



**Évaluation et application de MERRAero, une réanalyse des
aérosols atmosphériques développée par la NASA**

Thèse

Simon Provençal

Doctorat en sciences géographiques

Philosophiæ doctor (Ph. D.)

Québec, Canada

© Simon Provençal, 2017

**Évaluation et application de MERRAero, une réanalyse des
aérosols atmosphériques développée par la NASA**

Thèse

Simon Provençal

Sous la direction de

Nathalie Barrette, directrice de recherche

Résumé

La *Modern-Era Retrospective Analysis for Research and Application* (MERRA) est une réanalyse développée par le *Global Modeling and Assimilation Office* (GMAO) à la *National Aeronautics and Space Administration* (NASA) aux États-Unis qui intègre des données observées et des données modélisées pour reproduire une base de données complète dans le temps et l'espace de plusieurs variables atmosphériques (température, vitesse et direction du vent, humidité, pressions, etc.) depuis 1979. Afin de reproduire une analyse intégrée du système terrestre, le GMAO effectue d'autres réanalyses en parallèle : une réanalyse des océans (MERRAOcean), une réanalyse de la surface solide de la Terre (MERRALand) et une réanalyse de la composition de l'atmosphère (MERRAero), cette dernière constituant le sujet central de cette thèse. La 1^{ère} version de MERRAero intègre des données de la profondeur optique des aérosols (AOD) mesurée par MODIS-Terra et MODIS-Aqua, en orbite autour de la Terre depuis 2000 et 2002 respectivement, et les données d'un modèle de chimie atmosphérique qui simule la concentration de cinq espèces dominantes d'aérosols, soit les particules de sulfate, de carbone organique, de carbone noir, de poussière et de sel de mer. La réanalyse reproduit donc la concentration de ces cinq espèces d'aérosols partout sur la Terre, avec une résolution de 0,5° de latitude, 0,625° de longitude et 72 niveaux en altitude, à une fréquence horaire, en plus de leur contribution individuelle à l'AOD totale. Une reconstruction peut ensuite être appliquée pour obtenir la concentration totale des matières particulaires, un contaminant couramment pris en compte pour évaluer la qualité de l'air.

MERRAero constitue une avancée importante dans l'étude de la composition atmosphérique à l'échelle globale. Elle met à la disposition de la communauté scientifique un outil novateur qui lui permet d'étudier une

vaste gamme de problèmes liées à la pollution atmosphérique qu'aucun réseau de surveillance ne peut accomplir, particulièrement dans les régions dépourvues de toute surveillance fiable. MERRAero doit cependant traverser un processus d'évaluation rigoureux avant d'être jugée apte à accomplir ses fonctions. Certaines de ses capacités ont déjà été évaluées à certains endroits, notamment sa simulation de l'AOD au-dessus de certaines régions du monde et sa simulation de la concentration des oxydes de soufre aux États-Unis. L'objectif de cette thèse est de poursuivre les travaux d'évaluation avec une emphase sur la concentration des différentes espèces d'aérosols simulées à la surface par MERRAero dans plusieurs régions du monde. Une fois que l'évaluation ait été jugée favorable, MERRAero a ensuite été appliquée à une étude sur la pollution urbaine de l'air à l'échelle globale.

La concentration de plusieurs espèces d'aérosols simulée par MERRAero à la surface depuis 2003 a été comparée à des données d'observations provenant de différents réseaux de surveillance autour du monde : le *Interagency Monitoring of Protected Visual Environments* (IMPROVE) aux États-Unis, le *European Monitoring and Evaluation Programme* (EMEP) en Europe, celui du Ministère de la protection environnementale en Israël et celui de l'Administration de la protection environnementale à Taïwan. Plusieurs indicateurs statistiques ont été calculés, et des analyses spatiales et temporelles ont été effectuées pour évaluer l'exactitude de MERRAero, identifier ses lacunes importantes et formuler des recommandations pour améliorer ses versions subséquentes.

L'évaluation aux É.-U. et en Europe en milieu rural a démontré que MERRAero reproduit bien la concentration des particules de sulfate et de carbone d'origine anthropique. La concentration des particules de carbone d'origine naturelle, provenant notamment des feux de forêt, a cependant été largement surestimée, causant ainsi un biais important en été. MERRAero a surestimé aussi la concentration des particules de sable de sources lointaines, telles que le Sahara et les déserts en l'Asie de l'Est qui affectent

légèrement la composition des aérosols aux É.-U. L'évaluation a reproduit des résultats favorables en milieu urbain malgré la résolution de MERRAero qui ne capture pas toutes les sources d'aérosols, causant ainsi des fluctuations saisonnières non conformes aux observations.

L'évaluation a reproduit des résultats très favorables en Israël. Sa proximité au Sahara et aux déserts du Moyen-Orient suggère que MERRAero simule très bien la concentration des particules de sable d'origine locale. À Taïwan, MERRAero a reproduit la concentration des aérosols généralement bien à l'exception des mois d'hiver, lorsque Taïwan est le plus affecté par l'advection de pollution d'origine chinoise.

Malgré les lacunes identifiées, dans l'ensemble, l'évaluation a reproduit des résultats jugés suffisamment favorables pour que MERRAero soit appliquée dans une multitude de problématiques, notamment à l'étude de la pollution urbaine de l'air à l'échelle globale. Cette analyse a démontré l'impact que les politiques environnementales et la récession économique des dernières années ont eu sur la pollution atmosphérique des villes d'Amérique du Nord, d'Europe et d'Asie de l'Est. Même l'air des villes chinoises, lesquelles sont aux prises avec de sérieux problèmes de pollution depuis plusieurs années, s'est amélioré grâce à une initiative du gouvernement à réduire les émissions de contaminants atmosphériques. Les villes de l'Inde et du Bangladesh sont les seules à avoir vu leur situation se détériorer, due à une forte urbanisation et industrialisation. La qualité de l'air des villes d'Amérique du Sud et d'Afrique subsaharienne s'est aussi améliorée par un ralentissement des activités de déforestation au cours des dix dernières années, particulièrement dans la forêt amazonienne.

Table des matières

Résumé	iii
Liste des tableaux.....	x
Liste des figures.....	xii
Abréviations et symboles	xvi
Remerciements	xix
Avant-propos	xx
1 Introduction générale	1
1.1 Introduction	1
1.1.1 Propriétés des contaminants atmosphériques	2
1.1.2 La chimie des aérosols	3
1.1.3 Les observations des aérosols.....	5
1.1.4 La modélisation des aérosols	7
1.1.5 L'évaluation des modèles.....	9
1.1.6 La <i>Modern-Era Retrospective Analysis for Research and Application</i>	15
1.2 Problématique et objectifs	18
1.3 Méthodologie	20
1.3.1 La reconstruction de la concentration des PM.....	20
1.3.2 L'évaluation de MERRAero	22
1.3.3 Les incertitudes.....	26
1.3.4 L'application de MERRAero à l'étude de la pollution atmosphérique urbaine	27
1.4 Structure de la thèse	28
Références	30
2 Evaluation of PM chemical speciation simulated by NASA's MERRA Aerosol Reanalysis with the IMPROVE network in the United States	35
2.1 Introduction	36
2.2 Methods	38
2.3 Results and discussion.....	41
2.3.1 Ensemble evaluation	41
2.3.2 Evaluation of the annual and seasonal fluctuations.....	42
2.3.3 Evaluation in urban environments	46
2.3.4 The contribution of NO ₃	48

2.4	Conclusion	48
	References	50
3	Evaluation of PM surface concentrations simulated by Version 1 of NASA’s MERRA Aerosol Reanalysis over Europe	53
3.1	Introduction	54
3.2	Methods	56
3.3	Results	59
3.4	Discussion.....	65
3.5	Conclusion	68
	References	70
4	Evaluation of PM _{2.5} surface concentrations simulated by Version 1 of NASA’s MERRA Aerosol Reanalysis over Israel and Taiwan	73
4.1	Introduction	74
4.2	Locations and methods.....	77
4.2.1	Israel and Taiwan.....	77
4.2.2	Evaluation method	78
4.3	Results and discussion.....	81
4.3.1	Israel.....	81
4.3.2	Taiwan	84
4.4	Conclusion	86
	References	88
5	AOD distributions and trends of major aerosol species over a selection of the world’s most populated cities based on the 1st Version of NASA’s MERRA Aerosol Reanalysis.....	92
5.1	Introduction	93
5.2	Methodology and data.....	97
5.2.1	MERRA Aerosol Reanalysis.....	97
5.2.2	Method.....	99
5.3	AOD distributions of aerosol speciation (2003–2015).....	100
5.3.1	North and Central America.....	100
5.3.2	South America	103
5.3.3	Africa	105
5.3.4	Europe, including Russia and Turkey.....	107
5.3.5	Western and Central Asia.....	109

5.3.6	Eastern Asia.....	110
5.3.7	Southeastern Asia and Oceania.....	113
5.4	AOD trends of aerosol speciation (2003–2015)	114
5.4.1	Total AOD	114
5.4.2	AOD from SO ₄ aerosols	116
5.4.3	AOD from POM and BC aerosols.....	120
5.5	Discussion and conclusion	124
	References	128
6	Conclusion générale	136
6.1	Introduction	136
6.2	Les résultats de l'évaluation.....	136
6.2.1	États-Unis.....	136
6.2.2	Europe	138
6.2.3	Israël et Taïwan.....	138
6.3	L'application à l'étude de la pollution de l'air urbain à l'échelle globale	139
6.4	Conclusion et perspectives.....	140
	Références	144
A1	Une analyse statistique entre la concentration de particules fines et d'ozone en présence de brume sèche dans le Sud du Québec.....	145
A1.1	Introduction	145
A1.2	Méthodologie	149
A1.3	Résultats	153
A1.4	Discussion et conclusion	160
	Références	162
A2	Thermal comfort in Quebec City, Canada: sensitivity analysis of the UTCI and other popular thermal comfort indices in a mid-latitude continental city	165
A2.1	Introduction	166
A2.2	Materials and method.....	169
A2.2.1	The UTCI and other popular thermal comfort indices.....	169
A2.2.2	Location and data	170
A2.3	Results	173
A2.3.1	Climatic comparison between the stations.....	173

A2.3.2 Sensitivity analysis between the indices	176
A2.3.3 Identifying hazardous hot and cold weather events	180
A2.4 Discussion.....	184
A2.5 Conclusion	186
References	188

Liste des tableaux

Tab. 2.1: Performance statistics for the ensemble of the 163 rural stations. AOC stands for “average observed concentration.”	41
Tab. 2.2: Performance statistics for the ensemble of the 163 rural stations.	45
Tab. 2.3: Performance statistics for the ensemble of the 14 urban stations. AOC stands for “average observed concentration.”	46
Tab. 3.1: Performance statistics for the ensemble of locations. AOC stands for “average observed concentration.”	59
Tab. 3.2: Performance statistics for the ensemble of locations between April and September. AOC stands for “average observed concentration.”	66
Tab. 3.3: Average concentrations simulated by MERRAero for the ensemble of locations in Fig. 3.1 over the study period.	67
Tab. 3.4: Performance statistics for the ensemble of locations without the Italian stations. AOC stands for “average observed concentration.”	68
Tab. 4.1: Performance statistics for the ensemble of locations in Israel and Taiwan. AOC stands for “average observed concentration.”	82
Tab. 4.2: Average concentration simulated by MERRAero for the ensemble of locations in Fig. 4.1 over the study period.	84
Tab. A1.1 : Statistiques des concentrations de PM _{2.5} et d'O ₃ à Montréal, Québec et Gatineau jusqu'en 2013. Bien que la surveillance de l'O ₃ ait commencé en 2000 à Québec, seulement les données à partir du 1 ^{er} avril 2003 ont été utilisées pour calculer ces statistiques.....	152
Tab. A1.2 : Distribution des observations de brume sèche en fonction de la concentration de PM _{2.5} et d'O ₃	153
Tab. A1.3 : Distribution des observations estivales (juin, juillet et août) de brume sèche en fonction de la concentration de PM _{2.5} et d'O ₃	157
Tab. A1.4 : Distribution des observations hivernales (décembre, janvier et février) de brume sèche en fonction de la concentration de PM _{2.5} et d'O ₃ à Montréal.....	157

Tab. A1.5 : Distribution des observations diurnes (de 7h à 17h) de brume sèche au cours de l'été (juin, juillet et août) en fonction de la concentration de PM _{2.5} et d'O ₃	158
Tab. A2.1: Physical environment of the three stations.	172
Tab. A2.2: Clothing values used for calculating the PET.	173
Tab. A2.3: Slope (S) and coefficient of determination (R^2) for comparison between the variables ($T_{mrt,off}$, e and v_{10}) and the offset of the indices (UTCI _{off} and PET _{off}) at the three stations.	178
Tab. A2.4: Total number of hourly values for the UTCI, PET, HX and WC according to stress or comfort level at JL and SS. Stress levels for the UTCI are taken from Błażejczyk <i>et al.</i> (2013), comfort/stress levels for the PET are taken from Matzarakis <i>et al.</i> (1999), and HX and WC comfort levels are taken from Błażejczyk <i>et al.</i> (2012).	181

Liste des figures

Fig. 1.1 : Distribution de la concentration d'un contaminant en fonction de la distance de la source d'après le modèle gaussien.....	7
Fig. 1.2 : Système de coordonnées (a) lagrangien et (b) eulérien.....	8
Fig. 1.3 : Exemple de l'agencement d'une campagne d'évaluation. Le traceur est relâché de l'origine (0, 0) et sa concentration est mesurée aux différents points.....	10
Fig. 1.4 : Réservoir servant de laboratoire de Deardorff et Willis.	11
Fig. 1.5 : Exemple d'un tunnel aérodynamique pour étudier la dispersion en milieu urbain.....	12
Fig. 1.6 : Exemple d'une comparaison entre des données d'un modèle (lignes) et des données d'observations (points) à différentes distances d'une source.	14
Fig. 1.7 : Quantité et source des données (a) disponibles et (b) assimilées dans GEOS-5. TOVS (<i>TIROS Operational Vertical Sounder</i>), SSMI (<i>Special Sensor Microwave Imager</i>), ATOVS (<i>Advanced TIROS Operational Vertical Sounder</i>) et AIRS (<i>Advanced Infrared Sounder</i>) sont des sondeurs installés sur différents satellites.	17
Fig. 2.1: Locations of IMPROVE stations classified by regions.....	40
Fig. 2.2: Annual (left) and monthly (right) averages of (a) PM ₁₀ , (b) PM _{2.5} , (c) (NH ₄) ₂ SO ₄ , (d) OC, (e) BC, (f) DS _{2.5} and (g) SS _{2.5} concentrations measured by IMPROVE and simulated by MERRAero for the ensemble of the 163 rural stations.	43
Fig. 2.3: Monthly averages of OC concentrations measured by IMPROVE and simulated by MERRAero in (a) the northeast and (b) the northwest.	44
Fig. 2.4: Monthly averages of DS _{2.5} concentrations measured by IMPROVE and simulated by MERRAero in (a) the southeast and (b) the southwest..	45
Fig. 2.5 : Annual (left) and monthly (right) averages of (a) PM ₁₀ , (b) PM _{2.5} , (c) (NH ₄) ₂ SO ₄ , (d) OC and (e) BC concentrations measured by IMPROVE and simulated by MERRAero for the ensemble of the 14 urban stations.....	47
Fig. 3.1: Locations of monitoring stations in Europe.....	58

Fig. 3.2: Density scatter plots between observations and simulations of PM concentrations and species over the ensemble of European locations.60

Fig. 3.3: Maps of the mean bias for PM concentrations and species.64

Fig. 3.4: Monthly averages of PM concentration and species observations and simulations over the ensemble of European locations.65

Fig. 3.5: Monthly averages of PM concentration and species observations and simulations over the ensemble of European locations without the Italian stations.68

Fig. 4.1: Locations of monitoring stations in Israel and Taiwan.80

Fig. 4.2: Density scatter plot for (a) observed and simulated [PM_{2.5}], and (b) log-transformed observed and simulated [PM_{2.5}] for the ensemble of locations in Israel.82

Fig. 4.3: (a) Yearly and (b) monthly average of [PM_{2.5}] observation, simulation and bias, and (c–d) similarly for the SD and *FAC2*, for the ensemble of locations in Israel.82

Fig. 4.4: Density scatter plot for (a) observed and simulated [PM_{2.5}], and (b) log-transformed observed and simulated [PM_{2.5}] for the ensemble of locations in Taiwan.84

Fig. 4.5: (a) Yearly and (b) monthly average of [PM_{2.5}] observation, simulation and bias, and (c–d) similarly for the SD and *FAC2*, for the ensemble of locations in Taiwan.86

Fig. 5.1: Proportion of AOD speciation for a selection of cities in North and Central America. Mean AOD is provided for a few cities. The reader is referred to the supplementary material for such information for all the cities.101

Fig. 5.2: AOD of total and aerosol species averaged by month in (a) Los Angeles and (b) New York City.102

Fig. 5.3: Proportion of AOD speciation for a selection of cities in South America.104

Fig. 5.4: AOD of total and aerosol species averaged by month in (a) Brasilia and (b) Santiago.105

Fig. 5.5: Proportion of AOD speciation for a selection of cities in Africa. .106

Fig. 5.6: Proportion of AOD speciation for a selection of cities in Europe.	108
Fig. 5.7: AOD of total and aerosol species averaged by month in Naples.	108
Fig. 5.8: Proportion of AOD speciation for a selection of cities in Western and Central Asia.....	110
Fig. 5.9: Proportion of AOD speciation for a selection of cities in Eastern Asia.	112
Fig. 5.10: AOD of total and aerosol species averaged by month in Guangzhou.	112
Fig. 5.11: Proportion of AOD speciation for a selection of cities in Southeastern Asia and Oceania.	114
Fig. 5.12: Linear trend for total AOD in all cities between 2003 and 2015.	115
Fig. 5.13: Linear trend for AOD from SO ₄ aerosols in all cities between 2003 and 2015.....	117
Fig. 5.14: AOD of total and aerosol species averaged by year in (a) New York City, (b) London, (c) Moscow and (d) Tokyo.....	118
Fig. 5.15: AOD of total and aerosol species averaged by year in (a) Guangzhou and (b) Beijing.....	120
Fig. 5.16: Linear trend for AOD from POM aerosols in all cities between 2003 and 2015.....	122
Fig. 5.17: Linear trend for AOD from BC aerosols in all cities between 2003 and 2015.....	123
Fig. 5.18: AOD of total and aerosol species averaged by year in Sacramento.	123
Fig. A1.1 : Carte du Sud du Québec (supérieur gauche) et localisation des stations météorologiques et de qualité de l'air à Québec (supérieur droit), Gatineau (inférieur gauche) et Montréal (inférieur droit).....	151
Fig. A1.2 : Fréquence mensuelle des observations de brume sèche et concentration moyenne mensuelle de PM _{2.5} et d'O ₃ à (a) Montréal entre 1997	

et 2013, (b) Québec entre 2003 et 2013, et (c) Gatineau entre 2003 et 2013.
 155

Fig. A1.3 : Fréquence horaire des observations de brume sèche et concentration moyenne horaire de $PM_{2.5}$ et d' O_3 à (a) Montréal entre 1997 et 2013, (b) Québec entre 2003 et 2013, et (c) Gatineau entre 2003 et 2013.
 156

Fig. A1.4 : Proportion (en %) des observations horaires de brume sèche en fonction de la direction du vent (en degrés) à (a) Montréal entre 1997 et 2013, (b) Québec entre 2003 et 2013, et (c) Gatineau entre 2003 et 2013. 159

Fig. A2.1: Map of Quebec City and location of the Jean-Lesage, Sainte-Foy and Saint-Sauveur stations. 172

Fig. A2.2: Monthly averaged (a) T , (b) e and (c) v_{10} at the three stations from March 2013 to February 2014. 174

Fig. A2.3: Monthly averaged (a) UTCI, (b) PET, (c) HX and WC at the three stations from March 2013 to February 2014. 174

Fig. A2.4: Monthly average of the difference between SS and JL for (a) T , (b) e and (c) v_{10} from March 2013 to February 2014. 175

Fig. A2.5: Monthly average of the difference between SS and JL for (a) the UTCI, (b) the PET, (c) the HX and the WC from March 2013 to February 2014.
 176

Fig. A2.6: Comparison between $UTCI_{off}$ and (a) $T_{mrt,off}$, (b) e and (c) v_{10} at SF, and (d-f) similarly for PET_{off} . The trend line is included, as well as its slope (S) and the coefficient of determination (R^2). 178

Fig. A2.7: Comparison between e and (a) $UTCI_{off}$, (b) PET_{off} and (c) HX_{off} at SF when $T \geq 21^\circ C$. The trend line and its slope (S) are included. 179

Fig. A2.8: Comparison between v_{10} and (a) $UTCI_{off}$, (b) PET_{off} and (c) WC_{off} at SF when $T \leq 0^\circ C$ and $v_{10} > 0$ m/s. The trend line and its slope (S) are included. 179

Fig. A2.9: Hourly (a) observations of T , T_{mrt} and v_{10} , (b) computations of the indices, and (c) computations of the indices in the shade for July 15–17, 2013, at SF. 182

Fig. A2.10: Hourly (a) observations of T , T_{mrt} and v_{10} , and (b) computations of the indices for January 1–3, 2014, at SF. 183

Abréviations et symboles

$(\cdot)_{ln}/(\cdot)_{log}$	Valeur log-transformée
$(\cdot)_{off}$	Différence avec T (<i>offset</i>)
$\overline{(\cdot)}$	Moyenne
AERONET	<i>Aerosol Robotic Network</i>
Al	Aluminium
AOD	Profondeur optique des aérosols (<i>aerosol optical depth</i>)
AMS	<i>American Meteorological Society</i>
AT	Température apparente (<i>Apparent temperature</i>)
AVHRR	<i>Advanced Very High Resolution Radiometer</i>
β	Coefficient d'extinction massique
B	Biais
BC	Particules de carbone noir (<i>black carbon</i>)
Ca	Calcium
CALIOP	<i>Cloud-Aerosol Lidar with Orthogonal Polarization</i>
CALIPSO	<i>Cloud-Aerosol Lidar and Infrared Pathfinder Satellite Observations</i>
Cl	Ion de chlorure
C_o	Concentration observée
C_s	Concentration simulée
CSN	<i>Chemical Speciation Network</i>
$\Delta(\cdot)$	Différence entre SS et JL
e	Pression de vapeur d'eau
EMEP	<i>European Monitoring and Evaluation Programme</i>
EPA	<i>Environmental Protection Agency</i>
e_s	Pression vapeur saturante de l'eau
F	Fraction
FAC2	Facteur de 2

Fe	Fer
GEOS	<i>Goddard Earth Observing System</i>
GMAO	<i>Global Modeling and Assimilation Office</i>
GOCART	<i>Goddard Ozone Chemistry, Aerosol, Radiation and Transport</i>
HI	Indice de chaleur (<i>Heat index</i>)
HX	Humidex
IMPROVE	<i>Interagency Monitoring of Protected Visual Environments</i>
JL	Jean-Lesage
MERRA	<i>Modern-Era Retrospective Analysis for Research and Application</i>
MERRAero	<i>Modern-Era Retrospective Analysis for Research and Application Aerosol Reanalysis</i>
MISR	<i>Multangle Imaging Spectroradiometer</i>
MODIS	<i>Moderate Resolution Imaging Spectroradiometers</i>
NASA	<i>National Aeronautics and Space Administration</i>
NCEP	<i>National Centers for Environmental Protection</i>
NH ₄	Ammoniac
NH ₄ NO ₃	Particules de nitrate d'ammonium
(NH ₄) ₂ SO ₄	Particules de sulfate d'ammonium
NO ₃	Particules de nitrate
NOAA	<i>National Oceanic and Atmospheric Administration</i>
NO _x	Oxydes d'azote
O ₃	Ozone
OC	Particules de carbone organique (<i>organic carbon</i>)
PET	Température physiologique équivalente (<i>Physiological equivalent temperature</i>)
PM	Matière particulaire (<i>particulate matter</i>)
PM _{0.1}	Nanoparticules
PM ₁	Particules très fine
PM ₁₀	Particules respirables

PM _{2.5}	Particules fines
PMV	Vote moyen prévisible (<i>Predicted mean vote</i>)
POM	Particules organiques (<i>particulate organic matter</i>)
PS/DS	Particules de poussière (<i>dust</i>)
PS _{2.5} /DS _{2.5}	Particules fines de poussière (<i>fine dust</i>)
R	Coefficient de corrélation
R ²	Coefficient de détermination
S	Pente (<i>slope</i>)
SD-B	Écart type du biais (<i>standard deviation of the bias</i>)
SET	Température effective standard (<i>Standard effective temperature</i>)
SF	Sainte-Foy
Si	Silicium
SM/SS	Particules de sel de mer (<i>sea salt</i>)
SM _{2.5} /SS _{2.5}	Particules fines de sel de mer (<i>fine sea salt</i>)
SO ₄	Particules de sulfate
SO _x	Oxydes de soufre
SS	Saint-Sauveur
T	Température
TC	Particules de carbone (<i>total carbon</i>)
Ti	Titane
T _{mrt}	Température moyenne radiante (<i>Mean radiant temperature</i>)
T _r	Température du point de rosée
UTCI	Indice universel du climat thermique (<i>Universal thermal climate index</i>)
v _x	Vitesse du vent à x m
WBGT	Température au thermomètre-globe mouillé (<i>Wet-bulb Globe Temperature</i>)
WC	Indice de refroidissement éolien (<i>Wind chill index</i>)

Remerciements

Je profite de cette occasion pour exprimer ma sincère reconnaissance envers ceux qui m'ont accompagné au long de ce parcours et qui ont contribué à son succès.

Notamment, je remercie le Prof. Pinhas Alpert, M. Pavel Kishcha et Mme Emily Elhacham de l'Université de Tel Aviv en Israël pour m'avoir accueilli en tant que stagiaire et m'avoir introduit au projet de recherche qui a pris une place prédominante dans mes études doctorales, en plus d'avoir fourni des données d'observations.

Je remercie le Prof. Sheng-Hsiang Wang de l'Université nationale centrale à Taïwan pour avoir fourni d'autres données d'observations.

Ensuite, je remercie M. Arlindo da Silva, Mme Virginie Buchard et M. Ravi Govindaraju de la NASA aux États-Unis qui ont fourni toutes les données nécessaires au succès de ce projet ainsi que des commentaires essentiels aux analyses.

Et finalement, et non les moindres, je remercie la Prof. Nathalie Barrette et M. Richard Leduc de l'Université Laval pour m'avoir supervisé au cours des six dernières années. Leur support, leur expertise et leurs conseils se sont avérés indispensables au succès de ce projet.

Avant-propos

Cette thèse regroupe l'ensemble des travaux effectués au cours de mes études doctorales et présente leurs objectifs, leur méthodologie, leurs résultats et leurs contributions à la communauté scientifique. Ces travaux ont été effectués en grande partie sous la direction de Mme Nathalie Barrette, professeure titulaire au Département de géographie de l'Université Laval, et de M. Richard Leduc, professeur associé à la même institution.

Cette thèse est présentée sous forme de six chapitres et de deux annexes. À l'exception de l'introduction générale (Chap. 1) et de la conclusion générale (Chap. 6), les chapitres sont rédigés en anglais sous forme de quatre articles scientifiques indépendants les uns des autres, mais tous reliés au sujet central de la thèse, soit l'évaluation et l'application de MERRAero :

Chapitre 2 : *Evaluation of PM chemical speciation simulated by NASA's MERRA Aerosol Reanalysis with the IMPROVE network in the United States*, par Simon Provençal, article à soumettre prochainement.

Ce chapitre présente la première tentative d'évaluer la concentration de toutes les espèces de matières particulaires (PM) simulée par MERRAero aux États-Unis à l'aide du réseau IMPROVE, soit le réseau de surveillance des PM le plus complet au monde, composé principalement de stations localisées en milieu rural. Le territoire des É.-U. ayant une certaine diversité géographique, cet article permet d'identifier rapidement des espèces de PM que MERRAero simule très bien, soit les particules de sulfate et de carbone d'origine anthropique, et d'autres qui sont moins bien représentées, telles que les particules de carbone d'origine naturelle, en analysant leur cycle saisonnier dans différentes régions des É.-U.

Chapitre 3 : *Evaluation of PM surface concentrations simulated by Version 1*

of NASA's MERRA Aerosol Reanalysis over Europe, par Simon Provençal, Virginie Buchard, Arlindo M. da Silva, Richard Leduc et Nathalie Barrette, article publié dans *Atmospheric Pollution Research* en 2017 (vol. 8, pp. 374–382).

Ce chapitre poursuit l'évaluation de MERRAero en Europe avec le réseau EMEP. La plupart des stations de l'EMEP sont aussi situées en région rurale malgré que plusieurs d'entre elles soient localisées à proximité d'un quartier résidentiel. Bien que cet article permette d'approfondir l'évaluation de MERRAero, il identifie aussi une de ses lacunes importantes, par sa résolution trop peu fine, qui représente mal les sources de PM d'origine résidentielle. L'analyse a reproduit une fluctuation saisonnière incohérente, expliquée par les émissions résidentielles hivernales de particules de carbone provenant des feux de foyer et du chauffage au bois, lesquelles ne sont pas représentées par MERRAero.

Chapitre 4 : *Evaluation of PM_{2.5} Surface Concentrations Simulated by Version 1 of NASA's MERRA Aerosol Reanalysis over Israel and Taiwan*, par Simon Provençal, Virginie Buchard, Arlindo M. da Silva, Richard Leduc, Nathalie Barrette, Emily Elhacham et Sheng-Hsiang Wang, article publié dans *Aerosol and Air Quality Research* en 2017 (vol. 17, pp. 253–261).

Les évaluations aux É.-U. et en Europe ont fourni de l'information utile pour juger de l'exactitude de MERRAero et ont permis d'identifier certaines de ses lacunes. La distribution des PM aux É.-U. et en Europe n'est cependant pas représentative de plusieurs autres régions du monde, d'où l'intérêt de poursuivre l'évaluation dans d'autres régions. Comme les réseaux fiables de surveillance se font rares à l'extérieur des pays occidentaux, une autre évaluation a été menée en Israël et à Taïwan. Bien que ces deux pays aient un territoire plutôt restreint, ces évaluations ont néanmoins fourni de l'information additionnelle sur l'applicabilité de MERRAero; en Israël par sa proximité au Sahara et

aux déserts du Moyen-Orient, et à Taïwan par sa position à l'intérieur d'une région du monde aux prises avec de sérieux problèmes de pollution atmosphérique. L'évaluation s'est révélée être très favorable en Israël, mais biaisée à Taïwan. L'absence des particules de nitrate dans la simulation de MERRAero, une de ses plus importantes lacunes, a occasionné des biais importants en hiver, lorsque Taïwan est le plus affecté par l'advection de pollution d'origine chinoise.

Chapitre 5 : *AOD distributions and trends of major aerosol species over a selection of the world's most populated cities based on the 1st Version of NASA's MERRA Aerosol Reanalysis*, par Simon Provençal, Pavel Kishcha, Arlindo M. da Silva, Emily Elhacham et Pinhas Alpert, article publié dans *Urban Climate* en 2017 (vol. 20, pp. 168–191).

L'évaluation de MERRAero ayant reproduit des résultats généralement favorables, ce chapitre applique la réanalyse à l'étude de la pollution urbaine de l'air à l'échelle globale en analysant l'AOD au cours d'une période de 13 ans (2003–2015) et au-dessus de 200 villes parmi les plus peuplées au monde. Une analyse aussi détaillée et à aussi grande échelle est à ce jour inédite, d'autant plus que les données fournies par MERRAero par sa discrimination des différentes espèces d'aérosols procurent de l'information que les réseaux de surveillance standards ne peuvent reproduire. Notamment, il a été possible d'observer les conséquences directes que l'urbanisation, l'industrialisation, les politiques environnementales et la récession économique des dernières années ont eues sur la qualité de l'air urbain.

Au cours de mes études doctorales, j'ai également participé parallèlement à d'autres projets de recherche qui ont fait l'objet de publications scientifiques. Celles-ci sont présentées en annexe :

Annexe 1 : *Une analyse statistique entre la concentration de particules fines et d'ozone en présence de brume sèche dans le Sud du Québec*, par Simon

Provençal, Richard Leduc et Nathalie Barrette, article publié dans *Pollution Atmosphérique* en 2016 (no. 228).

Cette annexe introduit la notion de brume sèche (ou de visibilité réduite) causée par une accumulation de particules fines comme indicateur de mauvaise qualité de l'air. Les particules fines sont souvent accompagnées d'autres contaminants gazeux, tels que l'ozone, bien qu'ils proviennent de processus physiques et chimiques différents. La brume sèche peut donc être utilisée comme indicateur simple de mauvaise qualité de l'air dans des régions dépourvues de surveillance. Cette annexe explore donc cette possibilité en utilisant le sud du Québec comme étude de cas, et documente les limites que comporte cette approche et les circonstances lors desquelles elle est plus efficace.

Annexe 2 : *Thermal comfort in Quebec City, Canada: sensitivity analysis of the UTCI and other popular thermal comfort indices in a mid-latitude continental city*, par Simon Provençal, Onil Bergeron, Richard Leduc et Nathalie Barrette, article rédigé en anglais et publié dans *International Journal of Biometeorology* en 2016 (vol. 60, pp. 591–603).

La deuxième annexe porte sur le confort thermique à Québec et documente la valeur ajoutée d'implanter un indice de confort universel, soit le nouvel indice universel du climat thermique (UTCI), aux dépens des indices traditionnels plus simples, tels que l'humidex et le facteur vent, dans une région où la fluctuation climatique saisonnière est particulièrement grande, comme c'est le cas à Québec. Tous les articles publiés auparavant n'avaient évalué l'applicabilité de l'UTCI que dans des régions au climat doux ou tempéré.

Je suis le premier auteur de chacun des articles. J'ai réalisé toutes les étapes de la recherche, soit le recensement des techniques modernes d'évaluation de modèles par une revue de la littérature complète; la collecte des données nécessaires à l'évaluation dans certains cas; la manipulation des données et leur analyse à l'aide d'indices statistiques; l'illustration et

l'analyse des résultats de manière à faire ressortir les forces et les faiblesses des évaluations et des applications; et la rédaction, dans leur totalité, de tous les articles. M. Arlindo da Silva, qui apparait sur plusieurs articles, est l'architecte de MERRAero. Les autres co-auteurs ont agi à titre de relecteurs et certains d'eux ont fourni des données.

1 Introduction générale

1.1 Introduction

La révolution industrielle a eu un impact profond sur la société des pays occidentaux, tant sur le plan de l'économie, de la politique et de l'environnement. La transition d'une main-d'œuvre artisanale et agricole vers une main-d'œuvre ouvrière a radicalement changé la fonctionnalité des sociétés. Bien que la révolution ait introduit des défis sociétaux majeurs, tels que l'exploitation d'ouvriers, la dégradation environnementale et la propagation d'épidémies, la révolution industrielle a néanmoins amélioré le sort des sociétés. Les progrès en science, en technologie et en médecine qui l'ont accompagnée ont favorisé la mobilisation des ressources, réduit les disettes, amélioré la qualité de vie et prolongé son espérance.

La pollution de l'eau, de la terre et de l'air causée par la révolution industrielle a constitué un défi majeur auquel les pays occidentaux ont dû faire face. Par exemple, l'accumulation de déchets dans la Tamise à Londres a mené à l'épisode du *Great Stink* au cours des mois de juillet et août 1858, durant lesquelles la chaleur estivale exacerbait les odeurs nauséabondes émanant de la rivière, ce qui a poussé les autorités à construire le système d'égouts londonien (Jackson, 2014). La pollution de l'air était aussi un problème récurrent à Londres. L'épisode de smog du 5 au 9 décembre 1952, responsable de 4 000 morts prématurées, est souvent cité comme étant l'élément déclencheur d'une prise de conscience du public et des autorités britanniques par rapport au lien entre la qualité de l'air et la santé. Quelques années plus tard, le Royaume-Uni introduisit l'une des premières réglementations modernes qui visait à contrôler et diminuer la pollution de l'air, le *Clean Air Act* de 1956. D'autres pays aux prises avec des problèmes de pollution semblables ont suivi l'exemple du Royaume-Uni en introduisant à leur tour de telles mesures préventives.

Le succès de la réglementation introduite dans les pays industrialisés est aujourd'hui bien évident. La concentration de plusieurs contaminants atmosphériques a considérablement diminué au cours des dernières décennies aux États-Unis (Hand *et al.*, 2012; 2013), au Mexique (Molina et Molina, 2004a; b), en Europe (Vestreng *et al.*, 2007; Tørseth *et al.*, 2012) et au Japon (Wakamatsu *et al.*, 2013). La pollution de l'air demeure néanmoins une préoccupation constante, particulièrement dans les environnements urbains où les sources de pollution sont nombreuses, puisque les standards fixés par les autorités locales sont parfois dépassés. D'autant plus, des pays émergents, tels que l'Inde et la Chine, ont récemment développé de sérieux problèmes de pollution atmosphérique causés par une forte urbanisation et industrialisation (Lu *et al.*, 2011).

1.1.1 Propriétés des contaminants atmosphériques

La pollution est présente dans l'air sous forme gazeuse, solide et liquide, et provient de diverses sources, tant naturelles qu'anthropiques. Les contaminants solides et liquides sont communément surnommés des aérosols, soit des particules microscopiques en suspension dans l'air. Comme leur temps de résidence dans l'air est limité (quelques minutes à plusieurs semaines), leur concentration varie grandement dans le temps et l'espace (Haywood et Boucher, 2000), où elle est généralement plus élevée près des sources d'émissions. Contrairement aux contaminants gazeux, les aérosols ont plusieurs particularités qui stimulent un intérêt de la part de la communauté scientifique qui s'étend au-delà de leurs impacts nocifs sur la santé, notamment celle de jouer un rôle dans l'équilibre climatique terrestre. En tant que noyaux de condensation, les aérosols sont essentiels à la formation des nuages. Ils influencent leur contenu en eau liquide, leur épaisseur et leur durée de vie. Ils affectent donc indirectement l'albédo terrestre (Haywood et Boucher, 2000; Lohmann et Feichter, 2005). Les

aérosols affectent aussi directement le budget de rayonnement global. Ils ont la capacité d'absorber le rayonnement solaire (et le rayonnement terrestre, dans une moindre mesure) qui contribue au réchauffement de l'air, et de réfléchir le rayonnement solaire, ce qui contribue à son refroidissement (Haywood et Boucher, 2000). De ce fait, les aérosols jouent un rôle important dans l'étude des changements climatiques. Cependant, l'évaluation du forçage radiatif auquel contribuent les aérosols regorge d'incertitudes au point tel que la plus grande part de l'incertitude du forçage anthropique total leur est attribuée (Forster *et al.*, 2007, sect. 2.2). Finalement, lorsque la concentration des aérosols est suffisamment élevée, la visibilité peut être significativement réduite (Charlson, 1969), des événements généralement associés à la brume sèche, au smog et aux tempêtes de sable.

À la surface terrestre, les aérosols sont considérés être une forme de pollution nocive à la santé, associés aux maladies cardiovasculaires, respiratoires et allergiques, et à la mortalité prématurée (Pöschl, 2005; Tager, 2013). Dans ce contexte, il est courant de les surnommer des matières particulaires (*particulate matter*, PM). Elles sont classées en fonction de leur grosseur : grosses particules (particules dont le diamètre $> 10 \mu\text{m}$), particules respirables (PM_{10} , diamètre $\leq 10 \mu\text{m}$), particules fines ($\text{PM}_{2.5}$, diamètre $\leq 2,5 \mu\text{m}$), particules très fines (PM_1 , diamètre $\leq 1 \mu\text{m}$) et nanoparticules ($\text{PM}_{0.1}$, diamètre $\leq 0,1 \mu\text{m}$).

1.1.2 La chimie des aérosols

L'intensité et la gravité des impacts énumérés dans la Sect. 1.1.1 dépendent de la composition chimique des aérosols. Il est donc pertinent de faire la distinction entre les principales espèces :

- Les particules de sulfate (SO_4) sont des particules liquides d'acide sulfurique neutralisées totalement ou partiellement par l'ammoniac (NH_4), lesquelles sont surnommées des particules de sulfate

- d'ammonium ((NH₄)₂SO₄). Elles sont produites par l'oxydation du dioxyde de soufre (SO₂). Les émissions globales de SO₂ proviennent principalement de la combustion de combustibles fossiles (~72%) et de biomasse (~2%), des phytoplanctons marins (~19%), et des volcans (~7%) (Forster *et al.*, 2007, sect. 2.4.4.1; Haywood et Boucher, 2000);
- Les particules de nitrate (NO₃) sont produites par l'oxydation des oxydes d'azote (NO_x) si du NH₄ est toujours disponible dans l'air suite à la neutralisation complète des SO₄ (Forster *et al.*, 2007, sect. 2.4.4.5), surnommées des particules de nitrate d'ammonium (NH₄NO₃). Les sources des NO_x sont nombreuses et incluent la combustion de combustibles fossiles et de biomasse, l'activité microbienne du sol, et les éclairs. Delmas *et al.* (1997) estiment à 83% la contribution anthropique des émissions globales de NO_x;
 - Les particules organiques (*particulate organic matter*, POM) sont un mélange complexe de composés organiques contenant du carbone (surnommé du carbone organique (*organic carbon*, OC)). Des centaines de composés organiques différents ont été identifiés dans l'air. Elles sont émises directement dans l'air suite à la combustion de combustibles fossiles, de biocarburants et de biomasse (Forster *et al.*, 2007, sect. 2.4.4.2);
 - Les particules de carbone noir (*black carbon*, BC) sont émises directement dans l'air par des processus de combustion incomplète et proviennent des mêmes sources que les POM (Forster *et al.*, 2007, sect. 2.4.4.3);
 - La poussière (PS) contient plusieurs types de minéraux et provient en grande partie de l'érosion éolienne naturelle, particulièrement dans les régions arides. Les activités humaines, telles que la déforestation, l'agriculture et les activités industrielles, représentent aussi des sources anthropiques appréciables de PS (Forster *et al.*, 2007, sect. 2.4.4.6; Denman *et al.*, 2007, sect. 7.5.1.1);

- Les particules de sel de mer (SM) proviennent des océans. Leur libération dans l'air dépend de facteurs météorologiques, tels que la température et la vitesse du vent à la surface océanique (Denman *et al.*, 2007, sect. 7.5.1.2).

Il est important de mentionner que les aérosols d'origine naturelle ne sont pas nécessairement considérés être des contaminants atmosphériques, notamment la PS et le SM.

1.1.3 Les observations des aérosols

Les pays industrialisés ont mis sur pied des réseaux de surveillance et d'échantillonnage de la qualité de l'air de surface. Les objectifs des réseaux sont variés, mais les principaux objectifs consistent à assurer le respect des normes environnementales à court et long terme, et à informer le public des conditions extérieures en temps réel. Pour y parvenir, les réseaux mesurent plusieurs contaminants, y compris la concentration massique des PM, sur une base régulière. La fréquence des mesures dépend cependant des contaminants, mais les PM_{2.5} sont généralement mesurées à une fréquence horaire pour combler des objectifs à court terme. Très peu de réseaux de surveillance dans le monde mesurent la composition chimique des PM. Deux réseaux de ce type couvrent le territoire des É.-U., soit la *Interagency Monitoring of Protected Visual Environments* (IMPROVE, <http://vista.cira.colostate.edu/improve/>) (Malm *et al.*, 1994), qui contient principalement des stations rurales, et le *Chemical Speciation Network* (CSN, <http://www.epa.gov/ttnamti1/speciepg.html>), qui contient davantage de stations urbaines. En Europe, le *European Monitoring and Evaluation Programme* (EMEP, <http://www.emep.int/>) (Tørseth *et al.*, 2012) regroupe plusieurs stations d'échantillonnage qui mesurent les contaminants standards (PM₁₀, PM_{2.5}, SO₂, etc.) alors que certaines d'entre elles mesurent certaines espèces de PM.

Les stations d'échantillonnage sont ponctuelles et représentatives de leur milieu immédiat, et bien que les stations mesurant les PM soient bien répandues dans les pays développés, l'inventaire disponible est insuffisant pour étudier le comportement des aérosols à l'échelle globale et en haute atmosphère. Les outils de télédétection s'avèrent donc être fort utiles pour combler le vide. L'*Aerosol Robotic Network* (AERONET, <http://aeronet.gsfc.nasa.gov/>) (Holben *et al.*, 1998) est le plus grand réseau global de surveillance de surface des aérosols par télédétection. Ce réseau de 1 960 photomètres (abolies ou toujours en opération) répartis à travers le monde mesure la profondeur (ou l'épaisseur) optique des aérosols (*aerosol optical depth*, AOD). L'AOD correspond à la masse des aérosols à l'intérieur de la colonne atmosphérique multipliée par leur coefficient d'extinction massique β . La valeur de β varie en fonction de la composition chimique et la grosseur des aérosols, de l'humidité relative, et de la longueur d'onde. Bien que ces instruments surveillent la colonne atmosphérique complète, les observations demeurent ponctuelles et très rares au-dessus des océans et des pôles. À partir de l'espace, les deux *Moderate Resolution Imaging Spectroradiometers* (MODIS, <http://modis.gsfc.nasa.gov/>) (Remer *et al.*, 2005) à bord des satellites Terra et Aqua, en orbite autour de la Terre depuis 2000 et 2002 respectivement, le *Multiangle Imaging Spectroradiometer* (MISR, <https://www-misr.jpl.nasa.gov/>) (Kahn *et al.*, 2005) à bord de Terra, et le *Cloud-Aerosol Lidar with Orthogonal Polarization* (CALIOP) à bord du *Cloud-Aerosol Lidar and Infrared Pathfinder Satellite Observations* (CALIPSO, https://www.nasa.gov/mission_pages/calipso/main/index.html) (Winker *et al.*, 2009; 2010), en orbite depuis 2006, quant à eux, permettent une surveillance des aérosols globale et quasi constante. Bien que certains instruments de télédétection aient la capacité de discerner la grosseur des aérosols, aucun d'eux ne peut faire la distinction au niveau de leur composition chimique.

1.1.4 La modélisation des aérosols

Les modèles de qualité de l'air ont été développés pour combler le manque ou les lacunes des systèmes d'observations. Le premier modèle a cependant été développé bien avant que la technologie ne permette sa surveillance : le modèle gaussien qui date des années 1930. Bosanquet et Pearson (1936) avaient conceptualisé une expression mathématique qui reproduit une distribution normale de la concentration d'un contaminant, plus ou moins intense en fonction de l'éloignement de la source (Fig. 1.1). Le modèle gaussien est encore utilisé de nos jours pour des applications simples.

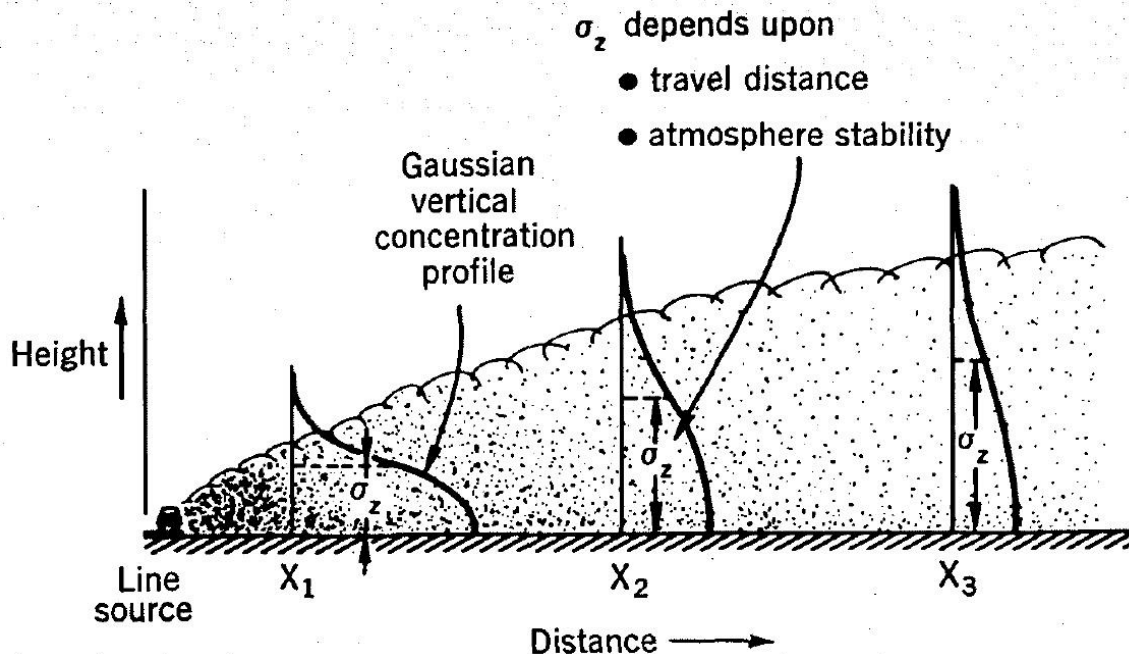


Fig. 1.1 : Distribution de la concentration d'un contaminant en fonction de la distance de la source d'après le modèle gaussien.
Source : Johnson *et al.*, 1973

Les progrès en informatique ont permis de développer des modèles numériques à grande échelle avec une précision remarquable. Les années 1970 ont marqué une percée importante en conceptualisant différentes approches à la modélisation de dispersion de contaminants dans l'air. Reynolds *et al.* (1973) ont introduit le premier modèle de dispersion eulérien, soit un système d'équations différentielles de conservation appliquées à

l'intérieur d'un domaine fixe dans l'espace. Pendant ce temps, les modèles de dispersion lagrangiens, c'est-à-dire des modèles qui simulent la trajectoire de contaminants dans l'espace en utilisant un système d'équations différentielles stochastiques (e.g., Rodhe, 1975), gagnaient de plus en plus de popularité. La Fig. 1.2 schématise la différence entre un modèle lagrangien, dont le système de coordonnées est fixe par rapport au contaminant qui se disperse, et eulérien, dont le système de coordonnées est fixe dans l'espace.

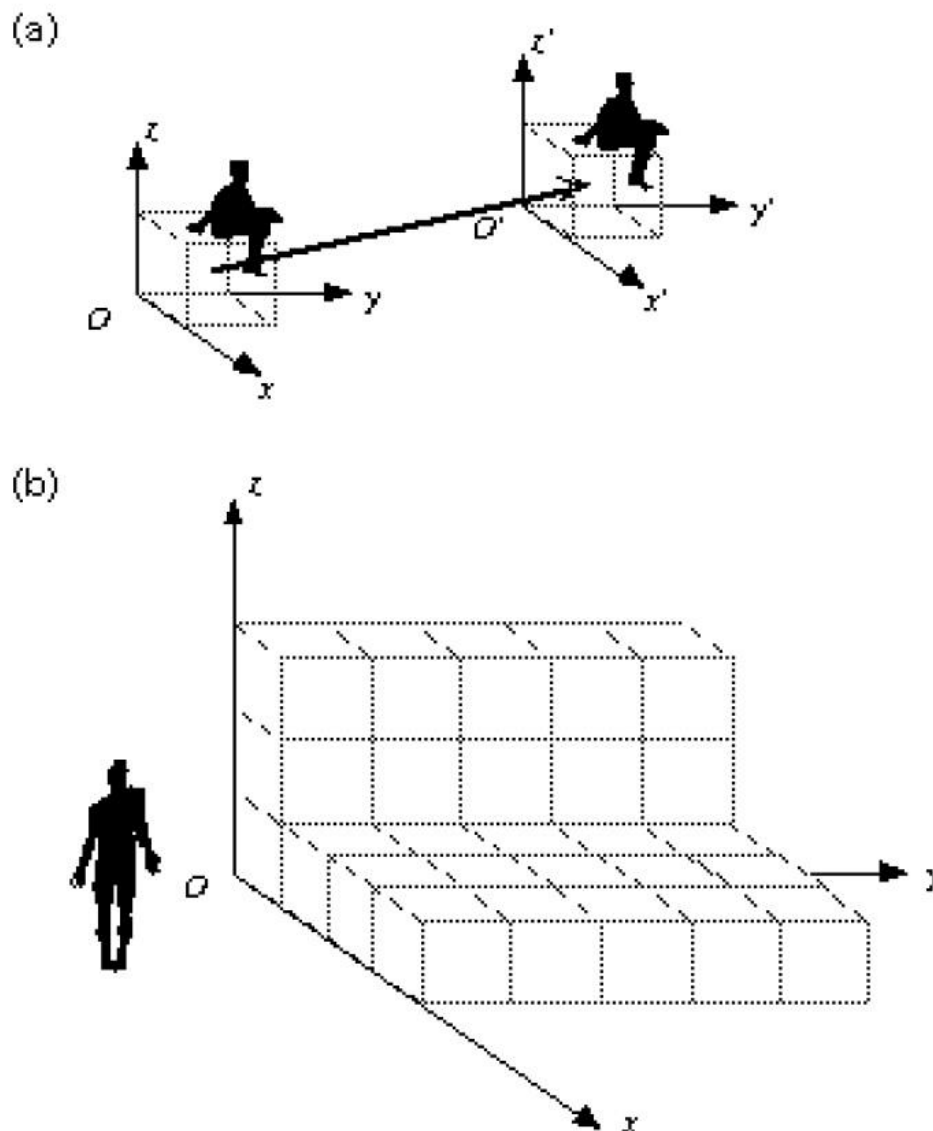


Fig. 1.2 : Système de coordonnées (a) lagrangien et (b) eulérien.
Source : Byun *et al.*, 2003

Aujourd'hui, plusieurs modèles complexes qui intègrent la météorologie, les propriétés de la surface terrestre et diverses sources de pollution ont été développés par des groupes de recherche académiques et gouvernementaux, tels que AERMOD et CALPUFF (https://www3.epa.gov/scram001/dispersion_prefrec.htm) développés par la *Environmental Protection Agency* (EPA) et la *American Meteorological Society* (AMS) aux É.-U. Ces modèles sont utilisés par de nombreux chercheurs pour leur recherche.

1.1.5 L'évaluation des modèles

En plus d'être des outils de prévision et de prévention, la couverture globale et temporelle des modèles fournit de l'information qu'aucun réseau de surveillance ne peut procurer. En contrepartie, un modèle comporte inévitablement des erreurs et des simplifications d'ordre physique, en plus des incertitudes que comportent les intrants (paramètres météorologiques, émissions de contaminants, etc.). Il est donc essentiel que les modèles soient soumis à un processus d'évaluation rigoureux pour qu'ils soient utilisés avec une certaine confiance.

L'évaluation des modèles se fait en comparant leur simulation à des données d'observations, soit mesurées par des réseaux de surveillance, soit lors de campagnes sur le terrain ou en laboratoire. Les campagnes sur le terrain sont généralement effectuées au cours de quelques jours durant lesquels des stations d'observations sont réparties sur des arcs à différentes distances de la source (e.g., Fig. 1.3). Un traceur est relâché de l'origine et sa concentration est mesurée à différents endroits sur le territoire. Les campagnes sur le terrain étant cependant dispendieuses, les équipements de laboratoire sont alors couramment utilisés pour compenser. Willis et Deardorff (1974; 1976; 1978; 1981; Deardorff et Willis, 1982) ont publié plusieurs travaux sur la dispersion d'un traceur à l'intérieur d'un réservoir rempli d'eau (Fig. 1.4), des expériences qui ont été utilisées pour évaluer de

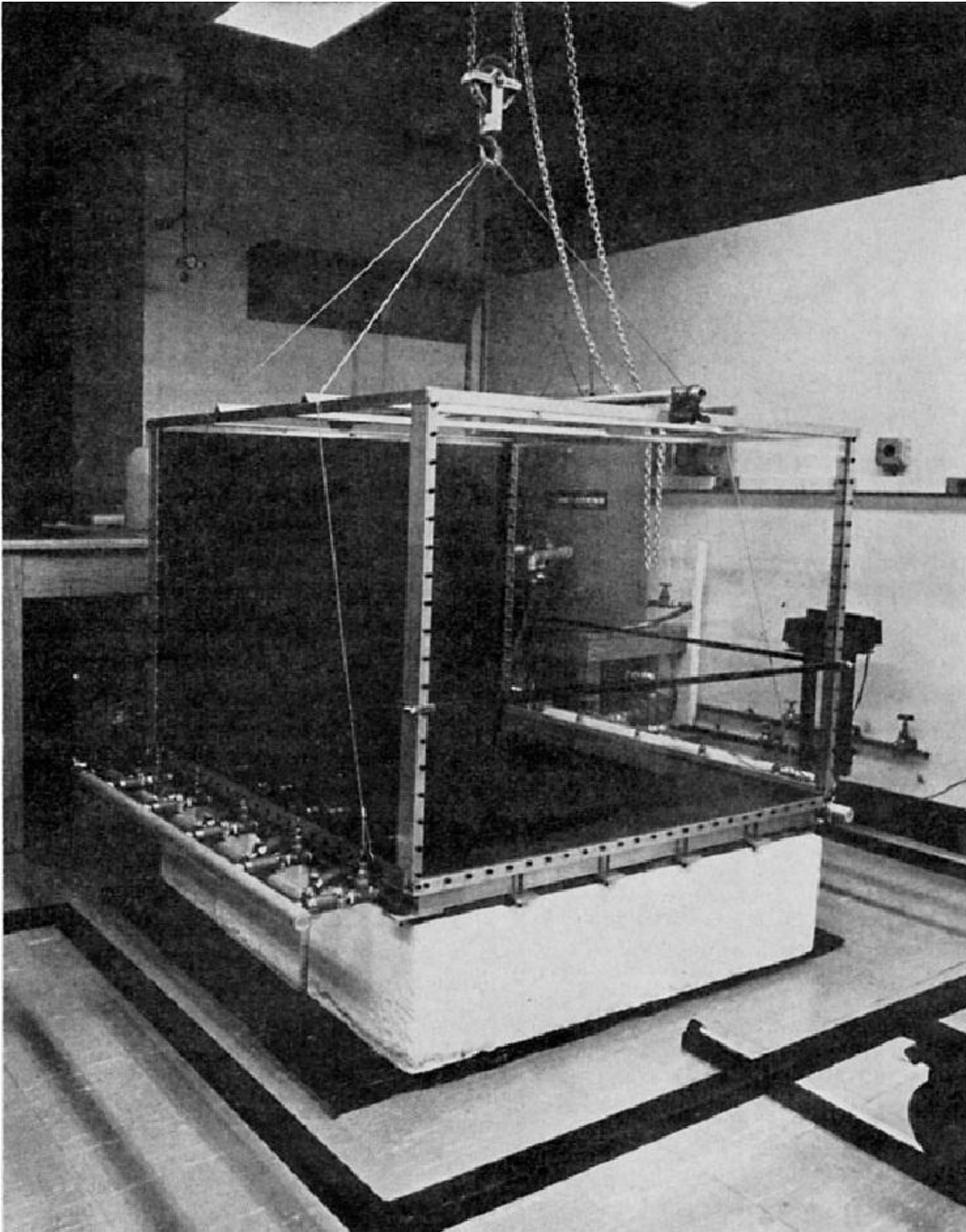


Fig. 1.4 : Réservoir servant de laboratoire de Deardorff et Willis.
Source : Willis et Deardorff, 1974

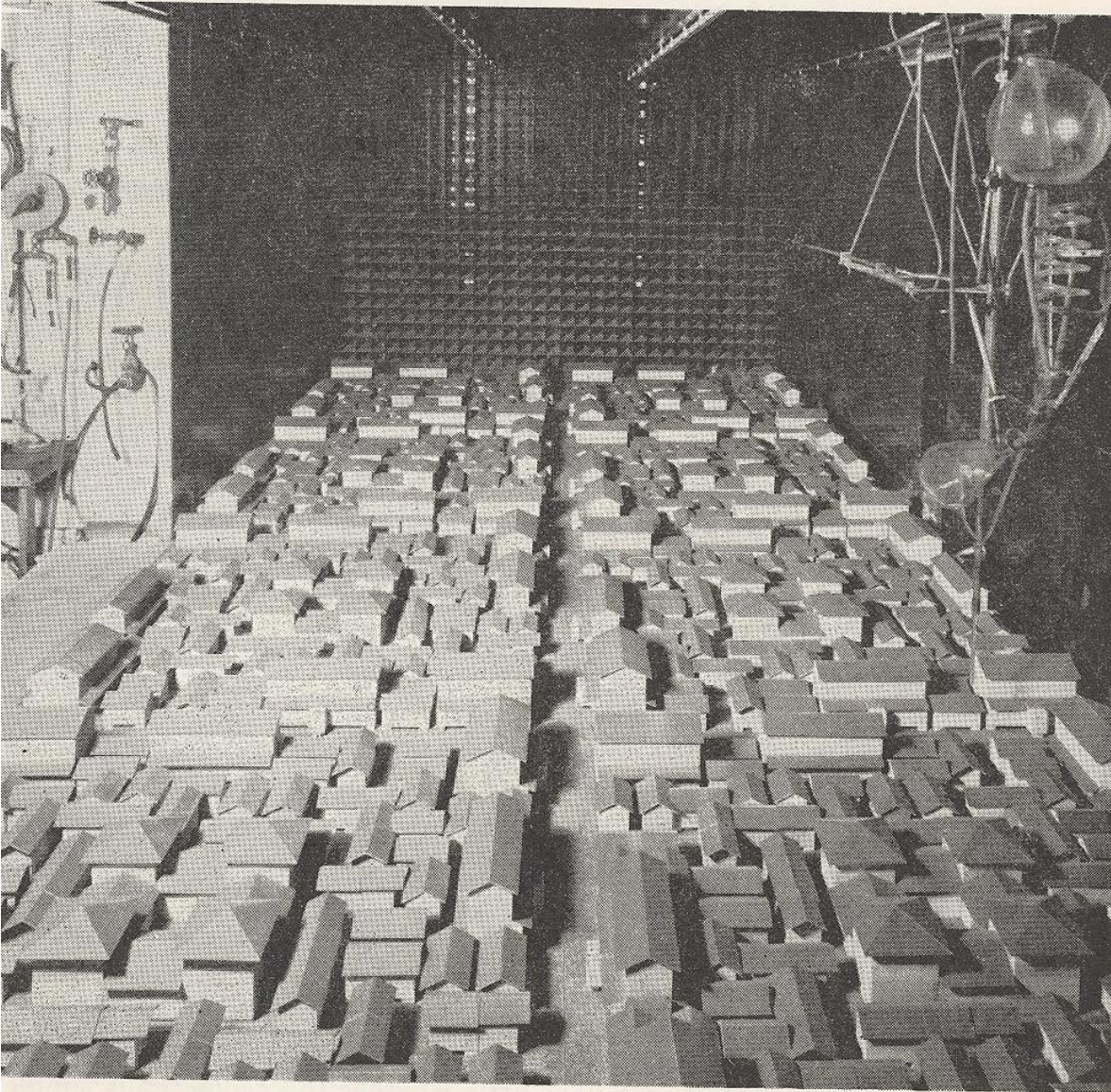


Fig. 1.5 : Exemple d'un tunnel aérodynamique pour étudier la dispersion en milieu urbain.

Source : Rouse, 1951

Les campagnes sur le terrain ont l'avantage d'être effectuées dans un environnement naturel, tandis que les expériences en laboratoire offrent la possibilité de contrôler les conditions dans lesquelles elles sont effectuées. Ces deux approches ont toutefois comme lacune de reproduire des résultats d'évaluation restreints tant dans l'espace que dans le temps. Elles sont effectivement trop limitées pour évaluer de manière exhaustive des modèles d'envergure régionale ou mondiale. Les réseaux d'observations s'avèrent donc essentiels pour évaluer de tels modèles.

Peu importe le modèle à être évalué et l'approche utilisée pour ce faire, l'évaluation consiste à comparer des données de concentrations simulées par le modèle à des données de concentrations observées. Historiquement, cette comparaison se faisait « à l'œil » (e.g., Fig. 1.6), laissant ainsi place à des interprétations subjectives quant à la qualité d'un modèle. Suite à un intérêt de la part de la communauté scientifique de standardiser la procédure d'évaluation, plusieurs indicateurs statistiques de performance ont été introduits afin de calculer différentes variantes du biais entre la concentration observée (C_o) et simulée (C_s), notamment :

- le biais moyen : $\bar{C}_s - \bar{C}_o$
- le biais moyen au carré : $\overline{(C_s - C_o)^2}$
- le biais moyen absolu : $\overline{|C_s - C_o|}$
- le biais de la moyenne géométrique : $\exp(\overline{\ln C_s} - \overline{\ln C_o})$

et plusieurs autres. L'efficacité de ces indicateurs est limitée puisque la simplification d'erreurs, c'est-à-dire la simplification des valeurs surestimées par celles sous-estimées, peut reproduire une évaluation favorable malgré les lacunes du modèle. Le coefficient de corrélation (R) est aussi un indicateur couramment utilisé malgré que Willmott (1982) le critique puisqu'il ne compare pas directement C_o et C_s , en plus d'être disproportionnellement influencé par des paires de données extrêmes. Il est effectivement possible qu'un modèle de bonne qualité produise un R faible ou même négatif.

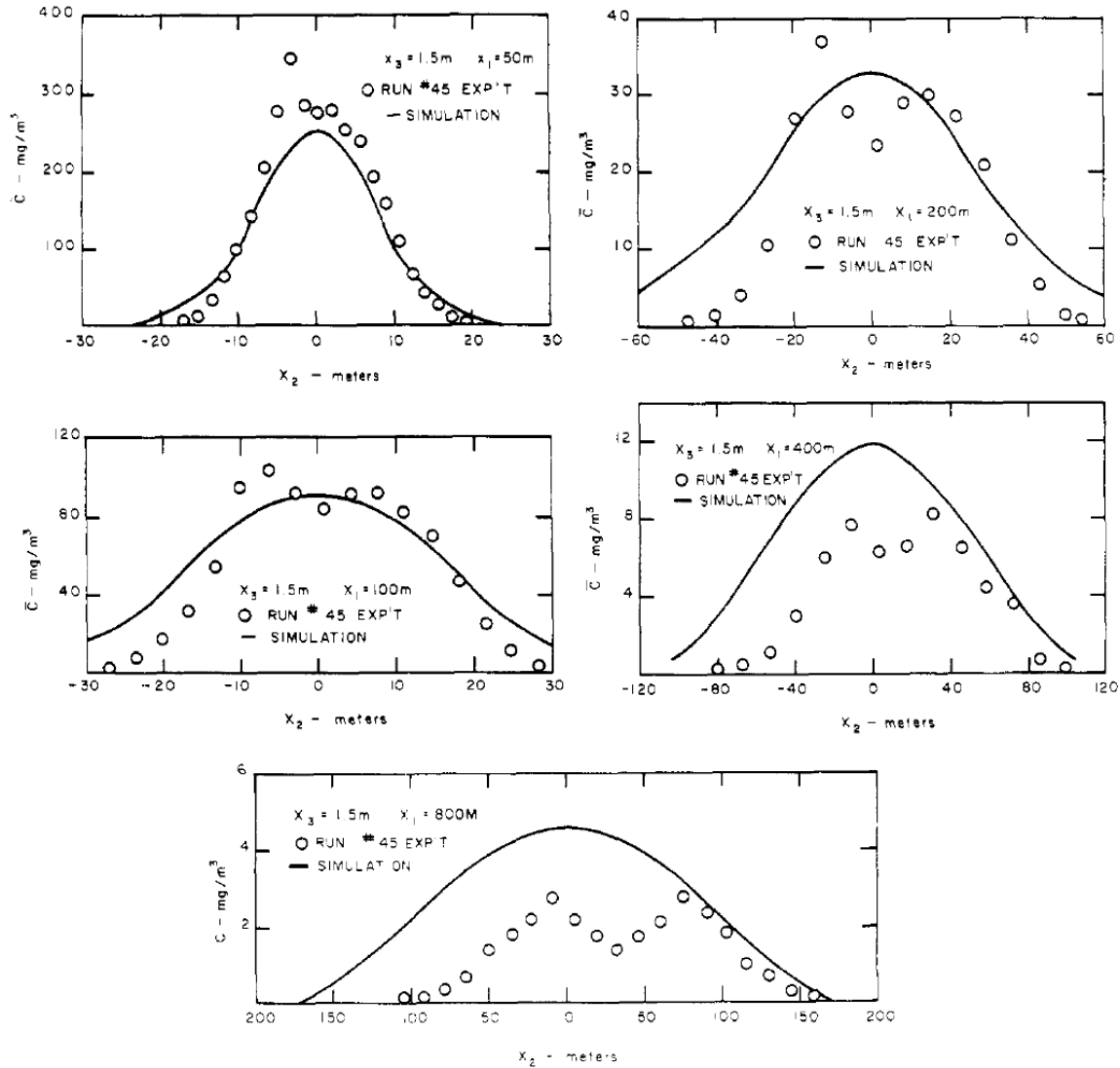


Fig. 1.6 : Exemple d'une comparaison entre des données d'un modèle (lignes) et des données d'observations (points) à différentes distances d'une source.

Source : Bullin et Dukler, 1974

Chang et Hanna (2004) ont introduit un indicateur d'évaluation plus fiable, soit la proportion des paires de données qui satisfont $0,5 \leq C_o / C_s \leq 2,0$ (FAC2, i.e. facteur de deux), un indicateur qui n'est pas affecté par la simplification d'erreurs ou par des paires de données extrêmes. Cet indicateur, utilisé en parallèle avec d'autres, encadre l'évaluation des modèles. Cet encadrement demeure néanmoins subjectif puisque des cibles quant à la valeur des indicateurs ne sont pas fixées, laissant ainsi place à des interprétations personnelles. Chang et Hanna (2004), quant à eux,

suggèrent une valeur minimale de $FAC2 = 0,5$ pour l'évaluation favorable d'un modèle.

1.1.6 La *Modern-Era Retrospective Analysis for Research and Application*

Les analyses rétrospectives (ou « réanalyses ») sont des outils qui harmonisent des modèles avec des réseaux d'observations pour recréer une base de données climatiques complète dans le temps et l'espace. De tels outils se sont avérées être très utiles pour la recherche en environnement.

Il y a plusieurs années, le *Global Modeling and Assimilation Office* (GMAO, <https://gmao.gsfc.nasa.gov/>) de la *National Aeronautics and Space Administration* (NASA, <https://www.nasa.gov/>) a introduit la *Modern-Era Retrospective Analysis for Research and Application* (MERRA, <http://gmao.gsfc.nasa.gov/research/merra/>) (Rienecker *et al.*, 2011), une réanalyse dont l'objectif principal est de concerter la suite du système d'observations satellitaires de la NASA, particulièrement depuis que Terra et Aqua sont en orbite, dans un contexte climatique, avec une emphase sur le cycle hydrologique. MERRA est bâtie à partir de plusieurs composantes faisant partie de la 5^e version du *Goddard Earth Observing System* (GEOS-5, <http://gmao.gsfc.nasa.gov/GEOS/>), un ensemble de modèles qui intègre un système d'assimilation de données développé par le GMAO pour adresser différentes problématiques concernant le système terrestre. GEOS-5 inclut un modèle de circulation générale, semblable à un modèle de prévisions météorologiques, couplé à un modèle hydrologique de surface, dans lequel les processus physiques, tels que l'humidité (évaporation, condensation, formation et composition des nuages, précipitations), le rayonnement solaire et terrestre, la turbulence, et l'interaction entre la surface et l'atmosphère, sont représentés. Le modèle *Goddard Ozone Chemistry, Aerosol, Radiation and Transport* (GOCART, Chin *et al.*, 2000; 2002) est aussi intégré pour

simuler la composition de l'atmosphérique en ozone et en aérosols qui interagissent avec le rayonnement et, par le fait même, jouent un rôle important dans le budget énergétique de la Terre.

MERRAero utilise un algorithme d'assimilation de données observées basé sur une interpolation statistique aux points de grille (Wu *et al.*, 2002) et un algorithme d'analyse différentielle qui applique une correction au modèle à mesure qu'il progresse dans le temps (Bloom *et al.*, 1996). Une description approfondie de la dynamique de GEOS-5 est documentée dans Rienecker *et al.* (2008).

Des données d'observations provenant de divers réseaux et plateformes sont assimilées dans GEOS-5. Des instruments de surveillance conventionnels, telles que des radiosondes, des catasondes, des profileurs de vent, des bouées et des stations météorologiques installées à la surface, dans des avions et sur des navires, fournissent des données météorologiques (vitesse et direction du vent, température, humidité, pression). Bien que les satellites ne mesurent aucune de ces variables directement, leur couverture beaucoup plus grande leur permet de contribuer la majorité des données d'observations assimilées par GEOS-5. La luminance énergétique mesurée à différentes longueurs d'onde par différents instruments installés sur plusieurs satellites permet d'inférer, entre autres, le profil vertical de la température, de l'humidité et de la concentration d'ozone. GEOS-5 assimile des données provenant de plusieurs générations de satellites de la NOAA, des *Geostationary Operational Environmental Satellites* et du *Defense Meteorological Satellite Program* (Rienecker *et al.*, 2008, sect. 3.5.2). La Fig. 1.7(a) présente l'évolution de la quantité de données d'observations disponible pour l'assimilation. Une augmentation importante est observée depuis le début des années 2000, qui atteint près de 4 millions de données par période de 6 heures, suite au lancement d'Aqua en orbite. Cette quantité est cependant trop volumineuse pour que chaque donnée soit assimilée dans GEOS-5. Une

série de programmes et d'algorithmes propres aux sources de données est exécutée pour effectuer un contrôle de la qualité et ainsi en exclure plus de la moitié (Fig. 1.7(b)).

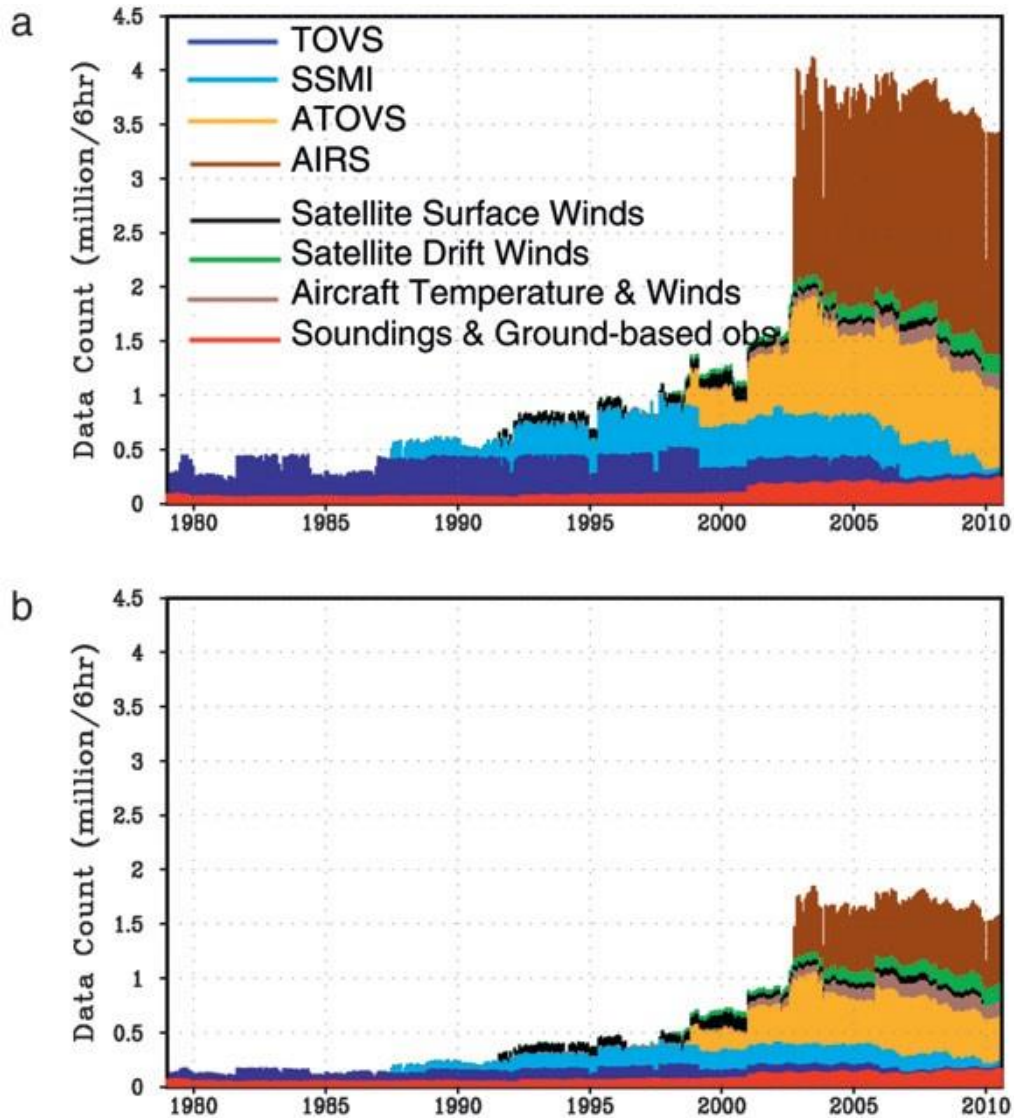


Fig. 1.7 : Quantité et source des données (a) disponibles et (b) assimilées dans GEOS-5. TOVS (*TIROS Operational Vertical Sounder*), SSMI (*Special Sensor Microwave Imager*), ATOVS (*Advanced TIROS Operational Vertical Sounder*) et AIRS (*Advanced Infrared Sounder*) sont des sondeurs installés sur différents satellites.

Source : Rienecker *et al.*, 2011

Alors que MERRA est une réanalyse des conditions météorologiques, le GMAO effectue d'autres réanalyses en parallèle : MERRAOcean, une réanalyse des conditions océaniques; MERRALand, une réanalyse de la surface terrestre; et MERRAero, une réanalyse des aérosols atmosphériques,

ce dernier constituant l'objet central de cette thèse.

Le modèle de circulation générale de GEOS-5 et le modèle GOCART constituent les principales composantes de MERRAero. GOCART simule les sources, les puits, le transport, la concentration et la taille de toutes les espèces d'aérosols énumérées dans la Sect. 1.1.2 à l'exception des NO_3 (Colarco *et al.*, 2010). Le modèle simule la concentration du OC et la multiplie par 1,4 pour estimer la concentration des POM. Les émissions de PS et de SM sont uniquement fonctions des propriétés de la surface et de la vitesse du vent à la surface, tandis que celles des autres espèces sont issues d'inventaires, incluant leurs précurseurs. GOCART utilise les émissions de SO_2 de 2005 reproduites par la version 4.1 de la *Emissions Database for Global Atmospheric Research* (EDGAR, <http://edgar.jrc.ec.europa.eu/>), un inventaire d'émissions anthropiques développé par la Commission européenne. Le SO_2 est ensuite oxydé dans la simulation pour former des SO_4 . GOCART utilise aussi la version 2.1 du *Quick Fire Emission Dataset* (QFED, https://gmao.gsfc.nasa.gov/research/science_snapshots/global_fire_emissions.php) (Darmenov et da Silva, 2015) pour les émissions de OC et de BC. De plus, MERRAero assimile les données corrigées d'AOD observées par MODIS-Terra et MODIS-Aqua pour reproduire une base de données globale des cinq espèces d'aérosols (concentration et AOD) à une résolution de $0,5^\circ$ de latitude, $0,625^\circ$ de longitude et 72 niveaux en altitude (de la surface à ~ 80 km d'altitude) depuis 2002.

1.2 Problématique et objectifs

MERRAero constitue une avancée importante dans l'étude des aérosols et de la qualité de l'air à l'échelle globale, particulièrement par sa distinction de la composition chimique des aérosols. Elle estime la concentration de cinq espèces dominantes d'aérosols en fonction de leur taille partout sur la Terre et en haute atmosphère, et leur contribution individuelle à l'AOD. Afin

qu'elle soit appliquée avec une certaine confiance, une évaluation complète, dans la mesure du possible, était nécessaire. Sa simulation de l'AOD a été évaluée au-dessus de l'Afrique, de l'Amérique du Sud, du centre et de l'est de l'Asie par Buchard *et al.* (2015); Nowottnick *et al.* (2015) ont évalué la structure verticale des aérosols spécifique à l'advection de sable provenant du Sahara au-dessus de l'Atlantique; et aux É.-U., la concentration de SO₂ et des PM_{2.5} à la surface a été évaluée par Buchard *et al.* (2014; 2016). MERRAero étant une réanalyse de très grande envergure, ces travaux, bien qu'ils aient contribué significativement à l'évaluer, demeuraient restreints tant sur le plan de ses capacités de simulation que de sa géographie. Afin d'optimiser la fiabilité de MERRAero pour qu'elle soit appliquée à diverses problématiques, des évaluations supplémentaires étaient nécessaires. Ce travail a donc proposé de poursuivre l'évaluation de MERRAero, avec une emphase sur sa simulation de la concentration des différentes espèces chimiques d'aérosols, des PM₁₀ et des PM_{2.5} à la surface terrestre, dans différentes régions du monde qui ont des profils d'aérosols distincts.

L'objectif de ce travail était donc de poursuivre l'évaluation de MERRAero en utilisant divers réseaux de surveillance autour du monde. Le réseau IMPROVE aux É.-U. était incontournable pour ses mesures de la concentration des PM₁₀, PM_{2.5} et de leurs espèces chimiques. Le réseau EMEP en Europe a procuré aussi des données de concentration des PM₁₀, PM_{2.5} et de certaines espèces chimiques. Le profil des aérosols aux É.-U. et en Europe étant quelque peu similaire, il était donc souhaitable de poursuivre l'évaluation dans d'autres régions du monde, malgré que les réseaux de surveillance soient beaucoup moins répandus à l'extérieur des pays occidentaux. Une évaluation de la concentration des PM_{2.5} a néanmoins été possible en Israël et à Taïwan, deux pays où de telles mesures sont disponibles. Bien que ces évaluations aient été limitées, les résultats ont néanmoins fourni de l'information utile quant à la performance de MERRAero, puisque leur profil d'aérosols est dominé par des espèces

chimiques spécifiques. En Israël, la concentration des PM_{2.5} est relativement élevée et principalement composée de particules d'origine naturelle due à sa proximité au Sahara et aux déserts du Moyen-Orient. La concentration des PM_{2.5} à Taïwan est aussi relativement élevée mais composée principalement de particules anthropiques dues aux activités industrielles en Chine continentale.

L'évaluation dans toutes ces régions du monde a permis d'examiner plus largement la portée et les limites de MERRAero, et de suggérer des améliorations pour perfectionner ses versions subséquentes. Dans l'ensemble, comme l'évaluation a reproduit des résultats favorables, MERRAero a ensuite été appliquée pour analyser la situation récente et courante de la qualité de l'air urbain à l'échelle globale. Comme plusieurs pays, particulièrement ceux en développement, sont dépourvus de toute surveillance malgré le fait qu'ils abritent des villes très peuplées aux prises avec des problèmes de pollution récurrents et croissants, les satellites et les modèles sont les seuls outils disponibles pour effectuer une analyse d'une telle ampleur. MERRAero étant une réanalyse fondée sur des modèles et des observations, elle fournit de l'information supplémentaire que les observations à elles seules ne peuvent procurer, notamment par sa capacité de décomposer l'AOD parmi les différentes espèces d'aérosols. Cette information est particulièrement utile puisqu'elle permet d'identifier spécifiquement les sources de pollution majeures qui affectent une ville; cette information n'étant pas fournie par les outils de télédétection ou les réseaux ne mesurant que la concentration des PM.

1.3 Méthodologie

1.3.1 La reconstruction de la concentration des PM

MERRAero estime la concentration de cinq espèces de PM : SO₄, OC,

BC, PS et SM, à l'échelle globale, à différents niveaux dans l'atmosphère et à une fréquence horaire. La concentration des particules de PS et de SM est classée en fonction de leur diamètre. À partir de celles-ci, il est possible d'appliquer une reconstruction pour estimer la concentration totale des PM. Plusieurs reconstructions ont été recensées dans la littérature et appliquées à l'aide d'observations pour évaluer leur exactitude (Chow *et al.*, 2015), mais chacune d'elles utilisait cette équation comme fondement :

$$(1.1) \quad [PM] = \begin{array}{l} \text{[ions inorganiques]} \\ + \text{ [particules organiques]} \\ + \text{ [particules de carbone noir]} \\ + \text{ [particules minérales]} \\ + \text{ [particules de sel]} \\ + \text{ [autres particules de trace]} \end{array}$$

Les crochets [] indiquent la concentration. Chaque composante de l'Éq. 1.1 était généralement estimée ainsi :

- Les ions inorganiques incluent les SO₄, les NO₃ et le NH₄. Comme la concentration du NH₄ est très rarement mesurée par les réseaux de surveillance, les SO₄ et les NO₃ étaient présumés être complètement neutralisés par le NH₄ sous forme de (NH₄)₂SO₄ et de NH₄NO₃, respectivement. La concentration des ions inorganiques était donc estimée ainsi : $1,375 \times [SO_4] + 1,29 \times [NO_3]$ (Chow *et al.*, 2015). La contribution des NO₃ était occasionnellement omise si leur concentration était manquante ou peu fiable (e.g., Malm *et al.*, 1994);
- La concentration des POM était estimée à partir des mesures de la concentration du OC en la multipliant par un coefficient qui habituellement prenait une valeur de 1,4 (Chow *et al.*, 2015). Cette valeur a cependant été critiquée par Turpin et Lim (2001) qui recommandent un coefficient plus élevé en fonction du milieu : $1,6 \pm 0,2$ pour le OC en milieu urbain et $2,1 \pm 0,2$ pour le OC vieilli (milieu rural);
- La concentration du BC était directement mesurée;

- Les particules minérales incluent plusieurs minéraux retrouvés dans la poussière, la terre et le sable mais dont seulement quelques-uns sont régulièrement mesurés. Pour estimer leur concentration totale, le réseau IMPROVE utilisait, par exemple, une équation empirique à partir de la concentration d'aluminium (Al), de silicium (Si), de titane (Ti), de calcium (Ca) et de fer (Fe) qui tenait compte des minéraux manquants (Malm et Hand, 2007);
- La concentration des particules de sel était obtenue à partir de la concentration des ions de chlorure (Cl) multipliée par 1,8 (Malm et Hand, 2007);
- Les autres particules de trace incluent, entre autres, l'oxyde de cuivre, l'oxyde de zinc et l'oxyde de plomb. Leur concentration était cependant très rarement incluse dans la reconstruction considérant leur contribution négligeable à la concentration totale des PM (Chow *et al.*, 2015).

Considérant toutes les espèces de PM simulées par MERRAero, la reconstruction de la simulation peut se faire le plus précisément possible à l'aide de ces deux équations :

$$(1.2) \quad [PM_{10}] = 1,375 \times [SO_4] + a \times [OC] + [BC] + [PS] + [SM]$$

$$(1.3) \quad [PM_{2.5}] = 1,375 \times [SO_4] + a \times [OC] + [BC] + [PS_{2.5}] + [SM_{2.5}]$$

Les Éq. 1.2 et 1.3 présument que les SO_4 , le OC et le BC sont sous forme de $PM_{2.5}$, et omettent la contribution des NO_3 . Tel que mentionné précédemment, a varie en fonction du milieu.

1.3.2 L'évaluation de MERRAero

La concentration à la surface des SO_4 , du OC, du BC, de la $PS_{2.5}$, du $SM_{2.5}$, des PM_{10} et des $PM_{2.5}$ simulée par MERRAero a été comparée à des observations dans la mesure où elles le permettaient à ces endroits :

- aux É.-U. contigus à l'aide du réseau IMPROVE;
- en Europe à l'aide du réseau EMEP;
- en Israël à l'aide du réseau du Ministère israélien de la protection environnementale;
- à Taïwan à l'aide du réseau de l'Administration taïwanaise de la protection environnementale.

IMPROVE est un réseau d'échantillonnage qui inclut plus de 200 stations abolies ou toujours en opération réparties dans la plupart des 50 états américains, dont une en Ontario. Le réseau mesure la concentration des PM₁₀ et des PM_{2.5} ainsi que celle de différentes espèces chimiques individuellement, soit les SO₄, les NO₃, le OC, le BC, l'Al, le Si, le Ti, le Ca, le Fe et le Cl. La reconstruction est ensuite appliquée pour obtenir la concentration des (NH₄)₂SO₄, des NH₄NO₃, des POM, de la PS et du SM. Le principal objectif d'IMPROVE est de surveiller la tendance à long terme de l'état de la qualité de l'air et de la visibilité, et donc n'échantillonne pas ces contaminants à une fréquence horaire. Les sites sont échantillonnés plusieurs fois au cours d'une période de 24 heures tous les trois jours, et les données, publiées sous forme de moyennes quotidiennes, sont disponibles publiquement dans la *Federal Land Manager Environmental Database* (<http://views.cira.colostate.edu/fed/>).

L'évaluation consistait à comparer la concentration des différentes espèces d'aérosols simulée par MERRAero à la surface à celle mesurée par IMPROVE aux endroits où les stations d'IMPROVE sont localisées et en opération à tout moment au cours de la période 2003–2013, soit à 176 endroits répartis dans les 48 états contigus et en Ontario (voir le Chap. 2, Fig. 2.1). Par étape, l'évaluation consistait à :

- Extraire la concentration horaire de toutes les espèces d'aérosols simulée par MERRAero aux endroits où les stations d'IMPROVE sont localisées;
- Calculer la moyenne quotidienne de la concentration des espèces

entre 0h et 23h en fonction de l'heure locale;

- Extraire les données quotidiennes de la concentration des mêmes espèces échantillonnées par IMPROVE;
- Comparer les concentrations simulées et observées lors des journées au cours desquels l'échantillonnage d'IMPROVE a eu lieu à l'aide d'indicateurs statistiques et d'éléments visuels, tels que des graphiques et des cartes.

Un contrôle de la qualité des données a été effectué en utilisant un algorithme de cohérence spatiale. Comme la concentration des contaminants à l'état de trace tend à avoir une distribution log-normale, le biais entre le logarithme de la concentration modélisée et le logarithme de la concentration observée ($B_{ln} = \ln(C_m) - \ln(C_o)$) a été calculé à toutes les stations à l'intérieur d'une région pour une journée spécifique. La moyenne et l'écart type de B_{ln} ont ensuite été calculés pour l'ensemble des stations et utilisés pour définir un intervalle de confiance qui justifie ~95% de la distribution normale : $\overline{B_{ln}} \pm 2\sigma_{B_{ln}}$. Toutes les paires de données qui ne satisfaisaient pas à cet intervalle ont été exclues de l'échantillon.

Plusieurs indicateurs statistiques ont été calculés pour quantifier la performance de MERRAero :

- la fraction moyenne : $\overline{F} = \overline{C_m} / \overline{C_o}$
- le biais moyen : $\overline{B} = \overline{C_m} - \overline{C_o}$
- l'écart type du biais;
- le biais moyen entre les concentrations log-transformées :

$$\overline{B_{ln}} = \overline{\ln(C_m)} - \overline{\ln(C_o)}$$

- l'écart type du biais entre les concentrations log-transformées;
- le R ;
- le R entre les concentrations log-transformées;
- le $FAC2$.

La \overline{F} quantifie proportionnellement la disparité entre les deux

concentrations tandis que le \bar{B} et son écart type quantifient l'écart brut entre les deux. Comme le R est un indicateur très répandu dans la littérature, il a été calculé pour évaluer MERRAero, mais le $FAC2$ demeure un indicateur plus fiable. Le \bar{B} , son écart type et le R ont aussi été calculés à partir des concentration log-transformées puisque les particules de trace ont tendance à épouser une distribution log-normale. En plus de ces indicateurs, la visualisation de l'évaluation a été réalisée à l'aide de nuages de points et de diagrammes à lignes qui comparent les moyennes annuelles et mensuelles.

Une démarche semblable a été utilisée pour l'évaluation en Europe avec le réseau EMEP. L'EMEP n'est cependant pas aussi complet qu'IMPROVE qui mesure toutes les espèces de PM systématiquement à toutes les stations au cours des mêmes journées. L'EMEP résulte d'une collaboration entre plusieurs pays européens qui partagent leurs données via cette base de données commune. Bien que des standards soient établis pour la publication des données (Tørseth *et al.*, 2012), la quantité des contributions varie grandement d'un pays à l'autre. Par exemple, l'Espagne fournit des données de la concentration de plusieurs espèces de PM tandis que la France ne fournit que la concentration des PM_{10} et des $PM_{2.5}$. Néanmoins, entre 2003 et 2014, la concentration des PM_{10} et des $PM_{2.5}$ est disponible à 52 endroits en Europe, la concentration des SO_4 à 32 endroits, la concentration du OC et du BC à 23 endroits, et la concentration du Cl à 24 endroits (voir le Chap. 3, Fig. 3.1). Les données sont disponibles sous forme de moyennes quotidiennes.

Les réseaux de surveillance en Israël et à Taïwan ne fournissent que des données de la concentration des $PM_{2.5}$. Bien que l'évaluation soit limitée à ce contaminant, les observations sont effectuées à une fréquence horaire, ce qui a permis de comparer un échantillon beaucoup plus grand. L'évaluation en Israël a été effectuée à l'aide de 11 stations entre 2003 et 2014 tandis que celle à Taïwan a été effectuée à l'aide de 13 stations entre 2005 et 2014 (voir le Chap. 4, Fig. 4.1).

1.3.3 Les incertitudes

Plusieurs incertitudes reliées à cette évaluation sont à noter :

- La résolution de MERRAero est de $0,5^\circ$ de latitude et $0,625^\circ$ de longitude. Si des stations d'échantillonnage sont situées à proximité de sources localisées de PM, celles-ci peuvent avoir biaisé l'évaluation. La grande majorité des stations utilisées dans cette évaluation sont situées en milieu rural, donc les sources localisées sont sans doute peu nombreuses. Certaines sont par contre localisées en milieu urbain;
- MERRAero utilise un inventaire d'émissions du SO_2 de 2005. Les émissions de SO_2 à l'échelle globale ont évolué depuis cette date, ce qui a compromis la simulation de la concentration des SO_4 après 2005;
- MERRAero ne simule pas la concentration des NO_3 . Ceci a donc constitué un manque pour la reconstruction des PM_{10} et des $\text{PM}_{2.5}$. Cependant, les NO_3 ne représentent qu'une faible proportion de la masse totale des PM_{10} et des $\text{PM}_{2.5}$, particulièrement en milieu rural;
- Peu de précisions quant aux procédures d'échantillonnage aux stations d'IMPROVE et de l'EMEP sont disponibles. Il n'y a pas d'information concernant la fréquence et les périodes d'échantillonnage au cours des périodes de 24 heures. Il n'y avait donc pas moyen de vérifier si les moyennes quotidiennes étaient véritablement représentatives de l'ensemble des journées spécifiques;
- Les méthodes d'échantillonnage des différentes espèces de PM ne sont pas exactes. Notamment, le niveau d'acidité des SO_4 dépend de la quantité du NH_4 disponible dans l'air pour neutraliser l'acide sulfurique formé à partir du SO_2 . Cependant, sans mesure ou simulation de la concentration du NH_4 , le niveau d'acidité demeure inconnu. La reconstruction a donc présumé que les SO_4 étaient tous sous forme de $(\text{NH}_4)_2\text{SO}_4$ complètement neutralisés, ce qui représente une limite maximale de la concentration réelle (Hand *et al.*, 2011, sect. 2.1.1);
- Les mesures du BC sont aussi sujettes à des biais importants. Les

méthodes courantes d'échantillonnage ont recourt à une variété de techniques d'évolution thermique pour mesurer la concentration totale des particules de carbone ($[TC] = [OC] + [BC]$) qui sont toutes raisonnablement fiables (Chow *et al.*, 1993). Là où les techniques diffèrent est la répartition du TC entre le OC et le BC. Comme la concentration du OC est beaucoup plus élevée que celle du BC, les différentes techniques peuvent reproduire des différences de concentration jusqu'à un facteur de 2 pour le BC (Chow *et al.*, 1993), tandis que l'impact est beaucoup moins important pour la concentration du OC;

- Comme les sources de PS sont nombreuses et sa composition est variée, sa concentration est estimée à partir d'une méthode générale qui additionne la concentration des oxydes des éléments qui se retrouvent généralement dans la PS, soit l'Al, le Si, le Ca, le Fe et le Ti. La concentration de chacun de ces éléments est multipliée par un coefficient qui représente la concentration de leur forme oxydée et tient compte des composés manquants. Malm et Hand (2007) estiment que la concentration de la PS mesurée par IMPROVE est sous-estimée d'environ 20% en moyenne;
- Finalement, la concentration du SM est estimée à partir de la concentration du Cl et la multiplie par 1,8. Les méthodes d'échantillonnage du Cl sont cependant biaisées en faveur d'une sous-estimation puisqu'une certaine quantité de Cl, qui n'est pas quantifiée par Hand *et al.* (2011, sect. 2.1.5), s'évapore au cours de la mesure.

1.3.4 L'application de MERRAero à l'étude de la pollution atmosphérique urbaine

Afin d'appliquer MERRAero à une étude sur la qualité de l'air urbain à l'échelle globale, sa simulation de l'AOD au-dessus de 200 villes parmi les

plus peuplées du monde, inspirées de la liste des plus grandes agglomérations de Brinkhoff (*City Population*, <http://www.citypopulation.de>), a été analysée entre 2003 et 2015. La population métropolitaine de chacune d'elles est d'au moins 2 millions d'habitants.

Une première analyse a été effectuée en calculant la moyenne de l'AOD au cours de la période de 13 ans au-dessus de chacune des villes en les regroupant par région géographique pour déterminer leur profil d'aérosols. Ensuite, une seconde analyse a été effectuée en calculant la moyenne de l'AOD par année, en calculant la régression linéaire annuelle au cours des 13 années et en effectuant un test *t* de Student pour évaluer la significativité de la pente. Ces analyses ont permis d'évaluer, d'une part, les conséquences qu'ont eues l'urbanisation et l'industrialisation sur la qualité de l'air urbain, et d'autre part, l'efficacité des réglementations à contrôler la pollution de l'air urbain, à l'échelle globale.

1.4 Structure de la thèse

Les Chap. 2, 3 et 4 détaillent les résultats et les particularités de l'évaluation de MERRAero dans les quatre régions du monde mentionnées précédemment : les É.-U. (Chap. 2), l'Europe (Chap. 3), Israël et Taïwan (Chap. 4). Le Chap. 5 constitue l'application de MERRAero aux villes les plus peuplées du monde et le Chap. 6 synthétise les résultats et les contributions de ce travail.

L'Annexe 1 présente les résultats d'une analyse statistique entre la fréquence de brume sèche et la concentration de contaminants atmosphériques effectuée dans les trois régions métropolitaines les plus peuplées du Québec : Montréal, Québec et Gatineau. Cette étude a permis d'identifier si la brume sèche est un indicateur simple mais fiable de mauvaise qualité de l'air afin d'être utilisé dans des régions dépourvues de surveillance. Et finalement, l'Annexe 2 est une étude sur le confort

thermique qui permet d'évaluer si un nouvel indice universel de confort, l'indice universel du climat thermique (*universal thermal climate index*, UTCI), peut être appliqué plus efficacement à des régions qui subissent des fluctuations importantes de température entre la saison chaude et froide, comme celle de Québec, comparativement à des indices traditionnels, tels que l'humidex et le facteur vent.

Références

Bloom, S.C., Takacs, L.L., da Silva, A.M. et Ledvina, D. (1996). Data assimilation using incremental analysis updates. *Mon. Weather Rev.* 124 : 1256–1271.

Buchard, V., da Silva, A.M., Colarco, P., Krotkov, N., Dickerson, R.R., Stehr, J.W., Mount, G., Spinei, E., Arkinson, H.L. et He, H. (2014). Evaluation of GEOS-5 sulfur dioxide simulations during the Frostburg, MD 2010 field campaign. *Atmos. Chem. Phys.* 14 : 1929–1941.

Buchard, V., da Silva, A.M., Colarco, P.R., Darmenov, A., Randles, C.A., Govindaraju, R., Torres, O., Campbell, J. et Spurr, R. (2015). Using the OMI aerosol index and absorption aerosol optical depth to evaluate the NASA MERRA Aerosol Reanalysis. *Atmos. Chem. Phys.* 15 : 5743–5760.

Buchard, V., da Silva, A.M., Randles, C.A., Colarco, P., Ferrare, R., Hair, J., Hostetler, C., Tackett, J. et Winker, D. (2016). Evaluation of the surface PM_{2.5} in Version 1 of the NASA MERRA Aerosol Reanalysis over the United States. *Atmos. Environ.* 125 : 100–111.

Bosanquet, C.H. et Pearson, J.L. (1936). The spread of smoke and gases from chimneys. *Trans. Farad. Soc.* 32 : 1249–1263.

Bullin, J.A. et Dukler, A.E. (1974). Stochastic modeling of turbulent diffusion with hybrid computer. *Environ. Sci. Technol.* 8 : 156–165.

Byun, D.W., Lacser, A., Yamartino, R. et Zannetti, P. (2003). *Eulerian dispersion models*. Dans : Zannetti, P. *Air quality modeling: theories, methodologies, computational techniques, and available databases and software—Volume I: Fundamentals*. EnviroComp Institute et Air & Waste Management Association, pp. 213–291.

Chang, J.C. et Hanna, S.R. (2004). Air quality model performance evaluation. *Meteorol. Atmos. Phys.* 87 : 167–196.

Charlson, R.J. (1969). Atmospheric visibility related to aerosol mass concentration. *Environ. Sci. Technol.* 3 : 913–918.

Chin, M., Rood, R.B., Lin, S.J., Müller, J.F. et Thompson, A.M. (2000). Atmospheric sulfur cycle simulated in the global model GOCART: model description and global properties. *J. Geophys. Res.* 105 : 24671–24687.

Chin, M., Ginoux, P., Kinne, S., Torres, O., Holben, B.N., Duncan, B.N., Martin, R.V., Logan, J.A., Higurashi, A. et Nakajima, T. (2002). Tropospheric aerosol optical thickness from the GOCART model and comparisons with satellite and sun photometer measurements. *J. Atmos. Sci.* 59 : 461–483.

Chow, J.C., Watson, J.G., Pritchett, L.C., Pierson, W.R., Frazier, C.A. et Purcell, R.G. (1993). The DRI thermal/optical reflectance carbon analysis

system: description, evaluation and application in U.S. air quality studies. *Atmos. Environ.* 27A : 1185–1201.

Chow, J.C., Lowenthal, D.H., Antony Chen, L.W., Wang, X. et Watson, J.G. (2015). Mass reconstruction methods for PM_{2.5}: a review. *Air Qual. Atmos. Health* 8 : 243–263.

Colarco, P., da Silva, A., Chin, M. et Diehl, T. (2010). Online simulations of global aerosol distributions in the NASA GEOS-4 model and comparisons to satellite and ground-based aerosol optical depth. *J. Geophys. Res.* 115 : D14207.

Darmenov, A.S. et da Silva, A. (2015). The Quick Fire Emissions Dataset (QFED): Documentation of versions 2.1, 2.2 and 2.4. *Technical Report Series on Global Modeling and Data Assimilation*, vol. 38. NASA/TM–2015–104606.

Deardorff, J.W. et Willis, G.E. (1982). Ground-level concentrations due to fumigation into an entraining mixed layer. *Atmos. Environ.* 16 : 1159–1170.

Delmas, R., Serça, D. et Jambertm C. (1997). Global inventory of NO_x sources. *Nutr. Cycl. Agroecosyst.* 48 : 51–60.

Denman, K.L., Brasseur, G., Chidthaisong, A., Ciais, P., Cox, P.M., Dickinson, R.E., Hauglustaine, D., Heinze, C., Holland, E., Jacob, D., Lohmann, U., Ramachandran, S., da Silva Dias, P.L., Wofsy, S.C. et Zhang, X. (2007). *Couplings between changes in the climate system and biogeochemistry*. Dans : Solomon, S., Qin, D., Manning, M., Chen, Z., Marquis, M., Averyt, K.B., Tignor, M. et Miller, H.L. *Climate change 2007: the physical science basis*. Cambridge University Press, Cambridge, pp. 499–587.

Forster, P., Ramaswamy, V., Artaxo, P., Berntsen, T., Betts, R., Fahey, D.W., Haywood, J., Lean, J., Lowe, D.C., Myhre, G., Nganga, J., Prinn, R., Raga, G., Schulz, M. et van Dorland, R. (2007). *Changes in atmospheric constituents and in radiative forcing*. Dans : Solomon, S., Qin, D., Manning, M., Chen, Z., Marquis, M., Averyt, K.B., Tignor, M. et Miller, H.L. *Climate change 2007: the physical science basis*. Cambridge University Press, Cambridge, pp. 129–234.

Gryning, S.E. et Lyck, E. (2002), *The Copenhagen tracer experiments: reporting of measurements*. Risø National Laboratory.

Hand, J.L. et al. (2011). *Spatial and seasonal patterns and temporal variability of haze and its constituents in the United States—Report V*. Cooperative Institute for Research in the Atmosphere et Colorado State University, ISSN 0737-5352-87.

Hand, J.L., Schichtel, B.A., Malm, W.C. et Pitchford, M.L. (2012). Particulate sulfate ion concentration and SO₂ emission trends in the United States from the early 1990s through 2010. *Atmos. Chem. Phys.* 12 : 10353–10365.

- Hand, J.L., Schichtel, B.A., Malm, W.C. et Pitchford, M. (2013). Widespread reductions in sulfate across the United States since the early 1990s. *AIP Conf. Proc.* 1527 : 495–498.
- Haywood, J. et Boucher, O. (2000). Estimates of the direct and indirect radiative forcing due to tropospheric aerosols: a review. *Rev. Geophys.* 38 : 513–543.
- Holben, B.N., Eck, T.F. Slutsker, I., Tanré, D., Buis, J.P., Setzer, A., Vermote, E., Reagan, J.A., Kaufman, Y.J., Nakajima, T., Lavenue, F., Jankowiak, I. et Smirnov, A. (1998). AERONET—A federated instrument network and data archive for aerosol characterization. *Remote Sens. Environ.* 66 : 1–16.
- Jackson, L. (2014). *Dirty old London: the Victorian fight against filth*. Yale University Press, New Haven.
- Johnson, W.B., Ludwig, F.L., Dabbert, W.F. et Aallen, R.J. (1973). An urban diffusion simulation model for carbon monoxide. *J. Air Pollut. Control Assoc.* 23 : 490–498.
- Kahn, R.A., Gaitley, B.J., Martonchik, J.V., Diner, D.J., Crean, K.A. et Holben, B. (2005). Multiangle Imaging Spectroradiometer (MISR) global aerosol optical depth validation based on 2 years of coincident Aerosol Robotic Network (AERONET) observations. *J. Geophys. Res.* 110 : D10S04.
- Lohmann, U. et Feichter, J. (2005). Global indirect aerosol effects: a review. *Atmos. Chem. Phys.* 5 : 715–737.
- Lu, Z., Zhang, Q. et Streets, D.G. (2011). Sulfur dioxide and primary carbonaceous aerosol emissions in China and India, 1996–2010. *Atmos. Chem. Phys.* 11 : 9839–9864.
- Malm, W.C., Sister, J.F., Huffman, D., Eldred, R.A. et Cahill, T.A. (1994). Spatial and seasonal trends in particle concentration and optical extinction in the United States. *J. Geophys. Res.* 99 : 1347–1370.
- Malm, W.C. et Hand, J.L. (2007). An examination of the physical and optical properties of aerosols collected in the IMPROVE program. *Atmos. Environ.* 41 : 3407–3427.
- Molina, L.T. et Molina, M.J. (2004a). Improving air quality in megacities: Mexico City case study. *Ann. N.Y. Acad. Sci.* 1023 : 142–158.
- Molina, M.J. et Molina, L.T. (2004b). Megacities and atmospheric pollution. *J. Air Waste Manage. Assoc.* 54 : 644–680.
- Nowottnick, E.P., Colarco, P.R., Welton, E.J. et da Silva, A. (2015). Use of the CALIOP vertical feature mask for evaluating global aerosol models. *Atmos. Meas. Tech.* 8 : 3647–3669.
- Pöschl, U. (2005). Atmospheric aerosols: composition, transformation,

climate and health effects. *Angew. Chem. Int. Edit.* 44 : 7520–7540.

Remer, L.A., Kaufman, Y.J., Tanré, D., Mattoo, S., Chu, D.A., Martins, J.V., Li, R.R., Ichoku, C., Levy, R.C., Kleidman, R.G., Eck, T.F., Vermote, E. et Holben, B.N. (2005). The MODIS aerosol algorithm, products, and validation. *J. Atmos. Sci.* 62 : 947–973.

Reynolds, S.D., Roth, P.M. et Seinfeld, J.H. (1973). Mathematical modeling of photochemical air pollution—I: formulation of the model. *Atmos. Environ.* 7 : 1033–1061.

Rienecker, M.M., Suarez, M.J., Todling, R., Bacmeister, J., Takacs, L., Liu, H.C., Sienkiewick, M., Koster, R.D., Gelaro, R., Stajner, I. et Nielsen, J.E. (2008). The GEOS-5 Data Assimilation System—Documentation of Versions 5.0.1, 5.1.0, and 5.2.0. *Technical Report Series on Global Modeling and Data Assimilation*, vol. 27. NASA/TM–2008–104606.

Rienecker, M.M., Suarez, M.J., Gelaro, R., Todling, R., Bacmeister, J., Liu, E., Bosilovich, M.G., Schubert, S.D., Takacs, L., Kim, G.K., Bloom, S., Chen, J., Collins, D., Conaty, A., da Silva, A., Gu, W., Joiner, J., Koster, R.D., Lucchesi, R., Molod, A., Owens, T., Pawson, S., Pegion, P., Redder, C.R., Reichle, R., Robertson, F.R., Ruddick, A.G., Sienkiewick, M. et Woollen, J. (2011). MERRA: NASA's Modern-Era Retrospective Analysis for Research and Application. *J. Clim.* 24 : 3624–3648.

Rodhe, H. (1975). Some aspects of the use of air trajectories for the computation of large-scale dispersion and fallout patterns. *Adv. Geophys.* 18B : 95–109.

Rouse, H. (1951). Air-tunnel studies of diffusion in urban areas. *Meteorol. Monogr.* 1 : 39–41.

Tager, I.B. (2013). *Health effects of aerosols: mechanisms and epidemiology*. Dans : Ruzer, L.S. et Harley, N.H. *Aerosols handbook: measurement, dosimetry, and health effects*, 2^e éd. CRC Press, Boca Raton, pp. 565–636.

Tørseth, K., Aas, W., Breivik, K., Fjæraa, A.M., Fiebig, M., Hjellbrekke, A.G., Lund Myhre, C., Solberg, S. et Yttri, K.E. (2012). Introduction to the European Monitoring and Evaluation Programme (EMEP) and observed atmospheric composition change during 1972–2009. *Atmos. Chem. Phys.* 12 : 5447–5481.

Turpin, B.J. et Lim, H.J. (2001). Species contribution to PM_{2.5} mass concentration: revisiting common assumptions for estimating organic mass. *Aerosol Sci. Technol.* 35 : 602–610.

Vestreng, V., Myhre, G., Fagerli, H., Reis, S. et Tarrason, L. (2007). Twenty-five years of continuous sulfur dioxide emission reduction in Europe. *Atmos. Chem. Phys.* 7 : 3663–3681.

- Wakamatsu, S., Morikawa, T. et Ito, A. (2013). Air pollution trends in Japan between 1970 and 2012 and impact of urban air pollution countermeasures. *Asian J. Atmos. Environ.* 7 : 177–190.
- Willis, G.E. et Deardorff, J.W. (1974). A laboratory model of the unstable planetary boundary layer. *J. Atmos. Sci.* 31 : 1297–1307.
- Willis, G.E. et Deardorff, J.W. (1976). A laboratory model of diffusion into the convective planetary boundary layer. *Q. J. R. Meteorol. Soc.* 102 : 427–445.
- Willis, G.E. et Deardorff, J.W. (1978). A laboratory study of dispersion from an elevated source within a modeled convective planetary boundary layer. *Atmos. Environ.* 12 : 1305–1311.
- Willis, G.E. et Deardorff, J.W. (1981). A laboratory study of dispersion from a source in the middle of the convective mixed layer. *Atmos. Environ.* 15 : 109–117.
- Willmott, C.J. (1982). Some comments on the evaluation of model performance. *Bull. Am. Meteorol. Soc.* 63 : 1309–1313.
- Winker, D.M., Vaughan, M.A., Omar, A., Hu, Y., Powell, K.A., Liu, Z., Hunt, W.H. et Young, S.A. (2009). Overview of the CALIPSO mission and CALIOP data processing algorithms. *J. Atmos. Ocean. Technol.* 26 : 2310–2323.
- Winker, D.M., Pelon, J., Coakley, J.A., Ackerman, S.A., Charlson, R.J., Colarco, P.R., Flamant, P., Fu, Q., Hoff, R.M., Kittaka, C., Kubar, T.L., Le Treut, H., McCormick, M.P., Mégie, G., Poole, L., Powell, K., Treppe, C., Vaughan, M.A. et Wielicki, B.A. (2010). The CALIPSO mission: a global 3D view of aerosols and clouds. *Bull. Am. Meteorol. Soc.* 91 : 1211–1229.
- Wu, W.S., Purser, R.J. et Parrish, D.F. (2002). Three-dimensional variational analysis with spatially inhomogeneous covariances. *Mon. Weather Rev.* 130 : 2905–2916.

2 Evaluation of PM chemical speciation simulated by NASA's MERRA Aerosol Reanalysis with the IMPROVE network in the United States

Abstract

This paper evaluates the Aerosol Reanalysis of the Modern-Era Retrospective Analysis for Research and Application's (MERRAero) ability to simulate the concentration of particulate matter (PM) and its speciation over the contiguous United States at the surface. Measurement data from the Interagency Monitoring of Protected Visual Environments (IMPROVE) network were used. MERRAero reproduced well the concentration of PM_{10} and $PM_{2.5}$ at both rural and urban locations. The concentration of sulfate particles was also well simulated, but inconsistencies surfaced with respect to the concentrations of carbon particles and their sources: they were overestimated in summer, especially in the Western U.S., caused by a misrepresentation of wildfire emissions, and underestimated in winter at urban locations, caused by the lack of residential wood burning emissions. The concentration of fine dust is overall overestimated, especially in spring and summer when the U.S. is most impacted by long distance transport of sand dust originating from distant deserts. Fine sea salt concentration is consistently overestimated by MERRAero but contributes little to total $PM_{2.5}$ concentration.

Résumé

Cet article évalue la capacité de MERRAero, soit la Modern-Era Retrospective Analysis for Research and Application Aerosol Reanalysis, de simuler la concentration des matières particulaires (PM) et de leur composition chimique à la surface des États-Unis contigus à l'aide de données d'observations mesurées par le réseau Interagency Monitoring of Protected Visual Environments (IMPROVE). MERRAero reproduit adéquatement la concentration des PM_{10} , des $PM_{2.5}$ et des particules de sulfate dans les régions rurales et urbaines. Des incohérences sont survenues par rapport à la concentration des particules de carbone et de leurs sources; elle est surestimée en été, particulièrement dans l'Ouest des É.-U., en raison d'une mauvaise représentation des émissions provenant des feux de forêt, et sous-estimée en hiver en région urbaine due aux sources résidentielles de carbone qui ne sont pas considérées par MERRAero. La concentration des particules de poussière est généralement surestimée, particulièrement au printemps et

en été lorsque les É.-U. sont le plus affectés par le transport de sable provenant de déserts lointains. La concentration des particules de sel de mer est constamment surestimée par MERRAero mais contribue peu à la concentration totale des PM_{2.5}.

2.1 Introduction

Particulate matter (PM) is an airborne pollutant hazardous to human health that is linked to cardiovascular, respiratory and allergic diseases (Pöschl, 2005; Tager, 2013). In high enough concentration, it can also significantly reduce visibility (Charlson, 1969). Such events are usually associated with haze, smog or dust storms. The seriousness of these impacts depends on the chemical composition and size of PM. PM does indeed originate from a variety of sources and contain different chemical particles.

Generally, all developed countries maintain at least one surveillance network of air quality at the surface. The goals of these networks vary, but their primary purpose is to assure short and long term fulfillment of environmental standards. Relatively speaking, mass concentration measurements of PM_{2.5} (PM with diameter $\leq 2.5 \mu\text{m}$) at short (hourly) frequencies are widespread in developed countries. However, these networks typically concentrate their monitoring stations in urban areas where air pollution problems are typically more frequent. This leaves large geographical gaps which are left unmonitored, notably in rural areas. Many underdeveloped countries (e.g., South American, African and Middle Eastern countries) and emerging economies (e.g., India and China) have unreliable, scarce or no air quality monitoring at all, even though air pollution is increasingly becoming a source of concern in those countries. Furthermore, very few networks distinguish between the different chemical species that compose PM_{2.5}.

Remote sensing and modeling are innovative tools used to fill in those voids. Such a tool is NASA's 5th version of the Goddard Earth Observing

System (GEOS-5), a data assimilation system which includes different components such as a general circulation model, atmospheric composition, terrestrial and oceanic surface properties, and an aerosol component (Colarco *et al.*, 2010). The aerosol component is inspired by the Goddard Chemistry, Aerosol, Radiation and Transport (GOCART) model (Chin *et al.*, 2002) which simulates the sources, sinks, transport and concentration of five aerosol species: sulfate (SO₄), organic carbon (OC), black carbon (BC), mineral dust (DS) and sea salt (SS) particles. DS and SS emissions are a function of surface properties and wind speed at the surface, and their respective concentrations are classified in different diameter bins. Sources of other species are simulated from emission inventories, including their precursors. Sulfur dioxide (SO₂, the precursor of SO₄) anthropogenic emissions are input from the Emission Database for Global Atmospheric Research (EDGAR) version 4.1 inventory from 2005 and biomass burning emissions are input from the NASA Quick Fire Emission Dataset (QFED) version 2.1 (Buchard *et al.*, 2015a). Also, GEOS-5 includes an atmospheric data assimilation system based on the Grid-point Statistical Interpolation algorithm (Wu *et al.*, 2002) which assimilates corrected aerosol optical depth (AOD) data monitored by the Moderate Resolution Imaging Spectroradiometers (MODIS) on board the Terra and Aqua satellites.

Many years ago, NASA introduced the Modern-Era Retrospective Analysis for Research and Application (MERRA, Rienecker *et al.*, 2011), a reanalysis tool whose main goal is to organize NASA's Earth observation systems since the beginning of the satellite era within a climatic context. With the ultimate goal of building an integrated analysis of the Earth system, many reanalyses are produced in parallel with other environmental components such as the composition of the atmosphere, the oceans and the surface. The MERRA Aerosol Reanalysis (MERRAero) assimilates GEOS-5 and MODIS data, and reproduces a global database of the AOD and concentration of five aerosol species with a resolution of 0.5° latitude by

0.625° longitude and 72 vertical levels (from the surface to 80 km), since 2002 (Buchard *et al.*, 2015a).

MERRAero is an innovative tool to study air pollution at the global scale, particularly with its ability to distinguish the chemical speciation of PM. MERRAero is currently being evaluated: Buchard *et al.* (2014) evaluated concentrations of SO₂ and SO₄ simulated by GEOS-5 in the United States, Buchard *et al.* (2015) evaluated MERRAero's assimilation of AOD with many remote sensing instruments in Africa, South America, Central and Eastern Asia, and Buchard *et al.* (2016) used a variety of remote sensing and *in situ* networks of observations to further evaluate MERRAero in the U.S. The goal of this paper is to evaluate MERRAero's chemical speciation of PM at the surface against a broad surveillance network measuring the same chemical species, the Interagency Monitoring of Protected Visual Environments (IMPROVE, Malm *et al.*, 1994) in the U.S.

2.2 Methods

MERRAero simulates the concentration of five PM species every hour: SO₄, OC, BC, DS and SS. From these, it is possible to estimate the total concentration of PM₁₀ as follows:

$$(2.1) \quad [\text{PM}_{10}] = 1.375 \times [\text{SO}_4] + 1.4 \times [\text{OC}] + [\text{BC}] + [\text{DS}] + [\text{SS}]$$

Brackets denote concentration. Eq. 2.1 assumes that all SO₄ is neutralized by ammonium (NH₄) in the form of ammonium sulfate ((NH₄)₂SO₄), which is a common assumption in mass reconstructions of PM (Chow *et al.*, 2015). [SO₄] is therefore multiplied by 1.375. [OC] is multiplied by 1.4 to account for other organic compounds found in particulate organic matter (POM). Furthermore, since MERRAero classifies different sizes of [DS] and [SS], it is also possible to estimate [PM_{2.5}] as follows:

$$(2.2) \quad [\text{PM}_{2.5}] = 1.375 \times [\text{SO}_4] + 1.4 \times [\text{OC}] + [\text{BC}] + [\text{DS}_{2.5}] + [\text{SS}_{2.5}]$$

Eqs. 2.1 and 2.2 assume that all SO₄, OC and BC are in the form of PM_{2.5}. Both of them lack the concentration of nitrate (NO₃) particles which can be substantial in urban environments (e.g., Kundu and Stone, 2014) but has also been dropped from the reconstruction when it was lacking or unreliable (e.g., Malm *et al.*, 1994).

IMPROVE is a surveillance network including more than 200 monitoring stations either discontinued or still in operation spread throughout most of the 50 U.S. states, most of which are located in rural areas. The network measures [PM₁₀] and [PM_{2.5}] independently, as well as [SO₄], [NO₃], [OC] and [BC]. Additionally, the network measures the concentrations of aluminium, silicon, calcium, iron and titanium to estimate the total concentration of fine soil particles (comparable to DS_{2.5}), and the concentration of chloride ions to estimate [SS_{2.5}]. IMPROVE's main objective is to monitor the long term trend of air quality and visibility in the U.S. and therefore only samples these pollutants a number of times over a 24-hour period every third day. Measurement data are publically available in the Federal Land Manager Environmental Database (<http://views.cira.colostate.edu/fed/>) in the form of daily averages.

Hourly MERRAero data are averaged on a daily basis and paired at 163 rural and 14 urban locations where IMPROVE sampling is available within the continental U.S. between 2003 and 2013 (Fig. 2.1). A spatial consistency algorithm is applied to assure reliability of the observed and simulated data which goes as follows: since trace concentrations are usually lognormally distributed, the bias between log-simulated concentration and log-observed concentrations ($B_{log} = \ln(C_s) - \ln(C_o)$; C_s : simulated concentration, C_o : observed concentration) is calculated at all locations within a geographical area on a given day; the average and standard deviation of B_{log} are calculated and used to define a reliability bracket which justifies ~95% of the normal distribution: $\overline{B_{log}} \pm 2\sigma_{B_{log}}$; all data pairs that fall outside this bracket are excluded.

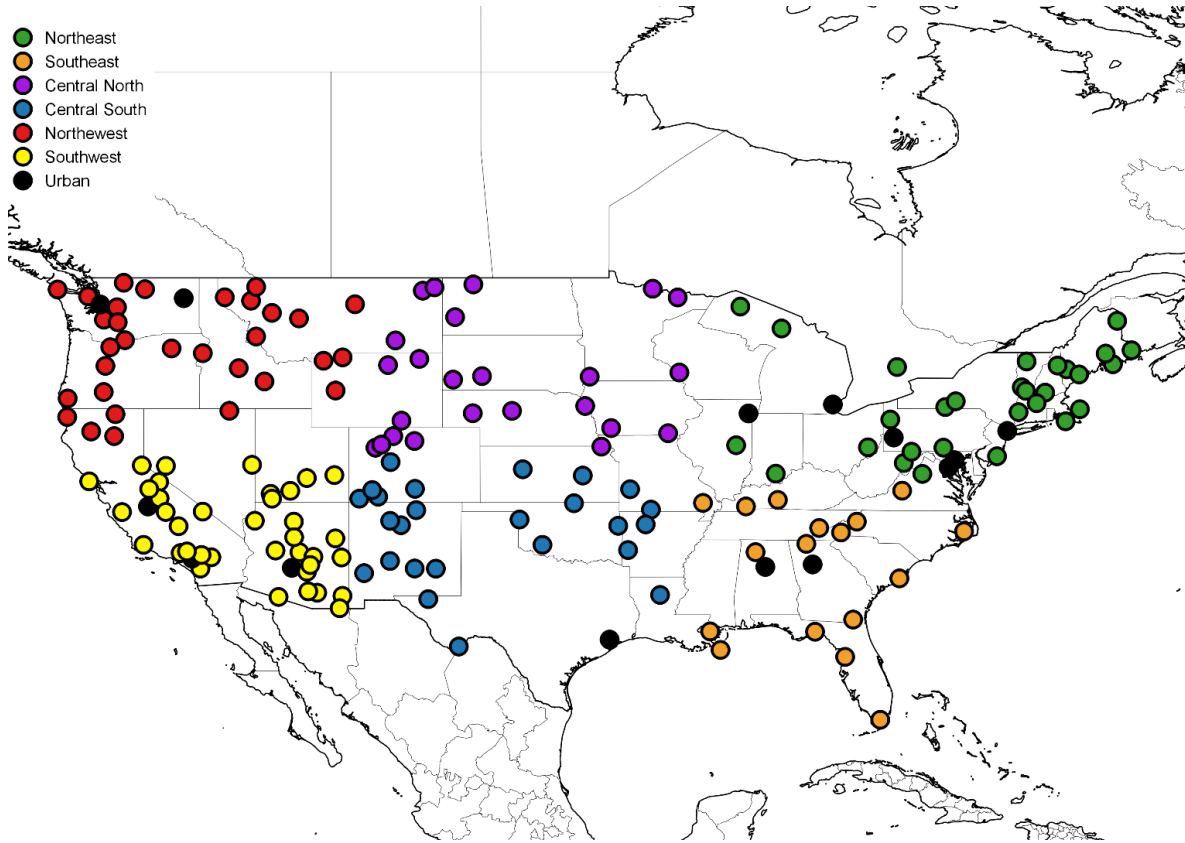


Fig. 2.1: Locations of IMPROVE stations classified by regions.

Many performance statistics are calculated to quantify MERRAero's accuracy: the mean fraction $\bar{F} = \bar{C}_s / \bar{C}_o$, the mean bias $\bar{B} = \bar{C}_s - \bar{C}_o$, the standard deviation of the bias ($SD-B$) and the correlation coefficient (R). Given the lognormally distribution of trace concentrations, it is also relevant to compute log-transformed statistics: $\overline{B_{log}} = \overline{\log(C_s)} - \overline{\log(C_o)}$, $SD-B_{log}$ and R_{log} . \bar{F} , \bar{B} and $\overline{B_{log}}$ can be misleading indices due to simplification of errors, which is why they need to be interpreted alongside $SD-B$ and $SD-B_{log}$. Willmott (1982) discouraged the use of R to evaluate the performance of a model since R is not a direct comparison between simulated and observed data; large differences between C_s and C_o can reproduce a high R , just as a good agreement between C_s and C_o can reproduce a low or even negative R . Chang and Hanna (2004) recommended using the proportion of simulated data which falls within a factor of 2 of observed data ($FAC2$, i.e. proportion of the data which satisfies $0.5 \leq C_o / C_s \leq 2.0$) as a rigorous index to

evaluate air quality models since this index is not disproportionately sensitive to extreme values and is unaffected by simplification of errors. Interpreting the numerical results is obviously subjective but Chang and Hanna (2004) considered a model’s performance to be reasonably good if $FAC2 \geq 0.5$.

2.3 Results and discussion

2.3.1 Ensemble evaluation

Performance statistics for the ensemble of the 163 rural stations are show in Tab. 2.1. Despite the fact that MERRAero doesn’t simulate NO_3 , it overestimates $[PM_{10}]$ by a factor of 1.34, which represents an additional $3.3 \mu\text{g}/\text{m}^3$ on average. $[PM_{2.5}]$ is overestimated by a factor of 1.38 ($1.9 \mu\text{g}/\text{m}^3$). There is some scatter within the data as seen from high $SD-B$ and moderate R values, however, $SD-B$ values tend to be disproportionately affected by extreme data pairs. For instance, if pairs of data that fall outside a factor of 10 between observed and simulated concentrations are excluded from the samples, which represent 1.3% of the PM_{10} and 0.7% of $PM_{2.5}$ samples, B and $SD-B$ are reduced to $3.0 \mu\text{g}/\text{m}^3$ and $11.6 \mu\text{g}/\text{m}^3$ for PM_{10} , and to $1.8 \mu\text{g}/\text{m}^3$ and $5.4 \mu\text{g}/\text{m}^3$ for $PM_{2.5}$, respectively. Nevertheless, the log-transformed data reproduce a good agreement and over 60% of simulated concentrations fall within a factor of 2 of observed concentrations ($FAC2 \geq 0.6$).

Tab. 2.1: Performance statistics for the ensemble of the 163 rural stations. AOC stands for “average observed concentration.”

	PM_{10}	$PM_{2.5}$	$(NH_4)_2SO_4$	OC	BC	$DS_{2.5}$	$SS_{2.5}$
n	176,371	177,179	179,525	176,365	175,645	176,873	180,069
AOC ($\mu\text{g}/\text{m}^3$)	9.5	5.0	1.9	1.0	0.2	0.6	0.1
\bar{F}	1.34	1.38	1.10	1.87	1.74	1.94	7.81
\bar{B} ($\mu\text{g}/\text{m}^3$)	3.3	1.9	0.2	0.9	0.1	0.6	0.7
$SD-B$ ($\mu\text{g}/\text{m}^3$)	12.7	6.7	1.7	5.1	0.4	1.4	1.4
\bar{B}_{log}	0.34	0.43	0.35	0.46	0.66	0.78	3.76
$SD-B_{log}$	0.79	0.63	0.71	0.77	0.80	0.99	2.46
R	0.42	0.52	0.71	0.55	0.52	0.57	0.59
R_{log}	0.56	0.70	0.73	0.69	0.62	0.59	0.46
FAC2	0.61	0.67	0.67	0.58	0.53	0.39	0.08

Before describing the performance results for the chemical speciation, it is important to mention that links can be made between MERRAero's ability to simulate the concentration of a given species to its ability to simulate total [PM₁₀] and [PM_{2.5}], but the performance statistics in Tab. 2.1 are not directly comparable between a given species and total PM due to different sample sizes and different measurement techniques. MERRAero slightly overestimates [SO₄] on average but the agreement is generally good overall. MERRAero overestimates [OC] by a factor of 1.87 (0.9 µg/m³) with important scatter in the data. OC appears to be the species most responsible for the overestimation of [PM_{2.5}] and scatter. [BC] is also overestimated by a factor of 1.74, but its concentration is generally so low (0.2 µg/m³ on average) that \bar{B} contributes very little to the overestimation of [PM_{2.5}] overall. DS_{2.5} and SS_{2.5} contribute little to PM_{2.5}, but MERRAero's overestimation of the concentrations of both these species by important factors (especially that of SS_{2.5}) results in non-negligible biases which together might contribute significantly to its overestimation of [PM_{2.5}]. *FAC2* values for these two species are also quite low.

2.3.2 Evaluation of the annual and seasonal fluctuations

Fig. 2.2 compares annual and monthly averaged [PM₁₀], [PM_{2.5}] and all species between MERRAero and IMPROVE. MERRAero overestimates [PM₁₀] and [PM_{2.5}] every year of the study period but the bias is particularly important during the spring and summer. Nevertheless, MERRAero simulates well the seasonal fluctuation despite the overestimation. The agreement for SO₄ is very good between 2003 and 2008 but diminishes afterward. This is the likely result of using a constant SO₂ emissions inventory of 2005 which isn't representative of real emissions since the end of the last decade in the U.S. Indeed, a transition from coal to natural gas for energy production since the 1990s resulted in a consistent decrease of

SO₂ emissions which is still ongoing today (de Gouw *et al.*, 2014). The simulation of the seasonal fluctuation is overall very good.

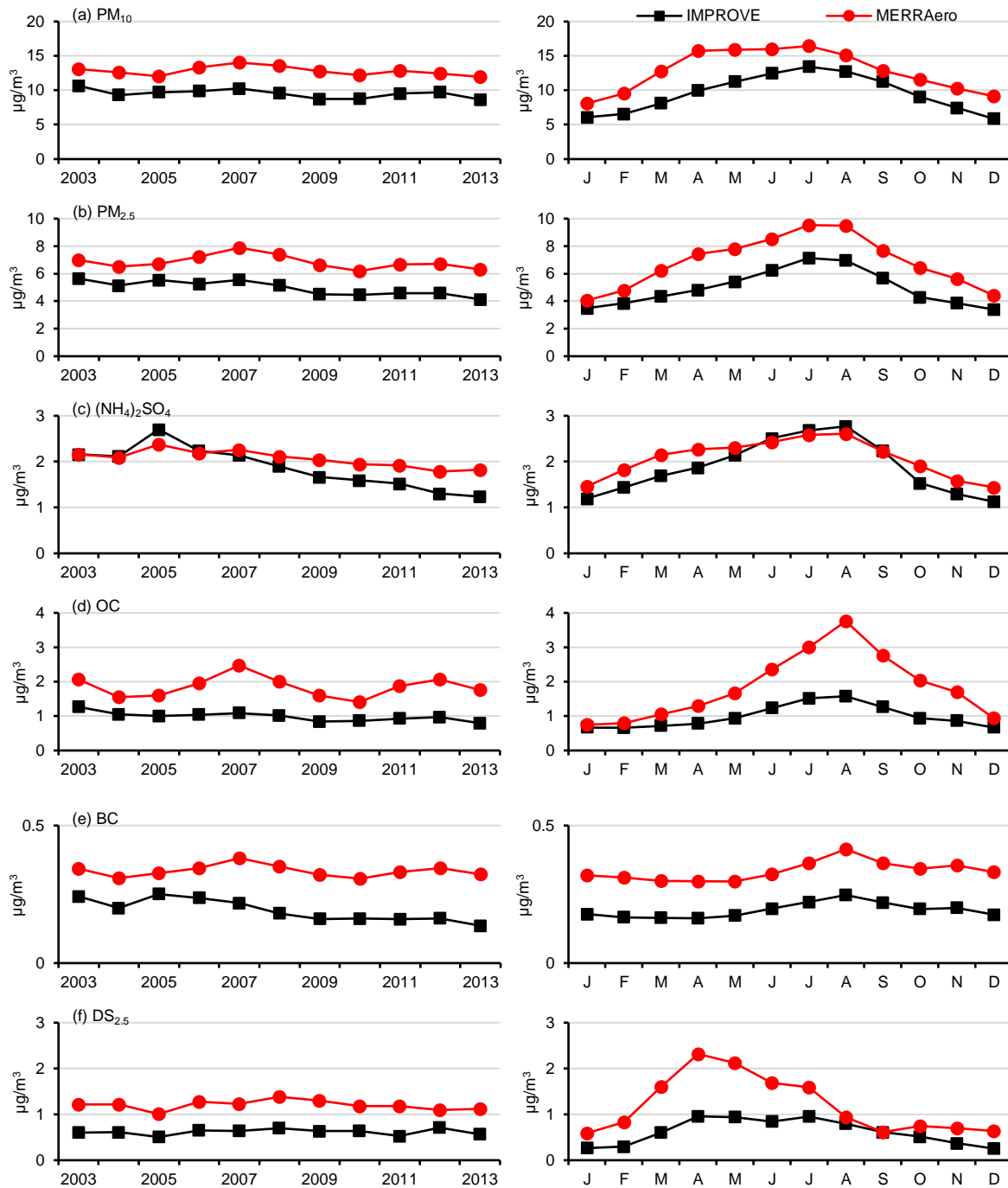


Fig. 2.2: Annual (left) and monthly (right) averages of (a) PM₁₀, (b) PM_{2.5}, (c) (NH₄)₂SO₄, (d) OC, (e) BC, (f) DS_{2.5} and (g) SS_{2.5} concentrations measured by IMPROVE and simulated by MERRAero for the ensemble of the 163 rural stations.

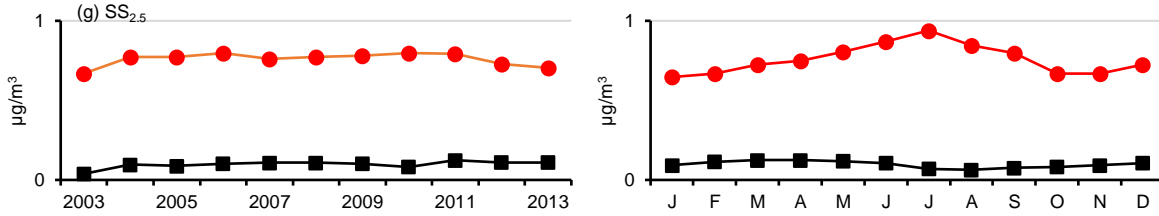


Fig. 2.2 (continued)

MERRAero's overestimation of [OC] is particularly noticeable in the summer which corresponds to the wildfire season. The Western U.S. is indeed a propitious region for recurring wildfires. Fig. 2.3 compares MERRAero's performance between a region where large wildfires seldom occur (northeast) and a region where they are recurrent (northwest) (see Fig. 2.1 for a definition of the regions). The northwest experiences a strong increase in [OC] between June and October which is captured but exaggerated by MERRAero. MERRAero estimated well [OC] the rest of the year in the northwest and generally well all year in the northeast. This suggests that MERRAero simulates well the carbon emissions from anthropogenic sources but exaggerates those from biomass burning. [BC] is also overestimated but in a more consistent fashion throughout the years and the seasons, but as mentioned previously, BC contributes little to total PM_{2.5}.

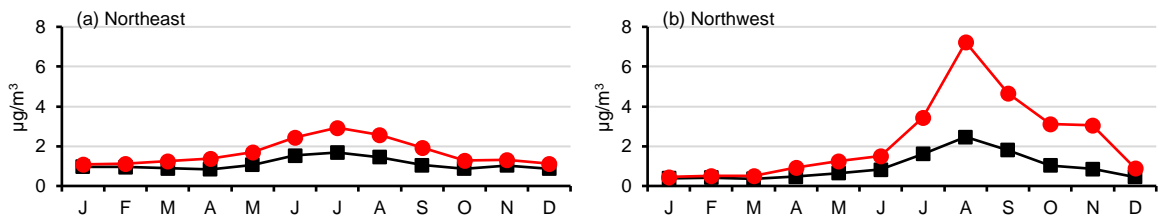


Fig. 2.3: Monthly averages of OC concentrations measured by IMPROVE and simulated by MERRAero in (a) the northeast and (b) the northwest.

MERRAero overestimates [DS_{2.5}], particularly during the spring and early summer. Some regions in the U.S. are influenced by important sources of DS on a seasonal basis, such as the arid region of the south and southwest (Stout, 2001), with an additional contribution from Eastern Asian deserts (Creamean *et al.*, 2014). Long distance transport of DS originating

from the Sahara desert also impacts the southeast in summer (Prospero, 1999). The seasonal fluctuation of $[DS_{2.5}]$ is well captured by MERRAero but periods of higher concentrations are exaggerated (Fig. 2.4). It is worth mentioning that measurements of soil particles by IMPROVE are biased toward a 20% underestimation on average (Malm and Hand, 2007). A 20% increase in soil concentration would undoubtedly improve the evaluation but would still be insufficient to close the gap between simulated and observed data.

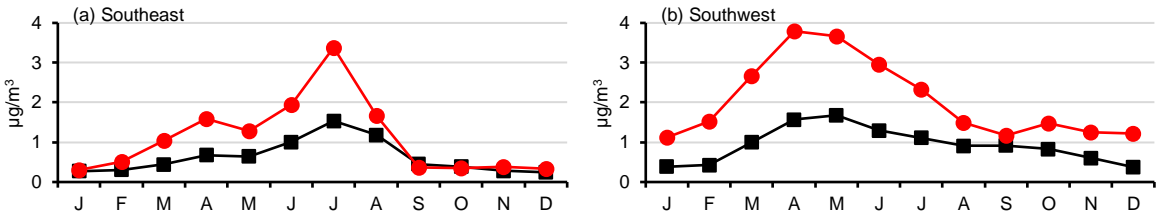


Fig. 2.4: Monthly averages of $DS_{2.5}$ concentrations measured by IMPROVE and simulated by MERRAero in (a) the southeast and (b) the southwest.

$[SS_{2.5}]$ is strongly and consistently overestimated by MERRAero, however, chloride measurements by IMPROVE are also biased toward an underestimation (Hand *et al.*, 2011, sect. 2.1.5). Observed $[SS_{2.5}]$ represents ~2% of $[PM_{2.5}]$ and only impacts coastal regions significantly. Despite simulating less than $1 \mu\text{g}/\text{m}^3$ of $SS_{2.5}$ on average, its overestimation by MERRAero can contribute to its overestimation of $[PM_{2.5}]$. Another comparison is performed between observed and simulated $[PM_{2.5}]$ by removing simulated $[SS_{2.5}]$ from $[PM_{2.5}]$ (Tab. 2.2). Almost all performance statistics has slightly yet visibly been improved.

Tab. 2.2: Performance statistics for the ensemble of the 163 rural stations.

	$PM_{2.5}$ (without $SS_{2.5}$)	$PM_{2.5}$ (without NH_4NO_3)	$PM_{2.5}$ (without $SS_{2.5}$ and NH_4NO_3)
n	176,973	176,158	175,983
\bar{F}	1.23	1.55	1.38
\bar{B} ($\mu\text{g}/\text{m}^3$)	1.1	2.4	1.7
SD-B ($\mu\text{g}/\text{m}^3$)	6.5	6.6	6.4
\bar{B}_{log}	0.30	0.56	0.43
SD-B _{log}	0.63	0.62	0.63
R	0.51	0.54	0.53
R _{log}	0.70	0.71	0.71
FAC2	0.71	0.61	0.67

2.3.3 Evaluation in urban environments

Evaluating MERRAero’s performance in urban environments is potentially problematic since urban sources of PM are plentiful with varying concentrations within short distances. Although PM sources from the downtown core of cities are taken into account by MERRAero, they tend to get diluted in its relatively coarse resolution, much like a single urban monitoring station is usually not representative of a city’s PM load as a whole. IMPROVE stations are located in 14 highly populated metropolitan areas: Atlanta, Baltimore, Birmingham, Chicago, Detroit, Fresno, Houston, Los Angeles, New York City, Phoenix, Pittsburgh, Seattle, Spokane and Washington (Fig. 2.1). These stations are generally located in suburbs and therefore are not representative of the downtown core of these cities. MERRAero’s performance is in many regards superior in the ensemble of these 14 cities (Tab. 2.3) compared to the ensemble of 163 rural locations (Tab. 2.1). Despite a lot of scatter in the data (reflected by high *SD-B* and low *R* values), the average simulated [PM_{2.5}] and [SO₄] are very close to average observed values. The *FAC2* is above 70% for both of these species. [PM₁₀], [OC], [BC] and [DS_{2.5}] are reasonably well simulated, but [SS_{2.5}] remains highly overestimated.

Tab. 2.3: Performance statistics for the ensemble of the 14 urban stations. AOC stands for “average observed concentration.”

	PM ₁₀	PM _{2.5}	(NH ₄) ₂ SO ₄	OC	BC	DS _{2.5}	SS _{2.5}
n	7,675	7,887	8,060	9,978	9,978	7,887	8,040
AOC (µg/m ³)	22.8	11.2	3.5	2.4	1.0	1.3	0.2
\bar{F}	0.85	0.96	0.95	1.18	0.75	1.19	4.32
\bar{B} (µg/m ³)	-3.4	-0.5	-0.2	0.4	-0.2	0.2	0.8
SD-B (µg/m ³)	20.0	8.5	2.6	3.2	0.8	2.5	1.5
\bar{B}_{log}	-0.18	0.01	0.14	0.12	-0.17	-0.13	1.94
SD-B _{log}	0.74	0.64	0.63	0.76	0.78	1.05	2.14
R	0.19	0.32	0.69	0.28	0.25	0.44	0.32
R _{log}	0.29	0.39	0.71	0.38	0.37	0.50	0.21
FAC2	0.66	0.75	0.73	0.67	0.64	0.50	0.19

MERRAero captures well the annual variation of [PM₁₀], [PM_{2.5}], [SO₄], [OC] and [BC] (Fig. 2.5). Seasonal fluctuations, however, reveal interesting features. Contrary to rural locations, MERRAero largely underestimates [PM₁₀] and [PM_{2.5}] in winter. Observed monthly averages of [PM_{2.5}] fluctuate

quite a lot: the summertime maximum is caused by SO_4 which is well reproduced by MERRAero; the wintertime maximum is caused by a combination of OC and BC, which are not at all reproduced by MERRAero. This wintertime surge in urban carbon load is the likely result of residential wood burning which is an important source of urban pollution in winter (Cooper, 1980; Sexton *et al.*, 1984; Hellén *et al.*, 2008; Pandis *et al.*, 2016). This anthropogenic source of carbon is not resolved by MERRAero.

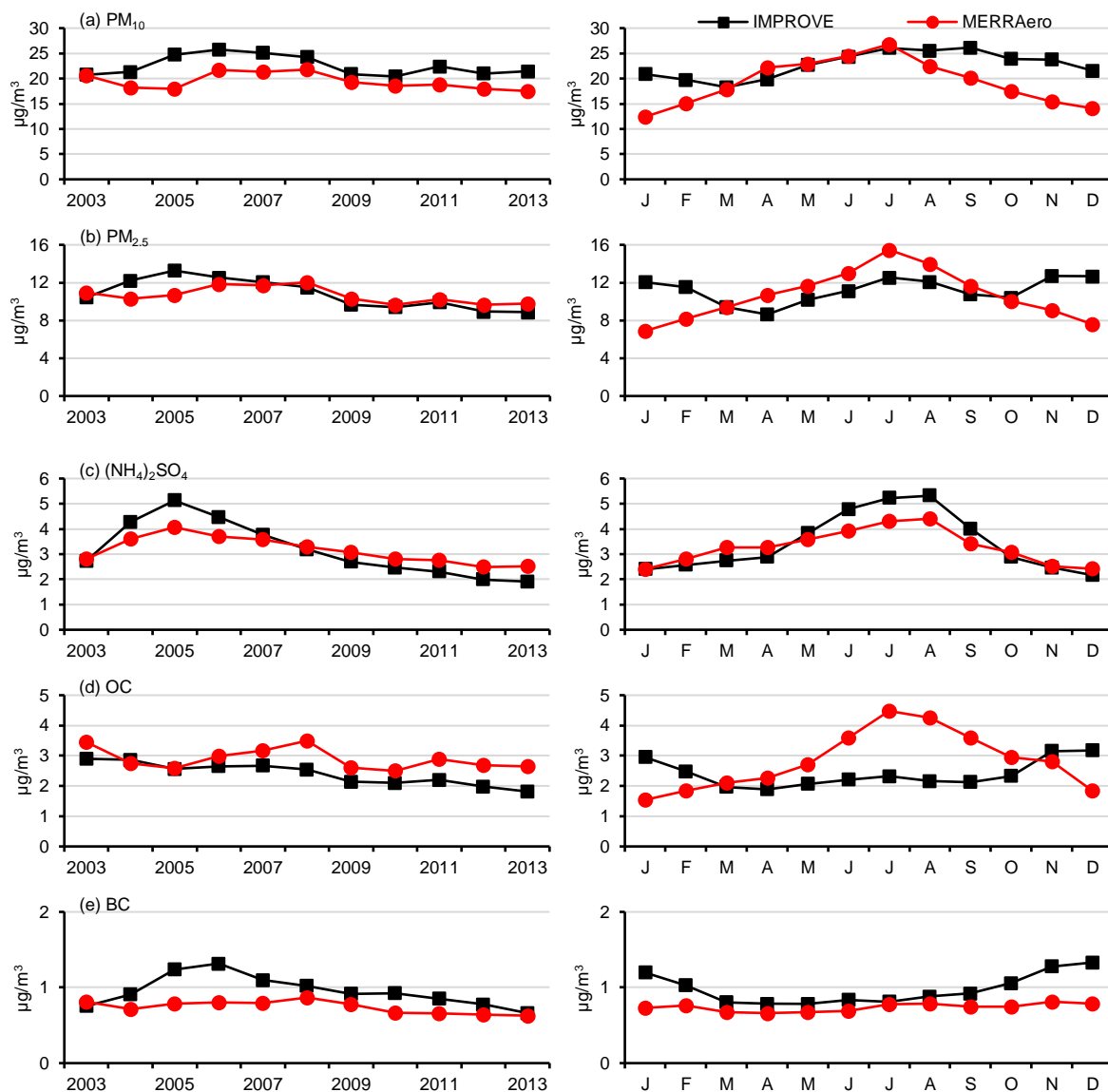


Fig. 2.5 : Annual (left) and monthly (right) averages of (a) PM_{10} , (b) $\text{PM}_{2.5}$, (c) $(\text{NH}_4)_2\text{SO}_4$, (d) OC and (e) BC concentrations measured by IMPROVE and simulated by MERRAero for the ensemble of the 14 urban stations.

2.3.4 The contribution of NO₃

The fact that MERRAero overestimates [PM_{2.5}] without even simulating NO₃ is a cause for concern. On average, observed ammonium nitrate (NH₄NO₃) concentration represents ~11% of total [PM_{2.5}] (this proportion grows to ~17% at urban locations). In order to evaluate how this shortcoming impacts MERRAero's ability to simulate [PM_{2.5}], we compare [PM_{2.5}] simulated by MERRAero with [PM_{2.5}] subtracted by [NH₄NO₃] observed by IMPROVE (Tab. 2.2). As expected, the evaluation worsened, but 61% of simulated data remain within a factor of 2 of observed data, which indicates that MERRAero simulates [PM_{2.5}] accurately in most instances despite this shortcoming. One last comparison is performed, between simulated [PM_{2.5}] without [SS_{2.5}] and observed [PM_{2.5}] without [NH₄NO₃] (Tab. 2.2). The values of the indices are very similar to those obtained in Tab. 2.1. This suggests that MERRAero's overestimation of [SS_{2.5}] somewhat compensates for its lack of NO₃.

2.4 Conclusion

We attempted to evaluate MERRAero's simulation of PM₁₀ and PM_{2.5} speciation at the surface over the U.S. Overall, MERRAero simulates well [SO₄] but its use of an SO₂ emissions inventory from 2005 is increasingly becoming antiquated. The simulation would benefit from using appropriate emission inventories proper to each year. The seasonal fluctuation is nevertheless very well simulated. The simulation of [OC] and [BC] is generally overestimated, particularly in the western U.S. and during the summer. This is an indication that biomass burning emissions of carbon particles are exaggerated by MERRAero. [OC] is generally well simulated during the winter. MERRAero overestimates [DS_{2.5}] in the spring and summer when the U.S. is most impacted by long distance transport of DS. [SS_{2.5}] is also consistently and significantly overestimated. DS_{2.5} and SS_{2.5}

measurements are both biased toward underestimations which explain in part the overestimated simulation of their respective concentration.

Despite the shortcomings listed in the previous paragraph, MERRAero simulates well $[PM_{10}]$ and $[PM_{2.5}]$, in part because $[SO_4]$ is also well simulated, given that $[(NH_4)_2SO_4]$ represents ~20% of total $[PM_{10}]$ and ~38% of total $[PM_{2.5}]$. The overestimation of $[PM_{2.5}]$ is mostly attributed to OC, and to $DS_{2.5}$ and $SS_{2.5}$ to a lesser degree. The fact that MERRAero doesn't simulate NO_3 somewhat compensates for the overestimated concentration of other species. The overestimation of $[BC]$ contributes little to $[PM_{2.5}]$.

MERRAero is capable to reliably simulate the PM load of metropolitan areas as a whole. There are, however, important discrepancies within the seasonal cycle with respect to the concentration of carbon particles which are underestimated in winter due to anthropogenic sources not taken into account by MERRAero. This is also reflected in the simulation of $[PM_{10}]$ and $[PM_{2.5}]$. Urban $[SO_4]$ is very well simulated.

References

Buchard, V., da Silva, A.M., Colarco, P., Krotkov, N., Dickerson, R.R., Stehr, J.W., Mount, G., Spinei, E., Arkinson, H.L. and He, H. (2014). Evaluation of GEOS-5 sulfur dioxide simulations during the Frostburg, MD 2010 field campaign. *Atmos. Chem. Phys.* 14: 1929–1941.

Buchard, V., da Silva, A.M., Colarco, P.R., Darmenov, A., Randles, C.A., Govindaraju, R., Torres, O., Campbell, J. and Spurr, R. (2015a). Using the OMI aerosol index and absorption aerosol optical depth to evaluate the NASA MERRA Aerosol Reanalysis. *Atmos. Chem. Phys.* 15: 5743–5760.

Buchard, V., da Silva, A.M., Randles, C.A., Colarco, P., Ferrare, R., Hair, J., Hostetler, C., Tackett, J. and Winker, D. (2016). Evaluation of the surface PM_{2.5} in Version 1 of the NASA MERRA Aerosol Reanalysis over the United States. *Atmos. Environ.* 125: 100–111.

Chang, J.C. and Hanna, S.R. (2004). Air quality model performance evaluation. *Meteorol. Atmos. Phys.* 87: 167–196.

Charlson, R.J. (1969). Atmospheric visibility related to aerosol mass concentration. *Environ. Sci. Technol.* 3: 913–918.

Chin, M., Ginoux, P., Kinne, S., Torres, O., Holben, B.N., Duncan, B.N., Martin, R.V., Logan, J.A., Higurashi, A. and Nakajima, T. (2002). Tropospheric aerosol optical thickness from the GOCART model and comparisons with satellite and sun photometer measurements. *J. Atmos. Sci.* 5: 461–483.

Chow, J.C., Lowenthal, D.H., Antony Chen, L.W., Wang, X. and Watson, J.G. (2015). Mass reconstruction methods for PM_{2.5}: a review. *Air Qual. Atmos. Health* 8: 243–263.

Colarco, P., da Silva, A., Chin, M. and Diehl, T. (2010). Online simulations of global aerosol distributions in the NASA GEOS-4 model and comparisons to satellite and ground-based aerosol optical depth. *J. Geophys. Res.* 115: D14207.

Cooper, J.A. (1980). Environmental impact of residential wood combustion emissions and its implications. *J. Air Pollut. Control Assoc.* 30: 855–861.

Creamean, J.M., Spackman, J.R., Davis, S.M. and White, A.B. (2014). Climatology of long-range transported Asian dust along the west coast of the United States. *J. Geophys. Res.: Atmos.* 119: 12171–12185.

de Gouw, J.A., Parrish, D.D., Frost, G.J. and Trainer, M. (2014). Reduced emissions of CO₂, NO_x, and SO₂ from U.S. power plants owing to switch from coal to natural gas with combined cycle technology. *Earth's Future* 2: 75–82.

Hand, J.L. *et al.* (2011). *Spatial and seasonal patterns and temporal*

variability of haze and its constituents in the United States—Report V. Cooperative Institute for Research in the Atmosphere and Colorado State University, ISSN 0737-5352-87.

Hellén, H., Hakola, H., Haaparanta, S., Pietarila, H. and Kauhaniemi, M. (2008). Influence of residential wood combustion on local air quality. *Sci. Total Environ.* 393: 283–290.

Kundu, S. and Stone, E.A. (2014). Composition and sources of fine particulate matter across urban and rural sites in the Midwestern United States. *Environ. Sci. Process. Impact* 16: 1360–1370.

Malm, W.C., Sister, J.F., Huffman, D., Eldred, R.A. and Cahill, T.A. (1994). Spatial and seasonal trends in particle concentration and optical extinction in the United States. *J. Geophys. Res.* 99: 1347–1370.

Malm, W.C. and Hand, J.L. (2007). An examination of the physical and optical properties of aerosols collected in the IMPROVE program. *Atmos. Environ.* 41: 3407–3427.

Pandis, S.N., Skyllakou, K., Florou, K., Kostenidou, E., Kaltsonoudis, C., Hasa, E. and Presto, A.A. (2016). Urban particulate matter pollution: a tale of five cities. *Farad. Discuss.* 189: 277–290.

Pöschl, U. (2005). Atmospheric aerosols: composition, transformation, climate and health effects. *Angew. Chem. Int. Edit.* 44: 7520–7540.

Prospero, J.M. (1999). Long-term measurements of the transport of African mineral dust to the southeastern United States: implications for regional air quality. *J. Geophys. Res.* 104: 15917–15927.

Rienecker, M.M., Suarez, M.J., Gelaro, R., Todling, R., Bacmeister, J., Liu, E., Bosilovich, M.G., Schubert, S.D., Takacs, L., Kim, G.K., Bloom, S., Chen, J., Collins, D., Conaty, A., da Silva, A., Gu, W., Joiner, J., Koster, R.D., Lucchesi, R., Molod, A., Owens, T., Pawson, S., Pegion, P., Redder, C.R., Reichle, R., Robertson, F.R., Ruddick, A.G., Sienkiewicz M. and Woollen, J. (2011). MERRA: NASA's Modern-Era Retrospective Analysis for Research and Application. *J. Clim.* 24: 3624–3648.

Sexton, K., Spengler, J.D., Treitman, R.D. and Turner, W.A. (1984). Winter air quality in a wood-burning community: a case study in Waterbury, Vermont. *Atmos. Environ.* 18: 1357–1370.

Stout, J.E. (2001). Dust and environment in the southern High Plains of North America. *J. Arid Environ.* 47: 425–441.

Tager, I.B. (2013). *Health effects of aerosols: mechanisms and epidemiology.* In: Ruzer, L.S. and Harley, N.H. *Aerosols handbook: measurement, dosimetry, and health effects*, 2nd ed., CRC Press, pp. 565–636.

Willmott, C.J. (1982). Some comments on the evaluation of model

performance. *Bull. Am. Meteorol. Soc.* 63: 1309–1313.

Wu, W.S., Purser, R.J. and Parrish, D.F. (2002). Three-dimensional variational analysis with spatially inhomogeneous covariances. *Mon. Weather Rev.* 130: 2905–2916.

3 Evaluation of PM surface concentrations simulated by Version 1 of NASA's MERRA Aerosol Reanalysis over Europe

Abstract

This article evaluates the concentrations of particulate matter (PM) and some of its chemical speciation such as sulfate, organic carbon, black carbon and sea salt particles simulated at the surface by Version 1 of the Aerosol Reanalysis of NASA's Modern-Era Retrospective Analysis for Research and Application (MERRAero) over Europe. Measurement data from the European Monitoring and Evaluation Programme database were used. The concentrations of coarse PM (PM_{10}), fine PM ($PM_{2.5}$), sulfate and black carbon particles are overall well simulated, despite a slight and consistent overestimation of PM_{10} concentration, and a slight and consistent underestimation of $PM_{2.5}$ and sulfate concentrations throughout most of the year. The concentration of organic carbon was largely underestimated, especially in winter, caused by two specific monitoring stations in Italy, resulting in an overall poor performance for this particular species. After removing these two stations from the sample, the evaluation of OC substantially improved but an underestimation in winter remained. Carbon emissions originating from anthropogenic sources, such as residential wood burning in winter, unresolved by MERRAero provide a plausible explanation for this discrepancy. The evaluation of $PM_{2.5}$, sulfate and organic carbon concentrations improved during the summer. The concentration of fine sea salt particles was consistently and largely overestimated, but contributes relatively little to total $PM_{2.5}$ concentration.

Résumé

Cet article évalue la concentration des matières particulaires (PM) et de quelques-unes de leurs espèces chimiques, telles que les particules de sulfate, de carbone organique, de carbone noir et de sel de mer, simulée à la surface par la réanalyse des aérosols MERRAero (Modern-Era Retrospective Analysis for Research and Application Aerosol Reanalysis) en Europe à l'aide de données d'observations mesurées par le European Monitoring and Evaluation Programme (EMEP). La concentration des PM_{10} , des $PM_{2.5}$, des particules de sulfate et de carbone noir est généralement bien simulée, malgré une légère et constante surestimation de la concentration des PM_{10} , et une sous-estimation de la concentration des $PM_{2.5}$ et des particules de carbone

noir tout au long de l'année. La concentration des particules de carbone organique est largement sous-estimée, particulièrement en hiver, due spécifiquement à des données d'observations provenant de deux stations en Italie. L'évaluation de cette espèce s'est substantiellement améliorée après avoir retiré ces deux stations de l'échantillon, mais la concentration est tout de même demeurée sous-estimée en hiver, quoique légèrement. Ce biais est expliqué par le fait que les émissions de carbone d'origine résidentielle, telles que le bois de chauffage, ne sont pas considérées par MERRAero. L'évaluation de la concentration des $PM_{2.5}$, des particules de sulfate et de carbone organique était très favorable en été. La concentration des particules de sel de mer est largement surestimée mais contribue peu à la concentration totale des $PM_{2.5}$.

3.1 Introduction

Many years ago, NASA introduced the first version of the Modern-Era Retrospective Analysis for Research and Application (MERRA), a reanalysis tool designed to simulate the hydrological cycle since the satellite era for climate research purposes (Rienecker *et al.*, 2011). MERRA integrates observations from NASA's Earth Observing System satellites and the 5th version of the Goddard Earth Observing System (GEOS-5) atmospheric model and data assimilation system (Rienecker *et al.*, 2008). Recently, MERRA was expanded to assimilate bias-corrected aerosol optical depth (AOD) observations from the Moderate Resolution Imaging Spectroradiometers (MODIS, Remer *et al.*, 2005) on board the Terra and Aqua satellites, and the Goddard Chemistry, Aerosol, Radiation and Transport (GOCART) model (Chin *et al.*, 2002). GOCART simulates the sources, sinks, transport and concentration of sulfate (SO_4), organic carbon (OC), black carbon (BC), dust (DS) and sea salt (SS) aerosols from the meteorological fields provided by GEOS-5 and emission inventories of different air pollutants. DS and SS emissions are a function of surface properties and wind speed at the surface, and their respective concentrations are classified in different diameter bins. Sources of other species are simulated from emission inventories, including their precursors.

Sulfur dioxide (SO₂, the precursor of SO₄) anthropogenic emissions are input from the Emission Database for Global Atmospheric Research (EDGAR) version 4.1 inventory from 2005 and biomass burning emissions (primarily OC and BC) are input from the NASA Quick Fire Emission Dataset (QFED) version 2.1 (Buchard *et al.*, 2015). Version 1 of MERRA's Aerosol Reanalysis is labeled "MERRAero."

MERRAero simulates the concentrations of the five aerosol species listed in the previous paragraph all over the world with a resolution of 0.5° latitude by 0.625° longitude and 72 vertical layers (from the surface to 80 km) between 2002 and 2015 (Buchard *et al.*, 2015). Considering that airborne particulate matter (PM) impacts public health and visibility differently depending on its size and its chemistry (e.g., Laden *et al.*, 2000; Schwartz and Neas, 2000; Groblicki *et al.*, 1981), MERRAero's ability to differentiate chemical speciation of aerosols is a significant improvement for studying a broad range of air quality issues around the world since very few monitoring networks make such an identification of local PM and its speciation observations, but particularly in regions with unreliable or scarce monitoring.

MERRAero is undergoing an evaluation process: Buchard *et al.* (2014) evaluated concentrations of SO₂ and SO₄ simulated by GEOS-5 during a field campaign in the United States; Buchard *et al.* (2015) evaluated MERRAero's assimilation of AOD with many remote sensing instruments over Africa, South America, Central and Eastern Asia; and Buchard *et al.* (2016) evaluated surface concentrations of fine PM speciation across the continental U.S. Buchard *et al.* (2016) obtained a stronger correlation between MERRAero and observations of fine PM concentration from rural networks as opposed to suburban networks. Suburban environments are more likely to contain local sources of pollution which are not captured by MERRAero's resolution. In terms of chemical speciation, overall, the concentrations of different fine PM species were well simulated, although

some biases were noticed, such as a large underestimation of OC concentration at suburban locations, especially in winter, and an excessive contribution of DS particles from local and remote sources. The goal of this paper is to expand MERRAero's reliability as a tool to study air quality issues around the world, as well as to identify shortcomings which will help improve subsequent versions, by evaluating the surface concentration of PM over Europe.

3.2 Methods

MERRAero simulates the concentration of five PM species every hour: SO_4 , OC, BC, DS and SS. Based on these, it is possible to estimate the total concentration of PM_{10} (PM with diameter ≤ 10 μm) as follows:

$$(3.1) \quad [\text{PM}_{10}] = 1.375 \times [\text{SO}_4] + 1.8 \times [\text{OC}] + [\text{BC}] + [\text{DS}] + [\text{SS}]$$

Brackets denote concentration. $[\text{SO}_4]$ is multiplied by 1.375 since SO_4 is assumed to be fully neutralized by ammonium (NH_4) in the form of ammonium sulfate ($(\text{NH}_4)_2\text{SO}_4$) and $[\text{OC}]$ is multiplied by 1.8 to account for other organic compounds found in particulate organic matter (POM). Furthermore, since MERRAero differentiates PM sizes of DS and SS, it is possible to estimate $[\text{PM}_{2.5}]$, a widely used air quality indicator, as follows:

$$(3.2) \quad [\text{PM}_{2.5}] = 1.375 \times [\text{SO}_4] + 1.8 \times [\text{OC}] + [\text{BC}] + [\text{DS}_{2.5}] + [\text{SS}_{2.5}]$$

Eqs. 3.1 and 3.2 assume that SO_4 , OC and BC are all in the form of $\text{PM}_{2.5}$ and lack the concentration of nitrate particles, which can make up a considerable portion of total $[\text{PM}_{2.5}]$ (Buchard *et al.*, 2016).

A European network of air quality surveillance stations is running under the European Monitoring and Evaluation Programme (EMEP), whose main goal is to provide to governments with information regarding the concentration of a broad range of air pollutants and their transport across

political boundaries (Tørseth *et al.*, 2012). This information is publically available on the EMEP database (<http://ebas.nilu.no>).

We evaluate MERRAero [PM] simulation and its chemical speciation at 55 locations across Europe where measurement data are available between 2003 and 2014 (Fig. 3.1). According to EMEP guidelines, monitoring stations should be regionally representative and therefore located in rural areas with minimal influence of local pollution sources (Tørseth *et al.*, 2012). A closer look at the locations reveals, however, that a large number of them in Fig. 3.1 are located in the outskirts of residential settlements, therefore some local sources of PM should be expected. Out of these 55 locations, 52 measure [PM₁₀] and [PM_{2.5}] over 24-hour periods, at varying frequencies. Chemical speciation of [PM_{2.5}] is also available at a number of locations but much less widespread: 32 stations measure [SO₄], 23 measure the concentration of carbonaceous particles and 24 measure the concentration of fine chloride ions (Cl_{2.5}). [Cl_{2.5}] is multiplied by 1.8 to obtain [SS_{2.5}] (Seinfeld and Pandis, 1998). Since few locations measure all necessary minerals to obtain a reasonable estimate of [DS_{2.5}], this species isn't evaluated. Hourly MERRAero data is averaged on a daily basis and paired at the 55 locations where concentration measurements are available. A spatial consistency algorithm is applied to assure reliability of the observed and simulated concentrations, which goes as follows: since trace concentrations are usually lognormally distributed, the bias between log-simulated concentration and log-observed concentration ($B_{log} = \ln(C_s) - \ln(C_o)$; C_s : simulated concentration, C_o : observed concentration) is calculated at all locations on a given day; the average and standard deviation of B_{log} are calculated and used to define a reliability interval which justifies ~95% of the normal distribution: $\overline{B_{log}} \pm 2\sigma_{B_{log}}$; all data pairs that fall outside this interval are excluded.



Fig. 3.1: Locations of monitoring stations in Europe.

Performance statistics are calculated to quantify MERRAero’s accuracy: the mean fraction $\bar{F} = \bar{C}_s / \bar{C}_o$, the mean bias $\bar{B} = \bar{C}_s - \bar{C}_o$, the standard deviation of the bias ($SD-B$) and the correlation coefficient (R); as well as log-transformed statistics: $\overline{B_{log}} = \overline{\log(C_s)} - \overline{\log(C_o)}$, $SD-B_{log}$ and R_{log} . Despite being widely applied, R is a criticized index for evaluating model performance since it doesn’t directly compare simulated with observed data (Willmott, 1982). Therefore, Chang and Hanna (2004) recommended as a rigorous index to evaluate air quality models the proportion of simulated data which falls

within a factor of 2 of observed data (*FAC2*, i.e. proportion of the data which satisfies $0.5 \leq C_o / C_s \leq 2.0$), since this index is not disproportionately sensitive to extreme values and is unaffected by simplification of errors. Chang and Hanna (2004) considered a model’s performance to be reasonably good if *FAC2* ≥ 0.5 .

3.3 Results

The spatial consistency algorithm excluded 4.0% of PM_{10} and 4.2% of $PM_{2.5}$ data pairs. Overall, on average, MERRAero overestimates $[PM_{10}]$ by a factor of 1.25, which represents an additional $4.1 \mu\text{g}/\text{m}^3$ (Tab. 3.1). $[PM_{2.5}]$, on the other hand, is underestimated by a factor of 1.25 ($2.1 \mu\text{g}/\text{m}^3$). As for chemical speciation, the algorithm excluded 4.5% of SO_4 , 0.7% of OC, 3.2% of BC and 1.0% of $SS_{2.5}$ data pairs. $[SO_4]$ and $[BC]$ are slightly underestimated, by $0.5 \mu\text{g}/\text{m}^3$ and $0.02 \mu\text{g}/\text{m}^3$, respectively. $[OC]$ is highly underestimated by a factor of 3.18, representing a discrepancy of $2.5 \mu\text{g}/\text{m}^3$, and $[SS_{2.5}]$ is also overestimated by a large factor of 2.11, but its actual average bias is lower ($1.0 \mu\text{g}/\text{m}^3$).

Tab. 3.1: Performance statistics for the ensemble of locations. AOC stands for “average observed concentration.”

	PM_{10}	$PM_{2.5}$	SO_4	OC	BC	$SS_{2.5}$
n	133,025	99,191	46,817	13,397	13,165	10,089
AOC ($\mu\text{g}/\text{m}^3$)	16.5	10.5	2.3	3.7	1.0	0.9
\bar{F}	1.25	0.80	0.77	0.31	0.98	2.11
\bar{B} ($\mu\text{g}/\text{m}^3$)	4.1	-2.1	-0.5	-2.5	-0.0	1.0
$SD-B$ ($\mu\text{g}/\text{m}^3$)	18.0	8.1	1.9	4.7	1.2	3.4
\overline{B}_{log}	0.18	-0.11	-0.21	-0.84	0.45	1.27
$SD-B_{log}$	0.72	0.62	0.65	0.93	0.94	1.54
R	0.44	0.47	0.48	0.16	0.52	0.25
R_{log}	0.48	0.59	0.60	0.39	0.60	0.44
FAC2	0.67	0.74	0.70	0.41	0.54	0.29

All species in Tab. 3.1, except for OC and $SS_{2.5}$, have a reasonably low B and B_{log} , however, there is quite a lot of scattering in the data, as reflected by $SD-B$ and $SD-B_{log}$ values which are much larger than their respective \bar{B} and \overline{B}_{log} , accompanied by low R and R_{log} values. It is worth mentioning that

SD's are disproportionately influenced by extreme data pairs. For example, if such pairs of data with a factor above 5 are excluded from the sample, which represents 3.4% of the PM_{10} and 1.5% of the $PM_{2.5}$ samples, the $SD-B$'s are reduced to $15.2 \mu\text{g}/\text{m}^3$ and $7.0 \mu\text{g}/\text{m}^3$, respectively. Fig. 3.2 presents density scatter plots which compare observed and simulated concentrations for all species. Although some scatter is clearly noticeable, the plots also show that the bulk of PM_{10} , $PM_{2.5}$ and SO_4 concentration data are reasonably well simulated. The slight underestimations of $[PM_{2.5}]$ and $[SO_4]$ are more noticeable in the log-transformed concentration plots (as well as the large underestimation of $[OC]$ and large overestimation of $[SS_{2.5}]$). Furthermore, the same species all have a $FAC2$ above 50%, supporting a favorable performance. With a $FAC2$ above 70%, $[PM_{2.5}]$ and $[SO_4]$ are overall very well estimated.

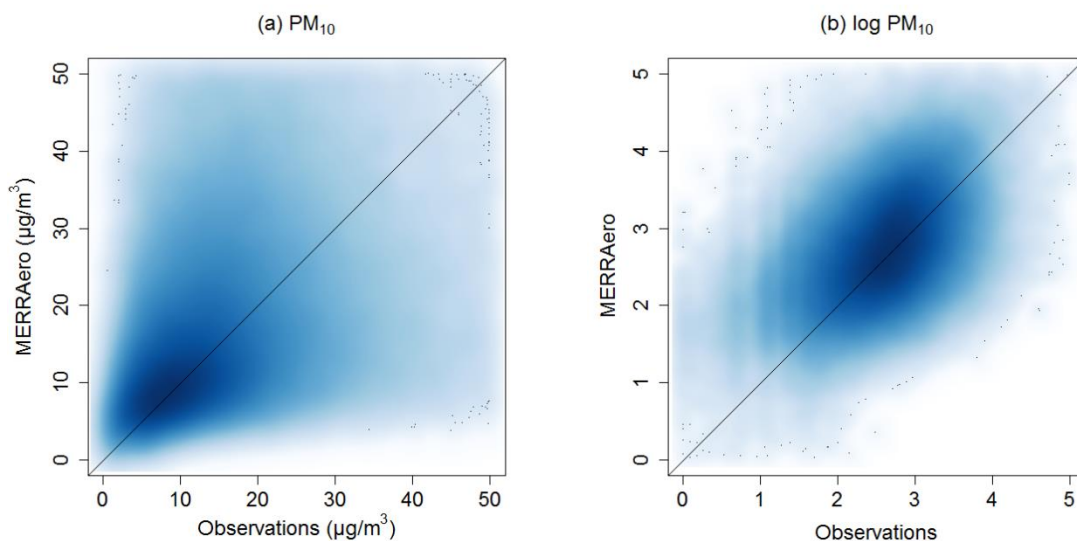


Fig. 3.2: Density scatter plots between observations and simulations of PM concentrations and species over the ensemble of European locations.

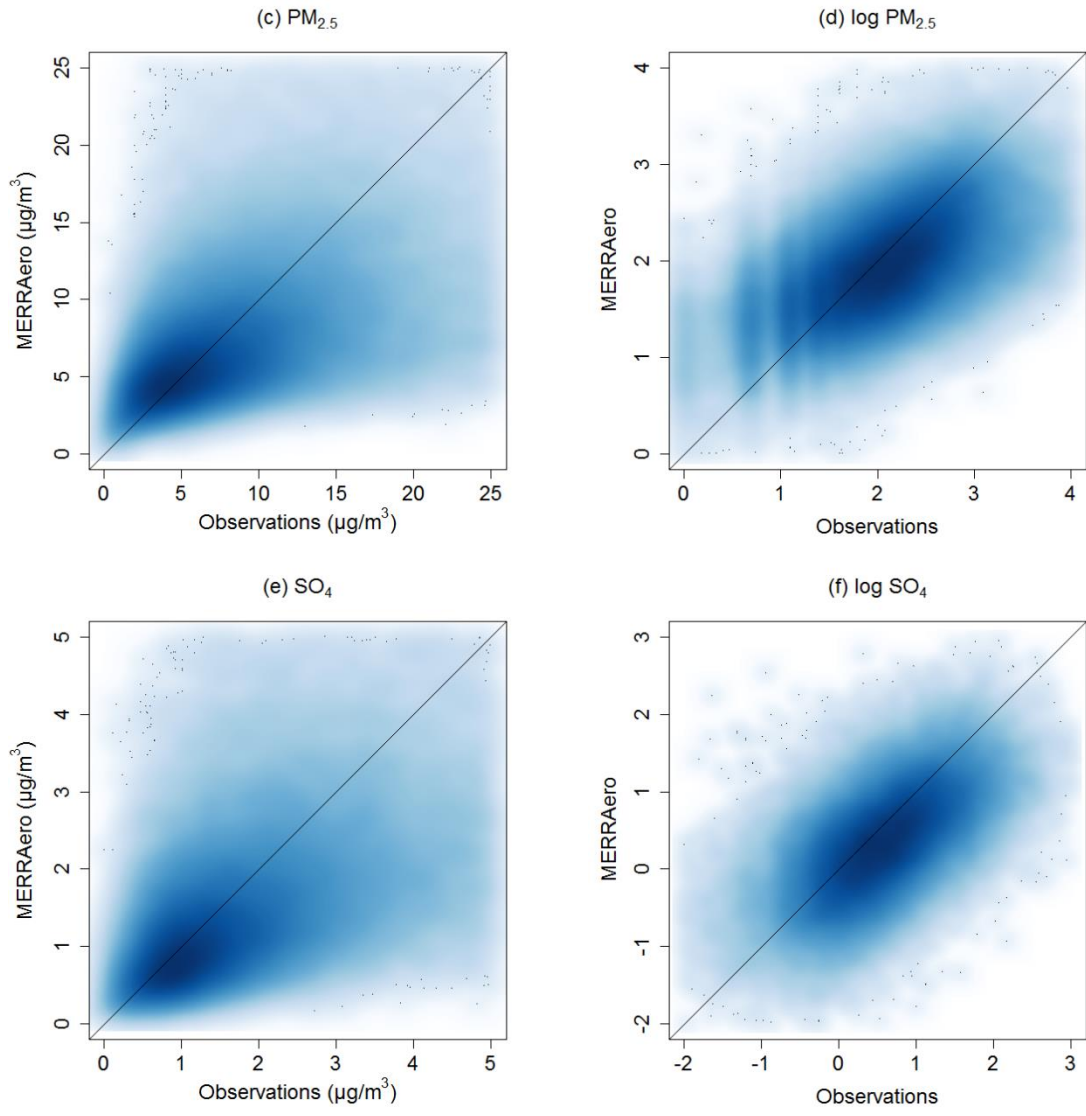


Fig. 3.2 (continued)

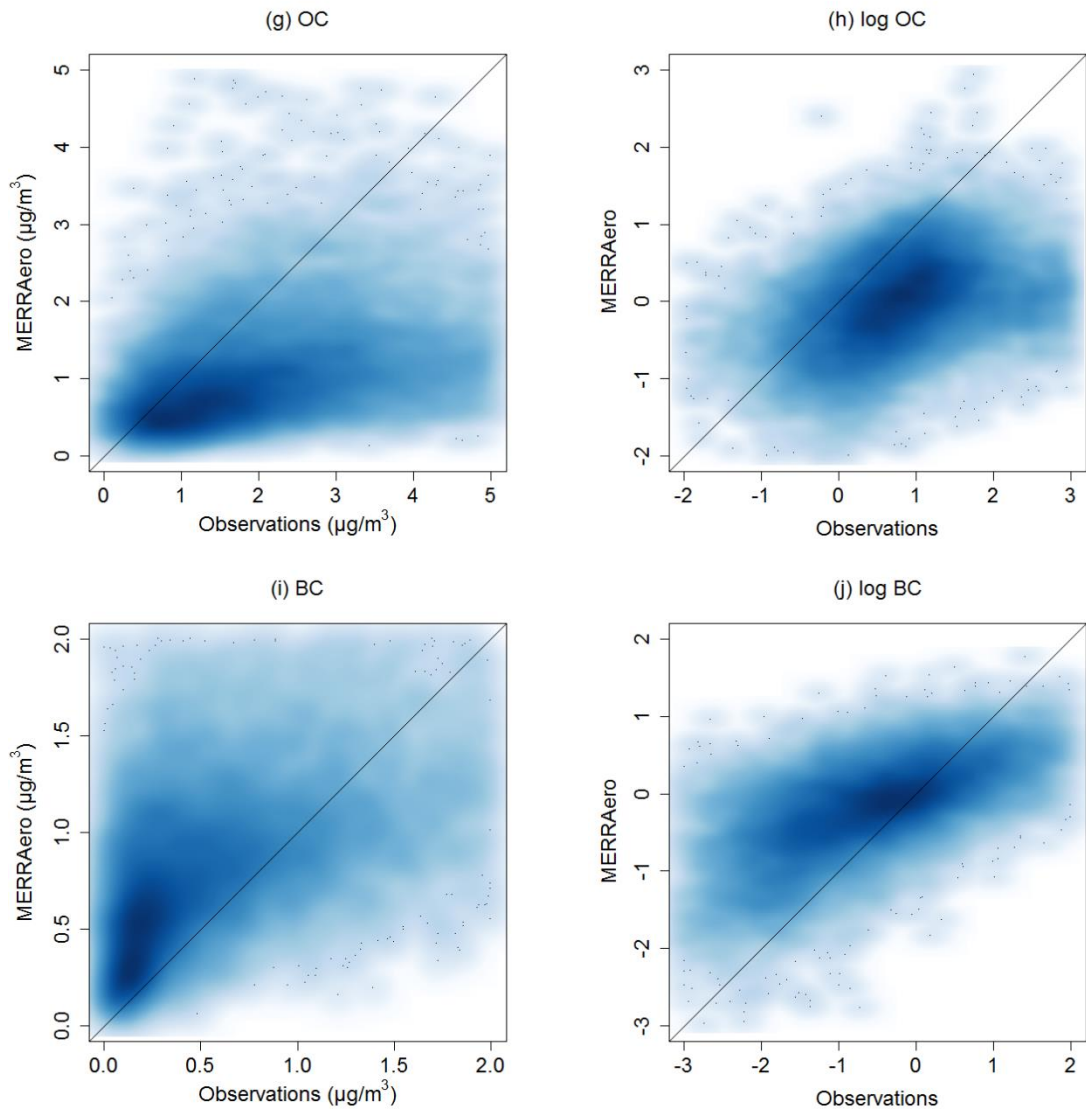


Fig. 3.2 (continued)

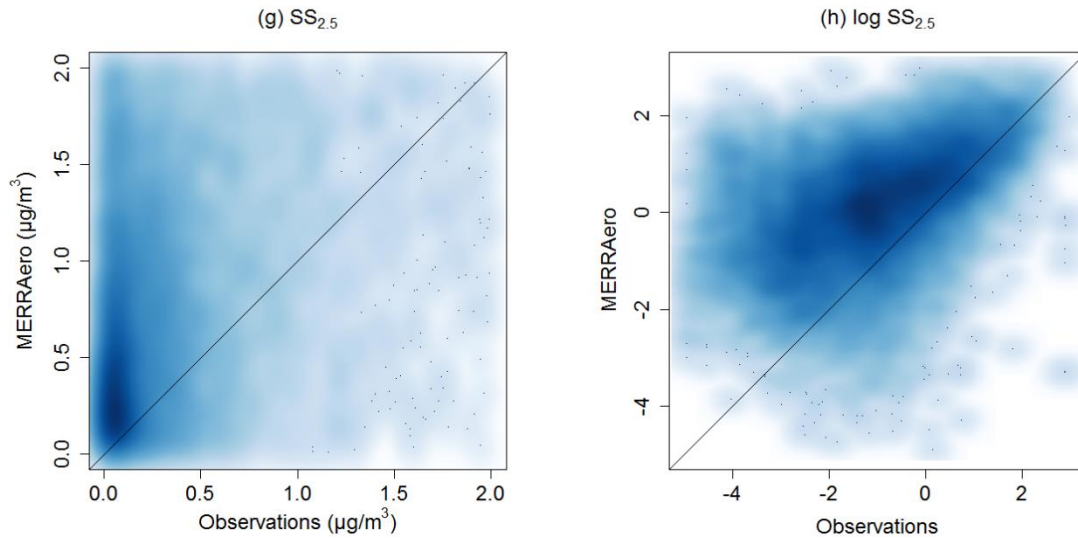


Fig. 3.2 (continued)

The geographical distribution of \bar{B} is mapped in Fig. 3.3. \bar{B} for $[\text{PM}_{10}]$ is reasonably close to zero across Europe except for a few locations where the overestimation is quite obvious: Cyprus, Ireland, Southwest Sweden, Western Denmark and the Spanish island of Minorca. $[\text{PM}_{2.5}]$ is mostly underestimated in central Europe, particularly in Italy, Eastern Austria and Eastern Germany. The mean bias for $[\text{SO}_4]$ is also close to zero except for the large overestimations observed in Southern England and Slovenia. $[\text{OC}]$ is underestimated across Europe, particularly in Italy. At the opposite, $[\text{BC}]$ is overestimated in most of Europe except, once again, in Italy where it is underestimated. $[\text{SS}_{2.5}]$'s overestimation is observed across Europe, but coastal locations tend to be most affected.

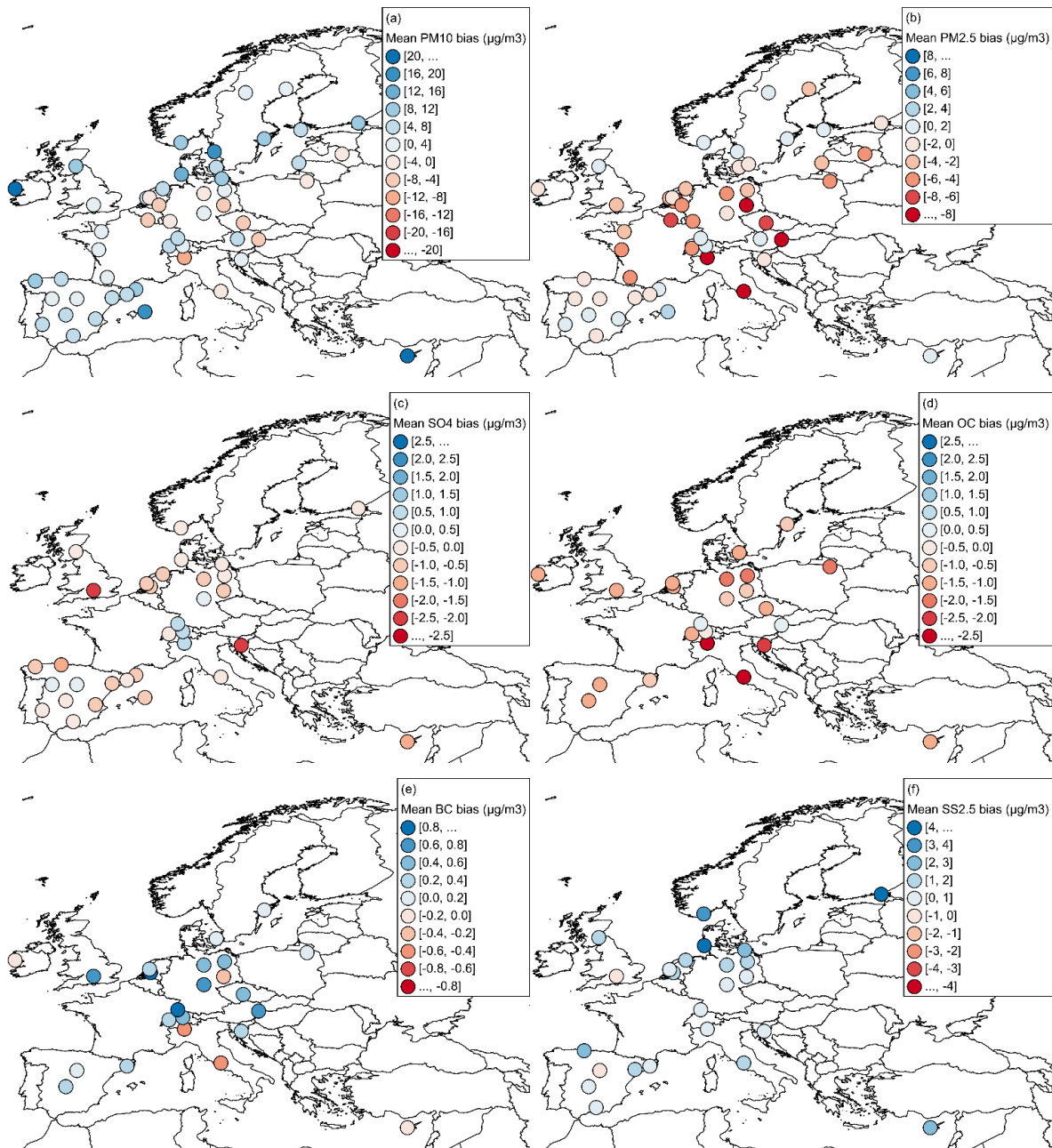


Fig. 3.3: Maps of the mean bias for PM concentrations and species.

Finally, a seasonal analysis is presented in Fig. 3.4 which graphs a comparison between observed and simulated concentrations for the six pollutants. $[\text{PM}_{10}]$ is overestimated throughout most of the year, while $[\text{PM}_{2.5}]$ is well simulated during most of the spring, summer and fall, but underestimated in winter. The underestimation is also larger in winter for $[\text{SO}_4]$, $[\text{OC}]$ and $[\text{BC}]$. The $[\text{OC}]$ underestimation is particularly noticeable

from November to February by factors up to 6.6. $[SS_{2.5}]$ is overestimated throughout the whole year.

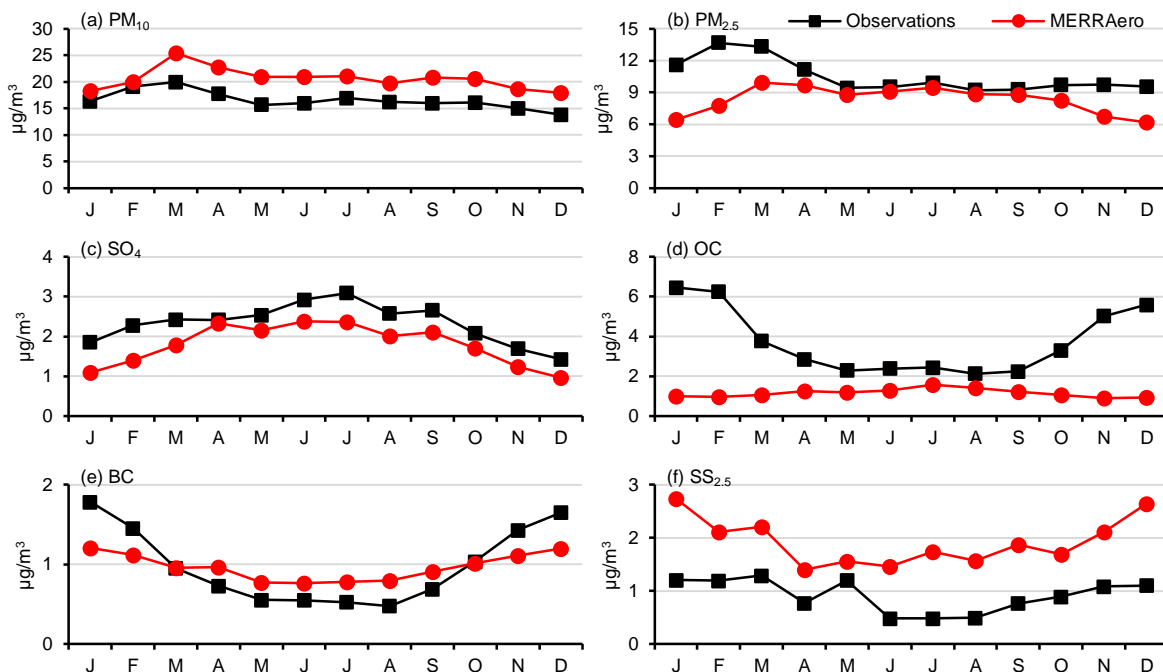


Fig. 3.4: Monthly averages of PM concentration and species observations and simulations over the ensemble of European locations.

3.4 Discussion

Although the comparisons of $[SO_4]$, $[OC]$, $[BC]$ and $[SS_{2.5}]$ in Fig. 3.4 are not directly comparable between each another or to those of $[PM_{2.5}]$ due to different samples and measurement techniques, they provide clues that explain the discrepancy between observed and simulated $[PM_{2.5}]$. Aside from the lack of nitrate particles, the wintertime underestimation of $[PM_{2.5}]$ is likely caused by a combination of $[SO_4]$, $[OC]$ and $[BC]$ underestimations during the same months. This concentration discrepancy for carbonaceous particles is similarly observed in suburban locations in the U.S. (Buchard *et al.*, 2016) where it was hypothesised that anthropogenic sources of such particles, such as residential wood burning, unaccounted for in MERRAero's resolution significantly increase a city or a town's PM load in winter (Cooper,

1980; Sexton *et al.*, 1984; Hellén *et al.*, 2008; Pandis *et al.*, 2016). There is indeed a stark contrast between these observations and those in rural U.S. where maximum [OC] and [BC] occur in summer, caused by seasonal wildfires (Buchard *et al.*, 2016). To a lesser extent, SO₂ is also emitted from biomass burning (Haywood and Boucher, 2000), which could explain the larger discrepancy between observed and simulated wintertime [SO₄]. Performance statistics were recalculated for [PM_{2.5}], [SO₄], [OC] and [BC] between April and September only, producing favorable results (Tab. 3.2), and, by extension, suggesting a misrepresentation of wintertime anthropogenic sources of PM by MERRAero. MERRAero reproduces a concentration of SO₄ larger than OC (Tab. 3.3), while the reverse is usually observed over Europe (Tab. 3.1; Putaud *et al.*, 2004, 2010). [SS_{2.5}] is consistently overestimated by MERRAero, a result also obtained in the U.S. (Buchard *et al.*, 2016), explained in part by measurement biases (Hand *et al.*, 2011). Since coastal locations tend to have the largest \bar{B} , this would suggest that SS emissions from the oceans are exaggerated. This overestimation of [SS_{2.5}] slightly compensates for the underestimation of the concentration of other species in simulating [PM_{2.5}].

Tab. 3.2: Performance statistics for the ensemble of locations between April and September. AOC stands for “average observed concentration.”

	PM _{2.5}	SO ₄	OC	BC
n	50,532	23,581	6,856	6,640
AOC (μg/m ³)	9.7	2.7	2.4	0.6
\bar{F}	0.93	0.82	0.56	1.42
\bar{B} (μg/m ³)	-0.6	-0.5	-1.1	0.2
SD-B (μg/m ³)	5.1	1.9	1.6	0.6
\bar{B}_{\log}	-0.03	-0.14	-0.51	0.64
SD-B _{log}	0.48	0.62	0.72	0.84
R	0.62	0.47	0.30	0.42
R _{log}	0.66	0.54	0.40	0.54
FAC2	0.85	0.73	0.54	0.54

Tab. 3.3: Average concentrations simulated by MERRAero for the ensemble of locations in Fig. 3.1 over the study period.

Species	Average concentration ($\mu\text{g}/\text{m}^3$)	Proportion of PM ₁₀ (%)	Proportion of PM _{2.5} (%)
PM ₁₀	21.7	—	—
PM _{2.5}	8.5	39.1	—
(NH ₄) ₂ SO ₄	2.3	10.7	27.2
POM	1.8	8.1	20.6
BC	0.7	3.0	7.7
DS	6.8	31.2	—
SS	10.2	47.1	—
DS _{2.5}	2.0	9.0	23.0
SS _{2.5}	1.8	8.4	21.5

The shortcomings identified in the previous paragraph regarding MERRAero’s simulation of [SO₄], [OC] and [BC] has relatively little impact on the overall simulation of [PM₁₀]. MERRAero’s overestimation of [PM₁₀] is rather consistent throughout most of the year compared to its inconsistent underestimation of [PM_{2.5}] (Fig. 3.4). Indeed, the simulation of [PM₁₀] is composed by 80% of DS and SS, compared to 47% for [PM_{2.5}] (Tab. 3.3). Europe certainly receives a significant amount of DS from the Sahara desert (d’Almeida, 1986), even in the northern region (Ansmann *et al.*, 2003), and SS from the surrounding seas (Tsyro *et al.*, 2011). MERRAero’s [PM₁₀] performance therefore relies predominantly on simulating particles originating from natural sources. Unfortunately, given the scarcity of direct coarse particle speciation measurements, we are unable to reliably evaluate this for the time being. If [SS] is overestimated to the same extent as [SS_{2.5}], this, coupled with the large underestimation of [OC], would conceivably reproduce the results obtained in Tab. 3.1.

At this point, it is difficult to speculate as to why MERRAero is performing better in some regions of Europe compared to others. A country where MERRAero is performing particularly poorly is Italy. [PM_{2.5}], [OC] and [BC] are all well underestimated at both Italian stations. Their respective average concentrations are measured at 21.7 $\mu\text{g}/\text{m}^3$, 7.4 $\mu\text{g}/\text{m}^3$ and 1.8 $\mu\text{g}/\text{m}^3$ in Northern Italy, and 20.0 $\mu\text{g}/\text{m}^3$, 11.7 $\mu\text{g}/\text{m}^3$ and 1.1 $\mu\text{g}/\text{m}^3$ in Central Italy, substantially higher than almost anywhere else in Europe. The station in Northern Italy is located in the vicinity of many small towns, 50

km away from Milan and close to the Alps. Its location is ideal to accumulate clustered pollutants originating from urban sources unaccounted for by MERRAero. The station in central Italy is also located west of the Apennine Mountains which cluster pollution originating from nearby towns. If those two stations are removed from the sample, the evaluations of $[PM_{2.5}]$ and $[OC]$ are indeed substantially improved (Tab. 3.4). The wintertime bias remains but is much less pronounced (Fig. 3.5). The fact that MERRAero doesn't simulate secondary organic carbon particles might also contribute to the underestimation.

Tab. 3.4: Performance statistics for the ensemble of locations without the Italian stations. AOC stands for "average observed concentration."

	PM _{2.5}	OC
n	95,514	9,737
AOC ($\mu\text{g}/\text{m}^3$)	10.1	2.2
F	0.82	0.50
\bar{B} ($\mu\text{g}/\text{m}^3$)	-1.9	-1.1
SD-B ($\mu\text{g}/\text{m}^3$)	7.5	1.8
\bar{B}_{\log}	-0.10	-0.59
SD-B _{log}	0.61	0.75
R	0.47	0.37
R _{log}	0.58	0.47
FAC2	0.75	0.50

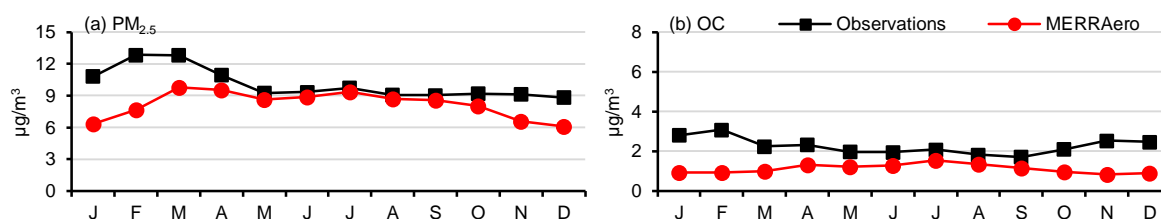


Fig. 3.5: Monthly averages of PM concentration and species observations and simulations over the ensemble of European locations without the Italian stations.

3.5 Conclusion

We evaluated MERRAero's simulation of PM_{10} and $PM_{2.5}$ speciation at the surface over Europe. Overall, MERRAero simulates well $[PM_{10}]$, $[PM_{2.5}]$, $[SO_4]$ and $[BC]$. Despite considerable scattering within the dataset, the average biases and, most importantly, the *FAC2*, a rigorous index to evaluate air quality models, reproduced favorable results. The evaluation of

[OC] wasn't as encouraging, revealing important underestimations overall, especially in winter. Wintertime underestimations were also obtained in the comparisons of [SO₄] and [BC], and by extension in [PM_{2.5}]. Anthropogenic emissions of carbon and sulfate in the form of residential wood burning, unresolved by MERRAero, are a likely explanation for this discrepancy. The evaluation of [PM_{2.5}], [SO₄] and [OC] did improve during the summer. By removing two stations from the sample where measurements of [OC] were particularly high, the evaluation of this species also improved substantially. MERRAero consistently overestimated [SS_{2.5}], by a factor of 2 on average. The bias was most evident at coastal locations which suggests that oceanic SS emissions are inflated.

This article demonstrated that MERRAero is a reliable tool to simulate the concentrations of major aerosol species in most circumstances. Some improvements are however feasible. The major shortcoming identified pertains to MERRAero's resolution, which hopefully will be improved in the foreseeable future. Inclusion of nitrate particles would also be a significant addition and would improve the simulation of [PM_{2.5}]. The simulation could also benefit from moderated sea salt emissions.

References

- Ansmann, A., Bösenberg, J., Chaikovsky, A., Comerón, A., Eckhardt, S., Eixmann, R., Freudenthaler, V., Ginoux, P., Komguem, L., Linné, H., Ángel López Márquez, M., Matthias, V., Mattis, I., Mitey, V., Müller, D., Music, S., Nickovic, S., Pelon, J., Sauvage, L., Sobolewsky, P., Srivastava, M.K., Stohl, A., Torres, O., Vaughan, G., Wandinger, U. and Wiegner, M. (2003). Long-range transport of Saharan dust to Northern Europe: the 11–16 October 2001 outbreak observed with EARLINET. *J. Geophys. Res.* 108: 4783.
- Buchard, V., da Silva, A.M., Colarco, P., Krotkov, N., Dickerson, R.R., Stehr, J.W., Mount, G., Spinei, E., Arkinson, H.L. and He, H. (2014). Evaluation of GEOS-5 sulfur dioxide simulations during the Frostburg, MD 2010 field campaign. *Atmos. Chem. Phys.* 14: 1929–1941.
- Buchard, V., da Silva, A.M., Colarco, P.R., Darmenov, A., Randles, C.A., Govindaraju, R., Torres, O., Campbell, J. and Spurr, R. (2015). Using the OMI aerosol index and absorption aerosol optical depth to evaluate the NASA MERRA Aerosol Reanalysis. *Atmos. Chem. Phys.* 15: 5743–5760.
- Buchard, V., da Silva, A.M., Randles, C.A., Colarco, P., Ferrare, R., Hair, J., Hostetler, C., Tackett, J. and Winker, D. (2016). Evaluation of the surface PM_{2.5} in Version 1 of the NASA MERRA Aerosol Reanalysis over the United States. *Atmos. Environ.* 125: 100–111.
- Chang, J.C. and Hanna, S.R. (2004). Air quality model performance evaluation. *Meteorol. Atmos. Phys.* 87: 167–196.
- Chin, M., Ginoux, P., Kinne, S., Torres, O., Holben, B.N., Duncan, B.N., Martin, R.V., Logan, J.A., Higurashi, A. and Nakajima, T. (2002). Tropospheric aerosol optical thickness from the GOCART model and comparisons with satellite and sun photometer measurements. *J. Atmos. Sci.* 59: 461–483.
- Cooper, J.A. (1980). Environmental impact of residential wood combustion emissions and its implications. *J. Air Pollut. Control Assoc.* 30: 855–861.
- d'Almeida, G.A. (1986). A model for Saharan dust transport. *J. Clim. Appl. Meteorol.* 25: 903–916.
- Groblicki, P.J., Wolff, G.T. and Countess, R.J. (1981). Visibility-reducing species in the Denver “brown cloud”—I. Relationships between extinction and chemical composition. *Atmos. Environ.* 15: 2473–2484.
- Hand, J.L. *et al.* (2011). *Spatial and Seasonal Patterns and Temporal Variability of Haze and its Constituents in the United States—Report V.* Cooperative Institute for Research in the Atmosphere and Colorado State University. ISSN 0737-5352-87.
- Haywood, J. and Boucher, O. (2000). Estimates of the direct and indirect

radiative forcing due to tropospheric aerosols: a review. *Rev. Geophys.* 38: 513–543.

Hellén, H., Hakola, H., Haaparanta, S., Pietarila, H. and Kauhaniemi and M. (2008). Influence of residential wood combustion on local air quality. *Sci. Total Environ.* 393: 283–290.

Laden, F., Neas, L.M., Dockery, D.W. and Schwartz, J. (2000). Association of fine particulate matter from different sources with daily mortality in six U.S. cities. *Environ. Health Persp.* 108: 941–947.

Pandis, S.N., Skyllakou, K., Florou, K., Kostenidou, E., Kaltsonoudis, C., Hasa, E. and Presto, A.A. (2016). Urban particulate matter pollution: a tale of five cities. *Farad. Discuss.* 189: 277–290.

Putaud, J.P., Raes, F., van Dingenen, R., Brüggemann, E., Facchini, M.C., Decesari, S., Fuzzi, S., Gehrig, R., Hüglin, C., Laj, P., Lorbeer, G., Maenhaut, W., Mihalopoulos, N., Müller, K., Querol, X., Rodriguez, S., Schneider, J., Spindler, G., ten Brink, H., Tørseth, K. and Wiedensohler, A. (2004). A European aerosol phenomenology—2, Chemical characteristics of particulate matter at kerbside, urban, rural and background sites in Europe. *Atmos. Environ.* 38: 2579–2595.

Putaud, J.P., van Dingenen, R., Alastuey, A., Bauer, H., Birmili, W., Cyrys, J., Flentje, H., Fuzzi, S., Gehrig, R., Hansson, H.C., Harrison, R.M., Herrmann, H., Hitzenberger, R., Hüglin, C., Jones, A.M., Kasper-Giebl, A., Kiss, G., Kousa, A., Kuhlbusch, T.A.J., Lefebvre, G., Maenhaut, W., Molnar, A., Moreno, T., Pekkanen, J., Perrino, C., Pitz, M., Puxbaum, H., Querol, X., Rodriguez, S., Salma, I., Schwarz, J., Smolik, J., Schneider, J., Spindler, G., ten Brink, H., Tursic, J., Viana, M., Wiedensohler, A. and Raes, F. (2010). A European aerosol phenomenology—3, Physical and chemical characteristics of particulate matter from 60 rural, urban, and kerbside sites across Europe. *Atmos. Environ.* 44: 1308–1320.

Remer, L.A., Kaufman, Y.J., Tanré, D., Mattoo, S., Chu, D.A., Martins, J.V., Li, R.R., Ichoku, C., Levy, R.C., Kleidman, R.G., Eck, T.F., Vermote, E. and Holben, B.N. (2005). The MODIS aerosol algorithm, products, and validation. *J. Atmos. Sci.* 62: 947–973.

Rienecker, M.M., Suarez, M.J., Todling, R., Bacmeister, J., Takacs, L., Liu, H.C., Sienkiewicz, M., Koster, R.D., Gelaro, R., Stajner, I. and Nielsen, J.E. (2008). The GEOS-5 Data Assimilation System—Documentation of Versions 5.0.1, 5.1.0, and 5.2.0. *Technical Report Series on Global Modeling and Data Assimilation*, vol. 27. NASA/TM-2008-104606.

Rienecker, M.M., Suarez, M.J., Gelaro, R., Todling, R., Bacmeister, J., Liu, E., Bosilovich, M.G., Schubert, S.D., Takacs, L., Kim, G.K., Bloom, S., Chen, J., Collins, D., Conaty, A., da Silva, A., Gu, W., Joiner, J., Koster, R.D., Lucchesi, R., Molod, A., Owens, T., Pawson, S., Pegion, P., Redder, C.R.,

- Reichle, R., Robertson, F.R., Ruddick, A.G., Sienkiewick and M., Woollen, J. (2011). MERRA: NASA's modern-era retrospective analysis for research and application. *J. Clim.* 24: 3624–3648.
- Schwartz, J. and Neas, L.M. (2000). Fine particles are more strongly associated than coarse particles with acute respiratory health effects in schoolchildren. *Epidemiology* 11: 6–10.
- Seinfeld, J.H. and Pandis, S.N. (1998). *Atmospheric chemistry and physics: from air pollution to climate change*. John Wiley, New York.
- Sexton, K., Spengler, J.D., Treitman, R.D. and Turner, W.A. (1984). Winter air quality in a wood-burning community: a case study in Waterbury, Vermont. *Atmos. Environ.* 18: 1357–1370.
- Tørseth, K., Aas, W., Breivik, K., Fjæraa, A.M., Fiebig, M., Hjellbrekke, A.G., Lund Myhre, C., Solberg, S. and Yttri, K.E. (2012). Introduction to the European monitoring and evaluation Programme (EMEP) and observed atmospheric composition change during 1972–2009. *Atmos. Chem. Phys.* 12: 5447–5481.
- Tsyro, S., Aas, W., Soares, J., Sofiev, M., Berge, H. and Spindler, G. (2011). Modelling of sea salt concentrations over Europe: key uncertainties and comparison with observations. *Atmos. Chem. Phys.* 11: 10367–10388.
- Willmott, C.J. (1982). Some comments on the evaluation of model performance. *Bull. Am. Meteorol. Soc.* 63: 1309–1313.

4 Evaluation of PM_{2.5} surface concentrations simulated by Version 1 of NASA's MERRA Aerosol Reanalysis over Israel and Taiwan

Abstract

Version 1 of the NASA MERRA Aerosol Reanalysis (MERRAero) assimilates bias-corrected aerosol optical depth (AOD) data from MODIS-Terra and MODIS-Aqua, and simulates particulate matter (PM) concentration data to reproduce a consistent database of AOD and PM concentration around the world from 2002 to the end of 2015. The purpose of this paper is to evaluate MERRAero's simulation of fine PM concentration against surface measurements in two regions of the world with relatively high levels of PM concentration but with profoundly different PM composition, those of Israel and Taiwan. Being surrounded by major deserts, Israel's PM load is characterized by a significant contribution of mineral dust, and secondary contributions of sea salt particles, given its proximity to the Mediterranean Sea, and sulfate particles originating from Israel's own urban activities and transported from Europe. Taiwan's PM load is composed primarily of anthropogenic particles (sulfate, nitrate and carbonaceous particles) locally produced or transported from China, with an additional contribution of springtime transport of mineral dust originating from Chinese and Mongolian deserts. The evaluation in Israel produced favorable results with MERRAero slightly overestimating measurements by 6% on average and reproducing an excellent year-to-year and seasonal fluctuation. The evaluation in Taiwan was less favorable with MERRAero underestimating measurements by 42% on average. Two likely reasons explain this discrepancy: emissions of anthropogenic PM and their precursors are largely uncertain in China, and MERRAero doesn't include nitrate particles in its simulation, a pollutant of predominately anthropogenic sources. MERRAero nevertheless simulates well the concentration of fine PM during the summer, when Taiwan is least affected by the advection of pollution from China.

Résumé

La 1^{ère} version de la réanalyse des aérosols MERRAero développée à la NASA assimile les données de profondeur optique des aérosols (AOD) mesurées par MODIS-Terra et MODIS-Aqua, et simule la concentration des matières particulaires (PM) pour reproduire une base de données cohérente

de l'AOD et de la concentration des PM autour du monde de 2002 à 2015. L'objectif de cet article est d'évaluer la simulation de la concentration des particules fines à l'aide d'observations à la surface dans deux régions du monde qui observent régulièrement des concentrations relativement élevées de PM mais dont leur composition est très différente, celles d'Israël et de Taïwan. Israël étant entouré de grands déserts, la composition des PM est caractérisée par une contribution significative de poussière minérale. Une contribution importante des particules de sel de mer, due à sa proximité à la Mer Méditerranée, et des particules de sulfate, due aux activités urbaines à l'intérieur même d'Israël et en Europe, est aussi observée. Les PM à Taïwan sont composées principalement de particules d'origine anthropique (sulfates, nitrates et particules de carbone) émises localement ou en provenance de la Chine. Une contribution additionnelle de PM au printemps provient de déserts en Chine et en Mongolie. L'évaluation en Israël a reproduit des résultats très favorables; MERRAero surestime légèrement la concentration observée de 6% en moyenne et a reproduit une excellente fluctuation annuelle et saisonnière. L'évaluation à Taïwan était moins favorable; MERRAero sous-estime les observations de 42% en moyenne. Deux raisons expliquent ce biais : 1) les émissions chinoises de particules anthropiques et de leurs précurseurs sont marquées par des incertitudes importantes, et 2) MERRAero ne simule pas la concentration des nitrates, un contaminant dont les sources sont largement anthropiques. Néanmoins, MERRAero simule bien la concentration de PM pendant l'été, lorsque Taïwan est le moins affecté par l'advection de pollution d'origine chinoise.

4.1 Introduction

NASA's Modern-Era Retrospective Analysis for Research and Application (MERRA, Rienecker *et al.*, 2011) is a reanalysis tool integrating satellite observations from the Earth Observing System and model data from the 5th version of the Goddard Earth Observing System (GEOS-5) atmospheric model and data assimilation system (Rienecker *et al.*, 2008) in order to produce a consistent database in both time and space of various environmental variables around the world since the beginning of the satellite era. Recently, bias-corrected aerosol optical depth (AOD) observations from the Moderate Resolution Imaging Spectroradiometers (MODIS, Remer *et al.*, 2005) on board the Terra and Aqua satellites, as well as the Goddard Chemistry, Aerosol, Radiation and Transport (GOCART) model (Chin *et al.*,

2002) were included in MERRA to create a reanalysis of aerosols labelled “MERRAero.” GOCART simulates the sources, sinks, transport and concentrations of sulfate (SO₄), organic carbon (OC), black carbon (BC), dust (DS) and sea salt (SS) aerosols (Chin *et al.*, 2002; Colarco *et al.*, 2010). DS and SS emissions are a function of surface properties and wind speed at the surface, and their respective concentrations are classified in different diameter bins. Sources of other species are simulated from emission inventories, including their precursors. Sulfur dioxide (SO₂, the precursor of SO₄) anthropogenic emissions are input from the Emission Database for Global Atmospheric Research (EDGAR) version 4.1 inventory from 2005 and biomass burning emissions (primarily OC and BC) are input from NASA’s Quick Fire Emission Dataset (QFED) version 2.1 (Buchard *et al.*, 2015).

MERRAero simulates the concentrations of the five aerosol species listed in the previous paragraph all over the world with a resolution of 0.5° latitude by 0.625° longitude and 72 vertical layers (from the surface to 80 km) from 2002 to the end of 2015 (Buchard *et al.*, 2015). Considering that these aerosol species, also referred to as airborne particulate matter (PM), affect public health and visibility differently depending on their size and chemistry (e.g., Groblicki *et al.*, 1981; Schwartz and Neas, 2000; Laden *et al.*, 2000), MERRAero’s differentiation of the aerosols’ chemical speciation is a significant improvement for studying a broad range of air quality issues around the world since very few monitoring networks make such a distinction of local PM observations, but especially in regions with unreliable or scarce monitoring.

Different components of MERRAero have been evaluated in different regions of the world. Its assimilation of AOD has been validated over Africa, South America, Central and Eastern Asia using many remote sensing instruments (Buchard *et al.*, 2015); in the United States, the surface concentrations of PM_{2.5}, their chemical speciation and SO₂ has been thoroughly evaluated (Buchard *et al.*, 2014; 2016); and in Europe, an

evaluation of the surface concentrations of PM₁₀, PM_{2.5} and some of their chemical speciation has been performed (Provençal *et al.*, 2016). The concentrations of PM₁₀, PM_{2.5} and SO₄ were generally well simulated in both the U.S. and Europe but Buchard *et al.* (2016) and Provençal *et al.* (2016) noticed an underestimation of carbonaceous concentrations in urban/suburban locations, particularly in winter, due to unresolved sources by MERRAero.

The U.S. and Europe have similar PM signatures in the sense that both regions are highly industrialized and therefore anthropogenic particles contribute significantly to their PM load. At the same time, implementation of air quality regulation has successfully reduced the emissions of various atmospheric pollutants across the U.S. and Europe over the last decades (e.g., Vestreng *et al.*, 2007; Granier *et al.*, 2011; Hand *et al.*, 2012; Klimont *et al.*, 2013; Xing *et al.*, 2013; de Gouw *et al.*, 2014) and, as a result, maintained relatively low levels of PM concentration. There are nevertheless important differences with respect to the chemical speciation of PM between the two regions such as a predominance of carbonaceous particles over the Western U.S. due to summer wildfires and a predominance of dust particles over Southern Europe due to its proximity to the Sahara desert.

The PM signature in the U.S. and Europe is not representative of many other regions in the world where PM sources and pollution control are profoundly different. In order for MERRAero to achieve optimal reliability for studying air quality issues around the world, the purpose of this article is to pursue MERRAero's evaluation in regions with different and distinct aerosol signatures, those of Israel and Taiwan. The evaluation in Israel, a region with a heavy PM load due to its proximity to major deserts, will ascertain MERRAero's ability to simulate the concentration of aerosol originating from natural sources. Taiwan being located in a region of the world which is routinely experiencing severe air pollution episodes, the evaluation there will provide insight on MERRAero's applicability in highly

polluted regions where its contribution would be most beneficial.

4.2 Locations and methods

4.2.1 Israel and Taiwan

Israel is located in Western Asia, surrounded by the Mediterranean Sea, the Sahara desert and the Middle Eastern deserts. Its PM concentration load is relatively high, composed largely of mineral DS (Kushelevsky *et al.*, 1983; Malenky *et al.*, 1983; Foner and Ganor, 1992) with an occasionally important contribution from SS particles when the wind is blowing inland (Foner and Ganor, 1992). PM concentrations in urban areas such as the coastal city of Tel Aviv are even higher due to anthropogenic SO₄ locally produced or transported from Europe (Foner and Ganor, 1992). Rural locations in Israel have also been impacted by the advection of SO₄ particles originating from Europe (Luria *et al.*, 1989).

Taiwan is an island located in Eastern Asia, separated from mainland China by the Taiwan Strait. Its concentration level of PM is fairly high, especially in urban areas (Chen *et al.*, 1999), caused by industrial and transportation activities within Taiwan but also due to wintertime synoptic features that transport polluted air from China (Lin *et al.*, 2005). SO₄, OC, BC, nitrate (NO₃) and ammonium (NH₄) particles together compose a large portion of PM concentration (Tsai and Cheng, 1999; Lin, 2002; Chen *et al.*, 2003; Tsai and Cheng, 2004; Tsai and Kuo, 2005; Lin *et al.*, 2008). Taiwan nevertheless enjoys cleaner air during the summer, coinciding with the typhoon season which sweeps the island with strong winds and heavy rain (Lin *et al.*, 2008). In spring, Taiwan is also impacted by the advection of dust originating from Chinese and Mongolian deserts (Chen *et al.*, 2004).

4.2.2 Evaluation method

MERRAero simulates the concentrations of five PM_{2.5} (PM with diameter $\leq 2.5 \mu\text{m}$) species every hour: SO₄, OC, BC, DS_{2.5} and SS_{2.5}. From these, it is possible to apply a mass reconstruction method to estimate the total concentration of PM_{2.5}. Chow *et al.* (2015) reviewed 11 commonly used equations to reconstruct PM mass from speciation measurements which are usually determined by the measurements available. The equations usually took the following form:

$$(4.1) \text{ PM} = \text{Inorganic ions} + \text{Organic matter} + \text{BC} + \text{DS} + \text{SS}$$

Inorganic ions include SO₄, NO₃ and NH₄ ions. When NH₄ measurements were lacking, SO₄ and NO₃ were assumed to be fully neutralized by NH₄ in the form of ammonium sulfate ((NH₄)₂SO₄) and ammonium nitrate (NH₄NO₃) by multiplying their respective concentrations by 1.375 and 1.29; (NH₄)₂SO₄ being composed of 73% of SO₄ by mass and NH₄NO₃ being similarly composed of 78% of NO₃. The concentration of inorganic ions was ultimately estimated by: $1.375 \times [\text{SO}_4] + 1.29 \times [\text{NO}_3]$ (brackets denote concentration). [NH₄NO₃] was occasionally omitted altogether when NO₃ measurements were lacking or unreliable (e.g., Malm *et al.*, 1994).

The concentration of particulate organic matter (POM) was estimated through OC measurements multiplied by a coefficient which took into account other organic compounds found in POM but not measured. Commonly and historically, a coefficient of 1.4 was used (Turpin and Lim, 2001; Chow *et al.*, 2015), but Turpin and Lim (2001) argued that such a value is often too low. They recommended a value of 1.6 ± 0.2 for urban carbonaceous particles, 2.1 ± 0.2 for aged (nonurban) particles and a value as high as 2.6 for biomass burning particles.

Taking into consideration the PM species simulated by MERRAero and given that this evaluation is performed in a combination of urban and non-urban locations, the following reconstruction is used:

$$(4.2) \quad [\text{PM}_{2.5}] = 1.375 \times [\text{SO}_4] + 1.8 \times [\text{OC}] + [\text{BC}] + [\text{DS}_{2.5}] + [\text{SS}_{2.5}]$$

Eq. 4.2 lacks the concentration of NO_3 particles whose sources are predominantly anthropogenic in nature (Delmas *et al.*, 1997).

MERRAero's simulation at the surface is compared to hourly observations of $[\text{PM}_{2.5}]$ measured at 11 locations in Israel between 2003 and 2014, and 13 locations in and around Taiwan between 2005 and 2014 (Fig. 4.1). A spatial consistency algorithm is applied to assure reliability of the observed and simulated data which goes as follows: since trace concentrations are usually lognormally distributed, the bias between log-simulated concentration and log-observed concentration ($B_{log} = \ln(C_s) - \ln(C_o)$; C_s : simulated concentration, C_o : observed concentration) is calculated at all locations within each study areas on a given hour; the average and standard deviation of B_{log} are calculated and used to define a reliability interval which justifies ~95% of the normal distribution: $\overline{B_{log}} \pm 2\sigma_{B_{log}}$; all data pairs that fall outside this interval are excluded.

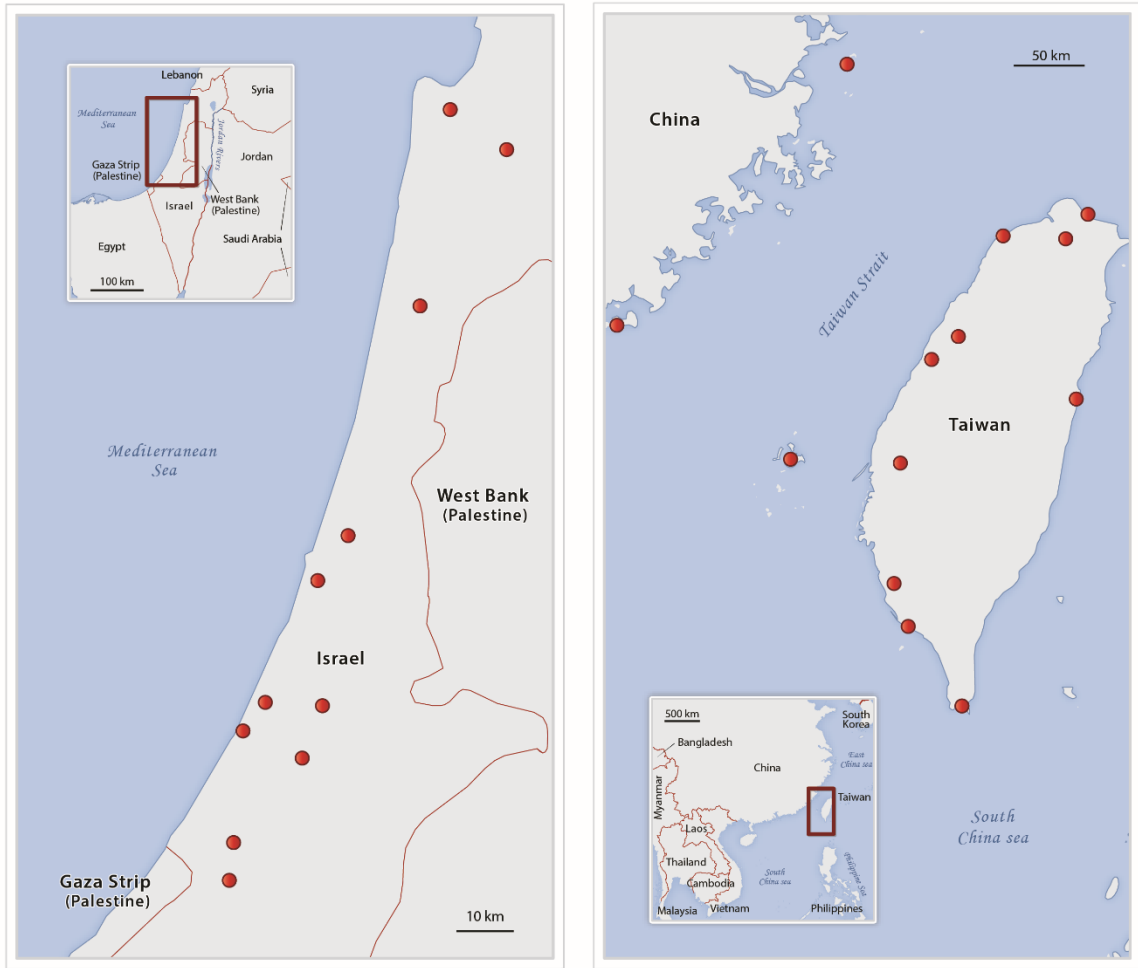


Fig. 4.1: Locations of monitoring stations in Israel and Taiwan.

Performance statistics are calculated to quantify MERRAero's accuracy: the mean fraction $\bar{F} = \bar{C}_s / \bar{C}_o$, the mean bias $\bar{B} = \bar{C}_s - \bar{C}_o$, the standard deviation of the bias ($SD-B$) and the correlation coefficient (R). Given that trace concentrations are lognormally distributed, it is also relevant to compute log-transformed statistics: $\overline{B_{log}} = \overline{\log(C_s)} - \overline{\log(C_o)}$, $SD-B_{log}$ and R_{log} . Willmott (1982) criticized the use of R to evaluate model performance since it doesn't directly compare simulated with observed data. Therefore, Chang and Hanna (2004) recommended as a rigorous index to evaluate air quality models the proportion of simulated data which falls within a factor of 2 of observed data ($FAC2$, i.e., proportion of the data which satisfies $0.5 \leq C_o / C_s \leq 2.0$) since this index is not disproportionately sensitive to

extreme values and is unaffected by simplification of errors. Chang and Hanna (2004) considered a model's performance to be reasonably good if $FAC2 \geq 0.5$.

4.3 Results and discussion

4.3.1 Israel

The spatial consistency algorithm excluded 5% of the data in Israel. At $22.5 \mu\text{g}/\text{m}^3$, the $\text{PM}_{2.5}$ load in Israel is high (Tab. 4.1) compared to Europe (Provençal *et al.*, 2017), rural and suburban U.S. (Buchard *et al.*, 2016). Overall, MERRAero simulates $[\text{PM}_{2.5}]$ very well in Israel by slightly overestimating its average concentration by 6% or $1.4 \mu\text{g}/\text{m}^3$ (Tab. 4.1). However, the high $SD-B$ value and modest R suggest significant scatter within the data and a low bias resulting from simplification of errors. On the other hand, it is worth mentioning that SD 's are disproportionately impacted by extreme data pairs. For instance, if such data which fall outside a factor of 5 between observed and simulated concentrations, which represent 2.6% of the sample, \bar{B} and $SD-B$ are reduced to $1.0 \mu\text{g}/\text{m}^3$ and $19.6 \mu\text{g}/\text{m}^3$, respectively. Furthermore, the density scatter plot of Fig. 4.2 reveals that although there is some scatter, the bulk of the data is generally well simulated. This is further supported by a high $FAC2$ value of 76%. The log-transformed data (Tab. 4.1; Fig. 4.2) support a similar analysis. Additionally, Fig. 4.3 compares the annual and monthly fluctuations between simulated and observed data, and illustrates an excellent identity between both datasets.

Tab. 4.1: Performance statistics for the ensemble of locations in Israel and Taiwan. AOC stands for “average observed concentration.”

	Israel	Taiwan
n	1,016,778	1,024,992
AOC ($\mu\text{g}/\text{m}^3$)	22.5	29.8
F	1.06	0.70
\bar{B} ($\mu\text{g}/\text{m}^3$)	1.4	-8.8
SD-B ($\mu\text{g}/\text{m}^3$)	23.8	22.7
\bar{B}_{\log}	0.07	-0.27
SD- B_{\log}	0.66	0.83
R	0.56	0.27
R_{\log}	0.50	0.30
FAC2	0.76	0.59

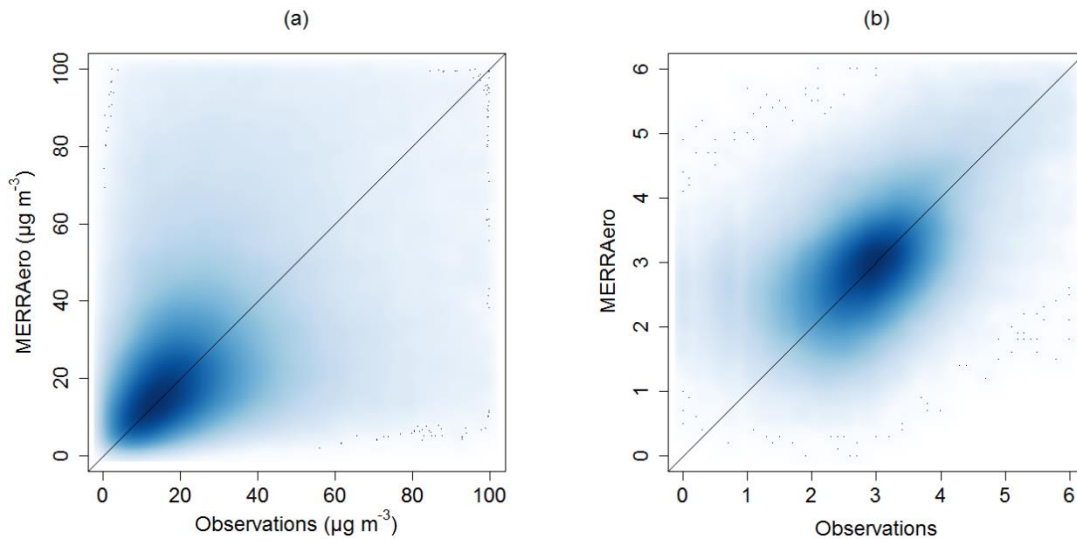


Fig. 4.2: Density scatter plot for (a) observed and simulated $[\text{PM}_{2.5}]$, and (b) log-transformed observed and simulated $[\text{PM}_{2.5}]$ for the ensemble of locations in Israel.

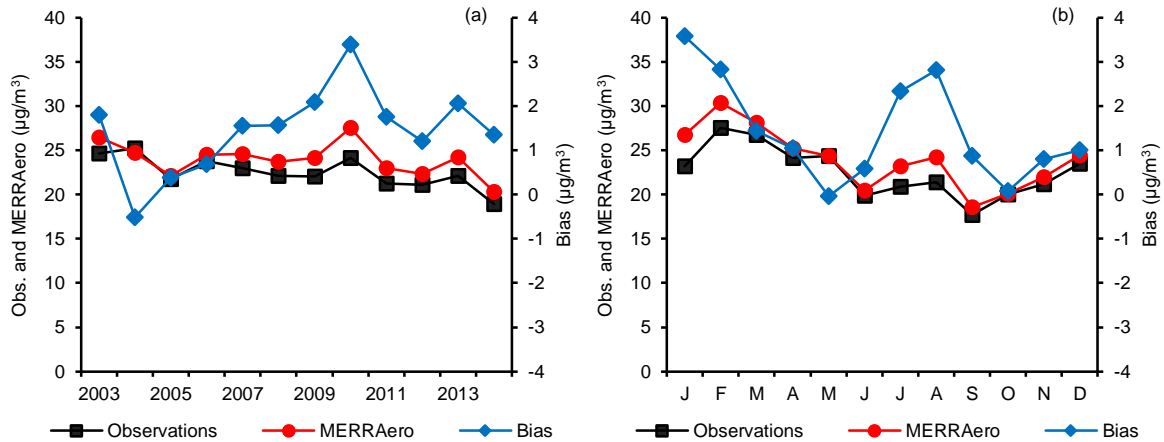


Fig. 4.3: (a) Yearly and (b) monthly average of $[\text{PM}_{2.5}]$ observation, simulation and bias, and (c-d) similarly for the SD and FAC2, for the ensemble of locations in Israel.

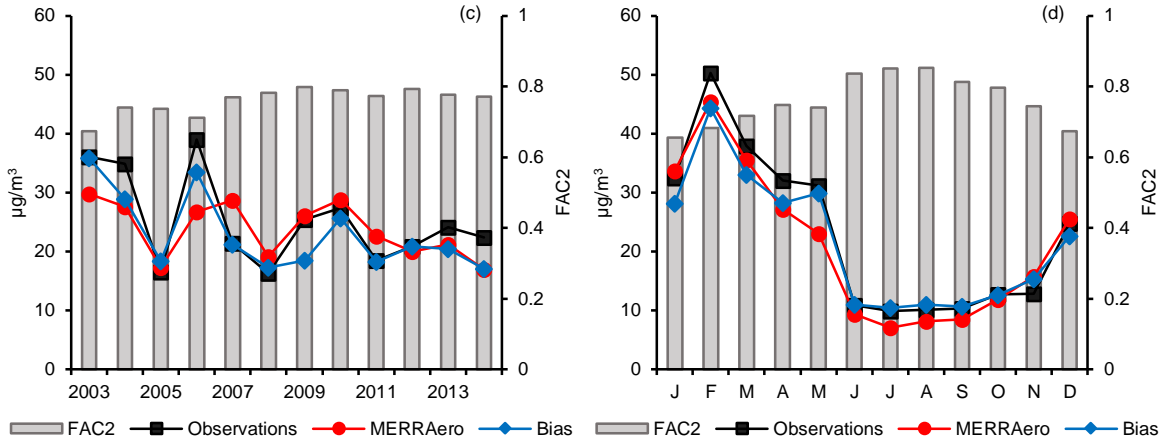


Fig. 4.3 (continued)

MERRAero's ability to accurately estimate $[PM_{2.5}]$ in Israel relies predominantly on its ability to simulate $[DS_{2.5}]$ since $[PM_{2.5}]$ is largely composed of this species (Tab. 4.2) and, to a lesser extent, its ability to simulate $[SO_4]$ and $[SS_{2.5}]$. The evaluation of $[DS_{2.5}]$ in the U.S. revealed important seasonal biases without much impact on the evaluation of $[PM_{2.5}]$ given its small contribution to $[PM_{2.5}]$ there (Buchard *et al.*, 2016). While the U.S. is mostly impacted by long range transport of DS, this evaluation in Israel would suggest that MERRAero performs well in simulating $[DS_{2.5}]$ originating from local sources. $[SO_4]$ has been shown to be well simulated in the U.S. and in Europe (Buchard *et al.*, 2016; Provençal *et al.*, 2016), we therefore have no reason to believe otherwise in this region. MERRAero largely overestimated $[SS_{2.5}]$ in both the U.S. and Europe due in part to measurement biases which could very well be the case in Israel. An overestimation of $[SS_{2.5}]$ could compensate the lack of nitrate particles in the simulation. In any case, the lack of NO_3 particles is likely a minor shortcoming given that they are less abundant than SO_4 and probably contribute little to $[PM_{2.5}]$.

Tab. 4.2: Average concentration simulated by MERRAero for the ensemble of locations in Fig. 4.1 over the study period.

Species	Israel		Taiwan	
	Average concentration ($\mu\text{g}/\text{m}^3$)	Proportion of $\text{PM}_{2.5}$ concentration (%)	Average concentration ($\mu\text{g}/\text{m}^3$)	Proportion of $\text{PM}_{2.5}$ concentration (%)
$\text{PM}_{2.5}$	24.0	—	20.9	—
$(\text{NH}_4)_2\text{SO}_4$	4.5	18.7	9.3	44.3
POM	1.3	5.4	3.0	14.1
BC	0.4	1.7	0.7	3.4
$\text{DS}_{2.5}$	13.9	57.9	2.0	9.3
$\text{SS}_{2.5}$	3.9	16.3	6.1	28.9

4.3.2 Taiwan

The spatial consistency algorithm excluded 3% of the data in Taiwan. The $\text{PM}_{2.5}$ load in Taiwan is higher than in Israel ($29.8 \mu\text{g}/\text{m}^3$; Tab. 4.1). Despite a *FAC2* of 59%, MERRAero’s performance in Taiwan is much less encouraging. On average, MERRAero underestimates total $[\text{PM}_{2.5}]$ by $8.8 \mu\text{g}/\text{m}^3$, a factor of 1.42. The *SD-B* is also high and *R* is positive but low. Fig. 4.4 reveals that the bulk of the simulated data, 66% to be precise, is indeed underestimated.

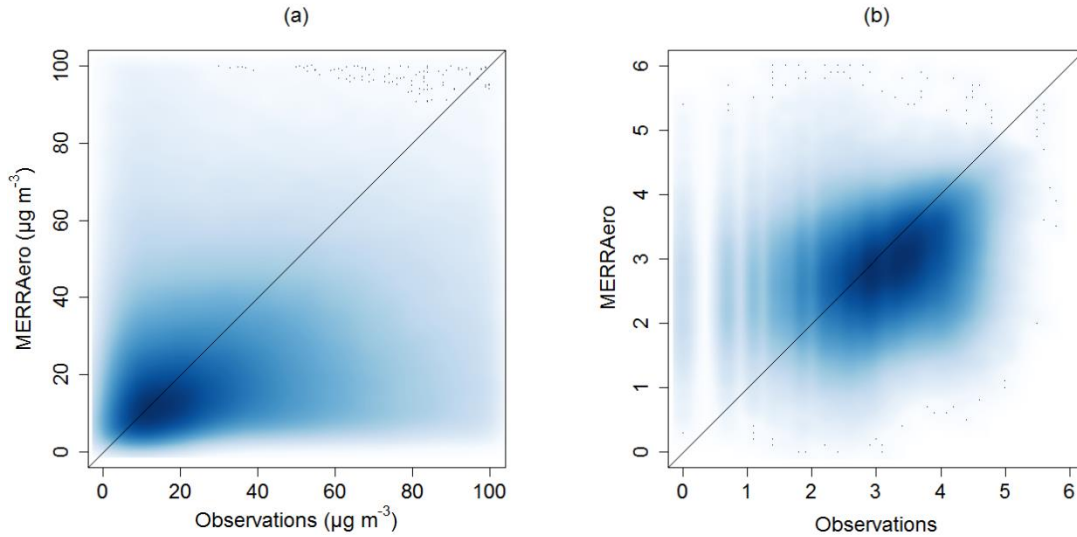


Fig. 4.4: Density scatter plot for (a) observed and simulated $[\text{PM}_{2.5}]$, and (b) log-transformed observed and simulated $[\text{PM}_{2.5}]$ for the ensemble of locations in Taiwan.

MERRAero’s simulation of $[\text{PM}_{2.5}]$ in Taiwan is mostly anthropogenic in nature (Tab. 4.2) with a significant proportion attributed to SO_4 . This information coupled with Fig. 4.5 which compares annually and monthly

averaged simulated and observed concentrations reveals a few clues as to why MERRAero's performance is less favorable in Taiwan. The evaluation performs well during the summer (typhoon) season but deteriorates during the rest of the year when Taiwan is most impacted by the advection of pollution from China. The use of a constant inventory of SO₂ emissions from 2005 is problematic in the long term since it is increasingly becoming antiquated with every passing year. Indeed, in 2005, China successfully implemented comprehensive policies to reduce SO₂ emissions. As a result, SO₂ emissions and, by extension, SO₄ concentrations have been decreasing since 2006 (Lu *et al.*, 2010; 2011; Wang and Hao, 2012; Zhang *et al.*, 2012; Klimont *et al.*, 2013; Zhao *et al.*, 2013a; Zhao *et al.*, 2013b). This is reflected in Fig. 4.5 with a near constant decrease of [PM_{2.5}] observations as opposed to the near constant year to year concentrations simulated by MERRAero. SO₂ emission estimates from China are also crippled with uncertainties (Smith *et al.*, 2011). The lack of nitrate particles in the simulation is much more troublesome in Taiwan given that [PM_{2.5}] is mostly composed of anthropogenic particles. This would certainly explain a significant portion of the underestimation. Another possible explanation for the wintertime discrepancy, one that's also been highlighted by Provençal *et al.* (2016) for the evaluation in Europe, is local sources of pollution unresolved by MERRAero. While MERRAero's simulation takes into account urban sources of pollution, its resolution is too coarse to capture the urban core of cities. Some monitoring stations in Taiwan (Fig. 4.1) are located in or around large cities, but none of them are located in their downtown core. We therefore don't expect them to be overly influenced by local sources of pollution. Nevertheless, some influence of unresolved sources should be anticipated. The springtime maximum observed in Fig. 4.5 is the likely contribution of long range transport of DS, well captured by MERRAero.

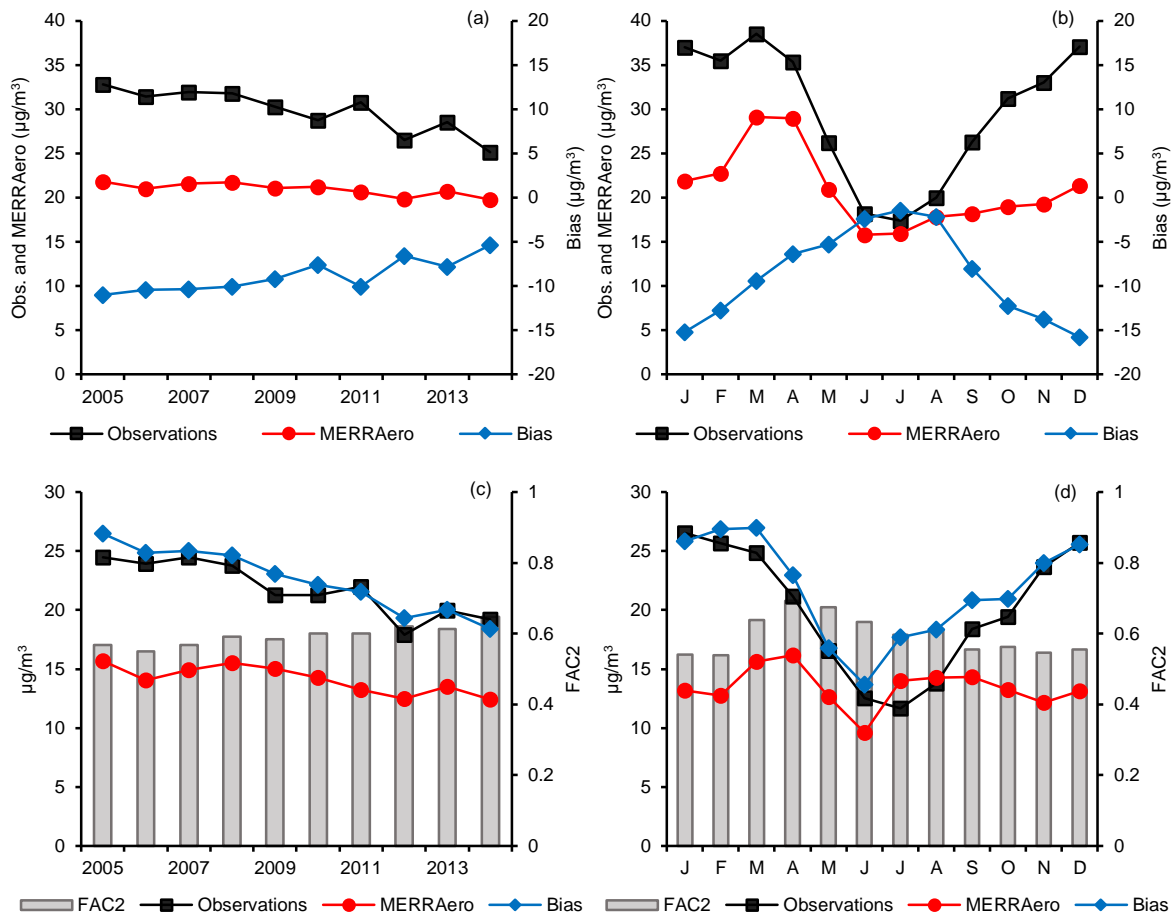


Fig. 4.5: (a) Yearly and (b) monthly average of $[\text{PM}_{2.5}]$ observation, simulation and bias, and (c-d) similarly for the SD and FAC2, for the ensemble of locations in Taiwan.

4.4 Conclusion

We evaluated version 1 of the MERRA Aerosol Reanalysis' ability to simulate the concentration of $\text{PM}_{2.5}$ in two regions of the world with relatively high levels of PM concentration but with profoundly different PM composition. Israel is characterized by a high concentration of $\text{PM}_{2.5}$ due to its proximity to major deserts and to the highly saline Mediterranean Sea. Its $\text{PM}_{2.5}$ load is composed mostly of natural particles (mineral dust and sea salt) with some contribution of anthropogenic particles (sulfate) originating from Israel's urban activities and advection from Europe. Taiwan's high $\text{PM}_{2.5}$ concentration is mostly anthropogenic in nature due to Taiwan's own

industrial activities and to advection of polluted air from China with some contribution of dust particles originating from East Asian deserts.

The evaluation reproduced favorable results in Israel where MERRAero slightly overestimated actual $PM_{2.5}$ concentrations by 6% on average. Although there is scatter within the distribution, most of the simulation is reasonably accurate with over 75% of the simulated data falling within a factor of 2 of measurements. Given that most of $PM_{2.5}$ in Israel is mineral dust, this evaluation supports the assumption that MERRAero performs well in simulating the concentration of fine dust originating from local and regional sources throughout the year.

The evaluation is not as favorable in Taiwan where MERRAero significantly underestimated measured $PM_{2.5}$ concentrations by 42% on average. Given that $PM_{2.5}$ in Taiwan is mostly composed of anthropogenic particles, many of which originate from China, two likely reasons explain this outcome: the uncertainty with respect to Chinese emissions and the lack of nitrate particles in the simulation. The simulation was indeed better during the summer when Taiwan is least impacted by advection of polluted air from China.

References

- Buchard, V., da Silva, A.M., Colarco, P., Krotkov, N., Dickerson, R.R., Stehr, J.W., Mount, G., Spinei, E., Arkinson, H.L. and He, H. (2014). Evaluation of GEOS-5 sulfur dioxide simulations during the Frostburg, MD 2010 field campaign. *Atmos. Chem. Phys.* 14: 1929–1941.
- Buchard, V., da Silva, A.M., Colarco, P.R., Darmenov, A., Randles, C.A., Govindaraju, R., Torres, O., Campbell, J. and Spurr, R. (2015). Using the OMI aerosol index and absorption aerosol optical depth to evaluate the NASA MERRA Aerosol Reanalysis. *Atmos. Chem. Phys.* 15: 5743–5760.
- Buchard, V., da Silva, A.M., Randles, C.A., Colarco, P., Ferrare, R., Hair, J., Hostetler, C., Tackett, J. and Winker, D. (2016). Evaluation of the surface PM_{2.5} in Version 1 of the NASA MERRA Aerosol Reanalysis over the United States. *Atmos. Environ.* 125: 100–111.
- Chang, J.C. and Hanna, S.R. (2004). Air quality model performance evaluation. *Meteorol. Atmos. Phys.* 87: 167–196.
- Chen, K.S., Lin, C.F. and Chou, Y.M. (2003). Determination of source contribution to ambient PM_{2.5} in Kaohsiung, Taiwan, using a receptor model. *J. Air Waste Manage. Assoc.* 51: 489–498.
- Chen, M.L., Mao, T.F. and Lin, I.K. (1999). The PM_{2.5} and PM₁₀ particles in urban areas of Taiwan. *Sci. Total Environ.* 226: 227–235.
- Chen, Y.S., Sheen, P.C., Chen, E.R., Liu, Y.K., Wu, T.N. and Yang, C.Y. (2004). Effects of Asian dust storm events on daily mortality in Taipei, Taiwan. *Environ. Res.* 95: 151–155.
- Chin, M., Ginoux, P., Kinne, S., Torres, O., Holben, B.N., Duncan, B.N., Martin, R.V., Logan, J.A., Higurashi, A. and Nakajima, T. (2002). Tropospheric aerosol optical thickness from the GOCART model and comparisons with satellite and sun photometer measurements. *J. Atmos. Sci.* 59: 461–483.
- Chow, J.C., Lowenthal, D.H., Antony Chen, L.W., Wang, X. and Watson, J.G. (2015). Mass reconstruction methods for PM_{2.5}: a review. *Air Qual. Atmos. Health* 8: 243–263.
- de Gouw, J.A., Parrish, D.D., Frost, G.J. and Trainer, M. (2014). Reduced emissions of CO₂, NO_x, and SO₂ from U.S. power plants owing to switch from coal to natural gas with combined cycle technology. *Earth's Future* 2: 75–82.
- Delmas, R., Serça, D. and Jambert, C. (1997). Global inventory of NO_x sources. *Nutr. Cycl. Agroecosyst.* 48: 51–60.
- Foner, H.A. and Ganor, E. (1992). The chemical and mineralogical composition of some urban atmospheric aerosols in Israel. *Atmos. Environ.*

26B: 125–133.

Granier, C., Bessagnet, B., Bond, T., d'Angiola, A., van der Gon, H.D., Frost, G.J., Heil, A., Kaiser, J.W., Kinne, S., Klimont, K., Kloster, S., Lamarque, J.F., Lioussé, C., Masui, T., Meleux, F., Mieville, A., Ohara, T., Raut, J.C., Riahi, K., Schultz, M.G., Smith, S.J., Thompson, A., van Aardenne, J., van der Werf, G.R. and van Vuuren, D.P. (2011). Evolution of anthropogenic and biomass burning emissions of air pollutants at global and regional scales during the 1980–2010 period. *Clim. Chang.* 109: 163–190.

Groblicki, P.J., Wolff, G.T. and Countess, R.J. (1981). Visibility-reducing species in the Denver “brown cloud”—I. Relationships between extinction and chemical composition. *Atmos. Environ.* 15: 2473–2484.

Hand, J.L., Schichtel, B.A., Malm, W.C. and Pitchford, M.L. (2012). Particulate sulfate ion concentration and SO₂ emission trends in the United States from the early 1990s through 2010. *Atmos. Chem. Phys.* 12: 10353–10365.

Klimont, Z., Smith, S.J. and Cofala, J. (2013). The last decade of global anthropogenic sulfur dioxide: 2000–2011 emissions. *Environ. Res. Lett.* 8: 014003.

Kushelevsky, A., Shani, G. and Haccoun, A. (1983). Effect of meteorological conditions on total suspended particulate (TSP) levels and elemental concentration of aerosols in a semi-arid zone (Beer-Sheva, Israel). *Tellus* 35B: 55–64.

Laden, F., Neas, L.M., Dockery, D.W. and Schwartz, J. (2000). Association of fine particulate matter from different sources with daily mortality in six U.S. cities. *Environ. Health Persp.* 108: 941–947.

Lin, C.H., Wu, Y.L., Lai, C.H., Watson, J.G. and Chow, J.C. (2008). Air quality measurements from the southern particulate matter supersite in Taiwan. *Aerosol Air Qual. Res.* 8: 233–264.

Lin, C.Y., Liu, S.C., Chou, C.C.K., Huang, S.J., Liu, C.M., Kuo, C.H. and Young, C.Y. (2005). Long-range transport of aerosols and their impact on the air quality of Taiwan. *Atmos. Environ.* 39: 6066–6076.

Lin, J.J. (2002). Characterization of the major chemical species in PM_{2.5} in the Kaohsiung City, Taiwan. *Atmos. Environ.* 36: 1911–1920.

Lu, Z., Streets, D.G., Zhang, Q., Wang, S., Carmichael, G.R., Cheng, Y.F., Wei, C., Chin, M., Diehl, T. and Tau, Q. (2010). Sulfur dioxide emissions in China and sulfur trends in East Asia since 2000. *Atmos. Chem. Phys.* 10: 6311–6331.

Lu, Z., Zhang, Q. and Streets, D.G. (2011). Sulfur dioxide and primary carbonaceous aerosol emissions in China and India, 1996–2010. *Atmos.*

Chem. Phys. 11: 9839–9864.

Luria, M., Lifschitz, B. and Peleg, M. (1989). Particulate sulfate levels at a rural site in Israel. *J. Atmos. Chem.* 8: 241–250.

Malenky, B., van Grieken, R., Van't Dack, L. and Luria, M. (1983). Atmospheric trace element concentration in Jerusalem, Israel. *Atmos. Environ.* 17: 819–822.

Malm, W.C., Sisler, J.F., Huffman, D., Eldred, R.A. and Cahill, T.A. (1994). Spatial and seasonal trends in particle concentration and optical extinction in the United States. *J. Geophys. Res.* 99: 1347–1370.

Provençal, S., Buchard, V., da Silva, A.M., Leduc, R. and Barrette, N. (2017a). Evaluation of PM surface concentration simulated by Version 1 of the NASA MERRA Aerosol Reanalysis over Europe. *Atmos. Pollut. Res.* 8: 374–382.

Remer, L.A., Kaufman, Y.J., Tanré, D., Mattoo, S., Chu, D.A., Martins, J.V., Li, R.R., Ichoku, C., Levy, R.C., Kleidman, R.H., Eck, T.F., Vermote E. and Holben, B.N. (2005). The MODIS aerosol algorithm, products, and validation. *J. Atmos. Sci.* 62: 947–973.

Rienecker, M.M., Suarez, M.J., Todling, R., Bacmeister, J., Takacs, L., Liu, H.C., Sienkiewick, M., Koster, R.D., Gelaro, R., Stajner, I. and Nielsen, J.E. (2008). The GEOS-5 data assimilation system—Documentation of versions 5.0.1, 5.1.0, and 5.2.0. *Technical Report Series on Global Modeling and Data Assimilation*, vol. 27, NASA/TM-2008-104606.

Rienecker, M.M., Suarez, M.J., Gelaro, R., Todling, R., Bacmeister, J., Liu, E., Bosilovich, M.G., Schubert, S.D., Takacs, L., Kim, G.K., Bloom, S., Chen, J., Collins, D., Conaty, A., da Silva, A., Gu, W., Joiner, J., Koster, R.D., Lucchesi, R., Molod, A., Owens, T., Pawson, S., Pegion, P., Redder, C.R., Reichle, R., Robertson, F.R., Ruddick, A.G., Sienkiewick, M. and Woollen, J. (2011). MERRA: NASA's Modern-Era Retrospective Analysis for Research and Application. *J. Clim.* 24: 3624–3648.

Schwartz, J. and Neas, L.M. (2000). Fine particles are more strongly associated than coarse particles with acute respiratory health effects in schoolchildren. *Epidemiology* 11: 6–10.

Smith, S.J., van Aardenne, J., Klimont, K., Andres, R.J., Volke, A. and Delgado Arias, S. (2011). Anthropogenic sulfur dioxide emissions: 1850–2005. *Atmos. Chem. Phys.* 11: 1101–1116.

Tsai, Y.I. and Cheng, M.T. (1999). Visibility and aerosol chemical composition near the coastal area in central Taiwan. *Sci. Total Environ.* 231: 37–51.

Tsai, Y.I. and Cheng, M.T. (2004). Characterization of chemical species in atmospheric aerosols in a metropolitan basin. *Chemosphere* 54: 1171–1181.

- Tsai, Y.I. and Kuo, S.C. (2005). PM_{2.5} aerosol water content and chemical composition in a metropolitan and a coastal area in southern Taiwan. *Atmos. Environ.* 39: 4827–4839.
- Turpin, B.J. and Lim, H.J. (2001). Species contribution to PM_{2.5} mass concentration: revisiting common assumptions for estimating organic mass. *Aerosol Sci. Technol.* 35: 602–610.
- Vestreng, V., Myhre, G., Fagerli, H., Reis, S. and Tarrasón, L. (2007). Twenty-five years of continuous sulfur dioxide emission reduction in Europe. *Atmos. Chem. Phys.* 7: 3663–3681.
- Wang, S. and Hao, J. (2012). Air quality management in China: issues, challenges, and options. *J. Environ. Sci.* 21: 2–13.
- Willmott, C.J. (1982). Some comments on the evaluation of model performance. *Bull. Am. Meteorol. Soc.* 63: 1309–1313.
- Xing, J., Pleim, J., Mathur, R., Pouliot, G., Hogrefe, C., Gan, C.M. and Wei, C. (2013). Historical gaseous and primary aerosol emissions in the United States from 1990–2010. *Atmos. Chem. Phys.* 13: 7531–7549.
- Zhang, Q., He, K. and Huo, H. (2012). Cleaning China's air. *Nature* 484: 161–162.
- Zhao, B., Wang, S., Dong, X., Wang, J., Duan, L., Fu, X., Hao, J. and Fu, J. (2013). Environmental effects of the recent emission changes in China: implications for particulate matter pollution and soil acidification. *Environ. Res. Lett.* 8: 024031.
- Zhao, Y., Zhang, J. and Nielsen, C.P. (2013). The effects of recent control policies on trends in emissions of anthropogenic atmospheric pollutants and CO₂ in China. *Atmos. Chem. Phys.* 13: 487–508.

5 AOD distributions and trends of major aerosol species over a selection of the world's most populated cities based on the 1st Version of NASA's MERRA Aerosol Reanalysis

Abstract

NASA recently extended the Modern-Era Retrospective Analysis for Research and Application (MERRA) with an atmospheric aerosol reanalysis which includes five particulate species: sulfate, organic matter, black carbon, mineral dust and sea salt. The MERRA Aerosol Reanalysis (MERRAero) is an innovative tool to study air quality issues around the world for its global and constant coverage and its distinction of aerosol speciation expressed in the form of aerosol optical depth (AOD). The purpose of this manuscript is to apply MERRAero to the study of urban air pollution at the global scale by analyzing the AOD over a period of 13 years (2003–2015) and over a selection of 200 of the world's most populated cities in order to assess the impacts of urbanization, industrialization, air quality regulations and regional transport which affect urban aerosol load. Environmental regulations and the recent global economic recession helped to decrease the AOD and sulfate aerosols in most cities of North America, Europe and Japan. Rapid industrialization in China over the last two decades resulted in Chinese cities having the highest AOD values in the world. China has nevertheless recently implemented emission control measures, which are showing early signs of success in many cities of Southern China, where AOD decreased substantially over the last 13 years. The AOD over South American cities, dominated by carbonaceous aerosols, also decreased over the last decade due to an increase in commodity prices which slowed deforestation activities in the Amazon rainforest. At the opposite, recent urbanization and industrialization in India and Bangladesh resulted in a strong increase of AOD, sulfate and carbonaceous aerosols in most cities of these two countries. The AOD over most cities in Northern Africa and Western Asia changed little over the last decade. Emissions of natural aerosols, which cities in these two regions tend to be mostly impacted by, don't tend to fluctuate significantly on an annual basis.

Résumé

La NASA a récemment introduit une réanalyse des aérosols

atmosphériques surnommée MERRAero (Modern-Era Retrospective Analysis for Research and Application Aerosol Reanalysis) qui inclut cinq espèces d'aérosols : les particules de sulfate, de matière organique, de carbone noir, de poussière et de sel de mer. MERRAero est un outil novateur pour étudier un large éventail de problématiques sur la qualité de l'air autour du monde par sa couverture globale et constante, et sa distinction des espèces d'aérosols exprimée par leur profondeur optique (AOD). L'objectif de cet article est d'appliquer MERRAero à l'étude de la pollution de l'air urbain à l'échelle globale en analysant l'AOD sur une période de 13 ans (2003–2015) au-dessus de 200 villes parmi les plus peuplées du monde, afin d'évaluer les impacts qu'ont l'urbanisation, l'industrialisation, les politiques environnementales et le transport régional qui affectent la charge des aérosols en milieu urbain. Les politiques environnementales et la récession économique récente ont contribué à réduire l'AOD et les particules de sulfate dans la plupart des villes d'Amérique du Nord, d'Europe et du Japon. La Chine a aussi récemment implanté des mesures de réduction des émissions qui démontrent des premiers signes encourageants dans des villes du sud de la Chine, où l'AOD a significativement diminué. L'AOD au-dessus des villes d'Amérique du Sud a aussi diminué au cours de la dernière décennie en raison d'un ralentissement des activités de déforestation dans la forêt amazonienne. À l'opposé, une forte urbanisation et industrialisation en Inde et au Bangladesh a causé une forte augmentation de l'AOD, des particules de sulfate et de carbone dans la plupart des villes de ces deux pays. L'AOD au-dessus des villes dans le nord de l'Afrique et dans l'ouest de l'Asie a peu changé au cours de la dernière décennie. Les villes dans ces deux régions du monde sont principalement affectées par des émissions d'aérosols d'origine naturelle qui n'ont pas tendance à fluctuer significativement d'une année à l'autre.

5.1 Introduction

Microscopic airborne aerosols have long been a prominent topic of study in the field of environmental science, predominantly in the atmospheric sciences. A considerable amount of literature has emerged in order to better understand the nature of these particles, but more specifically, to assess their impacts on various spheres of life and the environment. Aerosols are found in highly variable space and time distribution, size and chemical composition, and they originate from many sources, both natural and anthropogenic (Pöschl, 2005).

Aerosols considerably affect the environment and its living organisms.

It is well documented that aerosols are a serious health hazard to humans, fauna and flora. They are linked to cardiovascular, respiratory and allergic diseases, as well as enhanced mortality (Pöschl, 2005; Tager, 2013). Aerosols also affect weather and climate. Acting as cloud condensation nuclei, aerosols are an essential element of cloud formation. As such, they play an indirect role in increasing the clouds' and the Earth's albedo as a whole (Haywood and Boucher, 2000; Lohmann and Feichter, 2005). They also affect the Earth's radiation budget as absorbers of radiation, contributing to a warming of the atmosphere, and as reflectors of radiation, in which case they act as a cooling agent (Haywood and Boucher, 2000). Finally, in high enough concentrations, they can significantly reduce visibility (Charlson, 1969; Cheng and Tsai, 2000). This is often associated with episodes of haze, smog and dust storms.

The seriousness of the impacts listed in the previous paragraph is dependent on the aerosols' concentration and size, but particularly on their chemical composition. It is therefore relevant to distinguish between different aerosol species commonly found in the air:

- Sulfate (SO_4) aerosols originate from sulfur dioxide (SO_2) that has been neutralized by ammonium (NH_4) to form ammonium sulfate ($(\text{SO}_4)_2\text{NH}_4$; Forster *et al.*, 2007, sect. 2.4.4.1). SO_2 emissions emerge from fossil fuel and, to a much smaller extent, biomass burning, and therefore are vastly considered as anthropogenic. However, small natural contributions originate from volcanoes and the oceans (Haywood and Boucher, 2000);
- Nitrate (NO_3) aerosols originate from nitrogen oxides (NO_x) that have been neutralized by NH_4 to form ammonium nitrate (NO_3NH_4 ; Forster *et al.*, 2007, sect. 2.4.4.5). NO_3 emissions emanate from a variety of sources such as fossil fuel and biomass burning, bacteria and lightning. Delmas *et al.* (1997) estimated that 83% of NO_3 emissions are anthropogenic in nature;

- Particulate organic matter (POM), composed largely of organic carbon (OC), is the result of fossil fuel and biomass burning. The former is an anthropogenic source while the latter is either a natural or an anthropogenic source. As a whole, sources of POM are widely considered to be anthropogenic (Haywood and Boucher, 2000; Forster *et al.*, 2007, sect. 2.4.4.3);
- Black carbon (BC) particles are the result of incomplete combustion and originate from the same sources as POM (Haywood and Boucher, 2000; Forster *et al.*, 2007, sect. 2.4.4.2);
- Mineral dust (DS) is the product of wind erosion predominantly in arid environments. Sources are therefore considered natural. However, deforestation, agricultural and industrial practices are responsible for a portion of anthropogenic dust aerosols in the atmosphere (Haywood and Boucher, 2000; Forster *et al.*, 2007, sect. 2.4.4.6; Denman *et al.*, 2007, sect. 7.5.1.1);
- Sea salt (SS) aerosols originate from the oceans. The release of salt particles in the air depends on meteorological factors such as surface wind speed and sea surface temperature (Denman *et al.*, 2007, sect. 7.5.1.2).

There is scientific interest in studying aerosol pollution in cities because associated industries and road traffic are major sources of particulate matter and gaseous pollutants capable of forming aerosols through various chemical reactions and physical processes. Cities offer a wide variety of opportunities such as employment, education, health care, entertainment and other services which stimulate an ongoing and accelerating urbanization movement around the world (Moore *et al.*, 2003). The United Nations (2014) estimated that 30% of the world's population lived in an urban area in 1950. This proportion grew to 47% in 2000 and is expected to reach 66% in 2050 (United Nations, 2014). Particularly in developing countries, where the rate of urbanization is the greatest

(Subbotina, 2004, chap. 10), cities are lacking the means to adjust fast enough to fulfill the demand of their rapidly growing population and economic development. In this respect, urbanization comes with its fair share of environmental consequences (Sharma and Joshi, 2016). The phenomenon known as *global dimming*, which consists of a significant decrease in solar radiation flux around the world since the 1950s, is actually spatially inconsistent and much more pronounced over densely populated urban areas (Alpert *et al.*, 2005; Alpert and Kishcha, 2008). Indeed, atmospheric aerosol concentrations are significantly higher in populated cities as opposed to rural or remote areas (Cheng and Tsai, 2000), and the cities' population growth in developing countries tends to correlate with an increase of aerosol concentration (Kishcha *et al.*, 2011). Rapid urbanization and development in India and China resulted in a sharp increase of air pollutant emissions during the last decade (Lu *et al.*, 2011) and frequently recurring episodes of air pollution and haziness. On the other hand, urbanization in developed countries, albeit occurring at a slower rate, hasn't had such a negative impact. Developed countries did indeed struggle with severe air pollution issues in the past, but their economic and democratic situation provides them with the means to enforce clean air regulations and develop green technologies. As a result, air quality has significantly improved over the last decades in the United States (Hand *et al.*, 2012), Europe (Vestreng *et al.*, 2007; Tørseth *et al.*, 2012) and Japan (Wakamatsu *et al.*, 2013), even though their population and economy kept on growing.

Several years ago, NASA's Global Modeling and Assimilation Office (GMAO) introduced the Modern-Era Retrospective Analysis for Research and Application (MERRA, Rienecker *et al.*, 2011), a reanalysis tool incorporating satellite and model data to reproduce spatially consistent observations of many environmental variables. While the original MERRA included only meteorological parameters (wind, temperature, humidity, etc.), it has recently been extended to include assimilation of biased-corrected aerosol

optical depth (AOD) from the Moderate Resolution Imaging Spectroradiometers sensors (MODIS, Remer *et al.*, 2005) on board the Aqua and Terra satellites, which led to its rebranding as MERRAero. Although only total AOD is constrained by MODIS observations, the data assimilation algorithm in MERRAero provides speciated hourly data, with the relative contributions from five of the major aerosol species listed previously. Version 1 of MERRAero doesn't assimilate NO₃ particles. Nevertheless, MERRAero provides an innovative tool to the scientific community to study aerosol pollution issues around the world, especially in regions where reliable surface-based monitoring is scarce or unavailable. Examples of MERRAero's applicability can be found in Kessner *et al.* (2013), Colarco *et al.* (2014), Kishcha *et al.* (2014; 2015) and Yi *et al.* (2015).

In this study, AOD data from MERRAero is used to assess the state of air quality over a large selection of major metropolitan areas around the world (hereafter simply referred to as "cities") over the last thirteen years (2003–2015). Speciation data is used to determine which aerosol species contribute most to AOD over each city and a trend analysis is performed to evaluate how local and regional factors, as well as natural and anthropogenic factors, affect aerosol pollution in urban environments. Alpert *et al.* (2012) previously and similarly analyzed AOD trends over a selection of major cities around the world based on MODIS data. The advantage of using MERRAero as opposed to just MODIS data is its ability to distinguish between aerosol species which provides substantially more information for analysis.

5.2 Methodology and data

5.2.1 MERRA Aerosol Reanalysis

NASA's Version 1 of MERRAero incorporates the latest version of the

Goddard Earth Observing System (GEOS-5). It contains components for atmospheric circulation and composition (including atmospheric data assimilation), ocean circulation and biogeochemistry, and land surface processes. GEOS-5 also includes an atmospheric particulate matter (PM) module (Colarco *et al.*, 2010, and references therein). This module is based on a version of the Goddard Chemistry, Aerosol, Radiation and Transport (GOCART) model (Chin *et al.*, 2002). GOCART treats the sources, sinks and chemistry of SO₄, OC, BC, DS and SS particles. DS and SS emissions are a function of surface properties and wind speed at the surface. Sources of other species are simulated from emission inventories, including their precursors. SO₂ anthropogenic emissions are input from the Emission Database for Global Atmospheric Research (EDGAR) version 4.1 inventory from 2005 and biomass burning emissions (primarily OC and BC) are input from the NASA Quick Fire Emission Dataset (QFED) version 2.1 (Buchard *et al.*, 2015). PM species are treated as external mixtures and do not interact with each other. MERRAero also assimilates bias-corrected AOD observations from the MODIS sensors on both Terra and Aqua. MERRAero reproduces the concentrations of all five particulate species modeled by GOCART and their relative AOD contributions all over the world every hour with a resolution of 0.5° latitude by 0.625° longitude from mid-2002 to 2015.

A number of MERRAero components have been evaluated in different regions of the world. Its assimilation of AOD has been validated over Africa, South America, and Central and Eastern Asia using many remote sensing instruments by Buchard *et al.* (2015); Nowottnick *et al.* (2015) evaluated its aerosol speciation and vertical structure specific to Saharan dust transport using the Cloud-Aerosol Lidar with Orthogonal Polarization (CALIOP); in the United States, the surface concentrations of SO₂, fine PM and its chemical speciation has been thoroughly evaluated by Buchard *et al.* (2014; 2016); in Europe, an evaluation of the surface concentrations of PM, fine PM and some of their chemical speciation has been performed by Provençal *et al.* (2017a);

and finally, the surface concentration of fine PM in Israel and Taiwan was carried out by Provençal *et al.* (2017b).

5.2.2 Method

A selection of 200 of the world's most populated cities were chosen, inspired by Brinkhoff's major agglomerations list (City Population, <http://www.citypopulation.de>). All the selected cities have a population of at least 2 million inhabitants. Over each one of them, hourly AOD data from MERRAero were extracted for a period of 13 years, from 2003 to 2015, for total and every one of the five aerosol species. It is worth mentioning that MERRAero's resolution is too coarse to capture the urban core of cities. Urban aerosol load is obviously considered in the simulation, but urban grid points are broadly representative of the metropolitan areas, including the urban core and the surrounding suburbs.

A first analysis is performed by averaging the data over the 13-year period over each city and regrouping the cities by geographic region to determine their aerosol signature. A second analysis is performed by averaging the data by year over each city, calculating a regression trend over the 13 years and performing a Student's *t*-test to evaluate the trend's significance at the 90% confidence level. This quantifies the consequences of rapid urbanization with respect to air quality as well as ascertains the effectiveness of air pollution control over the last decade. The results are presented in map form. All the numerical data used to produce these maps are included in the supplementary material.

5.3 AOD distributions of aerosol speciation (2003–2015)

5.3.1 North and Central America

The proportions of aerosol species to total AOD for a selection of major cities in North and Central America are shown in Fig. 5.1. The reader is referred to the supplementary material for AOD values in all cities. The highest urban AOD values are observed in Central and Eastern United States and Canada, ranging from 0.133 in Miami to 0.190 in Houston. Denver is an exception with the lowest mean AOD in the whole region (0.095). The Northeastern United States is highly populated and industrialized, which explains the higher AOD values in Philadelphia (0.190), Cincinnati (0.189), Washington (0.188), New York City (0.187), Pittsburgh (0.184), Cleveland (0.181) and St. Louis (0.180). SO₄ aerosols account for a majority (> 50%) of total AOD in most North American cities. This is in line with Hand *et al.* (2012) who mentioned that the Eastern U.S. states emit substantially more SO₂, a precursor of SO₄ aerosols, compared to the other states. Overall, anthropogenic aerosols (SO₄, POM and BC) represent at least 85% of total AOD in all the northeastern cities. Nevertheless, overall, the mean AOD remains relatively low (< 0.2) in all cities. This is the result of effective air quality regulation in the U.S. known as the Clean Air Act, first adopted in 1970 and significantly amended in 1990. The success of this regulation has been highlighted by many (e.g., Granier *et al.*, 2011; de Meij *et al.*, 2012; Hand *et al.*, 2012; Xing *et al.*, 2013; de Gouw *et al.*, 2014) by documenting a substantial reduction of SO₂ emissions and/or concentration, among other air pollutants, across the U.S. during the last decades. SO₂ emissions and SO₄ concentrations are generally well correlated (Hand *et al.*, 2012; Xing *et al.*, 2013).

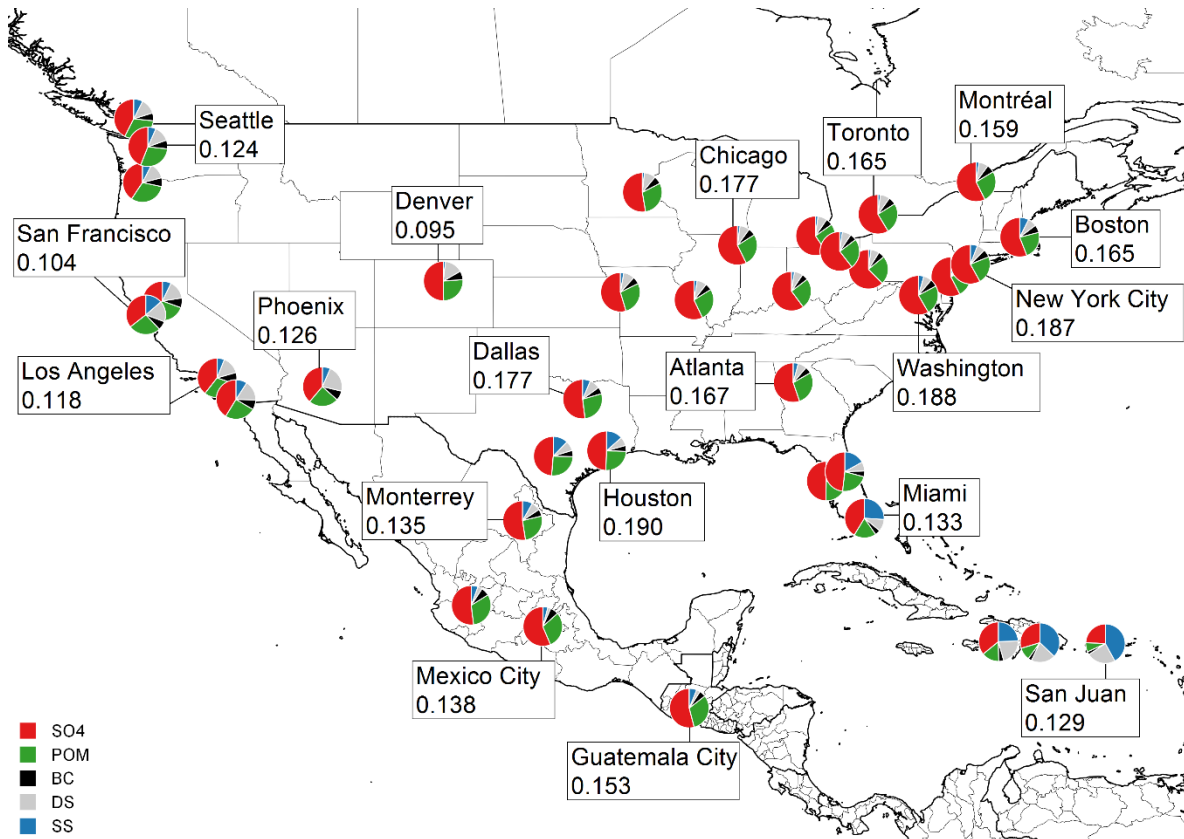


Fig. 5.1: Proportion of AOD speciation for a selection of cities in North and Central America. Mean AOD is provided for a few cities. The reader is referred to the supplementary material for such information for all the cities.

Mean AOD values in Orlando (0.157), Tampa (0.152) and Miami (0.133) are among the lowest in the Eastern U.S. with a significantly stronger contribution from SS aerosols to total AOD (from 16% in Tampa to 26% in Miami) given their proximity to the Atlantic Ocean and the Gulf of Mexico. However, Buchard *et al.* (2016) and Provençal *et al.* (2017a) documented a substantial overestimation of SS concentrations by MERRAero in coastal areas. Therefore these SS proportions are likely overestimated as well.

The mean AOD in cities of the west coast is lower, ranging from 0.107 in San Diego to 0.124 in Seattle, but the proportions of POM, BC and DS aerosols are higher. These cities are substantially affected by carbon emissions from wildfires occurring periodically in California. Indeed, Spracklen *et al.* (2007), who modeled OC emissions from summer wildfires in the Western U.S. between 1980 and 2004, concluded that the variability

of OC concentrations in the Western U.S. is largely due to the variability of wildfire emissions. Furthermore, AOD values from MERRAero averaged by month, shown in Fig. 5.2(a) for Los Angeles, also suggest this to be the case. Aside from an increase caused by DS in spring, POM is largely responsible for the fluctuation of total AOD, particularly during the wildfire season between July and October. The wintertime rainy season is also responsible, to a lesser extent, for the seasonal fluctuation. By contrast, the fluctuation of SO₄ AOD is barely perceivable. For the sake of comparison, the same graph is shown for New York City (Fig. 5.2(b)). The fluctuations of SO₄ and POM AOD are much more correlated which suggests that carbonaceous aerosols originate largely from energy consumption in that city. The higher DS proportion in Western U.S. cities is caused by advection of dust originating from the nearby deserts in the Southwestern U.S. and Northwestern Mexico.

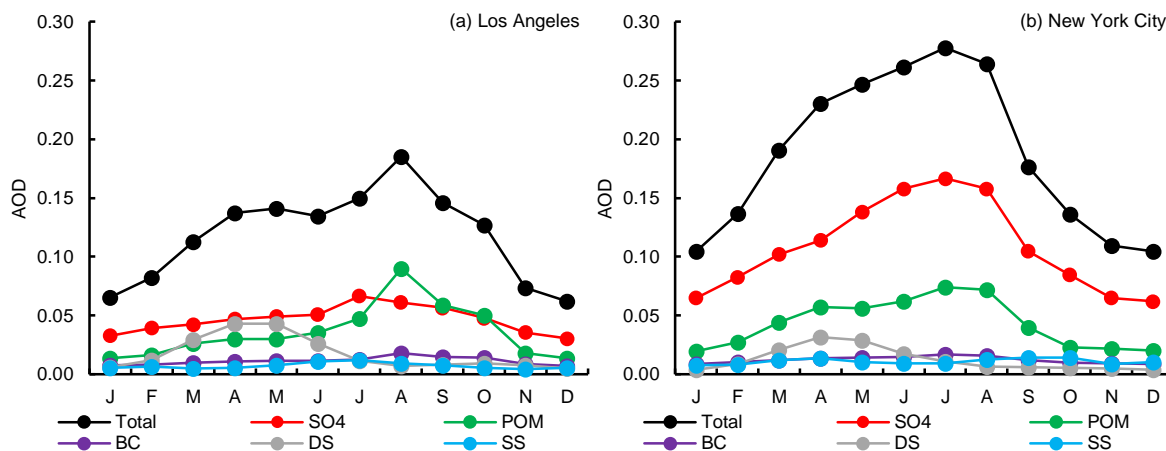


Fig. 5.2: AOD of total and aerosol species averaged by month in (a) Los Angeles and (b) New York City.

The mean AOD in Mexican cities is relatively low (below 0.140) while its speciation signature is similar to Northeastern U.S. cities, dominated by SO₄ and POM aerosols. The Mexican government also implemented successful management programs and incentives to improve urban air quality during the last decades (Molina and Molina, 2004; Parrish *et al.*, 2011). Finally, AOD in Caribbean cities is also low (below 0.140) but much less impacted

by anthropogenic aerosols. DS and SS compose over 50% of total AOD in Santo Domingo and San Juan. The Caribbean does indeed receive a large amount of DS originating from the Sahara desert (Prospero and Mayol-Bracero, 2013).

5.3.2 South America

The AOD distribution of aerosol speciation for cities located in South America is shown in Fig. 5.3. The mean AOD for cities in this region is somewhat lower compared to most cities in North America. Lima and Asunción are the only cities whose mean AOD is above 0.160. The speciation distribution is, however, quite different. The mean AOD in Buenos Aires and in cities of Southern Brazil is dominated by SO₄ and POM aerosols in more or less similar proportions. POM accounts for over half of total AOD in Goiânia, Brasília and Asunción. Deforestation and biomass burning for agricultural purposes in the Amazon rainforest are responsible for such a substantial presence of carbonaceous aerosols in the air (Sena *et al.*, 2013). Indeed, van der Werf *et al.* (2010) estimated that 14.5% of global carbon emissions from wildfires between 1997 and 2009 originate from South America. A synoptic circulation study published by Freitas *et al.* (2005) suggested that smoke plumes from wildfires in the Amazon are generally blown to the south, which explains why POM contributes much less to total AOD in cities on the east coast of Brazil.

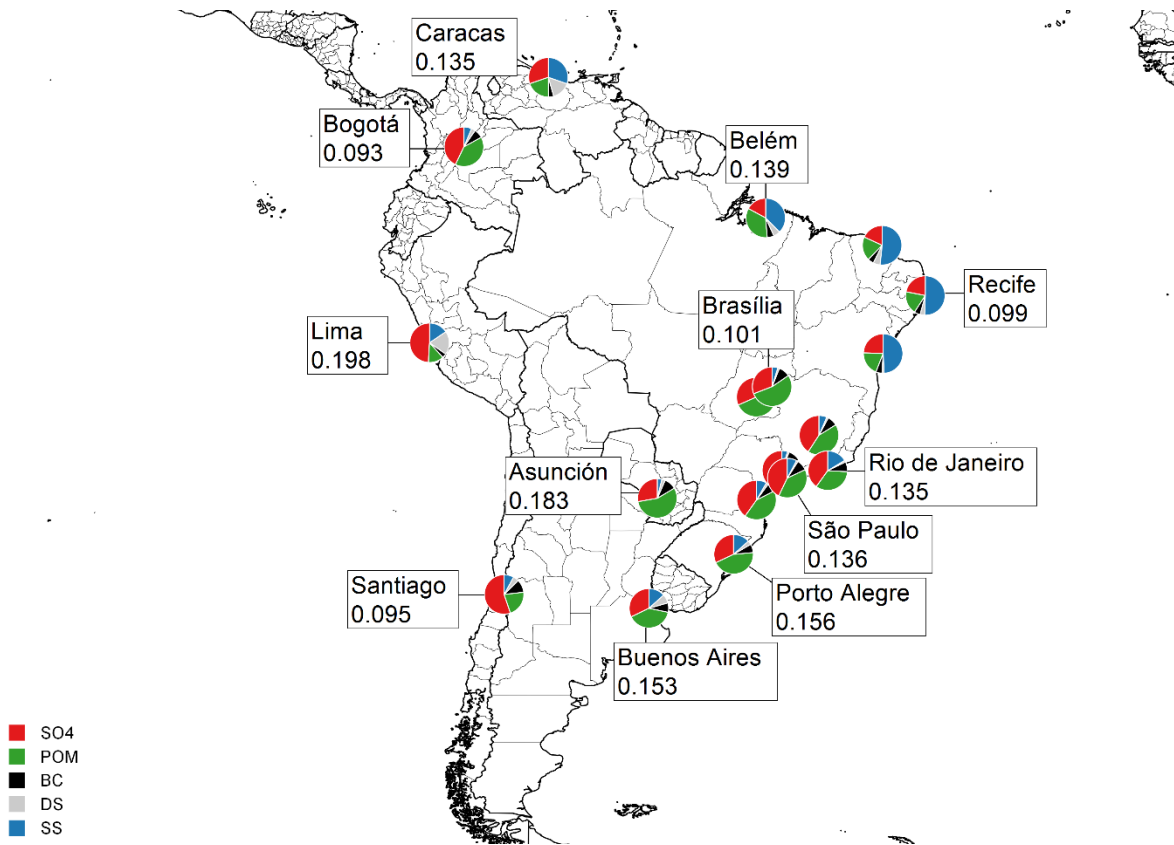


Fig. 5.3: Proportion of AOD speciation for a selection of cities in South America.

Fig. 5.4 compares the monthly averaged AOD between a city strongly impacted from wildfire emissions (Brasilia) and another one west of the Andes that is much less influenced by such emissions (Santiago). Brasilia is clearly affected by biomass burning emissions as shown by a sharp increase of POM, SO₄ and BC AOD during the wildfire season in the fall. Santiago, on the other hand, is slightly impacted by POM in the fall, but its AOD distribution is overall dominated by SO₄ aerosols throughout the year. The impact of the summertime rainy season on the aerosol load over the west coast of South America is also clearly illustrated in Fig. 5.4(b).

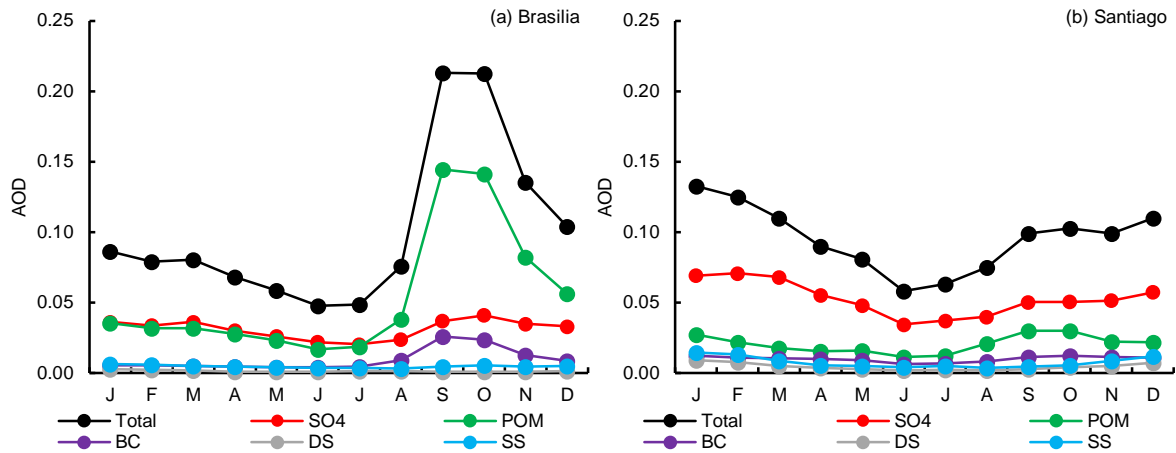


Fig. 5.4: AOD of total and aerosol species averaged by month in (a) Brasilia and (b) Santiago.

5.3.3 Africa

Fig. 5.5 displays the distribution of AOD speciation for cities located in Africa. The standout feature of Africa is obviously the Sahara desert, which covers most of the northern part of the continent. DS emissions from the desert contribute to high AOD values observed in cities in vicinity of the desert, such as Kano (0.472), Dakar (0.402) and Khartoum (0.389). DS contributes over 70% to total AOD in these three cities, while it contributes ~50% in all other cities of Northern Africa. It is important to mention that MERRAero doesn't assimilate AOD data over bright surfaces such as deserts. Therefore, over the source region, the data is constrained primarily by parameterized emissions determined by wind speed. However, the darker surface of cities might have been sufficient to provide assimilated data in and around them.

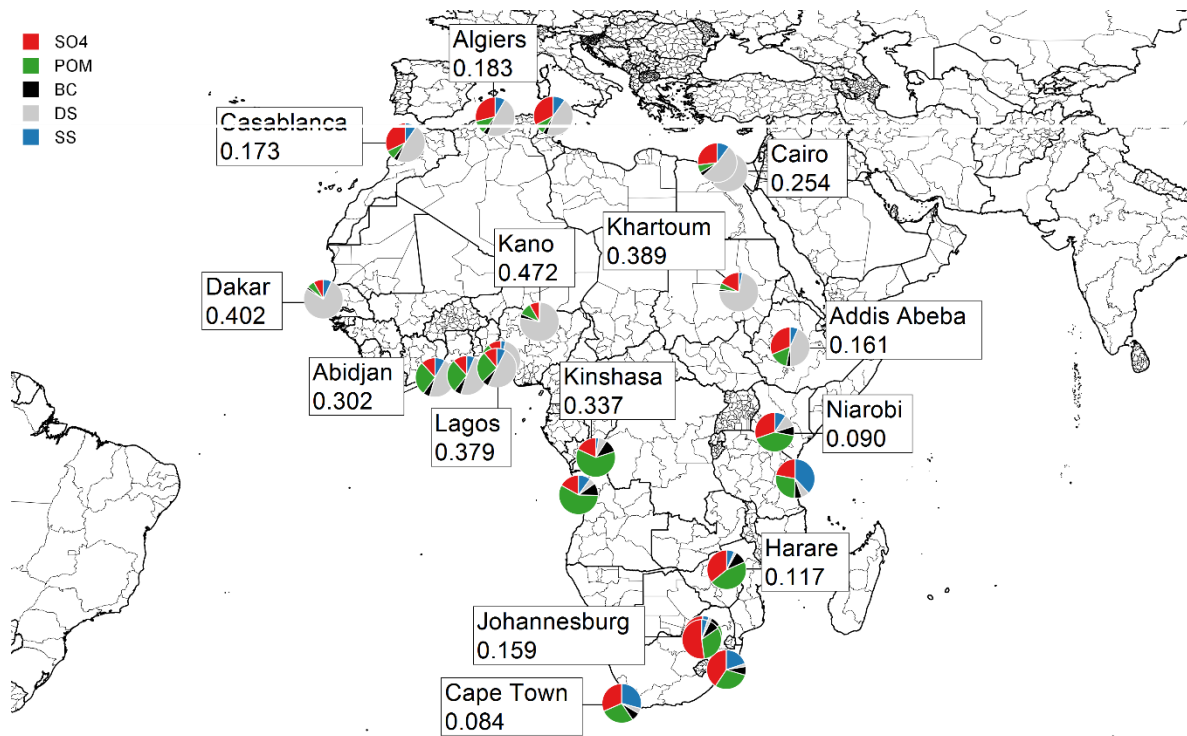


Fig. 5.5: Proportion of AOD speciation for a selection of cities in Africa.

The region of tropical Africa, south of the Sahara, is characterized by the savannah and rainforest where human-induced wildfire for agricultural purposes is a recurring practice and is an important source of aerosols (Archibald *et al.*, 2009; Eck *et al.*, 2003). Forest preservation initiatives have been implemented in Africa but Mercier (2012) essentially called them a failure. Over 50% of the world's carbon emissions from biomass burning does indeed originate from Africa (van der Werf *et al.*, 2010). Therefore, POM and BC aerosols together contribute over 73% to total AOD in Kinshasa, 68% in Luanda and 56% in Harare. The influence of biomass burning aerosols diminishes toward South Africa, where urban mean AOD is relatively low, ranging from 0.084 in Cape Town to 0.180 in Durban. The aerosol signature in South African cities resembles most that of North American cities.

5.3.4 Europe, including Russia and Turkey

The AOD proportions for cities located in Europe are shown in Fig. 5.6. The situation in European cities is, in many respects, similar to that of North American cities: mean AOD is relatively low while SO₄ aerosols contribute ~50% or more in most cities. Europe is indeed a heavily industrialized continent but effective air quality regulations have also been implemented in Europe, which has resulted in a consistent emission and concentration decrease of various air pollutants, notably PM and SO₂, over the last decades (Vestreng *et al.*, 2007; Granier *et al.*, 2011; Colette *et al.*, 2011; de Meij *et al.*, 2012; Tørseth *et al.*, 2012). Europe is, however, significantly impacted by the advection of DS originating from the Sahara desert, which represents over 10% of total AOD in all European cities in Fig. 5.4. Cities closer to the Mediterranean Sea are the most impacted, in line with Barkan *et al.* (2005), Querol *et al.* (2009) and Pey *et al.* (2013) who analyzed Saharan dust transport over the Mediterranean and into Europe. Indeed, DS contributes over 30% of total AOD in Izmir, Athens, Ankara and Naples, and to higher AOD values observed in cities such as Istanbul (0.206). Monthly averaged AOD values in Naples are offered as an example in Fig. 5.7 to show how much DS affects the AOD, especially in the spring when DS contributes almost as much as SO₄ to the total.

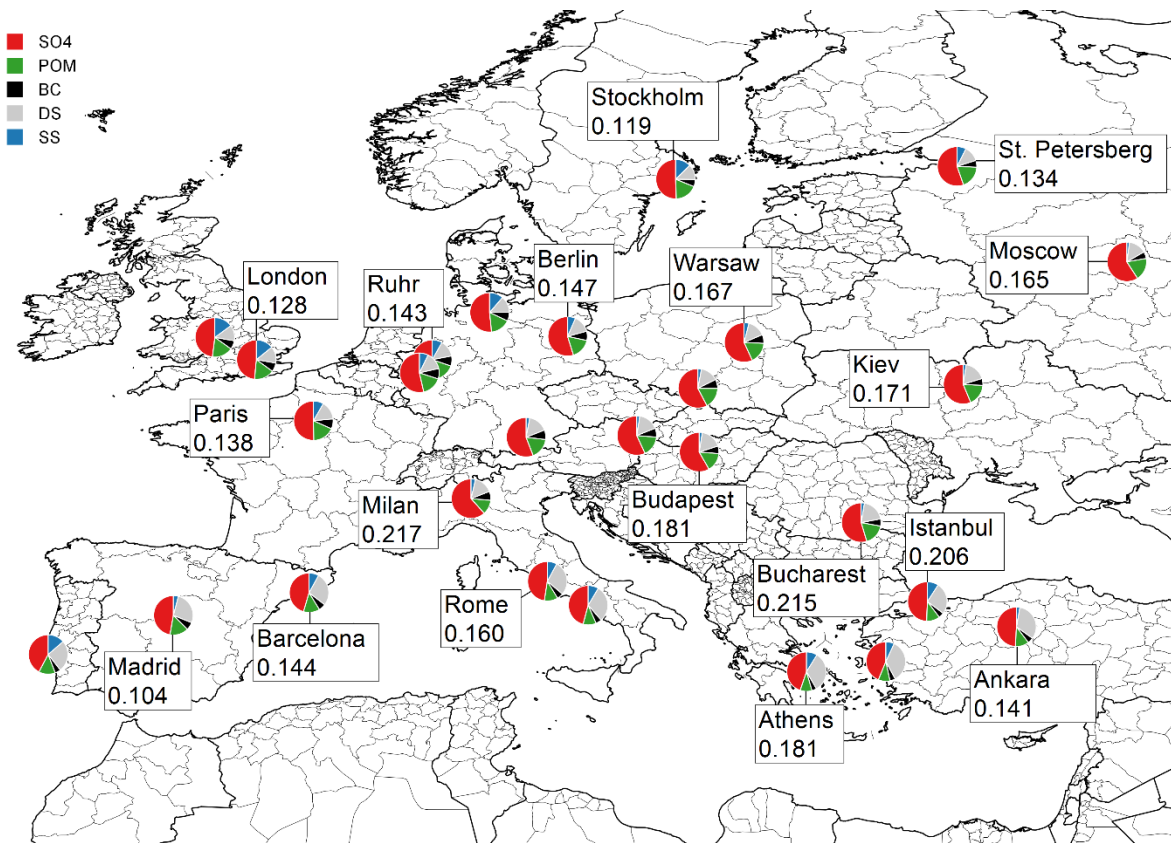


Fig. 5.6: Proportion of AOD speciation for a selection of cities in Europe.

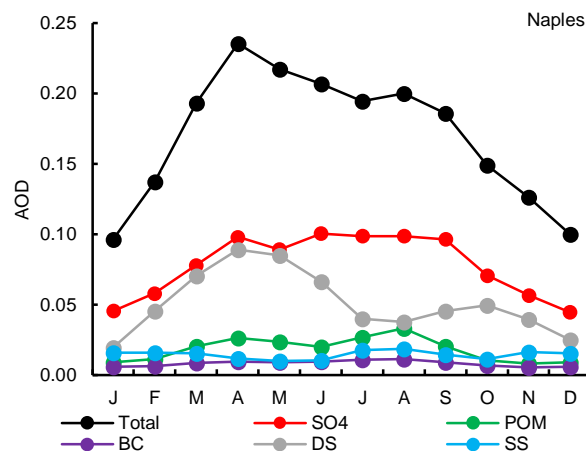


Fig. 5.7: AOD of total and aerosol species averaged by month in Naples.

The mean AOD in cities of the northern and western parts of Europe tends to be lower, for instance in Madrid (0.104), Stockholm (0.119), Birmingham (0.122) and Lisbon (0.126). Even in the megacities of London and Paris, the total AOD is fairly low (0.128 and 0.138, respectively), due to relatively low levels of SO₄ and to a substantial reduction of SO₂

concentrations in these two cities since the 1990s, but also in other European cities (Henschel *et al.*, 2013; Bigi and Harrison, 2010).

5.3.5 Western and Central Asia

This region includes a selection of cities west of China and Myanmar, shown in Fig. 5.8. Cities close to the Mediterranean Sea enjoy a relatively low aerosol load compared to other cities in this region, from an AOD of 0.163 in Damascus to 0.219 in Tel Aviv. The AOD tends to increase toward Pakistan; the mean AOD in all Pakistani cities is above 0.4, except in Rawalpindi where it lies at 0.370. All cities in Western Asia are characterized by the prominent presence of DS particles due to their location in the Middle Eastern deserts. DS accounts for over 40% of total AOD in all cities of Western Asia and close to 70% in Riyadh and Baghdad. The large presence of DS in Pakistani cities is compounded by the significant presence of SO₄ aerosols, which explains their large overall AOD. The mean AOD from SO₄ aerosols is indeed the highest in the Pakistani cities. Even if SO₄ AOD is lower in the other cities of Western Asia, SO₄ aerosols still provide an important contribution to total AOD in Tehran (41%), Aleppo (38%) and Tashkent (36%).

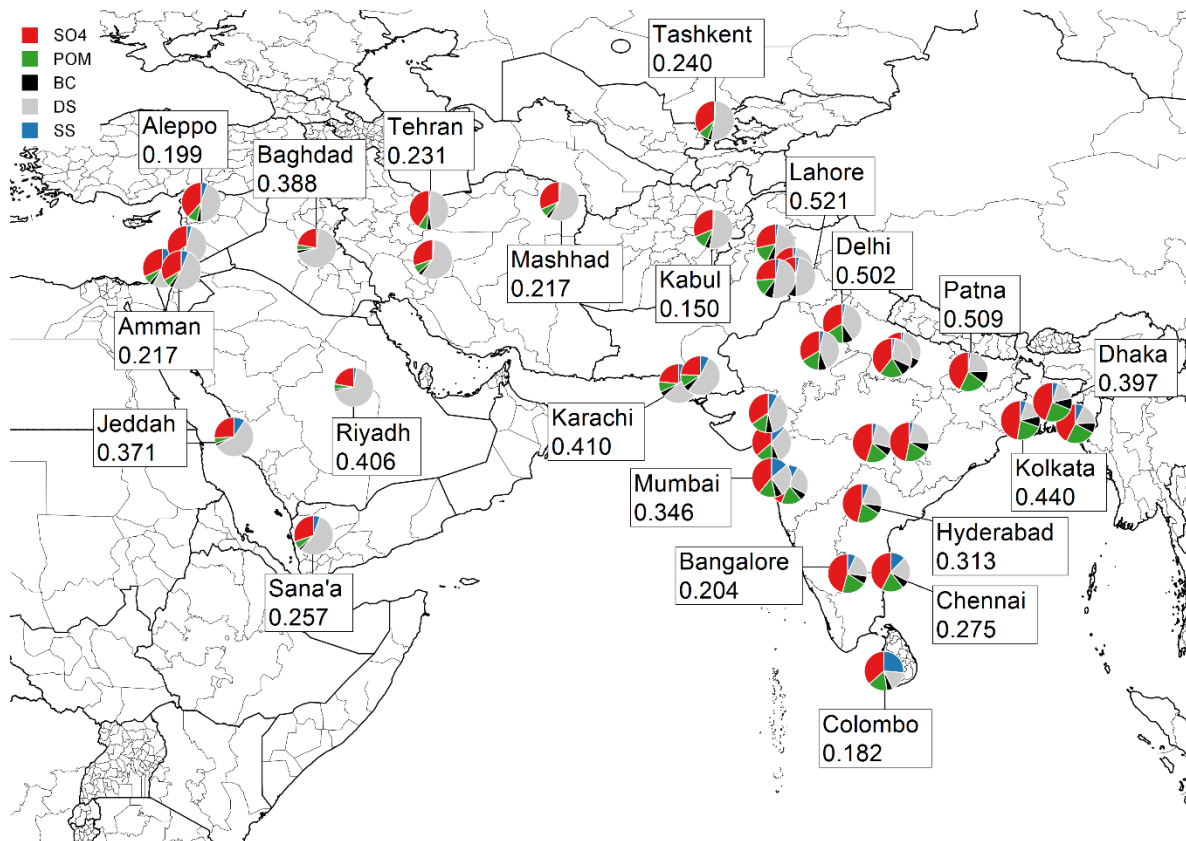


Fig. 5.8: Proportion of AOD speciation for a selection of cities in Western and Central Asia.

India is the world's second-most populated country. Fig. 5.8 includes 15 cities in India with a population over 2 million inhabitants. Its recent population and industrialization growth has resulted in a constant increase of fuel consumption and emissions of SO₂, OC and BC since the 1990s (Lu *et al.*, 2011; Klimont *et al.*, 2013). This resulted in high AOD values in most Indian cities; mean AOD is above 0.5 in Patna, Delhi, Kanpur and Lucknow. Indian cities are also highly affected by the advection of DS from nearby sources, especially in the northern part of India. DS aerosols contribute 40% to total AOD in Jaipur, 38% in Ahmedabad and in Delhi.

5.3.6 Eastern Asia

This region includes a selection of cities in China, Taiwan, North Korea, South Korea and Japan, shown in Fig. 5.9. China is the most populated

country in the world and has recently been surging economically at the cost of deteriorating air quality. Chinese cities record some of the highest speciated AOD averages in the world. Out of the 35 Chinese cities shown in Fig. 5.9, only three (Kunming, Ürümqi and Lanzhou) have a mean AOD value below 0.3. The highest mean AOD is observed in Chengdu (0.800), Wuhan (0.709) and Changsha (0.706). China is the world's largest anthropogenic aerosol emitter. Its energy consumption has increased drastically since 2000 as well as its emissions of SO₂, OC and BC (Lu *et al.*, 2011; Wang and Hao, 2012; Klimont *et al.*, 2013). SO₄ aerosols account for the majority (> 50%) of mean AOD in all Chinese cities except for Ürümqi located in the northwest, away from the densely populated eastern coast. The contribution of carbonaceous aerosols is also quite significant. Residential activities account for ~70% of OC and ~55% of BC emissions in China (Lu *et al.*, 2011). This results in a strong seasonal AOD fluctuation in many Chinese cities. The megacity of Guangzhou is presented as an example in Fig. 5.10 to highlight how fossil fuel and biomass burning, combined with frequent stagnating weather conditions, create very high levels of pollution in winter and early spring (Zhang and Cao, 2015). Additionally, springtime advection of DS from the Gobi desert in northern China and the Taklimakan desert in Western China (Sullivan *et al.*, 2007) is reflected in the higher DS proportions found in cities of Northern China.

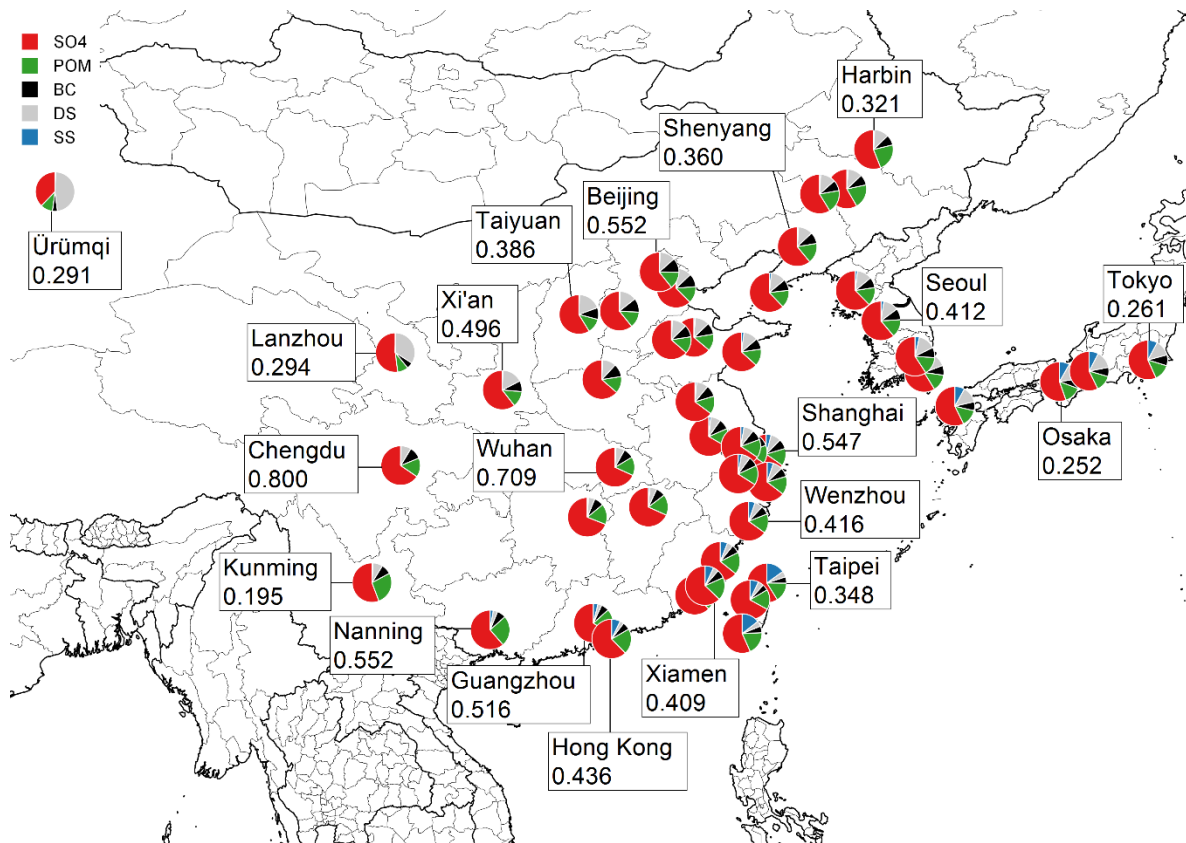


Fig. 5.9: Proportion of AOD speciation for a selection of cities in Eastern Asia.

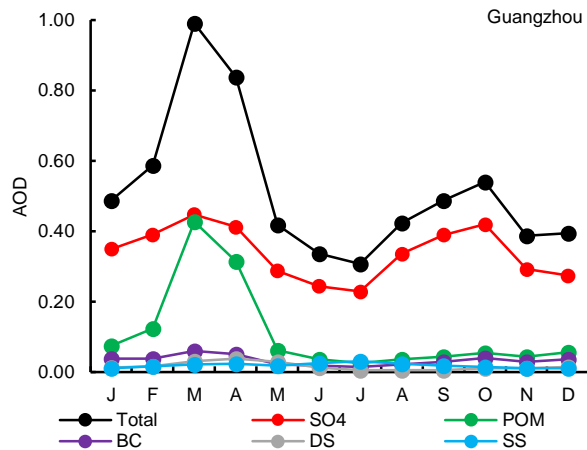


Fig. 5.10: AOD of total and aerosol species averaged by month in Guangzhou.

Cities in Taiwan, North Korea, South Korea and Japan are not as polluted as Chinese cities. They are nonetheless influenced by emissions and advection of pollutants from China. Lu *et al.* (2010) estimated that a 1% increase of SO₂ emissions in China leads to 1.15% and 0.71% increases in background SO₂ concentrations in South Korea and Japan respectively. The

mean AOD is indeed fairly high in Pyongyang (0.436), Seoul (0.412) and Taipei (0.348). The fact that Japan is farther away from China is reflected in its cities' lower AOD values, ranging from 0.250 in Nagoya to 0.295 in Fukuoka. Air quality policies have also been in place since the 1960s in Japan. SO₂ emissions and concentrations have decreased substantially since the 1970s (Kanada *et al.*, 2013; Wakamatsu *et al.*, 2013).

5.3.7 Southeastern Asia and Oceania

Fig. 5.11 maps the AOD distribution for cities located in Southeastern Asia and Australia. The highest mean AOD values in this part of the world are found in Bangkok (0.280), Jakarta (0.266) and Yangon (0.235). Cities in Indonesia (Jakarta, Bandung and Surabaya) are mostly impacted by SO₄ aerosols (ranging from 58% to 66% of total AOD). Yangon, Bangkok, Saigon, Kuala Lumpur and Singapore are affected by SO₄ and POM aerosols in more or less similar proportions. Deforestation in tropical Asia emits a substantial amount of carbonaceous particles in the air through biomass burning (Chang and Song, 2010). van der Werf *et al.* (2010) estimated that 9.5% of the world carbon emissions from wildfires originate from equatorial Asia. Manila and Cebu City in the Philippines are less impacted by POM and more affected by SS aerosols.

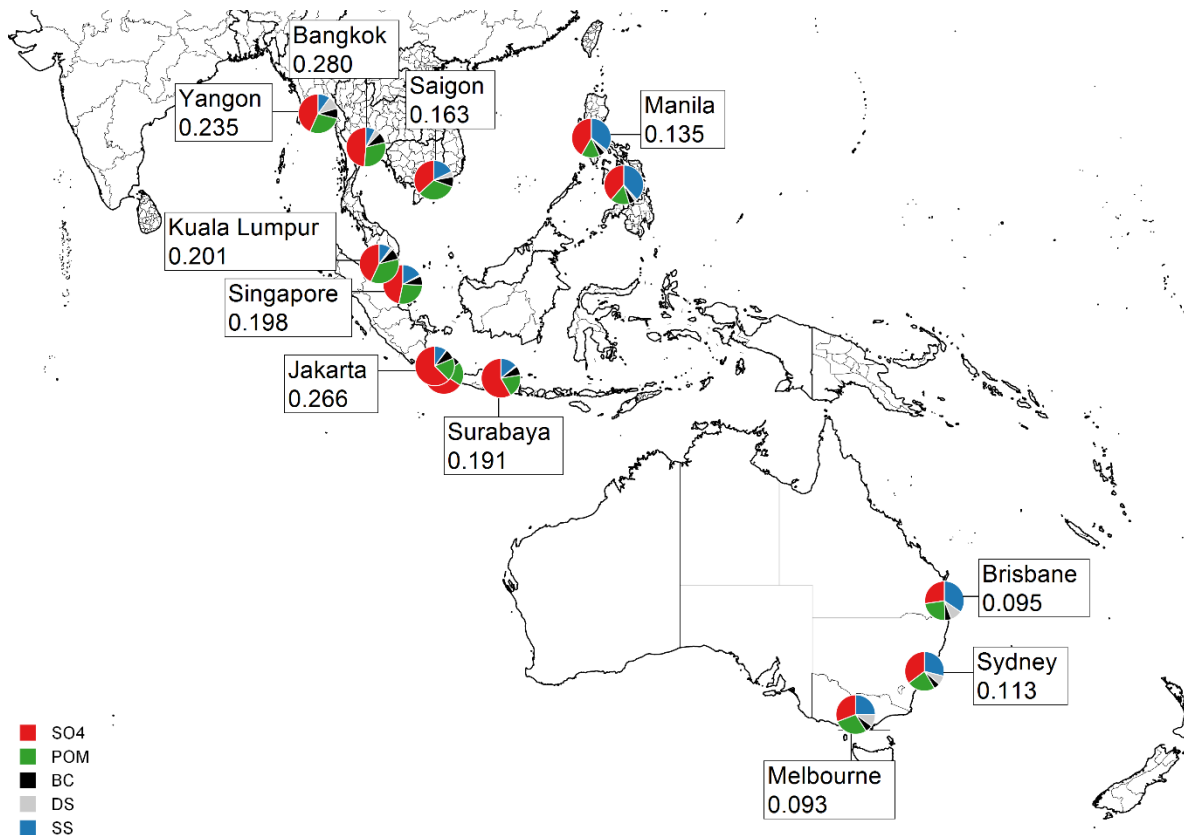


Fig. 5.11: Proportion of AOD speciation for a selection of cities in Southeastern Asia and Oceania.

The mean AOD in the three Australian cities is fairly low: 0.093 in Melbourne, 0.095 in Brisbane and 0.113 in Sydney. Like other industrialized countries, Australia maintains air quality guidelines, more restrictive than those in the U.S. and Europe, which are generally well respected (Broome *et al.*, 2015).

5.4 AOD trends of aerosol speciation (2003–2015)

5.4.1 Total AOD

The linear trend between 2003 and 2015 for total AOD and for all the cities is mapped in Fig. 5.12. The color grading is indicative of the level of change with lighter colors indicating an insignificant change. Globally, the AOD is decreasing in a wide majority of cities. The trends are negative in

every single city of the Americas, except in Sacramento and Santiago where they are positive but insignificant. The decreases are significant in cities of Eastern Canada and U.S., and the southeastern part of South America. The strongest decreases are observed in Washington and Asunción. Cities where the trend is insignificant tend to be those least affected by SO₄ aerosols, notably on the western coast of Canada and the U.S., in the Caribbean and in Eastern Brazil. Similarly, the trends are significantly negative in every European city, except in Stockholm, Kiev, Moscow and St. Petersburg where they are negative but insignificant.

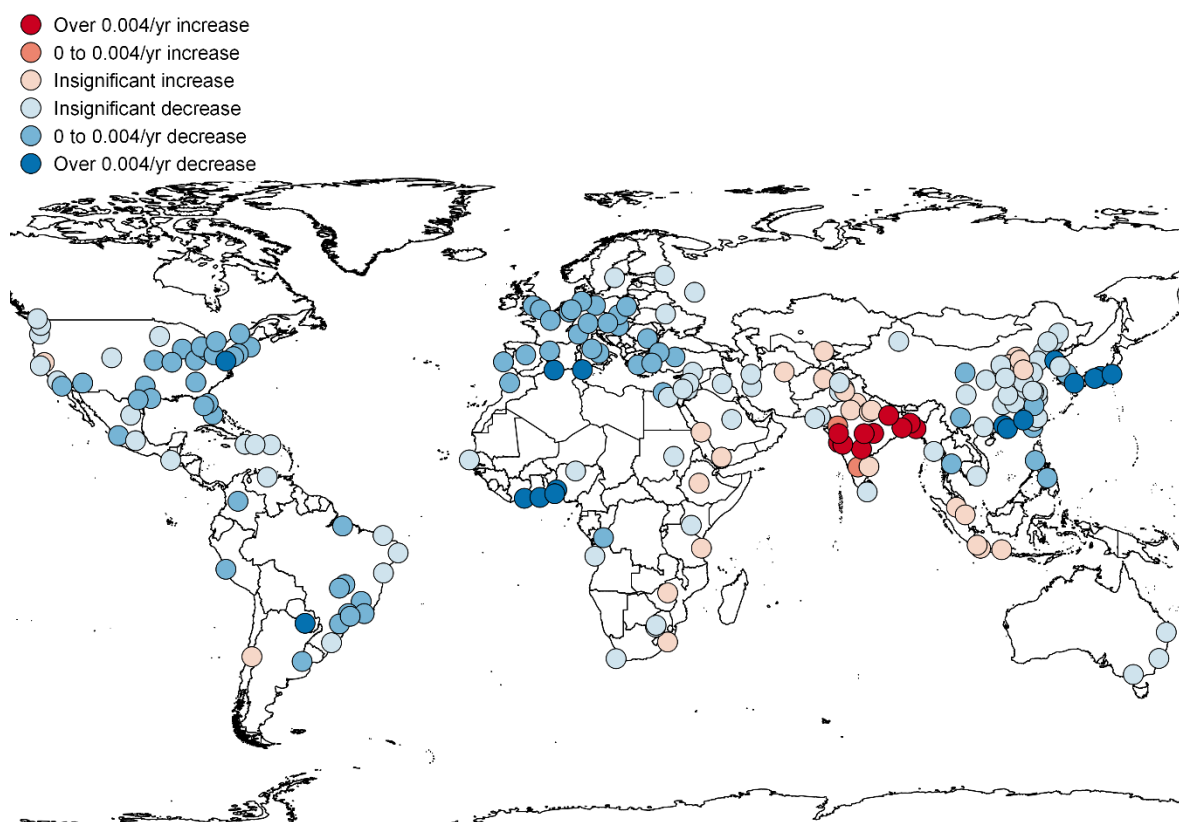


Fig. 5.12: Linear trend for total AOD in all cities between 2003 and 2015.

Trends in cities of Africa and Western Asia are generally insignificant, either positively or negatively. They are, however, significant and negatively strong (> 0.004 decrease per year) in the cities of Algiers, Accra, Abidjan, Ibadan, Lagos and Tunis. The situation in India and Bangladesh is quite different, where all cities exhibit a positive trend, many of which are

significant and strong (> 0.004 increase per year).

The AOD is decreasing in most of the 38 cities of China and Taiwan, albeit at an insignificant rate. The trend is nonetheless significant in a few cities and strongly decreasing in three cities of Southern China (Guangzhou, Xiamen and Hong Kong). Guangzhou, one of China's most populated cities, is in fact the city where the AOD trend is the strongest in the world (decrease of 0.0072 per year). The trends are also strongly negative in all Japanese cities and in the North Korean capital of Pyongyang. In Southeastern Asia, the trends tend to be insignificant, with the exception of Manila and Cebu City in the Philippines, and Bangkok in Thailand, which exhibit a significant AOD decrease. Finally, the three cities in Australia display an insignificant AOD decrease.

A similar analysis is performed in the following subsections for the trends of AOD speciation which will provide explanations for the AOD trends observed in Fig. 5.12. The reader is referred to the supplementary material for the trend values in all the cities and for all species.

5.4.2 AOD from SO₄ aerosols

SO₄ AOD trends are shown in Fig. 5.13. The trends are decreasing significantly in most cities of North America, especially in Eastern Canada and U.S., coinciding with the total AOD decrease observed in Fig. 5.12 and in line with the goals of the Clean Air Act referenced in Section 5.3.1. Over the years 2000–2010, SO₄ concentrations decreased in all regions of the U.S. but even more so over the Eastern U.S. (Hand *et al.*, 2012; 2013). Cities in Central and South America experienced insignificant changes in their SO₄ aerosol load, except in Santo Domingo where it significantly decreased and in Santiago where it significantly increased.

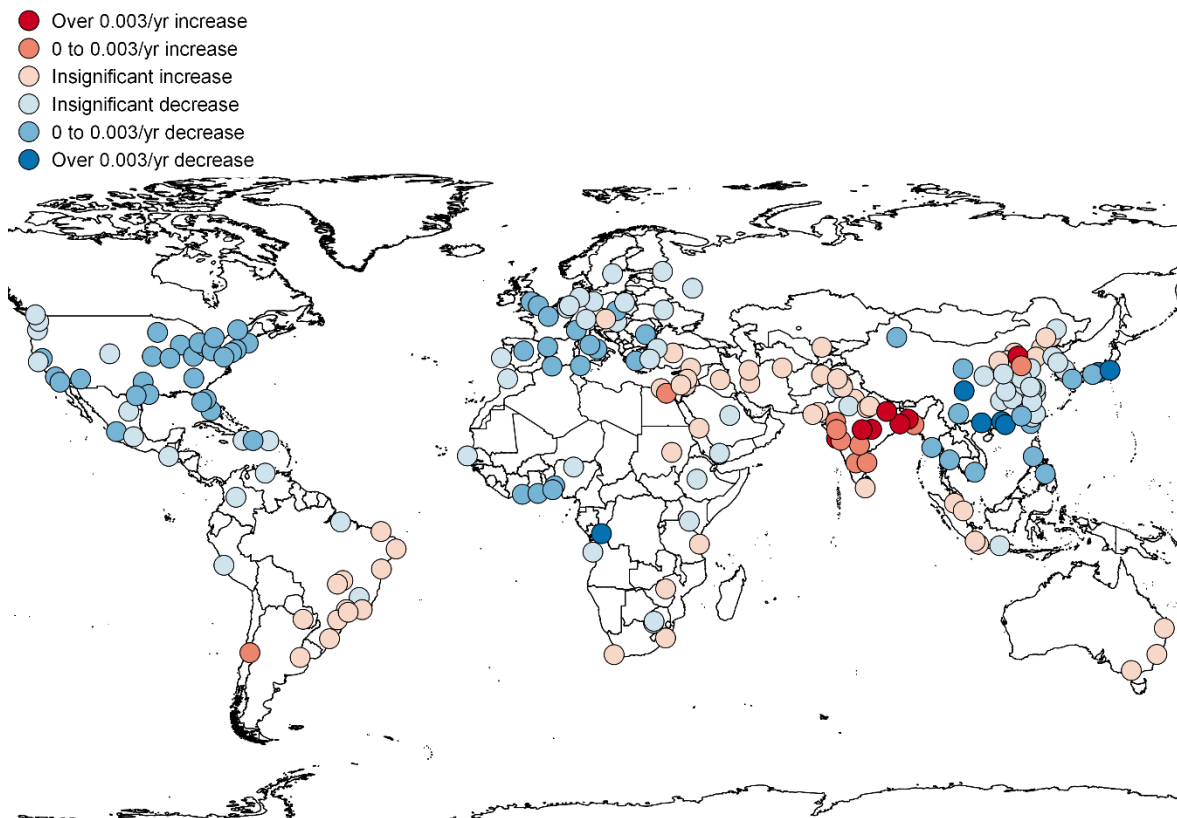


Fig. 5.13: Linear trend for AOD from SO_4 aerosols in all cities between 2003 and 2015.

In European cities, SO_4 AOD trends are generally decreasing significantly in Western Europe and insignificantly in Eastern Europe. They are increasing in only two cities, Vienna and Ankara, albeit at insignificant rates. This again is the result of effective air quality regulations implemented in Europe where SO_2 emissions and, by extension, SO_4 concentrations have decreased over the years 2001–2010 (de Meij *et al.*, 2012).

The decrease in North American and European cities was aided by the recent global economic recession. A few authors have dealt with the issue of economic slowdown and air quality, notably Vrekoussis *et al.* (2013) who documented a sharp decrease of various gaseous pollutants over Greece since 2008, Russell *et al.* (2012) who noticed a stronger-than-normal decrease of the NO_2 column over many U.S. cities during the recession, and Castellanos and Boersma (2012) who arrived at the same conclusion for the whole of Europe. Our data suggest that SO_4 aerosols were impacted in a

similar fashion, as shown in Fig. 5.14 for a selection of four megacities in the industrialized world. In New York City, the AOD of SO₄ aerosols started to decline in 2007 and took a sharp drop in 2010 before rebounding the following year; SO₄ AOD also suffered a sharp decline in 2010 in London; the AOD decreased in Moscow between 2007 and 2010; and the same variable has been steadily decreasing in Tokyo since 2006 but more steadily since 2008.

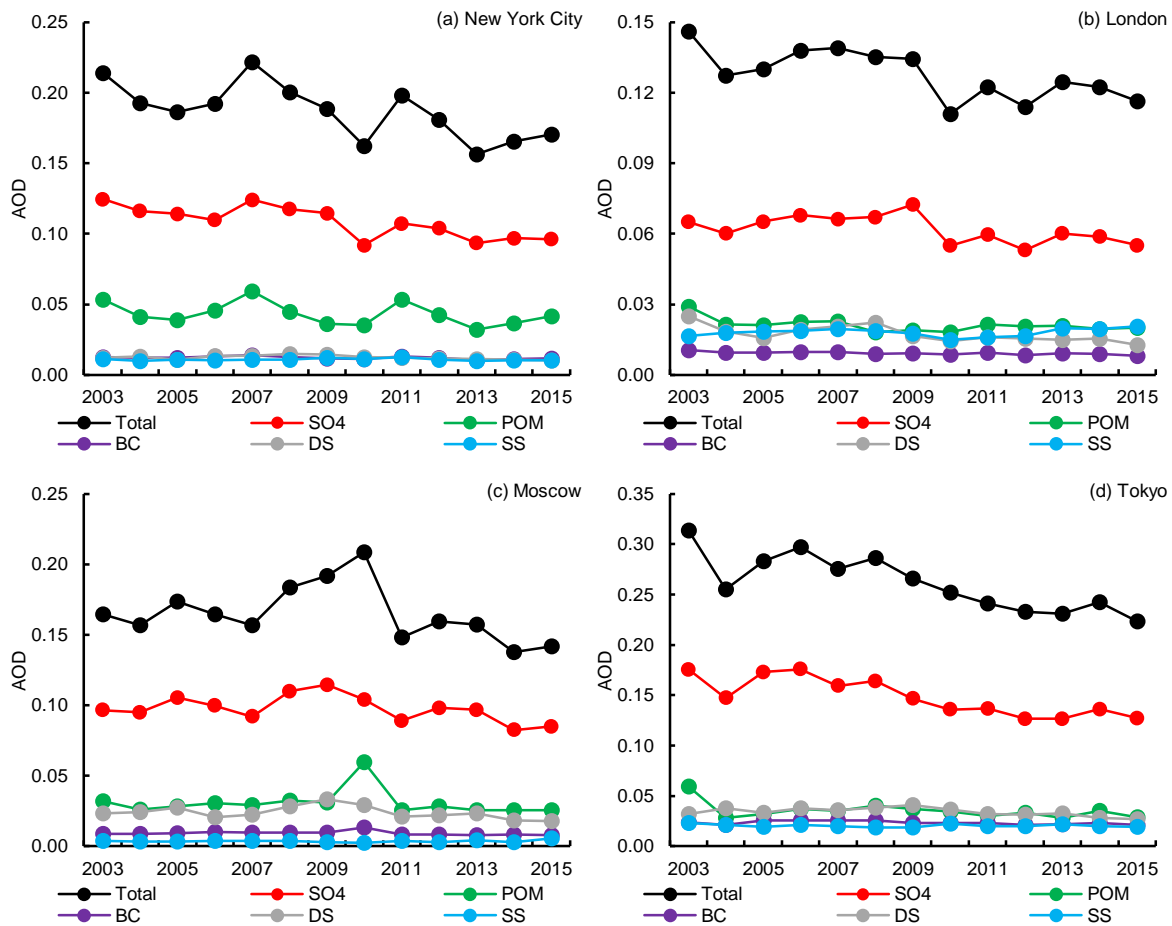


Fig. 5.14: AOD of total and aerosol species averaged by year in (a) New York City, (b) London, (c) Moscow and (d) Tokyo.

SO₄ AOD trends have changed insignificantly in most cities of Africa and Western Asia, where SO₄ aerosols generally contribute little to total AOD. There are some exceptions, for instance, Tunis, Algiers, Abidjan, Accra, Lagos and Ibadan where SO₄ AOD trends have significantly decreased, Kinshasa where it strongly decreased and Cairo where it significantly

increased. Although the trends are weak in cities in the north of India and in Bangladesh, Indian cities are rather unique in the global landscape in the sense that India is the only country where cities experienced a strong increasing SO₄ AOD trend. Tianjin in China is the only other city in the world with such a trend. In fact, the trend is increasing in all but one city in India (Jaipur), albeit insignificantly in three cities, including the megacity of Delhi. This is the likely result of recent industrial development and population growth in India. Lu *et al.* (2011) estimated that SO₂ emissions increased by 35% between 2004 and 2010 in India.

The trend is insignificant in most Chinese cities, positively in the northern part and negatively in the central part. Cities in Southern China experienced a significant decrease, quite strong in some cases (Guangzhou, Chengdu, Hong Kong and Nanning). Like India, China has also been experiencing rapid urbanization and industrialization over the last decade. A look at Fig. 5.13 is deceiving since only a small number of cities reveal an increasing trend, and an insignificant one in most of those cities for that matter. This is most likely due to emission patterns observed in China. Lu *et al.*'s (2011) estimates of Chinese SO₂ emissions showed little change between 2004 and 2010. However, this is the result of an 11% increase from 2004 to 2006 (peak year) and a slow decrease since then (9% decrease between 2006 and 2010). Other estimates vary by numbers but all agree with peak emissions in 2006 and a slow decrease since then (Lu *et al.*, 2010; Wang and Hao, 2012; Zhang *et al.*, 2012; Klimont *et al.*, 2013). Implementation of national comprehensive policies by the Chinese government in 2005 has been successful in this respect. The government also took advantage of international events such as the 2008 Beijing Olympics to temporarily and regionally push stricter air quality guidelines (Lin *et al.*, 2013). However, SO₂ emissions and their trends are very disproportionate throughout China (Zhao *et al.*, 2013a; Zhao *et al.*, 2013b). Guangzhou and Beijing are offered as examples in Fig. 5.15. Guangzhou

follows closely the national trend: peak SO_4 AOD in 2006 and a slow decrease since then, although not continuous. The SO_4 AOD trend in Beijing is fairly stable throughout the period, with slight fluctuations.

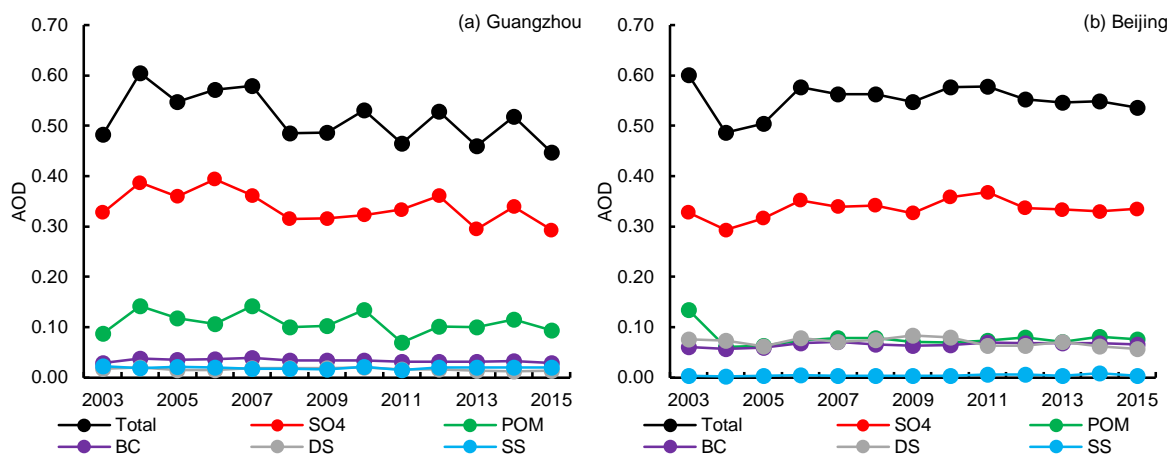


Fig. 5.15: AOD of total and aerosol species averaged by year in (a) Guangzhou and (b) Beijing.

The significant and occasionally strong SO_4 AOD decrease in all of Japan's cities is due to its air quality policies and to the recession, as mentioned previously, but also due to its position downwind from China. Since peak SO_4 AOD is observed in 2006 in Tokyo (Fig. 5.14(d)) and in other Japanese cities, coinciding with China's peak SO_4 emissions, it appears that Japan has also benefited from the air quality regulations implemented by the Chinese government. Trends are significantly decreasing in Yangon, Bangkok, Saigon and both Philipino cities of Cebu City and Manila, while it is insignificant in Kuala Lumpur, Singapore, the three cities in Indonesia and the three cities in Australia.

5.4.3 AOD from POM and BC aerosols

Since POM and BC particles originate from the same sources, their trends are similar across the cities (Figs. 5.16 and 5.17). Carbonaceous aerosols are also the by-product of fossil fuel burning. It is therefore intuitive to observe a decreasing AOD trend in cities where the SO_4 AOD is also

decreasing, and vice versa. This is the case for cities in the Eastern U.S., European, Indian and Japanese cities. However, trends for carbonaceous particles and SO₄ don't always parallel since carbon also originate from natural sources such as wildfires, whose contribution can explain the discrepancy between the two. For instance, the variability and recurrence of wildfires in the Western U.S. are largely responsible for the variability of OC concentrations in the same region (Spracklen *et al.*, 2007). Sacramento in California is offered as an example in Fig. 5.18. POM AOD fluctuated frequently according to the intensity of wildfires, as opposed to SO₄ AOD, which barely changed from one year to another. POM AOD has been steadily increasing since 2010, in conjunction with intensifying wildfire activities experienced in California in recent years. The trend was, however, deemed insignificant by the statistical test. A single episodic series of strong wildfires can also leave a profound impact on a city's aerosol signature. Western Russia was affected by an intense wildfire season during the summer of 2010 (Konovalov *et al.*, 2011), which explains the POM AOD peak in Moscow in 2010 (Fig. 5.14(c)). This peak is, however, probably underestimated since the smoke from the wildfires was so thick that MODIS occasionally and incorrectly identified it as clouds (van Donkelaar *et al.*, 2011). Mean AOD from the Aerosol Robotic Network (AERONET) observations in Moscow during July and August 2010 were above 1 for many days and reached a daily average peak of 3.6 on August 7 (Huijnen *et al.*, 2012). MERRAero's average of 1.5 for the same day pales in comparison. Without this wildfire episode, the POM AOD decrease in Moscow would have been significant.

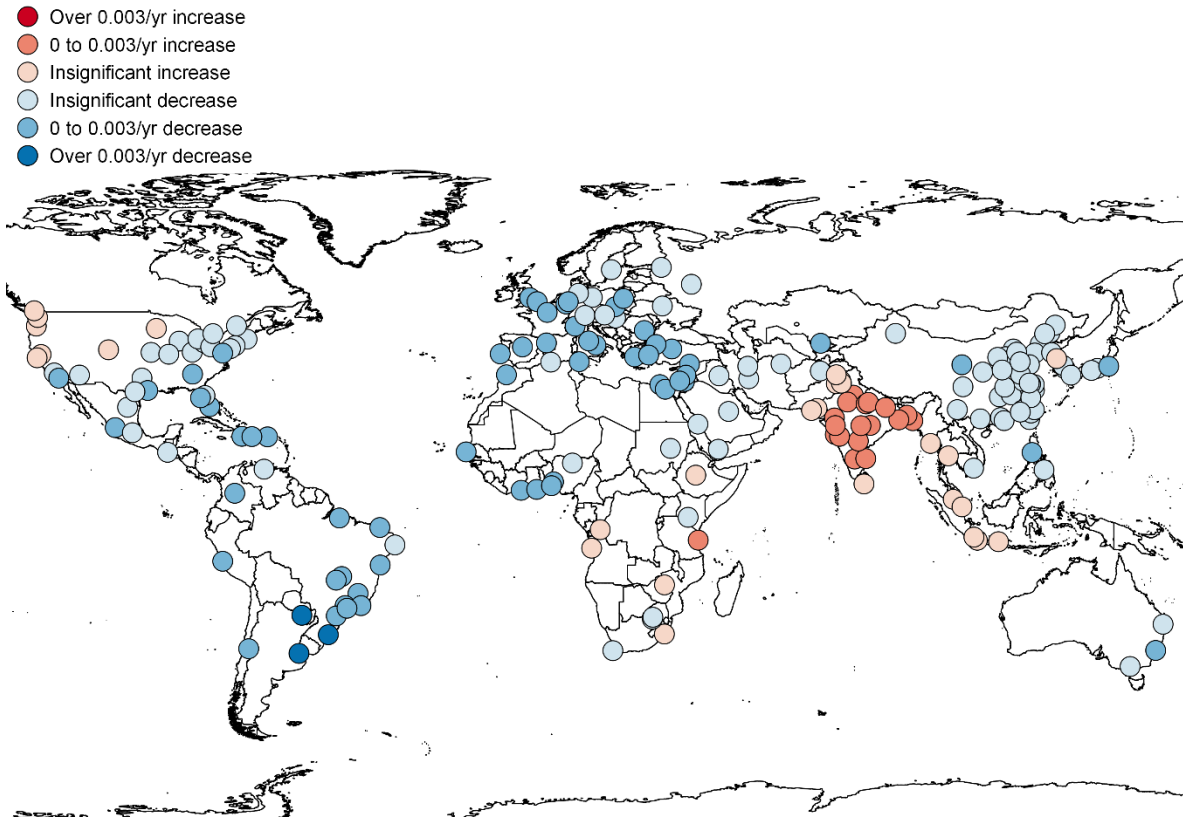


Fig. 5.16: Linear trend for AOD from POM aerosols in all cities between 2003 and 2015.

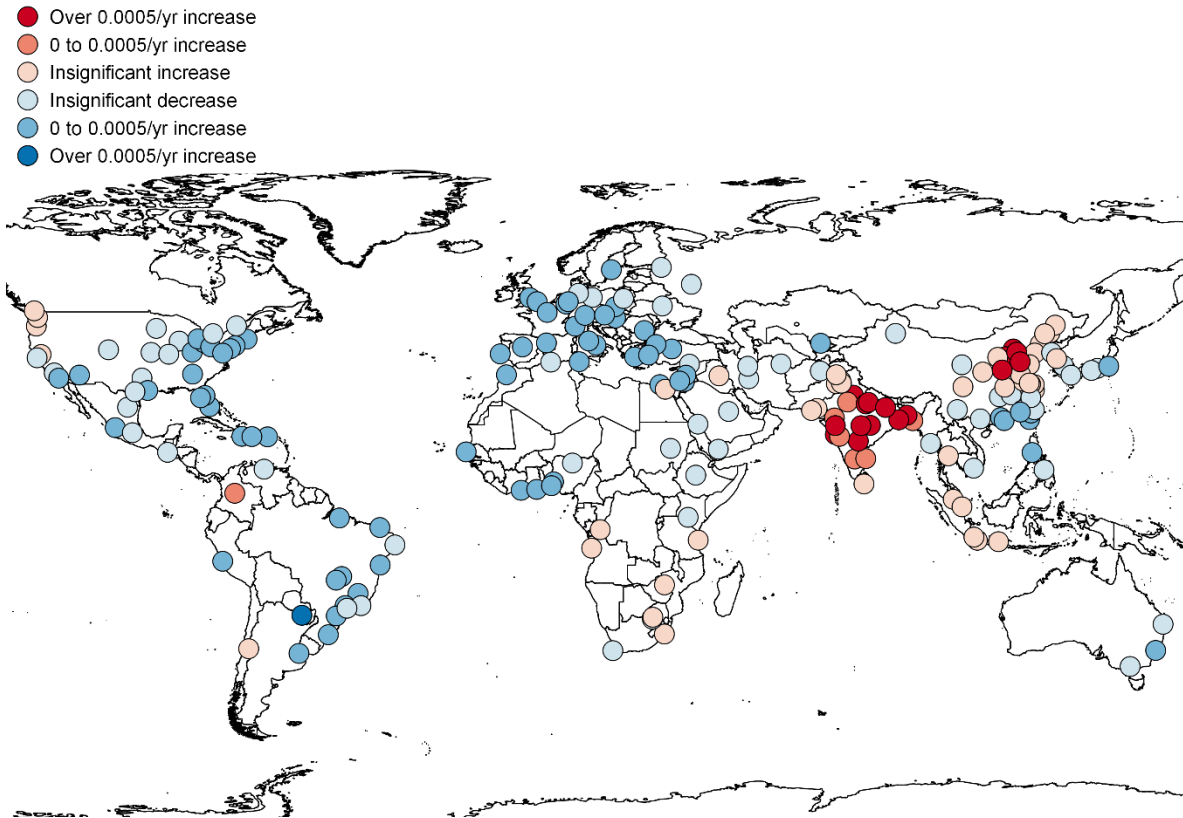


Fig. 5.17: Linear trend for AOD from BC aerosols in all cities between 2003 and 2015.

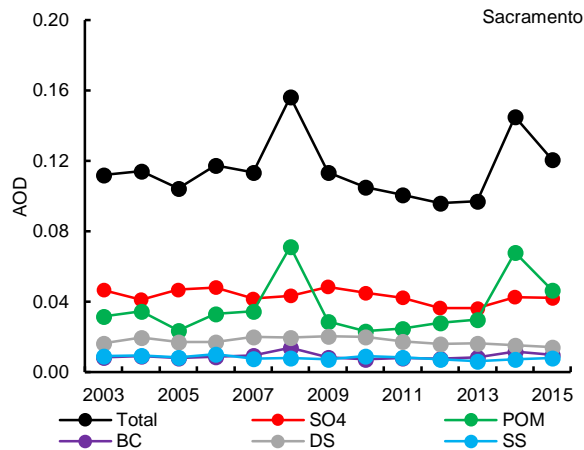


Fig. 5.18: AOD of total and aerosol species averaged by year in Sacramento.

As mentioned previously, wildfires in the Amazon rainforest are also an important source of carbonaceous aerosols in South America (Sena *et al.*, 2013). POM AOD is decreasing significantly in all both two South American cities, and quite strongly in three cities (Asunción, Porto Alegre and Buenos Aires). In accordance, deforestation in the Amazon has sharply decreased

since 2004, which appears to have been caused by conservation policies and economic factors (Malingreau *et al.*, 2012) that resulted in a decrease of carbon emissions (van der Werf *et al.*, 2010). Biomass burning also contributes a large amount of carbon aerosols in Equatorial Africa (Eck *et al.*, 2003); the POM and BC trends are however mostly insignificant in cities of that continent except right below the Sahara where the trends have decreased significantly. Carbon emission estimates also suggest a decrease during the first half of our study period in Northern Hemisphere Africa (Lehsten *et al.*, 2009; van der Werf *et al.*, 2010).

The BC trends in five cities of Northern China (Zibo, Zhengzhou, Tianjin, Shijiazhuang and Beijing) have increased strongly, which doesn't coincide with the POM trends. In Southeastern Asia and Australian cities, the trends for carbonaceous particles are insignificant in all cities, except in Manila and Sydney where they have decreased significantly.

5.5 Discussion and conclusion

The MERRA Aerosol Reanalysis was used to study urban air pollution issues around the world by using its assimilation of AOD observations and modeled concentrations of particulate matter over a 13-year period (2003–2015). MERRAero's differentiation of particle speciation makes it a unique and innovative tool capable of estimating the AOD of individual aerosol species with a global and constant coverage, unlike remote sensing instruments. This is particularly useful for studying urban air pollution since cities tend to exhibit a heterogeneous composition of aerosols.

The mean AOD was high (> 0.3) in most cities of China, India, the Middle East, Northern and tropical Africa. In contrast, it was relatively low (< 0.2) in most cities of North America, South America, Europe, Australia and South Africa. The high AOD values observed in Northern African and Western Asian cities are caused mostly by their proximity to large and sandy

deserts. Advection of DS also affects cities in India and Bangladesh but the high AOD averages in cities of these two countries is mostly the result of anthropogenic activities. Fossil fuel burning is responsible, for the most part, for the high AOD values observed in Chinese cities. However, advection of dust affects to some extent the AOD in cities of Northern China as well. High AOD averages in cities of tropical Africa are caused by deforestation and biomass burning activities.

Cities in North America, Europe, Japan, Southeastern Asia and Oceania tend to have a relatively low AOD on average, while SO_4 and POM aerosols contribute to it most. Even though fossil fuel consumption is a major source of pollution in those parts of the world, effective air quality regulations have been successful at keeping emissions and, as a consequence, AOD values low over the last decade. Cities in South America and on the west coast of the U.S. are affected by fossil fuel burning but carbon emissions from wildfires contribute a significant proportion to their mean AOD during the summer. European cities are also affected by DS transport from the Sahara.

Overall, SO_4 aerosols represented at least 10% of the mean AOD in all but two of the 200 cities presented in the various maps of this manuscript, those of Dakar in Senegal and Kano in Nigeria, for the only reason that their AOD is overwhelmed by DS particles due to their location close to the Sahara. POM aerosols represented at least 10% of the average in all but 24 cities, mostly located in Northern Africa or Western Asia. The presence of SS aerosols is significant in coastal cities but usually contributes little to the mean AOD.

The AOD decreased significantly between 2003 and 2015 in most cities of Eastern Canada and U.S., Europe and Japan, accompanied by an AOD decrease from SO_4 , POM and BC aerosols, a result of effective air quality regulations and the recent economic recession. Cities in South America,

most of which have also experienced a significant AOD decrease, owe this decrease to a declining AOD from POM aerosols due to a slowdown of deforestation activities in the Amazon rainforest. In contrast, all cities in India and Bangladesh experienced an increase of AOD from SO₄, POM and BC aerosols, which was quite strong in some cities due to recent and rapid urbanization and industrialization.

China has also been experiencing a strong urbanization and industrialization movement over the last few decades, which caused a strong increase in emissions of atmospheric pollutants. China nevertheless implemented air quality guidelines during our study period, resulting in insignificant AOD trends in most Chinese cities. The regulations are, however, showing early signs of success, with some cities in Southern China experiencing significant and strong decreases of AOD from SO₄ aerosols. The AOD values over Chinese cities remain, however, among the largest in the world.

Many cities in Africa and all cities of Western Asia have seen little change in their aerosol load. Cities in these parts of the world are mostly affected by aerosols originating from natural sources, which don't tend to fluctuate significantly on timescales of a year or more. Maps for AOD trends from DS and SS aerosols were not shown or discussed for the simple reason that the trends were relatively weak and/or insignificant in most cities.

As demonstrated in this paper, MERRAero is an innovative tool that provides to the scientific community with the means to study a broad range of aerosol pollution issues around the world. Some limitations pertaining to MERRAero are nevertheless worth raising. As mentioned previously, only MODIS AOD over oceans and dark land surfaces are assimilated. Furthermore, no vertically resolved aerosol information is available. NASA's Version 2 of MERRAero, MERRA-2, incorporates other remote sensing instruments, such as the Multi-angle Imaging Spectroradiometer (MISR)

and the Aerosol Robotic Network (AERONET), into its reanalysis to mitigate this shortcoming. MERRA-2 is currently being analyzed and results will be reported in forthcoming publications.

References

- Alpert, P., Kishcha, P., Kaufman, Y.J. and Schwarzbard, R. (2005). Global dimming or local dimming?: Effect of urbanization on sunlight availability. *Geophys. Res. Lett.* 32: L17802.
- Alpert, P. and Kishcha, P. (2008). Quantification of the effect of urbanization on solar dimming. *Geophys. Res. Lett.* 35: L08801.
- Alpert, P., Shvainshtein, O. and Kishcha, P. (2012). AOD trends over megacities based on space monitoring using MODIS and MISR. *Am. J. Clim. Chang.* 1: 117–131.
- Archibald, S., Roy, D.P., van Wilgen, B.W. and Scholes, R.J. (2009). Why limits fire? An examination of drivers of burnt area in Southern Africa. *Glob. Chang. Biol.* 15: 613–630.
- Barkan, J., Alpert, P., Kutiel, H. and Kishcha, P. (2005). Synoptics of dust transportation days from Africa toward Italy and central Europe. *J. Geophys. Res.* 110: D07208.
- Bigi, A. and Harrison, R.M. (2010). Analysis of the air pollution climate at a central urban background site. *Atmos. Environ.* 44: 2004–2012.
- Broome, R.A., Fann, N., Navin Cristina, T.J., Fulcher, C., Duc, H. and Morgan, G.G. (2015). The health benefits of reducing air pollution in Sydney, Australia. *Environ. Res.* 143: 19–25.
- Buchard, V., da Silva, A.M., Colarco, P., Krotkov, N., Dickerson, R.R., Stehr, J.W., Mount, G., Spinei, E., Arkinson, H.L. and He, H. (2014). Evaluation of GEOS-5 sulfur dioxide simulations during the Frostburg, MD 2010 field campaign. *Atmos. Chem. Phys.* 14: 1929–1941.
- Buchard, V., da Silva, A.M., Colarco, P.R., Darmenov, A., Randles, C.A., Govindaraju, R., Torres, O., Campbell, J. and Spurr, R. (2015). Using the OMI aerosol index and absorption aerosol optical depth to evaluate the NASA MERRA Aerosol Reanalysis. *Atmos. Chem. Phys.* 15: 5743–5760.
- Buchard, V., da Silva, A.M., Randles, C.A., Colarco, P., Ferrare, R., Hair, J., Hostetler, C., Tackett, J. and Winker, D. (2016). Evaluation of the surface PM_{2.5} in Version 1 of the NASA MERRA Aerosol Reanalysis over the United States. *Atmos. Environ.* 125: 100–111.
- Castellanos, P. and Boersma, K.F. (2012). Reduction in nitrogen oxides over Europe driven by environmental policy and economic recession. *Sci. Rep.* 2: 265.
- Charlson, R.J. (1969). Atmospheric visibility related to aerosol mass concentration. *Environ. Sci. Technol.* 3: 913–918.

Chang, D. and Song, Y. (2010). Estimates of biomass burning emissions in tropical Asia based on satellite-derived data. *Atmos. Chem. Phys.* 10: 2335–2351.

Cheng, M.T. and Tsai, Y.I. (2000). Characterization of visibility and atmospheric aerosols in urban, suburban, and remote areas. *Sci. Total Environ.* 263: 101–114.

Chin, M., Ginoux, P., Kinne, S., Torres, O., Holben, B., Duncan, B.N., Martin, R.V., Logan, J., Higurashi, A. and Nakajima, T. (2002). Tropospheric aerosol optical thickness from the GOCART model and comparisons with satellite and sun photometer measurements. *J. Atmos. Sci.* 59: 461–483.

Colarco, P., da Silva, A., Chin, M. and Diehl, T. (2010). Online simulations of global aerosol distributions in the NASA GEOS-4 model and comparisons to satellite and ground-based aerosol optical depth. *J. Geophys. Res.* 115: D14207.

Colarco, P.R., Kahn, R.A., Remer, L.A. and Levy, R.C. (2014). Impact of satellite viewing-swath width on global and regional aerosol optical thickness statistics and trends. *Atmos. Meas. Tech.* 7: 2313–2335.

Colette, A., Granier, C., Hodnebrog, Ø., Jakobs, H., Maurizi, A., Nyiri, A., Bessagnet, B., d'Angiola, A., d'Isidoro, M., Gauss, M., Meleux, F., Memmesheimer, M., Mieville, A., Rouil, L., Russo, F., Solberg, S., Stordal, F. and Tampieri, F. (2011). Air quality trends in Europe over the past decade: a first multi-model assessment. *Atmos. Chem. Phys.* 11: 11657–11678.

de Gouw, J.A., Parrish, D.D., Frost, G.J. and Trainer, M. (2014). Reduced emissions of CO₂, NO_x, and SO₂ from U.S. power plants owing to switch from coal to natural gas with combined cycle technology. *Earth's Future* 2: 75–82.

de Meij, A., Pozzer, A. and Lelieveld, J. (2012). Trend analysis in aerosol optical depths and pollutant emission estimates between 2000 and 2009. *Atmos. Environ.* 51: 75–85.

Delmas, R., Serça, D. and Jambertm C. (1997). Global inventory of NO_x sources. *Nutr. Cycl. Agroecosyst.* 48: 51–60.

Denman, K.L., Brasseur, G., Chidthaisong, A., Ciais, P., Cox, P.M., Dickinson, R.E., Hauglustaine, D., Heinze, C., Holland, E., Jacob, D., Lohmann, U., Ramachandran, S., da Silva Dias, P.L., Wofsy, S.C. and Zhang, X. (2007). *Couplings between changes in the climate system and biogeochemistry*. In: Solomon, S., Qin, D., Manning, M., Chen, Z., Marquis, M., Averyt, K.B., Tignor, M. and Miller, H.L. *Climate change 2007: the physical science basis*. Cambridge University Press, Cambridge, pp. 499–587.

Eck, T.F., Holben, B.N., Ward, D.E., Mukelabai, M.M., Dubovik, O., Smirnov, A., Schafer, J.S., Hsu, N.C., Piketh, S.J., Queface, A., le Roux, J., Swap, R.J.

and Slutsker, I. (2003). Variability of biomass burning aerosol optical characteristics in Southern Africa during the SAFARI 2000 dry season campaign and a comparison of single scattering albedo estimates from radiometric measurements. *J. Geophys. Res.* 108: 8477.

Forster, P., Ramaswamy, V., Artaxo, P., Berntsen, T., Betts, R., Fahey, D.W., Haywood, J., Lean, J., Lowe, D.C., Myhre, G., Nganga, J., Prinn, R., Raga, G., Schulz, M. and van Dorland, R. (2007). *Changes in atmospheric constituents and in radiative forcing*. In: Solomon, S., Qin, D., Manning, M., Chen, Z., Marquis, M., Averyt, K.B., Tignor, M. and Miller, H.L. *Climate change 2007: the physical science basis*. Cambridge University Press, Cambridge, pp. 129–234.

Freitas, S.R., Longo, K.M., Silva Dias, M.A.F., Silva Dias, P.L., Chatfield, R., Prins, E., Artaxo, P., Grell, G.A. and Recuero, F.S. (2005). Monitoring the transport of biomass burning emissions in South America. *Environ. Fluid Mech.* 5: 135–167.

Granier, C., Bessagnet, B., Bond, T., d'Angiola, A., van der Gon, H.D., Frost, G.J., Heil, A., Kaiser, J.W., Kinne, S., Klimont, Z., Kloster, S., Lamarque, J.F., Lioussé, C., Masui, T., Meleux, F., Mieville, A., Ohara, T., Raut, J.C., Riahi, K., Schultz, M.G., Smith, S.J., Thompson, A., van Aardenne, J., van der Werf, G.R. and van Vuuren, D.P. (2011). Evolution of anthropogenic and biomass burning emissions of air pollutants at global and regional scales during the 1980–2010 period. *Clim. Chang.* 109: 163–190.

Hand, J.L., Schichtel, B.A., Malm, W.C. and Pitchford, M.L. (2012). Particulate sulfate ion concentration and SO₂ emission trends in the United States from the early 1990s through 2010. *Atmos. Chem. Phys.* 12: 10353–10365.

Hand, J.L., Schichtel, B.A., Malm, W.C. and Pitchford, M. (2013). Widespread reductions in sulfate across the United States since the early 1990s. *AIP Conf. Proc.* 1527: 495–498.

Haywood, J. and Boucher, O. (2000). Estimates of the direct and indirect radiative forcing due to tropospheric aerosols: a review. *Rev. Geophys.* 38: 513–543.

Henschel, S., Querol, X., Atkinson, R., Pandolfi, M., Zeka, A., le Tertre, A., Analitis, A., Katsouyanni, K., Chanel, O., Pascal, M., Bouland, C., Haluza, D., Medina, S. and Goodman, P.G. (2013). Ambient air SO₂ patterns in 6 European cities. *Atmos. Environ.* 79: 236–247.

Huijnen, V., Flemming, J., Kaiser, J.W., Inness, A., Leitao, J., Heil, A., Eskes, H.J., Schultz, M.G., Benedetti, A., Hadji-Lazarou, J., Dufour, G. and Eremenko, M. (2012). Hindcast experiments of tropospheric composition during the summer 2010 fires over Western Russia. *Atmos. Chem. Phys.* 12: 4341–4364.

Kanada, M., Fujita, T., Fujii, M. and Ohnishi, S. (2013). The long-term impacts of air pollution control policy: historical links between municipal actions and industrial energy efficiency in Kawasaki City, Japan. *J. Clean. Prod.* 58: 92–101.

Kessner, A.L., Wang, J., Leby, R.C. and Colarco, P.R. (2013). Remote sensing of surface visibility from space: a look at the United States east coast. *Atmos. Environ.* 81: 136–147.

Kishcha, P., Starobinets, B., Kalashnikova, O. and Alpert, P. (2011). Aerosol optical thickness trends and population growth in the Indian subcontinent. *Int. J. Remote Sens.* 32: 9137–9149.

Kishcha, P., da Silva, A.M., Starobinets, B. and Alpert, P. (2014). Air pollution over the Ganges basin and northwest Bay of Bengal in the early postmonsoon season based on NASA MERRAero data. *J. Geophys. Res.: Atmos.* 119: 1555–1570.

Kishcha, P., da Silva, A., Starobinets, B., Long, C., Kalashnikova, O. and Alpert, P. (2015). Saharan dust as a causal factor of hemispheric asymmetry in aerosols and cloud cover over the tropical Atlantic Ocean. *Int. J. Remote Sens.* 36: 3423–3445.

Klimont, Z., Smith, S.J. and Cofala, J. (2013). The last decade of global anthropogenic sulfur dioxide: 2000–2011 emissions. *Environ. Res. Lett.* 8: 014003.

Konovalov, I.B., Beekmann, M., Kuznetsova, I.N., Yurova, A. and Zvyagintsev, A.M. (2011). Atmospheric impacts of the 2010 Russian wildfires: integrating modelling and measurements of an extreme air pollution episode in the Moscow region. *Atmos. Chem. Phys.* 11: 10031–10056.

Lehsten, V., Tansey, K., Balzter, H., Thonicke, K., Spessa, A., Weber, U., Smith, B. and Arneeth, A. (2009). Estimating carbon emissions from African wildfires. *Biogeosciences* 6: 349–360.

Lin, J.T., Pan, D. and Zhang, R.X. (2013). Trend and interannual variability of Chinese air pollution since 2000 in association with socioeconomic development: a brief overview. *Atmos. Ocean. Sci. Lett.* 6: 84–89.

Lohmann, U. and Feichter, J. (2005). Global indirect aerosol effects: a review. *Atmos. Chem. Phys.* 5: 715–737.

Lu, Z., Streets, D.G., Zhang, Q., Wang, S., Carmichael, G.R., Cheng, Y.F., Wei, C., Chin, M., Diehl, T. and Tau, Q. (2010). Sulfur dioxide emissions in China and sulfur trends in East Asia since 2000. *Atmos. Chem. Phys.* 10: 6311–6331.

Lu, Z., Zhang, Q. and Streets, D.G. (2011). Sulfur dioxide and primary

carbonaceous aerosol emissions in China and India, 1996–2010. *Atmos. Chem. Phys.* 11: 9839–9864.

Malingreau, J.P., Eva, H.D. and de Miranda, E.E. (2012). Brazilian Amazon: a significant five year drop in deforestation rates but figures are on the rise again. *AMBIO* 41: 309–314.

Mercier, J.R. (2012). Revisiting deforestation in Africa (1990–2010): one more lost generation. *Madag. Conserv. Ecol.* 7: 5–8.

Molina, L.T. and Molina, M.J. (2004). Improving air quality in megacities: Mexico City case study. *Ann. N.Y. Acad. Sci.* 1023: 142–158.

Moore, M., Gould, P. and Keary, B.S. (2003). Global urbanization and impact on health. *Int. J. Hyg. Environ. Health* 206: 269–278.

Nowottnick, E.P., Colarco, P.R., Welton, E.J. and da Silva, A. (2015). Use of the CALIOP vertical feature mask for evaluating global aerosol models. *Atmos. Meas. Tech.* 8: 3647–3669.

Parrish, D.D., Singh, H.B., Molina, L. and Madronich, S. (2011). Air quality progress in North American megacities: a review. *Atmos. Environ.* 45: 7015–7025.

Pey, J., Querol, X., Alastuey, A., Forastiere, F. and Stafoggia, M. (2013). African dust outbreaks over the Mediterranean basin during 2001–2011: PM₁₀ concentrations, phenomenology and trends, and its relation with synoptic and mesoscale meteorology. *Atmos. Chem. Phys.* 13: 1395–1410.

Pöschl, U. (2005). Atmospheric aerosols: composition, transformation, climate and health effects. *Angew. Chem. Int. Edit.* 44: 7520–7540.

Prospero, J.M. and Mayol-Bracero, O.L. (2013). Understanding the transport and impact of African dust on the Caribbean basin. *Bull. Am. Meteorol. Soc.* 94: 1329–1337.

Provençal, S., Buchard, V., da Silva, A.M., Leduc, R. and Barrette, N. (2017a). Evaluation of PM surface concentration simulated by Version 1 of NASA's MERRA Aerosol Reanalysis over Europe. *Atmos. Pollut. Res.* 8: 374–382.

Provençal, S., Buchard, V., da Silva, A.M., Leduc, R., Barrette, N., Elhacham, E. and Wang, S.H. (2017b). Evaluation of PM_{2.5} surface concentrations simulated by Version 1 of NASA's MERRA Aerosol Reanalysis over Israel and Taiwan. *Aerosol Air Qual. Res.* 17: 253–261.

Querol, X., Pey, J., Pandolfi, M., Alastuey, A., Cusack, M., Pérez, N., Monero, T., Viana, M., Mihalopoulos, N., Kallos, G. and Kleanthous, S. (2009). African dust contributions to mean ambient PM₁₀ mass-level across the Mediterranean basin. *Atmos. Environ.* 43: 4266–4277.

Remer, L.A., Kaufman, Y.J., Tanré, D., Mattoo, S., Chu, D.A., Martins, J.V.,

Li, R.R., Ichoku, C., Levy, R.C., Kleidman, R.G., Eck, T.F., Vermote E., Holben, B.N., 2005. The MODIS aerosol algorithm, products, and validation. *J. Atmos. Sci.* 62, 947–973.

Rienecker, M.M., Suarez, M.J., Gelaro, R., Todling, R., Bacmeister, J., Liu, E., Bosilovich, M.G., Schubert, S.D., Takacs, L., Kim, G.K., Bloom, S., Chen, J., Collins, D., Conaty, A., da Silva, A., Gu, W., Joiner, J., Koster, R.D., Lucchesi, R., Molod, A., Owens, T., Pawson, S., Pegion, P., Redder, C.R., Reichle, R., Robertson, F.R., Ruddick, A.G., Sienkiewicz, M. and Woollen, J. (2011). MERRA: NASA's Modern-Era Retrospective Analysis for Research and Application. *J. Clim.* 24: 3624–3648.

Russell, A.R., Valin, L.C. and Cohen, R.C. (2012). Trends in OMI NO₂ observations over the United States: effects of emission control technology and the economic recession. *Atmos. Chem. Phys.* 12: 12197–12209.

Sena, E.T., Artaxo, P. and A.L. Correia, A.L. (2013). Spatial variability of the direct radiative forcing of biomass burning aerosols and the effects of land use change in Amazonia. *Atmos. Chem. Phys.* 13: 1261–1275.

Shao, M., Tang, X., Zhang, Y. and Li, W. (2006). City clusters in China: air and surface water pollution. *Front. Ecol. Environ.* 4: 353–361.

Sharma, R. and Joshi, P.K. (2016). Mapping environmental impacts of rapid urbanization in the national capital region of India using remote sensing inputs. *Urban Clim.* 15: 70–82.

Spracklen, D.V., Logan, J.A., Mickley, L.J., Park, R.J., Yevich, R., Westerling, A.L. and Jaffe, D.A. (2007). Wildfires drive interannual variability of organic carbon aerosol in the western U.S. in summer. *Geophys. Res. Lett.* 34: L16816.

Subbotina, T.P. (2004). *Beyond economic growth: an introduction to sustainable development*, 2nd ed. The International Bank for Reconstruction and Development, Washington, USA.

Sullivan, R.C., Guazzotti, S.A., Sodeman, D.A. and Prather, K.A. (2007). Direct observations of the atmospheric processing of Asian mineral dust. *Atmos. Chem. Phys.* 7: 1213–1236.

Tager, I.B. (2013). *Health effects of aerosols: mechanisms and epidemiology*. In: Ruzer, L.S. and Harley, N.H. *Aerosols handbook: measurement, dosimetry, and health effects*, 2nd ed. CRC Press, Boca Raton, pp. 565–636.

Tørseth, K., Aas, W., Breivik, K., Fjæraa, A.M., Fiebig, M., Hjellbrekke, A.G., Lund Myhre, C., Solberg, S. and Yttri, K.E. 2012. Introduction to the European Monitoring and Evaluation Programme (EMEP) and observed atmospheric composition change during 1972–2009. *Atmos. Chem. Phys.* 12: 5447–5481.

United Nations (2014). World urbanization prospects, the 2014 revision. <http://esa.un.org/unpd/wup/CD-ROM/>. Accessed 1 December 2015.

van Donkelaar, A., Martin, R.V., Levy, R.C., da Silva, A.M., Krzyzanowski, M., Chubarova, N.E., Semutnikova, E. and Cohen, A.J. (2011). Satellite-based estimates of ground-level fine particulate matter during extreme events: a case study of the Moscow fires in 2010. *Atmos. Environ.* 45: 6225–6232.

van der Werf, G.R., Randerson, J.T., Giglio, L., Collatz, G.J., Mu, M., Kasibhatla, P.S., Morton, D.C., Defries, R.S., Jin, Y. and van Leeuwen, T.T. (2010). Global fire emissions and the contribution of deforestation, savanna, forest, agricultural, and peat fires (1997–2009). *Atmos. Chem. Phys.* 10: 11707–11735.

Vestreng, V., Myhre, G., Fagerli, H., Reis, S. and Tarrason, L. (2007). Twenty-five years of continuous sulfur dioxide emission reduction in Europe. *Atmos. Chem. Phys.* 7: 3663–3681.

Vrekoussis, M., Richter, A., Hilboll, A., Burrows, J.P., Gerasopoulos, E., Lelieveld, J., Barrie, L., Zarefos, C. and Mihalopoulos, N. (2013). Economic crisis detected from space: air quality observations over Athens/Greece. *Geophys. Res. Lett.* 40: 458–463.

Wakamatsu, S., Morikawa, T. and Ito, A. (2013). Air pollution trends in Japan between 1970 and 2012 and impact of urban air pollution countermeasures. *Asian J. Atmos. Environ.* 7: 177–190.

Wang, S. and Hao, J. (2012). Air quality management in China: issues, challenges, and options. *J. Environ. Sci.* 21: 2–13.

Xing, J., Pleim, J., Mathur, R., Pouliot, G., Hogrefe, C., Gan, C.M. and Wei, C. (2013). Historical gaseous and primary aerosol emissions in the United States from 1990–2010. *Atmos. Chem. Phys.* 13: 7531–7549.

Yi, B., Yang, P., Dessler, A. and da Silva, A.M. (2015). Response of aerosol direct radiative effect to the East Asian summer monsoon. *IEEE Geosci. Remote Sens. Lett.* 12: 597–600.

Zhang, Q., He, K. and Huo, H. (2012). Cleaning China's air. *Nature* 484: 161–162.

Zhang, Y.L. and Cao, F. (2015). Fine particulate matter (PM_{2.5}) in China at a city level. *Sci. Rep.* 5: 14884.

Zhao, B., Wang, S., Dong, X., Wang, J., Duan, L., Fu, X., Hao, J. and Fu, J. (2013a). Environmental effects of the recent emission changes in China: implications for particulate matter pollution and soil acidification. *Environ. Res. Lett.* 8: 024031.

Zhao, Y., Zhang, J. and Nielsen, C.P. (2013b). The effects of recent control

policies on trends in emissions of anthropogenic atmospheric pollutants and CO₂ in China. *Atmos. Chem. Phys.* 13: 487–508.

6 Conclusion générale

6.1 Introduction

MERRAero est un outil novateur pour étudier une vaste gamme de sujets sur les aérosols atmosphériques à l'échelle globale. Son assimilation de données modélisées et observées lui permet de reproduire la concentration et l'AOD de plusieurs espèces d'aérosols partout sur la Terre, à une fréquence horaire et avec une bonne résolution; de l'information qu'aucun réseau de surveillance ne peut fournir.

Comme tout modèle, MERRAero a dû traverser un processus d'évaluation rigoureux afin que sa simulation soit utilisée avec une certaine confiance. L'objectif de cette thèse était de poursuivre le travail de Buchard *et al.* (2014; 2015; 2016) qui ont évalué son assimilation de l'AOD, et sa simulation de la concentration de SO₂ et des SO₄ principalement aux É.-U. Une évaluation approfondie a été entreprise pour évaluer la concentration de toutes les espèces d'aérosols simulées par MERRAero aux É.-U. et en Europe, en plus d'une évaluation de la concentration des PM_{2.5} en Israël et à Taïwan. Israël est une région d'intérêt par sa proximité aux grands déserts qui sont une source importante de PM d'origine naturelle, et Taïwan est d'un intérêt tout aussi important par sa proximité à la Chine qui est aux prises avec de graves problèmes de pollution depuis plus d'une décennie.

6.2 Les résultats de l'évaluation

6.2.1 États-Unis

Le Chap. 2 a poursuivi une évaluation approfondie aux É.-U. en évaluant la concentration de toutes les espèces d'aérosols reproduites par MERRAero (SO₄, OC, BC, PS et SM) ainsi que la reconstruction des PM₁₀ et

PM_{2.5} avec le réseau IMPROVE entre 2003 et 2013.

En région rurale, dans l'ensemble, MERRAero a surestimé la concentration de toutes les espèces d'aérosols, par un facteur de 1,34 pour les PM₁₀, 1,38 pour les PM_{2.5}, 1,10 pour les SO₄, 1,87 pour le OC, 1,74 pour le BC, 1,94 pour la PS_{2.5} et 7,81 pour le SM_{2.5}. Ces valeurs sont cependant sujettes à des simplifications d'erreurs et influencées disproportionnellement par des paires de données extrêmes. En contrepartie, le *FAC2*, soit la proportion des paires de données qui satisfont un facteur de 2 entre la concentration observée et la concentration simulée, est un indicateur d'évaluation plus fiable puisqu'il n'est pas influencé par de tels biais. D'après cet indicateur, l'évaluation a reproduit des résultats favorables pour les PM₁₀ (61%), les PM_{2.5} (67%), les SO₄ (67%), le OC (58%) et le BC (53%). L'évaluation pour la PS_{2.5} et le SM_{2.5} a toutefois été défavorable due en partie à un biais systémique dans les observations.

L'évaluation dans l'Est des É.-U. était beaucoup plus favorable que dans l'Ouest. L'Est des É.-U. est une région fortement industrialisée, ce qui résulte à une concentration de PM d'origine anthropique plus élevée. L'Ouest des É.U. est affecté périodiquement par des feux de forêt qui contribuent à augmenter la concentration des PM pendant la saison estivale. MERRAero a largement exagéré cette contribution naturelle de OC et de BC, un constat qui nous permet de conclure que MERRAero éprouve davantage de difficulté à simuler la concentration de PM de sources naturelles comparativement aux particules de sources anthropiques. MERRAero a aussi exagéré la concentration de la PS d'origine lointaine, notamment dans le Sud-Ouest des É.-U. qui est influencé par l'advection de PS venant des déserts dans l'Est de l'Asie, et dans le Sud-Est, une région influencée par l'advection de PS venant du Sahara.

En région urbaine, l'évaluation a été tout aussi favorable mais MERRAero a sous-estimé la concentration des PM₁₀ et des PM_{2.5}, dû au

manque des NO_3 dans sa simulation. La sous-estimation a été particulièrement importante en hiver pour les PM_{10} , les $\text{PM}_{2.5}$, le OC et le BC. Le chauffage au bois et les feux de foyer sont une source importante de tels contaminants en hiver qui n'est pas simulée ou capturée par la résolution de MERRAero.

6.2.2 Europe

Le Chap. 3 a poursuivi l'évaluation en Europe avec le réseau EMEP entre 2003 et 2014. Dans l'ensemble, l'évaluation a été favorable pour la concentration des PM_{10} , des $\text{PM}_{2.5}$, des SO_4 et du BC. Comme en milieu urbain aux É.-U., MERRAero a sous-estimé largement la concentration des $\text{PM}_{2.5}$ et du OC en hiver dans l'ensemble de l'Europe. La plupart des stations d'observations en Europe sont situées à proximité de quartiers résidentiels qui sont source de contaminants anthropiques. Une analyse régionale a cependant permis d'identifier deux stations en Italie qui étaient responsables de cette forte concentration hivernale. Une des deux stations est située au nord de l'Italie, soit au pied des Alpes; une position idéale pour isoler les contaminants provenant des villes avoisinantes et de Milan, située à 50 km au sud. L'autre, située au centre de l'Italie, est localisée à l'ouest des Apennins, aussi bien positionnée pour capturer les contaminants provenant des villes dans l'ouest. Lorsque ces stations ont été exclues de l'échantillon, l'évaluation s'est nettement améliorée. La sous-estimation a cependant persisté pendant la saison hivernale mais était beaucoup moins prononcée.

6.2.3 Israël et Taïwan

Le Chap. 4 a poursuivi l'évaluation en Israël et à Taïwan avec des données de la concentration des $\text{PM}_{2.5}$ fournies par les autorités locales.

L'évaluation en Israël était d'un intérêt particulier puisque qu'il est situé à proximité de grands déserts, occasionnant une concentration élevée de $PM_{2.5}$ composée principalement de particules d'origine naturelle. L'évaluation à Taïwan était d'un intérêt tout aussi important puisque la Chine traverse depuis plus d'une décennie une importante croissance économique et industrielle qui a de sérieuses répercussions sur la qualité de l'air. Les épisodes de pollution intense y sont effectivement courants.

L'évaluation en Israël a reproduit des résultats très favorables, surestimant la concentration des $PM_{2.5}$ que de 6% en moyenne. Ceci indique que MERRAero simule bien la concentration des PM d'origine naturelle et locale. L'évaluation de MERRAero à Taïwan était moins favorable, sous-estimant la concentration par un facteur de 1,43. La sous-estimation est particulièrement prononcée au cours de l'hiver mais aussi présente au printemps et à l'automne. Deux raisons expliquent ce biais : 1) les émissions de SO_2 en Chine regorgent d'incertitudes et 2) le manque des NO_3 dans la simulation de MERRAero est beaucoup plus problématique dans cette région du monde très polluée. Effectivement, l'évaluation était davantage favorable pendant l'été, lorsque Taïwan est le moins affecté par la pollution d'origine chinoise. Cette période de l'année correspond à la saison des typhons, lorsque Taïwan est balayé par de forts vents et des pluies diluviennes, ce qui tend à assainir l'air.

6.3 L'application à l'étude de la pollution de l'air urbain à l'échelle globale

Malgré les biais identifiés au cours de cette recherche, les évaluations ont reproduit des résultats suffisamment favorables pour affirmer que MERRAero est un outil de réanalyse fiable dans l'ensemble. Comme des biais plus importants ont été signalés en milieux urbains, ou du moins dans des régions où les sources résidentielles d'aérosols sont considérables,

l'usage des données d'AOD aux dépens des données de concentration a été favorisé pour l'application à l'étude de la pollution de l'air urbain puisque MERRAero assimile directement des données d'AOD dans sa réanalyse.

Notamment, l'analyse a démontré l'impact que les politiques environnementales et la récession économique récente ont eu sur la pollution atmosphérique des villes dans les pays développés, par une baisse marquée des SO_4 dans presque toutes les villes d'Amérique du Nord, d'Europe et d'Asie de l'Est. Ce constat s'applique aussi aux villes chinoises malgré le fait qu'elles traversent depuis deux décennies une montée fulgurante d'urbanisation et d'industrialisation accompagnée par des épisodes récurrents de pollution. L'AOD au-dessus des villes chinoises est effectivement parmi les plus élevées au monde. Dans ce sens, l'initiative du gouvernement chinois à réduire les émissions de contaminants tout en conservant sa croissance économique démontre des premiers signes encourageants. Les villes de l'Inde et du Bangladesh, deux autres pays qui expérimentent une montée importante d'urbanisation et d'industrialisation depuis plusieurs années, ont, quant à elles, observé une croissance constante de l'AOD.

Des régions qui sont principalement affectées par la combustion de biomasse, soit l'Amérique du Sud et l'Afrique équatoriale, ont aussi vu leurs conditions s'améliorer au cours des dix dernières années. Les activités de déforestation ont substantiellement ralenti, particulièrement dans la forêt amazonienne, causées par une augmentation des prix des produits agricoles.

6.4 Conclusion et perspectives

Les conclusions de l'évaluation se résument ainsi :

- Dans l'ensemble, la concentration des SO_4 est bien estimée. Cependant, MERRAero bénéficierait d'un inventaire d'émissions de SO_2 qui fluctue

d'une année à l'autre. Comme les émissions de SO₂ ont beaucoup évolué au cours de la dernière décennie, l'inventaire de 2005 devient de plus en plus vétuste. Le biais entre la simulation et les observations se creuse depuis cette année tant aux É.-U. qu'en Europe et à Taïwan;

- La concentration anthropique du OC est bien estimée à l'exception des contributions résidentielles qui sont importantes en hiver. Ces sources ne sont pas assimilées par MERRAero;
- La concentration naturelle du OC issue des feux de forêt est largement surestimée;
- Comme le BC provient des mêmes sources que le OC, l'évaluation de la concentration du BC est sujette aux mêmes biais que celle du OC. Par contre, la concentration du BC est généralement mieux estimée que celle du OC. Le BC contribue très peu à la concentration totale des PM₁₀ et des PM_{2.5};
- L'évaluation de la concentration de la PS_{2.5} a reproduit des résultats contradictoires : bien estimée en Israël mais surestimée aux É.-U. Contrairement à Israël, les É.-U. sont affectés par des sources lointaines de PS. Ceci suggère possiblement que MERRAero ne simule pas adéquatement les puits d'aérosols, notamment par la déposition et les précipitations, et donc le transport d'aérosols sur de longues distances;
- La concentration des SM_{2.5} est surestimée de manière constante, tant aux É.-U. qu'en Europe. L'évaluation n'a pas permis d'identifier une cause certaine, mais comme la surestimation tend à être particulièrement évidente dans les régions côtières, il est probable que les sources de SM_{2.5} soient tout simplement exagérées. À l'extérieur des régions côtières, les SM_{2.5} contribuent très peu aux PM₁₀ et aux PM_{2.5};
- Dans l'ensemble, la concentration des PM_{2.5} est bien estimée mais est sujette aux mêmes biais que les différentes espèces;
- La concentration des PM₁₀ est généralement bien estimée mais

légèrement surestimée de manière constante. Les PM_{10} sont principalement composées de PS et de SM. Si la concentration du SM_{10} est surestimée dans la même mesure que celle du $SM_{2.5}$, ceci pourrait expliquer ce biais;

- La simulation bénéficierait de l'inclusion des NO_3 , particulièrement dans les régions urbaines et les régions polluées (e.g., Asie de l'Est).

La NASA a déjà apporté quelques améliorations à la version subséquente de MERRAero (MERRA-2) en assimilant des données provenant d'autres instruments de télédétection : MISR, AERONET et le *Advanced Very High Resolution Radiometer* (AVHRR, <http://noaasis.noaa.gov/NOAASIS/ml/avhrr.html>). Ces instruments permettent une meilleure assimilation de l'AOD au-dessus des surfaces claires, telles que les déserts, puisque MODIS éprouve effectivement des difficultés à mesurer l'AOD au-dessus de telles régions.

Cette évaluation a testé l'efficacité de MERRAero à simuler la concentration des aérosols à la surface dans plusieurs régions du monde qui ont des profils d'aérosols différents et où un réseau de mesures le permet. MERRAero étant une réanalyse de très grande envergure, des évaluations supplémentaires auraient pu être effectuées afin d'étoffer les résultats mais n'ont pu être poursuivies, faute de ressources disponibles. Notamment, des évaluations en Amérique du Sud et en Afrique subsaharienne auraient certainement contribué de l'information additionnelle à l'évaluation de la concentration simulée des particules de carbone effectuée aux É.-U. Ces deux régions sont cependant dépourvues de toute surveillance fiable. De plus, la capacité de MERRAero à simuler l'AOD de chacune des espèces d'aérosols est l'une de ses composantes qui ne peut être évaluée pour l'instant, puisque les instruments à notre disposition sont incapables de mesurer cette distinction.

Néanmoins, les travaux de recherche effectués au cours de cette thèse

permettront, d'une part, à la NASA d'apporter des améliorations aux versions subséquentes de MERRAero qui n'ont toujours pas été adressées, et d'autre part, à des chercheurs désirant utiliser MERRAero pour leurs propres travaux d'avoir une certaine confiance envers la qualité de la simulation et d'être conscients de ses lacunes. MERRAero permet d'étudier une vaste gamme de problématiques liées à la pollution de l'air à l'échelle globale que les réseaux de surveillance standards ne permettent pas. Comme l'a démontré le Chap. 5, MERRAero a permis d'effectuer une étude approfondie de la pollution urbaine de l'air, tout comme elle peut être utilisée pour étudier de nombreux autres sujets, tels que la chimie et la dispersion atmosphérique, l'influence des aérosols sur la formation des nuages et sur les changements climatiques, et les mécanismes de déposition des aérosols, pour ne nommer que quelques exemples.

Références

Buchard, V., da Silva, A.M., Colarco, P., Krotkov, N., Dickerson, R.R., Stehr, J.W., Mount, G., Spinei, E., Arkinson, H.L. et He, H. (2014). Evaluation of GEOS-5 sulfur dioxide simulations during the Frostburg, MD 2010 field campaign. *Atmos. Chem. Phys.* 14 : 1929–1941.

Buchard, V., da Silva, A.M., Colarco, P.R., Darmenov, A., Randles, C.A., Govindaraju, R., Torres, O., Campbell, J. et Spurr, R. (2015). Using the OMI aerosol index and absorption aerosol optical depth to evaluate the NASA MERRA Aerosol Reanalysis. *Atmos. Chem. Phys.* 15 : 5743–5760.

Buchard, V., da Silva, A.M., Randles, C.A., Colarco, P., Ferrare, R., Hair, J., Hostetler, C., Tackett, J. et Winker, D. (2016). Evaluation of the surface PM_{2.5} in Version 1 of the NASA MERRA Aerosol Reanalysis over the United States. *Atmos. Environ.* 125 : 100–111.

A1 Une analyse statistique entre la concentration de particules fines et d’ozone en présence de brume sèche dans le Sud du Québec

Résumé

La proximité du Sud de l’Ontario et du Nord-Est des États-Unis positionne le Québec dans une situation de vulnérabilité face à l’advection de contaminants atmosphériques en provenance de ces régions très industrialisées et peuplées. La visibilité réduite est un indicateur bien connu d’une piètre qualité de l’air lorsque les conditions atmosphériques sont sèches. Lorsque la visibilité est inférieure à 10 km et que l’humidité relative est faible, un épisode de brume sèche est signalé dans l’observation météorologique. Il est donc intuitif d’associer un épisode de brume sèche à un niveau élevé de contaminants atmosphériques. Plusieurs études associent la brume sèche à une concentration élevée d’ozone, et bien que l’ozone soit un gaz qui n’absorbe ni ne disperse la lumière, il est couramment utilisé comme indicateur de visibilité réduite. L’objectif de cette étude est de vérifier si l’ozone est effectivement un indicateur fiable de visibilité réduite au même titre que les particules fines qui, elles, réduisent véritablement la visibilité. À l’aide de données provenant de stations de surveillance météorologique et de qualité de l’air, une analyse statistique est effectuée entre la concentration de ces deux contaminants lorsque la brume sèche est signalée dans les trois régions métropolitaines les plus peuplées du Sud du Québec : Montréal, Québec et Gatineau. Les résultats suggèrent que la concentration de particules fines est élevée lorsque la brume sèche est signalée, mais, par contre, la concentration d’ozone est beaucoup plus variable. Moins de la moitié des observations de brume sèche est accompagnée d’une concentration élevée d’ozone. Les cycles annuels et quotidiens expliquent en partie cette variabilité; les épisodes de brume sèche estivaux et diurnes sont caractérisés par une concentration élevée d’ozone plus fréquente, contrairement aux épisodes hivernaux, alors qu’à peine quelques observations de brume sèche sont caractérisées ainsi.

A1.1 Introduction

Le Sud du Québec est localisé à proximité des régions fortement industrialisées et peuplées du Sud de l’Ontario et du Nord-Est des États-

Unis. Les activités industrielles et l'urbanisation ont des conséquences négatives sur plusieurs sphères de l'environnement, comme la pollution des terres, de l'eau et de l'air. Le Québec est particulièrement vulnérable quant à l'advection de contaminants atmosphériques provenant du sud, avec le potentiel de détériorer la qualité de son air, bien que le Sud du Québec soit, lui aussi, industrialisé et peuplé et contribue ainsi à polluer son propre air. Les contaminants toxiques de l'air ont de graves effets sur la santé des individus; ils sont associés à l'occurrence des maladies cardio-vasculaires et respiratoires (Brunekreff et Holgate, 2002). Ils peuvent aussi nuire aux récoltes agricoles (Heck *et al.*, 1982).

La combustion de combustibles fossiles émet des oxydes d'azote (NO_x) et des oxydes de soufre (SO_x) dans l'air. Suite à une chaîne de réactions chimiques et de processus physiques, ils peuvent produire des particules fines secondaires ($\text{PM}_{2.5}$, particules dont le diamètre est égal ou inférieur à $2,5 \mu\text{m}$), plus spécifiquement surnommées nitrates et sulfates. La combustion de combustibles fossiles et de biomasse libère aussi des $\text{PM}_{2.5}$ sous forme de particules carbonées. D'autres espèces chimiques se retrouvent dans les $\text{PM}_{2.5}$, telles qu'une variété de poussière minérale, mais les nitrates, les sulfates et les particules carbonées constituent la majeure partie de la concentration massique des $\text{PM}_{2.5}$ observée à travers le Canada (Brook et Dann, 1999; Jeong *et al.*, 2011). En présence de composés organiques volatils, les NO_x peuvent aussi produire de l'ozone (O_3). Dans le passé, les $\text{PM}_{2.5}$ et l' O_3 étaient alors traités comme des problèmes de pollution indépendants l'un de l'autre, mais il existe bien un couplage chimique entre les deux (Meng *et al.*, 1997).

Plusieurs études argumentent que l'advection de tels contaminants des États-Unis mène à des épisodes de pollution atmosphérique au Québec (Thibault *et al.*, 1995; Leduc et Roy-Loubier, 2005) et ailleurs au Canada (Munn, 1973; Vickers et Munn, 1977; Chung, 1977; 1978; Thurston *et al.*, 1994; Brook *et al.*, 2002). L'advection de contaminants en provenance de

l'Ontario impacte aussi le Québec (Leduc et Roy-Loubier, 2005). Une caractéristique géographique importante du Sud du Québec est la vallée du fleuve Saint-Laurent dont la topographie emprisonne les contaminants en provenant du sud et les canalise le long du fleuve. Plusieurs villes se retrouvent sur ses rives, notamment Montréal, Trois-Rivières et Québec.

Lorsque la concentration de contaminants atmosphériques est élevée, il est possible que la visibilité soit réduite. Si l'humidité relative est faible, il est d'usage de penser qu'une visibilité réduite est un indicateur de mauvaise qualité de l'air. Les standards canadiens prescrivent une observation de brume sèche lorsque la visibilité est inférieure à 10 km et que l'humidité relative est faible (Vickers et Munn, 1977 ; Environnement Canada, 2015). Donc il est intuitif d'associer un épisode de brume sèche à une concentration élevée de contaminants atmosphériques. Toutes les espèces de particules en suspension réduisent la visibilité, mais d'après des données provenant de stations de surveillance à travers le Canada, les sulfates et les nitrates contribuent particulièrement à obstruer la visibilité (McDonald et Shepherd, 2004).

Leduc et Pépin (1995) ont analysé l'évolution des observations de brume sèche dans plusieurs villes du corridor Windsor-Québec entre 1953 et 1990. Ils ont observé une fréquence maximale à London (Ontario) qui diminue progressivement jusqu'à Sept-Îles (Québec). Dans le même article, ils ont brièvement analysé le lien entre l'occurrence de brume sèche et la concentration d'O₃ à Montréal entre 1979 et 1990 à l'aide d'un tableau de fréquences simple. Ils ont conclu que la fréquence de brume sèche est plus élevée lorsque la concentration d'O₃ est élevée elle aussi. Lorsqu'ils ont publié cet article, les PM_{2.5} n'étaient pas mesurées au Québec. À cette époque, l'O₃ était alors utilisé comme indicateur de pollution photochimique et de visibilité réduite, bien que n'ayant aucun impact sur la visibilité. Des études de cas d'épisodes estivaux de brume sèche associent la brume sèche (ou la visibilité réduite) à de fortes concentrations d'O₃ (Wolff *et al.*, 1981;

1982; King et Vukovich, 1982; Diederer *et al.*, 1985; Aneja *et al.*, 2004; Taubman *et al.*, 2004). Une concentration élevée d'O₃ a aussi été observée dans la brume sèche arctique (Herbert *et al.*, 1989) et dans la fumée de feux de forêt (Radke *et al.*, 1978; Stith *et al.*, 1981; Delany *et al.*, 1985; Andreae *et al.*, 1988).

Il est important de noter que la composition chimique de la brume sèche peut différer et que celle-ci affecte la production d'O₃. Toutes les formes de combustion (charbon, mazout, gaz naturel, pétrole, biomasse, etc.) produisent des oxydes d'azote. En présence de composés organiques volatils, les oxydes d'azote sont très efficaces pour produire de l'O₃ suite à une série de réactions photochimiques complexe. C'est pour cette raison que la brume sèche issue de ces formes de combustion est communément surnommée le smog photochimique. Quant aux dérivés soufrés, ils sont produits principalement par la combustion de charbon. C'est pour cette raison que la brume sèche issue de cette forme de combustion est communément surnommée le smog industriel. Les sulfates sont cependant beaucoup moins efficaces que les oxydes d'azote pour produire de l'O₃. Il n'est donc pas prévu que le smog industriel soit nécessairement accompagné d'une forte concentration d'O₃. Au Québec, le charbon représente à peine 1% de la consommation totale d'énergie; le pétrole (38%) et le gaz naturel (14%), les hydrocarbures sont des sources d'énergie beaucoup plus importantes (Gouvernement du Québec, <http://hydrocarbures.gouv.qc.ca/consommation.asp>). La brume sèche observée au Québec et issue de sources de pollution québécoises serait donc davantage de nature photochimique et propice à la formation d'O₃. Elle peut néanmoins être de nature industrielle et présenter donc une faible concentration d'O₃ en raison des sources de pollution provenant de l'Ontario et des États-Unis, qui sont des régions où la consommation de charbon est plus importante.

L'objectif de cette étude est de vérifier, à l'aide de données récentes, si

l'O₃ est effectivement un indicateur fiable de visibilité réduite, au même titre que les PM_{2.5} dont les données sont maintenant disponibles. Ceci est effectué en analysant des données météorologiques et de qualité de l'air dans les trois régions métropolitaines (les régions métropolitaines seront désormais référées simplement comme des « villes ») les plus peuplées du Sud du Québec : Montréal, Québec et Gatineau.

A1.2 Méthodologie

Cette analyse est effectuée dans les trois villes les plus peuplées du Québec. Dans chacune d'elles, une station météorologique est choisie pour obtenir les observations horaires de brume sèche, signalée ou non. Une station de la qualité de l'air est aussi choisie pour obtenir les observations horaires de PM_{2.5} et d'O₃. Un certain effort a été déployé pour choisir une station située loin du centre-ville et de sources de pollution qui pourraient influencer les données à petite échelle, mais qui contient une série de données substantielle. Les trois villes sont les suivantes :

- Montréal, avec une population métropolitaine de 4 millions d'habitants, constitue près de la moitié de la population totale du Québec. Elle est localisée au creux de la vallée du fleuve Saint-Laurent, à 50 km de la frontière des États-Unis et à 60 km de la frontière de l'Ontario. La station météorologique choisie est à l'aéroport Pierre-Élliott-Trudeau, qui surveille les conditions météorologiques à Montréal depuis plusieurs décennies. La station de la qualité de l'air choisie est à Sainte-Anne-de-Bellevue, située dans une banlieue dans l'Ouest de l'Île de Montréal. Cette station mesure les PM_{2.5} et les O₃ depuis 1997.
- Québec a une population métropolitaine de 800 000 habitants. Elle est située à 230 km en aval de Montréal, donc plus loin des États-Unis et de l'Ontario que Montréal. Le choix d'une station de la qualité de l'air s'est arrêté sur la station Saint-Charles–Garnier qui mesure les deux

contaminants depuis 2003, bien que la station des Sables soit opérationnelle depuis 1998 mais située près du centre-ville et du port de Québec. Les données météorologiques proviennent de l'aéroport Jean-Lesage.

- Gatineau a une population de 275 000 habitants. Cependant, elle fait partie de la région métropolitaine d'Ottawa en Ontario, qui compte une population de 1,3 million d'habitants. Elle est située à 170 km à l'ouest de Montréal, directement sur la frontière ontarienne, et à 75 km de la frontière des États-Unis. La station de la qualité de l'air située dans le secteur Hull est utilisée, elle est en fonction depuis 2003. Les données météorologiques proviennent de l'aéroport Macdonald–Cartier à Ottawa.

Les données de population référencées dans le paragraphe précédent proviennent de Brinkhoff (*City Population*, <http://www.citypopulation.de>). Une carte des trois villes avec la localisation des stations d'observations est tracée dans la Fig. A1.1.

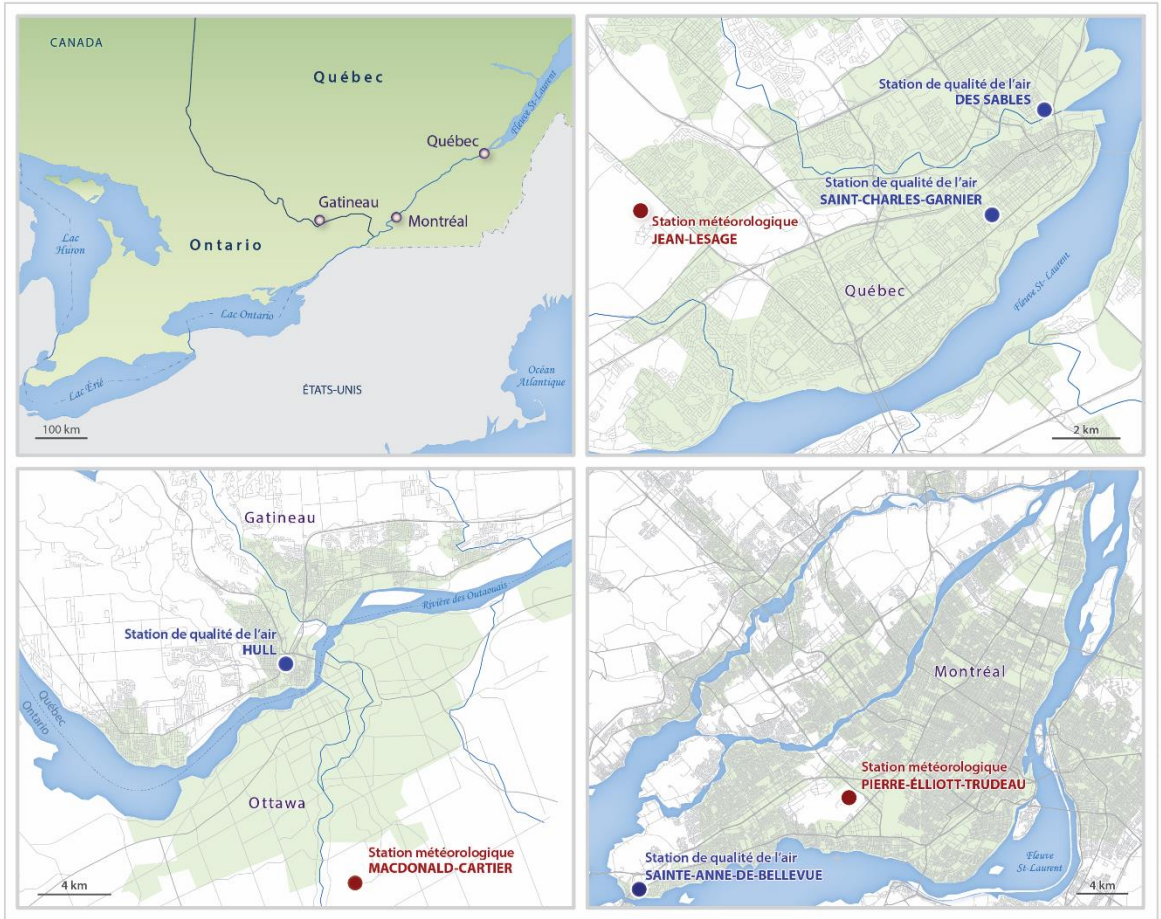


Fig. A1.1 : Carte du Sud du Québec (supérieur gauche) et localisation des stations météorologiques et de qualité de l'air à Québec (supérieur droit), Gatineau (inférieur gauche) et Montréal (inférieur droit).

Une analyse différente est effectuée dans chaque ville. La période d'étude dépend de la disponibilité des données : 1997–2013 pour Montréal, 2003–2013 pour Québec et 2003–2013 pour Gatineau.

Occasionnellement, il arrive qu'une observation de brume sèche soit signalée lorsque l'humidité relative est trop élevée pour la justifier. Afin d'éviter tout doute, un critère est appliqué lorsque la brume sèche est signalée. Ce critère est le même qu'ont utilisé Leduc et Pépin (1995) : $T - T_r > 2^\circ\text{C}$, où T est la température de l'air et T_r est la température du point de rosée. Si une observation de brume sèche est signalée lorsque les conditions ambiantes ne satisfont pas cette condition, cette observation est exclue. L'observation est aussi exclue si la valeur de T ou de T_r est

manquante.

Pour chacun des contaminants (PM_{2.5} et O₃), et dans chacune des trois villes, la série de données de la concentration est séparée en déciles, pour former dix classes de concentration équiprobables. Le premier et le dernier décile, ainsi que d'autres statistiques, sont présentés dans le Tab. A1.1.

Tab. A1.1 : Statistiques des concentrations de PM_{2.5} et d'O₃ à Montréal, Québec et Gatineau jusqu'en 2013. Bien que la surveillance de l'O₃ ait commencé en 2000 à Québec, seulement les données à partir du 1^{er} avril 2003 ont été utilisées pour calculer ces statistiques.

	Montréal		Québec		Gatineau	
	PM _{2.5}	O ₃	PM _{2.5}	O ₃	PM _{2.5}	O ₃
Début des observations	8/10/1997	19/09/1997	4/04/2003	7/09/2000	15/04/2003	1/01/2003
Moyenne	7,69 µg/m ³	24,00 ppb	8,09 µg/m ³	22,84 ppb	6,99 µg/m ³	23,54 ppb
Écart type	8,01 µg/m ³	14,07 ppb	7,54 µg/m ³	12,35 ppb	6,88 µg/m ³	13,16 ppb
1 ^{er} décile	0,85 µg/m ³	4,80 ppb	1,27 µg/m ³	5,59 ppb	0,88 µg/m ³	5,71 ppb
Médiane	5,45 µg/m ³	23,80 ppb	6,00 µg/m ³	23,08 ppb	5,00 µg/m ³	23,32 ppb
9 ^e décile	17,18 µg/m ³	41,80 ppb	17,00 µg/m ³	52,62 ppb	15,40 µg/m ³	40,01 ppb
Échantillon	135 146	138 967	87 799	87 125	89 675	89 818

Tout au long de ce texte, nous faisons référence à une concentration faible pour toute concentration dont la valeur fait partie de la première classe (premiers 10%), et à une concentration élevée pour toute concentration dont la valeur fait partie de la dernière classe (derniers 10%). Ensuite, lorsque la brume sèche est signalée, les données horaires de la concentration des contaminants sont réparties en fonction des classes de concentration des PM_{2.5} et d'O₃. Les Tableaux incluent une classe de concentration faible, une classe de concentration élevée, et deux classes de concentration intermédiaires sont séparées par la médiane. Si la valeur de concentration d'un des deux contaminants est manquante pour une observation spécifique de brume sèche, cette observation ne peut être prise en compte. Malheureusement, des données de qualité de l'air sont souvent manquantes en raison de la calibration fréquente et de la déficience des instruments de mesure.

A1.3 Résultats

L'analyse pour Montréal est effectuée entre 1997 et 2013. Au cours de cette période de 17 ans, 1 479 observations horaires de brume sèche ont été signalées; 272 d'entre elles ont été exclues puisqu'elles ne satisfont pas aux critères retenus. Les observations restantes sont réparties dans le Tab. A1.2 en fonction de leur concentration en PM_{2.5} et O₃. Une grande majorité (> 80%) de ces observations se produit lorsque la concentration des PM_{2.5} est élevée, alors la classe de concentration faible enregistre une fréquence négligeable (< 1%). La situation pour la concentration d'O₃ est bien différente : à peine 25% des observations se produisent lorsque la concentration est élevée. En fait, 12% d'entre elles se produisent lorsque la concentration est faible.

Tab. A1.2 : Distribution des observations de brume sèche en fonction de la concentration de PM_{2.5} et d'O₃.

Montréal		O ₃ (ppb)				Total
		[0, 4,80[[4,80, 23,80[[23,80, 41,80[[41,80, ∞[
PM _{2.5} (µg/m ³)	[0, 0,85[0	3	2	0	5 (0,4%)
	[0,85, 5,45[0	9	1	1	11 (0,9%)
	[5,45, 17,18[30	110	40	12	192 (15,9%)
	[17,18, ∞[119	333	255	292	999 (82,8%)
	Total	149 (12,3%)	455 (37,7%)	298 (24,7%)	305 (25,3%)	1 207
Québec		O ₃ (ppb)				Total
		[0, 5,59[[5,59, 23,08[[23,08, 52,62[[52,62, ∞[
PM _{2.5} (µg/m ³)	[0, 1,27[0	0	0	0	0 (0,0%)
	[1,27, 6,00[0	3	1	0	4 (1,2%)
	[6,00, 17,00[1	15	23	10	49 (15,0%)
	[17,00, ∞[10	56	75	132	273 (83,7%)
	Total	11 (3,4%)	74 (22,7%)	99 (30,4%)	142 (43,6%)	326
Gatineau		O ₃ (ppb)				Total
		[0, 5,71[[5,71, 23,32[[23,32, 40,01[[40,01, ∞[
PM _{2.5} (µg/m ³)	[0, 0,88[0	0	0	0	0 (0,0%)
	[0,88, 5,00[0	0	0	0	0 (0,0%)
	[5,00, 15,40[5	23	18	15	61 (16,6%)
	[15,40, ∞[16	68	87	136	307 (83,4%)
	Total	21 (5,7%)	91 (24,7%)	105 (28,5%)	151 (41,0%)	368

L'analyse pour Québec est effectuée entre 2003 et 2013. Au cours de cette période de 11 ans, 382 observations horaires de brume sèche ont été signalées, 56 d'entre elles ont été exclues puisqu'elles ne satisfont pas aux critères retenus. Les observations restantes sont réparties dans le Tab. A1.2. Comme à Montréal, la totalité des observations se produit lorsque la concentration des PM_{2.5} est élevée. En revanche, 74% des observations de

cette classe ont une concentration d'O₃ supérieure à la médiane.

L'analyse pour Gatineau est effectuée entre 2003 et 2013. Au cours de cette période de 11 ans, 441 observations horaires de brume sèche ont été signalées, 73 d'entre elles ont été exclues puisqu'elles ne satisfont pas aux critères retenus. Les observations restantes sont réparties dans le Tab. A1.2. La situation à Gatineau est semblable à celle de Québec : une grande majorité des observations se retrouve dans la classe de concentration élevée de PM_{2.5}, 41% d'entre elles se produisent au niveau élevé de concentration d'O₃, et 70% d'entre elles ont une concentration d'O₃ supérieure à la médiane.

Ces analyses démontrent, d'une part, le résultat peu surprenant que la concentration de PM_{2.5} est généralement élevée lors d'épisodes de brume sèche, et d'autre part, le résultat plus intéressant que la concentration d'O₃ est plus faible que prévu : plus d'une observation sur deux à Québec et Gatineau, et trois observations sur quatre à Montréal. Il est bien connu que la qualité de l'air manifeste un cycle quotidien et annuel distinct, ce qui est bien perceptible dans nos données (Fig. A1.2 et A1.3). La plus grande fréquence des observations de brume sèche se produit en juin, juillet et août, à l'exception de Montréal où la fréquence en février est particulièrement élevée. La concentration moyenne mensuelle de PM_{2.5} est plus élevée au cours des mois d'été et d'hiver, alors que la concentration moyenne mensuelle d'O₃ est élevée au cours du printemps et faible au cours de l'automne.

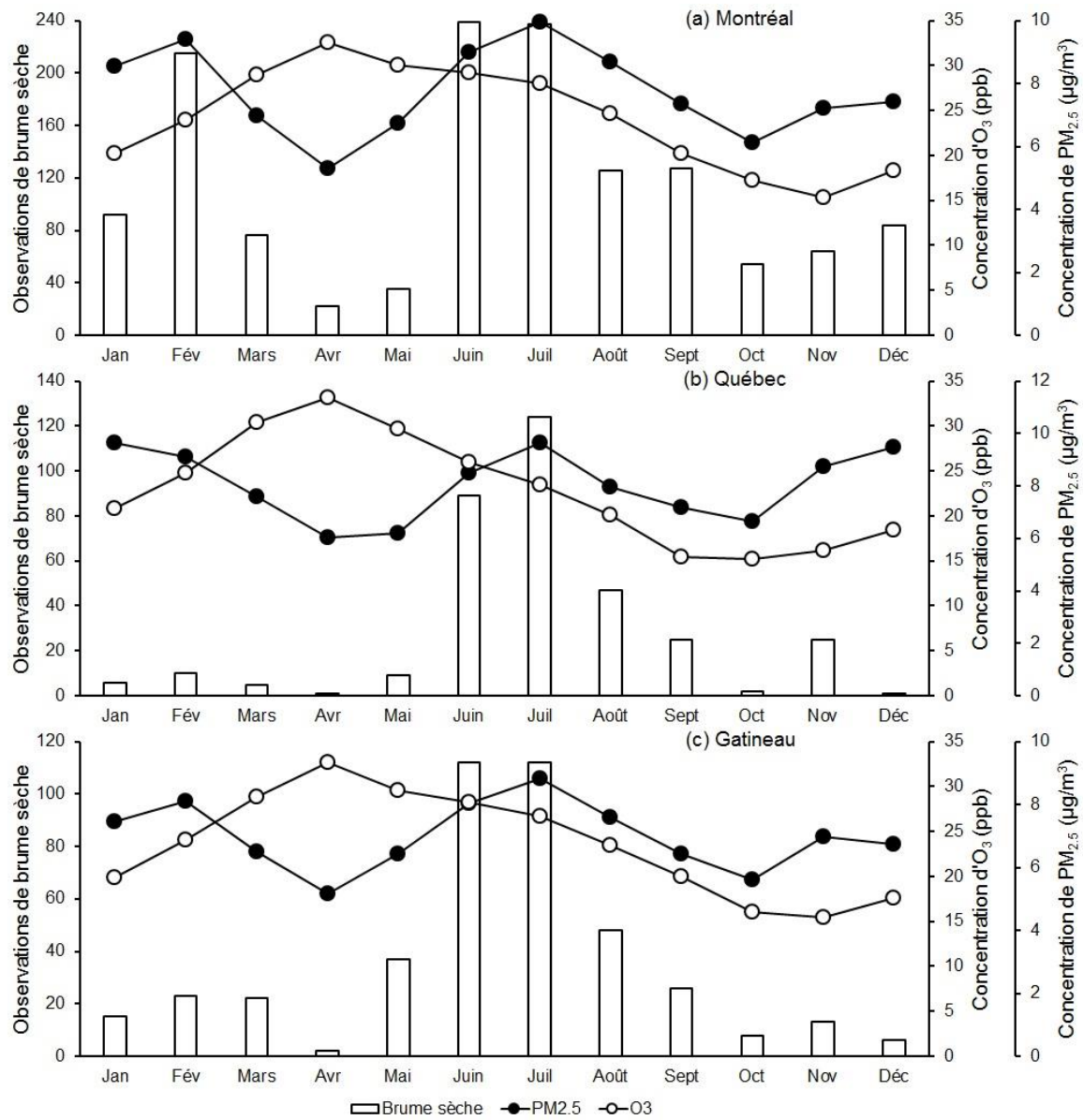


Fig. A1.2 : Fréquence mensuelle des observations de brume sèche et concentration moyenne mensuelle de $\text{PM}_{2.5}$ et d' O_3 à (a) Montréal entre 1997 et 2013, (b) Québec entre 2003 et 2013, et (c) Gatineau entre 2003 et 2013.

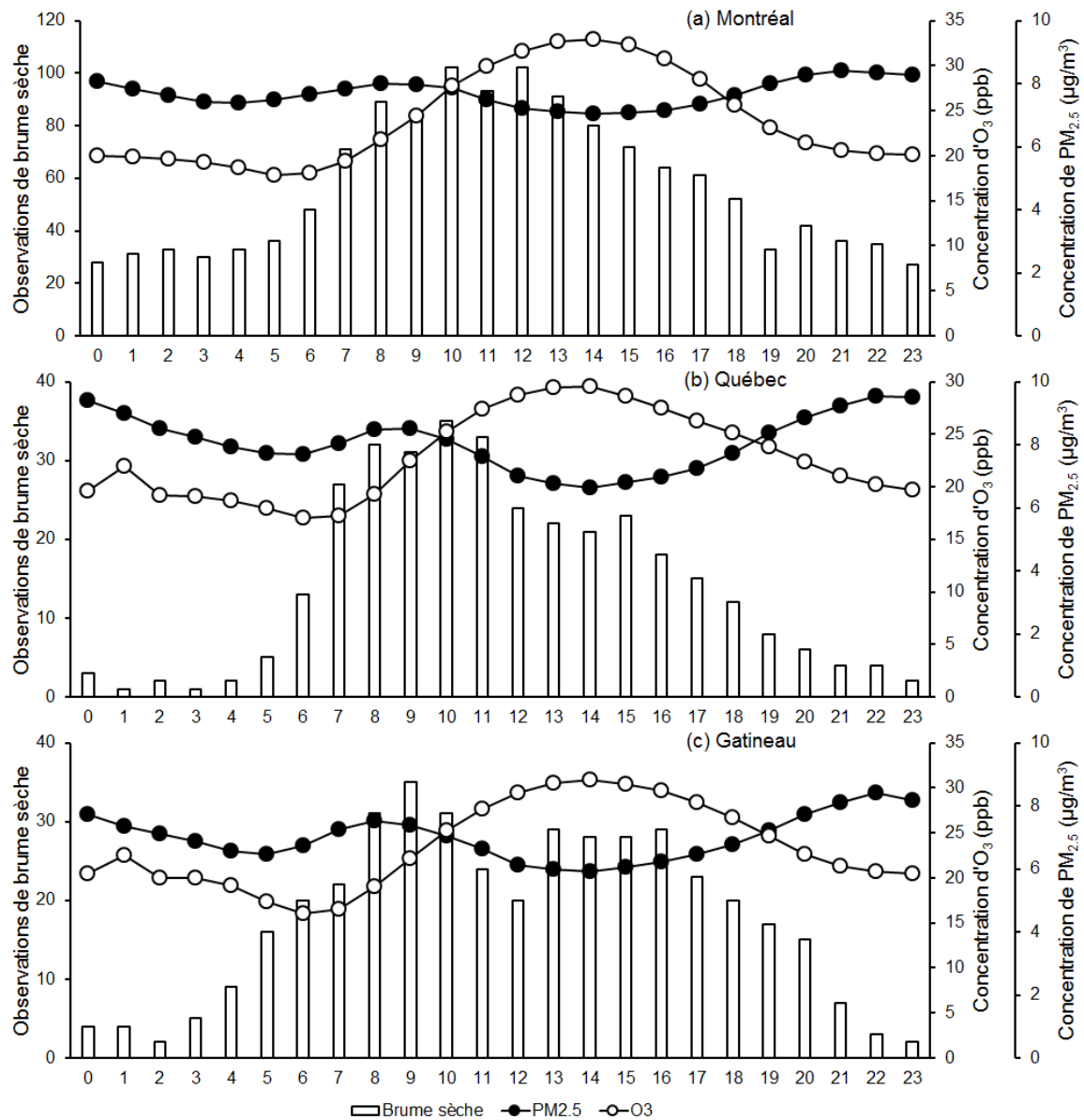


Fig. A1.3 : Fréquence horaire des observations de brume sèche et concentration moyenne horaire de PM_{2,5} et d'O₃ à (a) Montréal entre 1997 et 2013, (b) Québec entre 2003 et 2013, et (c) Gatineau entre 2003 et 2013.

Prenant ceci en considération, le Tab. A1.3, semblable au Tab. A1.2, ne contient que les observations de brume sèche survenues au cours des trois mois d'été (juin, juillet et août).

Tab. A1.3 : Distribution des observations estivales (juin, juillet et août) de brume sèche en fonction de la concentration de PM_{2.5} et d'O₃.

Montréal		O ₃ (ppb)				Total
		[0, 4,80[[4,80, 23,80[[23,80, 41,80[[41,80, ∞[
PM _{2.5} (µg/m ³)	[0, 0,85[0	0	0	0	0 (0,0%)
	[0,85, 5,45[0	1	1	1	3 (0,6%)
	[5,45, 17,18[1	19	21	7	48 (9,6%)
	[17,18, ∞[5	70	145	229	449 (89,8%)
	Total	6 (1,2%)	90 (18,0%)	167 (33,4%)	237 (47,4%)	500
Québec		O ₃ (ppb)				Total
		[0, 5,59[[5,59, 23,08[[23,08, 52,62[[52,62, ∞[
PM _{2.5} (µg/m ³)	[0, 1,27[0	0	0	0	0 (0,0%)
	[1,27, 6,00[0	3	1	0	4 (1,6%)
	[6,00, 17,00[0	14	19	8	41 (16,6%)
	[17,00, ∞[2	27	58	115	202 (81,8%)
	Total	2 (0,8%)	44 (17,8%)	78 (31,6%)	123 (49,8%)	247
Gatineau		O ₃ (ppb)				Total
		[0, 5,71[[5,71, 23,32[[23,32, 40,01[[40,01, ∞[
PM _{2.5} (µg/m ³)	[0, 0,88[0	0	0	0	0 (0,0%)
	[0,88, 5,00[0	0	0	0	0 (0,0%)
	[5,00, 15,40[2	9	10	15	36 (15,0%)
	[15,40, ∞[0	31	70	103	204 (85,0%)
	Total	2 (0,8%)	40 (16,7%)	80 (33,3%)	118 (49,2%)	240

Comparée au Tab. A1.2, la situation a peu changé pour la concentration de PM_{2.5} : la classe de concentration élevée enregistre une grande majorité des observations dans les trois villes. La proportion a même augmenté de 7% à Montréal. La situation a cependant changé pour la concentration d'O₃ : la proportion a augmenté dans la classe de concentration élevée de 22% à Montréal, 6% à Québec et 8% à Gatineau. Bien que plus de 80% des observations aient une concentration d'O₃ supérieure à la médiane dans les trois villes, ces proportions demeurent tout de même inférieures aux attentes. À des fins de comparaison, les observations de brume sèche pour les trois mois d'hiver sont réparties dans le Tab. A1.4 pour Montréal.

Tab. A1.4 : Distribution des observations hivernales (décembre, janvier et février) de brume sèche en fonction de la concentration de PM_{2.5} et d'O₃ à Montréal.

Montréal		O ₃ (ppb)				Total
		[0, 4,80[[4,80, 23,80[[23,80, 41,80[[41,80, ∞[
PM _{2.5} (µg/m ³)	[0, 0,85[0	3	2	0	5 (1,5%)
	[0,85, 5,45[0	3	0	0	3 (0,9%)
	[5,45, 17,18[18	43	1	1	63 (18,3%)
	[17,18, ∞[78	154	38	3	273 (79,4%)
	Total	96 (27,9%)	203 (59,0%)	41 (11,9%)	4 (1,2%)	344

La classe de concentration élevée d'O₃ compte à peine quelques observations. La situation est similaire à Québec et Gatineau, mais comme

la brume sèche est un phénomène beaucoup plus rare en hiver, la fréquence totale au cours de ces trois mois dans ces deux villes est trop faible pour obtenir une représentation significative, et donc n'est pas présentée.

Le cycle quotidien est présenté dans la Fig. A1.3. La fréquence des observations de brume sèche est faible entre le coucher et le lever du soleil. Elle augmente tôt le matin pour atteindre un maximum avant midi, et diminue progressivement au cours de l'après-midi et de la soirée. La concentration moyenne quotidienne maximale de PM_{2.5} est observée en matinée et en soirée. La concentration moyenne quotidienne maximale d'O₃ est observée tôt dans l'après-midi alors que le minimum se produit en matinée. La calibration de certains instruments de mesure est effectuée quotidiennement à 1h, ce qui occasionne une perte de données fréquente à cette heure. L'échantillon est donc beaucoup plus faible à cette heure comparativement aux autres périodes de la journée, ce qui explique la moyenne particulière obtenue à Québec et Gatineau à 1h. Le Tab. A1.5 cerne les épisodes estivaux et diurnes (entre 7h et 17h) de brume sèche. La proportion pour la classe de concentration élevée d'O₃ a encore augmenté, mais modestement, de 6% à Montréal, 5% à Québec et 1% à Gatineau.

Tab. A1.5 : Distribution des observations diurnes (de 7h à 17h) de brume sèche au cours de l'été (juin, juillet et août) en fonction de la concentration de PM_{2.5} et d'O₃.

Montréal		O ₃ (ppb)				Total
		[0, 4,80[[4,80, 23,80[[23,80, 41,80[[41,80, ∞[
PM _{2.5} (µg/m ³)	[0, 0,85[0	0	0	0	0 (0,0%)
	[0,85, 5,45[0	0	0	1	1 (0,3%)
	[5,45, 17,18[0	8	13	7	28 (9,4%)
	[17,18, ∞[1	30	89	154	274 (90,4%)
Total		1 (0,3%)	38 (12,5%)	102 (33,7%)	162 (53,5%)	303
Québec		O ₃ (ppb)				Total
		[0, 5,59[[5,59, 23,08[[23,08, 52,62[[52,62, ∞[
PM _{2.5} (µg/m ³)	[0, 1,27[0	0	0	0	0 (0,0%)
	[1,27, 6,00[0	3	1	0	4 (2,0%)
	[6,00, 17,00[0	12	16	7	35 (17,2%)
	[17,00, ∞[1	14	44	105	164 (80,8%)
Total		1 (0,5%)	29 (14,3%)	61 (30,1%)	112 (55,2%)	203
Gatineau		O ₃ (ppb)				Total
		[0, 5,71[[5,71, 23,32[[23,32, 40,01[[40,01, ∞[
PM _{2.5} (µg/m ³)	[0, 0,88[0	0	0	0	0 (0,0%)
	[0,88, 5,00[0	0	0	0	0 (0,0%)
	[5,00, 15,40[2	6	8	11	27 (15,9%)
	[15,40, ∞[0	18	50	75	143 (84,1%)
Total		2 (1,2%)	24 (14,1%)	58 (34,1%)	86 (50,6%)	170

Finalement, afin d'obtenir des indices sur l'origine et la nature des épisodes de brume sèche, la Fig. A1.4 illustre la proportion des observations de brume sèche en fonction de la direction du vent.

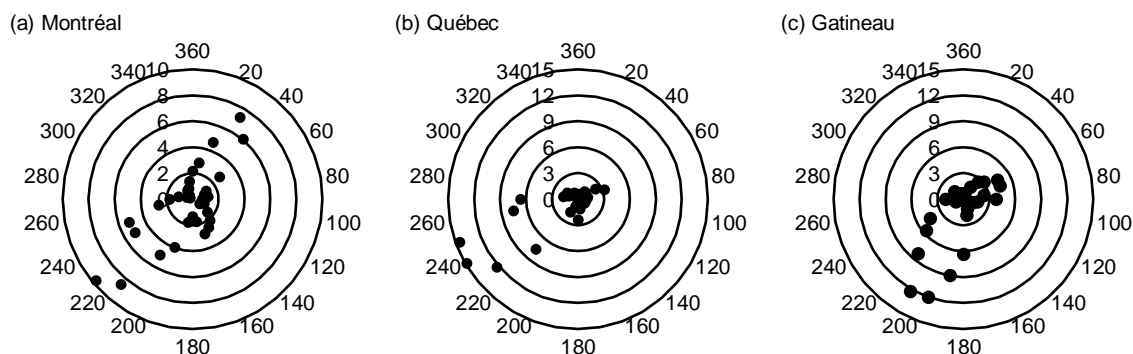


Fig. A1.4 : Proportion (en %) des observations horaires de brume sèche en fonction de la direction du vent (en degrés) à (a) Montréal entre 1997 et 2013, (b) Québec entre 2003 et 2013, et (c) Gatineau entre 2003 et 2013.

Montréal, 58% des observations se produisent lorsque le vent souffle du sud-est, sud, sud-ouest ou de l'ouest (entre 100 et 270°), ce qui suggère que ces sources de pollution proviennent principalement de l'Ontario et des États-Unis. De plus, 27% des observations surviennent lorsque le vent souffle du nord-est (entre 10 et 80°), en provenance de Québec. Montréal est la source de ses propres épisodes de brume sèche dans 6% des cas, lorsque le vent est calme. Montréal, l'Ontario et les États-Unis sont la source apparente de la grande majorité (69%) des observations de brume sèche à Québec (direction du vent entre 180 et 270°), alors que 8% de celles-ci se produisent en condition de vent calme. À Gatineau, 67% des observations sont accompagnées d'un vent provenant du sud-est, sud ou sud-ouest (entre 110 et 260°; provenant de l'Ontario et des États-Unis), et 23% d'entre elles surviennent lorsque le vent souffle du nord-est ou de l'est (entre 10 et 90°, provenant de Montréal et Québec). À peine 2% des observations surviennent lorsque le vent est calme.

A1.4 Discussion et conclusion

Nous avons tenté de vérifier si l'O₃ est un indicateur fiable de visibilité réduite en analysant des données de qualité de l'air lorsqu'une observation de brume sèche est signalée dans trois villes du Sud du Québec. Dans toutes les localités, la concentration de PM_{2.5} est élevée lors d'au moins 8 observations de brume sèche sur 10. Étant donné que les particules en suspension constituent un obstacle à la visibilité, ceci est un constat anodin. Lors d'épisodes de brume sèche, la concentration d'O₃ a tendance à être plus élevée, mais elle est beaucoup plus variable. La classe de concentration élevée enregistre une proportion appréciable (et supérieure à 10%), mais plus de la moitié des observations se retrouve à l'extérieur de cette classe. Il est effectivement fréquent que la brume sèche soit accompagnée d'une concentration d'O₃ faible.

Après avoir séparé les observations en fonction de la période de l'année et de la journée, ces variables ont démontré clairement le rôle important qu'elles exercent sur la distribution de la concentration d'O₃. Pendant l'été et pendant la journée, la proportion des observations de brume sèche accompagnées d'une concentration élevée d'O₃ a augmenté substantiellement, mais pas au même niveau que celui atteint par les PM_{2.5}. L'O₃ étant le produit de réactions photochimiques, ceci démontre à quel point le manque d'ensoleillement en hiver et pendant la nuit limite la production d'O₃, en dépit de la présence abondante de PM_{2.5}. Les épisodes estivaux et diurnes de brume sèche ont effectivement la plus grande chance d'être accompagnés d'une concentration élevée d'O₃. Ceci est cohérent avec les résultats de plusieurs études urbaines qui observent une forte corrélation positive entre la concentration d'O₃ et la température (Korsog et Wolff, 1991; Sillman et Samson, 1995; Pugliese *et al.*, 2014), particulièrement lorsqu'elle est supérieure à 20°C (Camalier *et al.*, 2007). La raison pour laquelle la proportion de la classe de concentration élevée d'O₃ dans le Tab. A1.2 est beaucoup plus faible à Montréal que dans les deux

autres villes est la fréquence plus élevée de brume sèche hivernale. La saisonnalité exerce peu d'influence sur la concentration des $PM_{2.5}$ lorsque la brume sèche est présente.

Bien que la concentration d' O_3 soit généralement plus élevée lorsque la brume sèche est présente, elle n'est pas un indicateur robuste de visibilité réduite dans le Sud du Québec. Elle est plus fiable lors d'épisodes de brume sèche estivaux et diurnes, mais les $PM_{2.5}$ demeurent un meilleur indicateur dans la plupart des cas. L' O_3 n'est pas du tout un bon indicateur de visibilité réduite lors d'épisodes de brume sèche hivernaux.

L'analyse de l'origine des épisodes de brume sèche permet de penser que le Québec contribue, par lui-même, à la formation d'une minorité des épisodes de brume sèche, tandis que l'Ontario et les États-Unis contribuent à la formation d'une proportion beaucoup plus importante d'épisodes. Les sources de pollution ontariennes et américaines, propices à la formation de smog industriel, peuvent expliquer, du moins en partie, les épisodes de brume sèche présentant une faible concentration d' O_3 observés en territoire québécois. Mais comme ces mêmes sources de pollution sont aussi propices à la formation de smog photochimique, cette explication demeure spéculative.

Références

- Andreae, M.O., Browell, E.V., Garstang, M., Gregory, G.L., Harriss, R.C., Hill, G.F., Jacob, J., Pereira, M.C., Sachse, W., Setzer, A.W., Silva Dias, P.L., Talbot, R.W., Torres, A.L. et Wofsy, S.C. (1988). Biomass-burning emissions and associated haze layers over Amazonia. *J. Geophys. Res.* 93 : 1509–1527.
- Aneja, V.P., Brittig, J.S., Kim, D.S. et Hanna, A. (2004). Ozone and other air quality-related variables affecting visibility in the Southeast United States. *J. Air Waste Manage. Assoc.* 54 : 681–688.
- Brook, J.R. et Dann, T.F. (1999). Contribution of nitrate and carbonaceous species to PM_{2.5} observed in Canadian cities. *J. Air Waste Manage. Assoc.* 49 : 193–199.
- Brook, J.R., Lillyman, C.D., Shepherd, M.F. et Mamedov, A. (2002). Regional transport and urban contributions to fine particle concentrations in southeastern Canada. *J. Air Waste Manage. Assoc.* 52 : 855–866.
- Brunekreff, B. et Holgate, S.T. (2002). Air pollution and health. *Lancet* 360 : 1233–1242.
- Camalier, L., Cox, W. et Dolwick, P. (2007). The effects of meteorology on ozone in urban areas and their use in assessing ozone trends. *Atmos. Environ.* 41 : 7127–7137.
- Chung, Y.S. (1977). Ground-level ozone and regional transport of air pollutants. *J. Appl. Meteorol.* 16 : 1127–1136.
- Chung, Y.S. (1978). The distribution of atmospheric sulphates in Canada and its relationship to long-range transport of air pollutants. *Atmos. Environ.* 12 : 1471–1480.
- Delany, A.C., Haagensen, P., Walters, S., Wartburg, A.F. et Crutzen, P.J. (1985). Photochemically produced ozone in the emission from large-scale tropical vegetation fires. *J. Geophys. Res.* 90 : 2425–2429.
- Diederer, H.S.M.A., Guicherit, R. et Hollander, J.C.T. (1985). Visibility reduction by air pollution in the Netherlands. *Atmos. Environ.* 19 : 377–383.
- Environnement Canada (2015). *MANOBS: Manuel d'observations météorologiques*, 7^e édition, modification 19, Gatineau, Canada.
- Heck, W.W., Taylor, O.C., Adams, R. Bingham, G., Miller, J., Preston, E. et Weinstein, L. (1982). Assessment of crop loss from ozone. *J. Air Pollut. Control Assoc.* 32 : 353–361.
- Herbert, G.A., Schnell, R.C., Bridgman, H.A., Bodhaine, B.A., Oltmans, S.J. et Shaw, G.E. (1989). Meteorology and haze structure during AGASP-II, part 1: Alaskan Arctic flights, 2–10 April 1986. *J. Atmos. Chem.* 9 : 17–48.

- Jeong, C.H., McGuire, M.L., Herod, D., Dann, I., Dabek-Zlotorzynska, E., Wang, D., Ding, L., Celio, V., Mathieu, D. et Evans, G. (2011). Receptor model based identification of PM_{2.5} sources in Canadian cities. *Atmos. Pollut. Res.* 2 : 158–171.
- King, W.J. et Vukovich, F.M. (1982). Some dynamic aspects of extended pollution episodes. *Atmos. Environ.* 16 : 1171–1181.
- Korsog, P.E. et Wolff, G.T. (1991). An examination of urban ozone trends in the northeastern U.S. (1973–1983) using a robust statistical method. *Atmos. Environ.* 25B : 47–57.
- Leduc, R. et Pépin, L. (1995). Brume sèche dans le corridor Windsor–Québec. *Pollut. Atmos.* 145 : 52–59.
- Leduc, R. et Roy-Loubier, K. (2005). Ozone dans le sud du Québec : origine et trajectoire. *Vecteur Environ.* 38 : 44–54.
- McDonald, K. et Shepherd, M. (2004). Characterization of visibility impacts related to fine particulate matter in Canada. *J. Air Waste Manage. Assoc.* 54 : 1061–1068.
- Meng, Z., Dabdub, D. et Seinfeld, J.H. (1997). Chemical coupling between atmospheric ozone and particulate matter. *Science* 277: 116–119.
- Munn, R.E. (1973). Secular increases in summer haziness in the Atlantic provinces. *Atmosphere* 11 : 156–161.
- Pugliese, S.C., Murphy, J.G., Geddes, J.A. et Wang, J.M. (2014). The impacts of precursor reduction and meteorology on ground-level ozone in the Greater Toronto area. *Atmos. Chem. Phys.* 14 : 8197–8207.
- Radke, L.F., Stith, J.L., Hegg, D.A. et Hobbs, P.V. (1978). Airborne studies of particles and gases from forest fires. *J. Air Pollut. Control Assoc.* 28 : 30–34.
- Sillman, S. et Samson, P.J. (1995). Impact of temperature on oxidant photochemistry in urban, rural and remote environments. *J. Geophys. Res.* 100 : 11497–11508.
- Stith, J.L., Radke, L.F. et Hobbs, P.V. (1981). Particle emissions and the production of ozone and nitrogen oxides from the burning of forest slash. *Atmos. Environ.* 15 : 73–82.
- Taubman, B.E., Marufu, L.T., Piety, C.A., Doddridge, B.G., Stehr, J.W. et Dickerson, R.R. (2004). Airborne characterization of the chemical, optical, and meteorological properties, and origins of a combined ozone-haze episode over the eastern United States. *J. Atmos. Sci.* 61 : 1781–1793.
- Thibault, D., Leduc, R. et Hufty, A. (1995). La pollution par l’ozone troposphérique au Québec méridional : analyse des épisodes du 7 et du 17–

18 juin 1995. *Vecteur Environ.* 30 : 34–43.

Thurston, G.D., Gorczynski, J.E., Currie, J.H., He, D., Ito, K., Hipfner, J., Waldman, J., Liou, P.J. et Lippmann, M. (1994). The nature and origins of acid summer haze air pollution in metropolitan Toronto, Ontario. *Environ. Res.* 65 : 254–270.

Vickers, G.G. et Munn, R.E. (1977). A Canadian haze climatology. *Clim. Chang.* 1 : 97–103.

Wolff, G.T., Kelly, N.A. et Ferman, M.A. (1981). On the sources of summertime haze in the eastern United States. *Science* 211 : 703–705.

Wolff, G.T., Kelly, N.A. et Ferman, M.A. (1982). Source regions of summertime ozone and haze episodes in the eastern United States. *Water Air Soil Pollut.* 18 : 65–81.

A2 Thermal comfort in Quebec City, Canada: sensitivity analysis of the UTCI and other popular thermal comfort indices in a mid-latitude continental city

Abstract

The newly developed Universal Thermal Climate Index (UTCI), along with the physiological equivalent temperature (PET), the humidex (HX) and the wind chill index (WC), was calculated in Quebec City, Canada, a city with a strong seasonal climatic variability, over a 1-year period. The objective of this study is twofold: evaluate the operational benefits of implementing the UTCI for a climate monitoring program of public comfort and health awareness as opposed to relying on traditional and simple indices, and determine whether thermal comfort monitoring specific to dense urban neighborhoods is necessary to adequately fulfill the goals of the program. In order to do so, an analysis is performed to evaluate each of these indices' sensitivity to the meteorological variables that regulate them in different environments. Overall, the UTCI was found to be slightly more sensitive to mean radiant temperature, moderately more sensitive to humidity and much more sensitive to wind speed than the PET. This dynamic changed slightly depending on the environment and the season. In hot weather, the PET was found to be more sensitive to mean radiant temperature and therefore reached high values that could potentially be hazardous more frequently than the UTCI and the HX. In turn, the UTCI's stronger sensitivity to wind speed makes it a superior index to identify potentially hazardous weather in winter compared to the PET and the WC. Adopting the UTCI broadly would be an improvement over the traditionally popular HX and WC indices. The urban environment produced favorable conditions to sustain heat stress conditions, where the indices reached high values more frequently there than in suburban locations, which advocates for weather monitoring specific to denser urban areas.

Résumé

Le nouvel indice universel du climat thermique (UTCI) ainsi que la température physiologique équivalente (PET), l'humidex (HX) et l'indice de refroidissement éolien (WC) ont été calculés à Québec (Canada), une ville dont la variabilité climatique saisonnière est très grande, au cours d'une période d'un an. Cette étude a deux objectifs : 1) évaluer les bénéfices opérationnels d'implanter l'UTCI comme programme de surveillance du climat pour le confort

et la santé du public aux dépens des indices simples et traditionnels utilisés présentement, et 2) déterminer si la surveillance du confort thermique spécifique aux quartiers urbains denses est nécessaire pour adéquatement combler les objectifs du programme. Une analyse est menée pour évaluer la sensibilité de chacun des indices aux variables météorologiques qui les gouvernent dans différents environnements. Généralement, l'UTCI est plus sensible à la température moyenne radiante, modérément plus sensible à l'humidité et beaucoup plus sensible à la vitesse du vent que la PET. Cette dynamique change légèrement en fonction de l'environnement et de la saison. Par temps chaud, la PET est plus sensible à la température moyenne radiante et, en conséquence, atteint des valeurs élevées qui peuvent potentiellement être dangereuses à la santé plus fréquemment que l'UTCI et l'HX. En contrepartie, l'UTCI est un indice supérieur pour identifier les périodes potentiellement dangereuses en hiver par sa plus forte sensibilité à la vitesse du vent, comparativement à la PET et au WC. L'environnement urbain reproduit des conditions favorables aux stress de chaleur, où les indices atteignent des valeurs élevées plus fréquemment qu'en banlieue. Ceci plaide pour une surveillance spécifique aux environnements urbains denses.

A2.1 Introduction

Meteorological monitoring and awareness programs contribute to the public's well-being and safety by informing people of current and forthcoming weather conditions which allows them to adapt their behaviour accordingly. Currently in the province of Quebec, warnings related to heat or cold weather are issued based on forecasts of air temperature and two thermal comfort indices: the humidex (HX; Santee and Wallace, 2005) and the wind chill index (WC; Osczevski and Bluestein, 2005). Both are simple two-variable indices which combine humidity or wind speed to air temperature, to represent human-perceived temperature during the hot and cold seasons, respectively. These indices are easy to calculate, but their use is limited to specific periods and they overlook other environmental variables which significantly influence thermal comfort.

Given the plethora of thermal comfort indices that surfaced in the literature over time (see Epstein and Moran (2006) for a lengthy yet incomplete list), choosing a proper index is not a straightforward process.

The choice usually results in a compromise between simplicity and universal applicability. Some indices did manage to stand out and pass the test of time, for example Fanger's (1970) pioneering predicted mean vote (PMV), the standard effective temperature (SET; Gagge *et al.*, 1971; 1986), Steadman's (1984; 1994) apparent temperature (AT), the physiological equivalent temperature (PET; Höppe, 1999; Matzarakis *et al.*, 1999), the wet bulb globe temperature (WBGT; Minard *et al.*, 1957) and the heat index (HI; Santee and Wallace, 2005). Originally designed to evaluate comfort indoors, the PMV was faced with important shortcomings when tested outdoors (Humphreys, 1994); the SET, the AT and the PET, despite being universally applicable, are still relatively simple models (Jendritzky *et al.*, 2012); the WBGT, aside from its exclusive application to warm weather, has been criticized for a variety of reasons (Taylor, 2006; Budd, 2008), such as its inadequate response to humidity and wind speed; and the HI is yet another simple two-variable comfort assessment index of warm weather. No index was unanimously proclaimed as a universal standard. Following a decade of research led by the International Society of Biometeorology, the Universal Thermal Climate Index (UTCI) was introduced in 2009, designed to be valid for all climate ranges and scales, and for all applications of human biometeorology (Jendritzky *et al.*, 2012). It was designed to be the universal standard of thermal comfort.

Although thermal indices are routinely part of weather bulletins around the world, recent studies of thermal comfort indices have almost exclusively focused on warm or temperate regions, where climatic seasonal fluctuation is moderate, such as the United Kingdom (Krüger *et al.*, 2013), Germany (Mayer *et al.*, 2008), Hungary (Kántor *et al.*, 2012), Portugal (Oliveira and Andrade, 2007), Greece (Bleta *et al.*, 2014), Turkey (Toy and Yilmaz, 2010), Israel (Cohen *et al.*, 2012), Sri Lanka (Johansson and Emmanuel, 2006), Bangladesh (Burkard *et al.*, 2011), Taiwan (Lin *et al.*, 2011), Japan (Thorsson *et al.*, 2007a), Malaysia (Makaremi *et al.*, 2012), Australia

(Spagnolo and de Dear, 2003), Brazil (Bröde *et al.*, 2012a) and many others. Apart from the WC, few recent studies made use of thermal comfort indices in cold environments. A notable exception is Błażejczyk *et al.* (2012) who compared the UTCI to other indices in different climates including the Arctic climate of the Svalbard archipelago.

Weather monitoring which serves as the foundation to weather alerts in the province of Quebec is performed at regionally representative stations which are located in the outskirts of denser urban areas where most people live. This is the case for Quebec City where it has been shown that considerable air temperature variability over the territory can produce significantly different thermal conditions from the downtown core to the suburbs (Leduc *et al.*, 1980; 1981; Bergeron, 2014). The urban climate is well documented for its differing characteristics compared to the surrounding rural areas. The air of cities tends to be warmer, a phenomenon famously known as the *urban heat island*. Additionally, cities are less windy, less humid and less sunlit (Landsberg, 1981). Given the urban heat island effect, a greater likelihood of potential heat stress circumstances within a city during a heat wave can be expected, however, high-rise buildings can provide shade. An urban street canyon can therefore become a so-called *cool island* and attenuate the effects of hot weather (Pearlmutter *et al.*, 1999).

This study aims at assessing the operational benefits of implementing the UTCI in neighborhoods of different urban densities within Quebec City, a city with a strong seasonal climatic variability. Specific objectives include (1) calculating the UTCI and other popular comfort indices in order to perform a sensitivity analysis with respect to the meteorological variables that influence them, and (2) calculate the indices in different environments, in order to document the necessity of expanding the network of urban weather stations.

A2.2 Materials and method

A2.2.1 The UTCI and other popular thermal comfort indices

The UTCI is based on Fiala *et al.*'s (1999; 2001) physiological model, a complex multi-node model which simulates the exchanges of energy between the body and the environment, and the corporal reactions to thermal stresses, in response to meteorological variables and personal behavior. An adaptive clothing model was included to estimate typical clothing habits of individuals based on temperature. The reader is referred to Havenith *et al.* (2012) for more information on the clothing model, and to Błażejczyk *et al.* (2013) and Fiala *et al.* (2012) for a detailed description of the UTCI.

Fiala's physiological model requires many iterations in order to calculate the UTCI, which is time-consuming (Bröde *et al.*, 2012b). This compromises the UTCI's applicability in real time or its computation for extensive series of data. To address this limitation, a simplified version of the UTCI was made available on its official website (www.utci.org) in the form of a Fortran code and an executable program. This program is the result of a six-degree regression analysis of the UTCI and reproduces an output index instantly. It requires four meteorological variables as inputs: air temperature (T), wind speed at a 10-m height (v_{10}), water vapor pressure (e) and the mean radiant temperature (T_{mrt} , an indicator of global radiation, see Kántor and Unger (2011) for more details). The clothing is taken into consideration by the clothing model and the physical activity is assumed to be light (i.e., walking). The website version of the UTCI is used throughout this study.

We calculate the UTCI, the HX and the WC, the last two being the indices most used by the Canadian weather service and most recognized by the Canadian public. For the sake of comparing the UTCI with another universal index, we also calculate the PET, a comfort index widely applied

in the literature. The PET requires the same four meteorological variables as the UTCI as inputs, except for v which is measured at body height (1.5 m). The physiological model driving the PET, the Munich energy-balance model for individuals (Höppe, 1993), is much simpler than Fiala’s model, however, users are able to modify activity and clothing values. The HX and the WC are simple two-variable indices. The HX is a heat comfort index meaningful when $T \geq 21^\circ\text{C}$ (Environment Canada, 2014). It is a function of T (in $^\circ\text{C}$) and e (in hPa):

$$(A2.1) \text{HX} = T + 0.5555 \times (e - 10)$$

The WC, a cold comfort index meaningful when $T \leq 0^\circ\text{C}$ (Environment Canada, 2015), is a function of T and v_{10} (in km/h):

$$(A2.2) \text{WC} = 13.12 + 0.6215 \times T - 11.37 \times v_{10}^{0.16} + 0.3965 \times T \times v_{10}^{0.16}$$

Throughout this text, we only compute the HX whenever $T \geq 21^\circ\text{C}$, and the WC when $T \leq 0^\circ\text{C}$ and $v_{10} > 0$ km/h, since, counterintuitively, Eq. A2.2 will produce values of the WC well above T for $v_{10} = 0$ km/h. All indices are expressed on a temperature scale in $^\circ\text{C}$.

A2.2.2 Location and data

Quebec City is located in Canada at 46.5° latitude. It has a continental cold and humid climate with a warm summer (Peel *et al.*, 2007). The average temperature difference between January and July is above 30°C (MDDELCC, 2015).

We use data from three meteorological stations spread across the city. The first is at Jean-Lesage airport (JL), in an open area with minimal urban influence, the second is in the Sainte-Foy (SF) neighbourhood, in an open area surrounded by residential, commercial and institutional buildings, and the third is in the Saint-Sauveur (SS) neighbourhood, a dense urban area

with low-rise buildings close to the downtown core. The three stations within the city are mapped in Fig. A2.1 and their physical environmental features are tabulated in Tab. A2.1. JL and SF are typical weather stations operated by the federal weather service where T and relative humidity (RH) are measured at a 2-m height, and v is measured at 10 m. Measurements for the same three variables are made at 4.5 m at SS, a station under the Quebec climate monitoring program. All three stations measure T , RH and v every hour. To estimate e from RH measurements, the Magnus approximation of saturated water vapour pressure (e_s) is used:

$$(A2.3) e_s = C_1 \exp\left(\frac{C_2 T}{C_3 + T}\right)$$

where $C_1 = 6.1094$, $C_2 = 17.625$ and $C_3 = 243.04^\circ\text{C}$ for $T \geq 0^\circ\text{C}$, and $C_1 = 6.1121$, $C_2 = 22.587$ and $C_3 = 273.86^\circ\text{C}$ for $T < 0^\circ\text{C}$ (Alduchov and Eskridge, 1996). e simply equals $e_s \times RH$. Since some indices require v at a different height (z) than where it is measured, a logarithmic profile is used to obtain v at the desired height:

$$(A2.4) \frac{v_{z_1}}{v_{z_2}} = \frac{\log(z_1/0.01)}{\log(z_2/0.01)}$$

This is the same used internally by the UTCI to obtain v at body level (Bröde *et al.*, 2012b). T_{mrt} is not directly measurable. In order to obtain an estimate, the RayMan software (Matzarakis *et al.*, 2007; 2010) is used. To estimate T_{mrt} , RayMan requires several pieces of information, such as geographical location and altitude (Tab. A2.1), time zone (UTC – 5), albedo, Bowen ratio, ratio of diffuse to global radiation, time of year and day, and meteorological parameters (T , e , $v_{1.5}$, and global radiation or cloud cover). Default values were used for the albedo (0.3), the Bowen ratio (1.3) and the ratio of diffuse to global radiation (0.2). Cloud cover data is available at JL and is used for the other two stations as well. Additionally, RayMan permits the input of the architectural and vegetation landscape surrounding the site of interest, which can influence T_{mrt} on small scales due to its shadow and radiation

effects. However, since the three stations are located in open spaces (including the SS station located in a parking lot), this feature was not used. RayMan also computes the PET based on meteorological and personal variables. Activity level is kept fixed at 135 W, which is the reference condition used by the UTCI (Bröde *et al.*, 2012b), and clothing values are adjusted according to Tab. A2.2, approximated from the UTCI clothing model (Havenith *et al.*, 2012). The indices are calculated every hour at the three stations for a 1-year period, between March 2013 and February 2014.



Fig. A2.1: Map of Quebec City and location of the Jean-Lesage, Sainte-Foy and Saint-Sauveur stations.

Tab. A2.1: Physical environment of the three stations.

Station	Latitude	Longitude	Altitude (m)	Proportion of natural surfaces	Proportion of paved surfaces
Jean-Lesage (non-urban)	46°48'	-71°23'	62	0.78	0.19
Sainte-Foy (suburban)	46°47'	-71°17'	90	0.47	0.41
Saint-Sauveur (urban)	46°49'	-71°14'	23	0.21	0.53

Tab. A2.2: Clothing values used for calculating the PET.

Temperature range	Clothing value (clo)
[30°C, +∞[0.2
[20°C, 30°C]	0.4
[10°C, 20°C]	0.9
[0°C, 10°C]	1.4
[-10°C, 0°C]	1.9
[-20°C, -10°C]	2.2
[-30°C, -20°C]	2.6
[-∞, -30°C]	2.9

A2.3 Results

A2.3.1 Climatic comparison between the stations

Monthly averaged data for T , e and v_{10} are graphed in Fig. A2.2(a–c) for the three stations. In order to obtain v_{10} at SS, the relationship of Eq. A2.4 is applied. Overall, JL is the coldest, windiest and most humid station. By contrast, SS is the warmest, least windy and humid station. SF falls in between; however, it is very similar to JL. T_{mrt} 's annual cycle is not shown but exhibits a similar pattern to T 's cycle. As expected, this falls in line with the urban/rural climate contrast described in the Introduction. There is an agreement among all stations that the summer is less windy than the winter season. The annual cycle of the indices (Fig. A2.3(a–c)) follows the temperature closely, but the influence of the other variables is noticeable, particularly during the winter when UTCI, PET and WC averages are well below T , and at SS where these indices tend to diverge away from those calculated at SF and JL. For the sake of comparing the HX between the stations without any bias, the restriction ($T \geq 21^\circ\text{C}$) had to be fulfilled simultaneously at all three stations in order for those data points to be included in the averages of Fig. A2.3(c). Interestingly, there is hardly any difference in the HX between the stations.

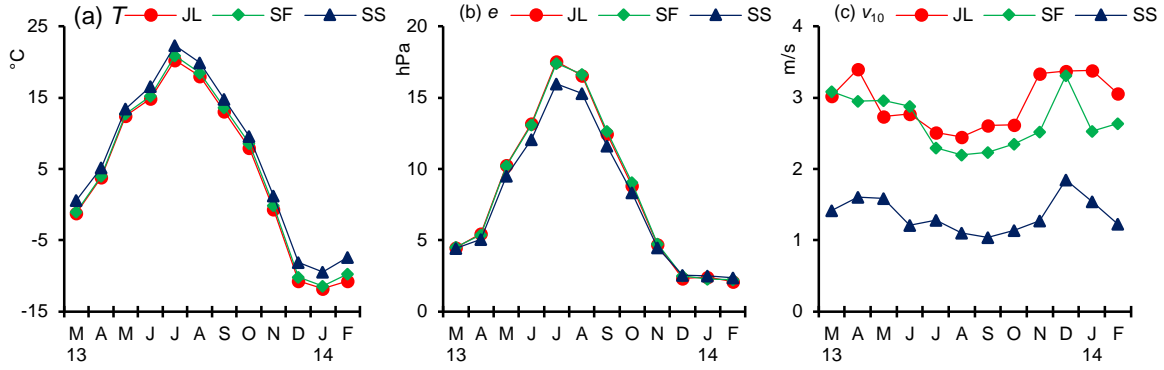


Fig. A2.2: Monthly averaged (a) T , (b) e and (c) v_{10} at the three stations from March 2013 to February 2014.

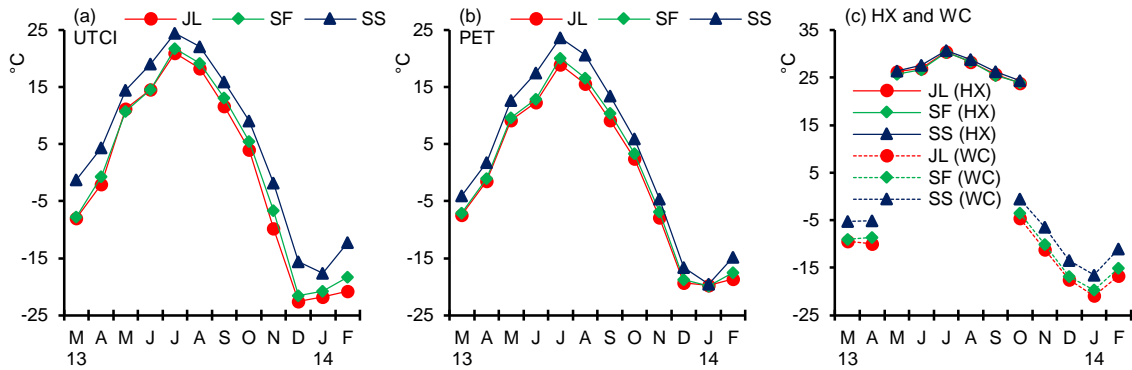


Fig. A2.3: Monthly averaged (a) UTCI, (b) PET, (c) HX and WC at the three stations from March 2013 to February 2014.

The urban heat island is in part responsible for the higher index values calculated at SS. It is well known that this effect is present all day, but stronger at night. Figure A2.4(a–c) shows the monthly average of the difference between SS and JL for T , e and v_{10} according to the period of the day. The difference of any variable or index between SS and JL will be labelled by Δ from here onward (e.g., $\Delta T = T_{SS} - T_{JL}$). The fluctuation of ΔT_{mrt} again follows ΔT closely and therefore is not shown either. We define daytime such that $T_{mrt} \geq T$ and otherwise for nighttime. ΔT is stronger in the summer and winter (Fig. A2.4(a)). Δe is larger in magnitude during the summer while there is virtually no difference between the stations during the winter (Fig. A2.4(b)), resulting from e values being typically low in cold weather (Fig. A2.2(b)). At the opposite, the magnitude of Δv_{10} is larger in the fall and winter (Fig. A2.4(c)). Regarding the night/day contrast, ΔT is stronger at night,

contrary to Δe and Δv_{10} . JL tends to be more humid and windy than SS, but particularly during the daytime.

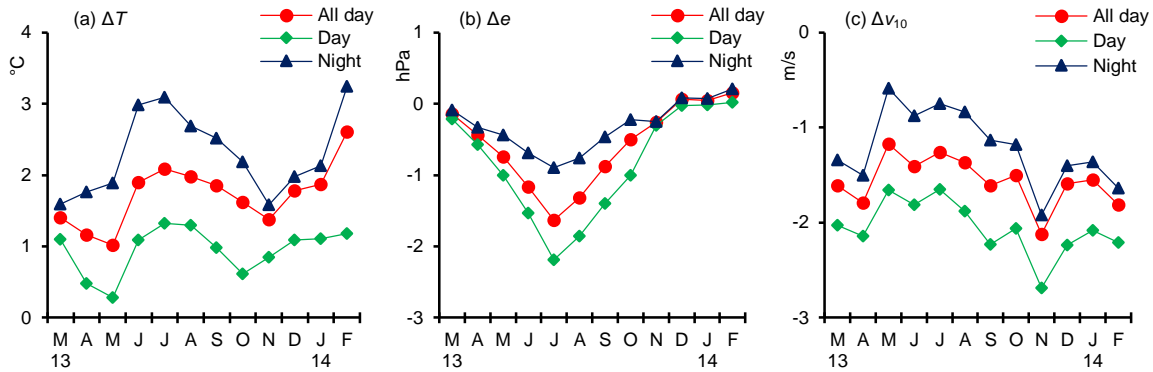


Fig. A2.4: Monthly average of the difference between SS and JL for (a) T , (b) e and (c) v_{10} from March 2013 to February 2014.

How the indices react to these climatic differences is shown in Fig. A2.5(a–c). For ΔPET (Fig. A2.5(b)), the urban/rural contrast varies in the same fashion as ΔT (Fig. A2.4(a)), from a low in the spring and fall to a high in the summer. At the opposite, ΔUTCI (Fig. A2.5(a)) shows a wider difference in the late fall and winter of about 8°C on average, accompanied by a larger Δv observed during the same months (Fig. A2.4(c)), compared to $\sim 4^\circ\text{C}$ in the summer. The urban/rural contrast is typically stronger during the daytime for both ΔUTCI and ΔPET (Fig. A2.5(a–b)), contrary to ΔT (Fig. A2.4(a)), but the difference is fairly constant throughout the summer daytime for ΔUTCI . A weaker v during the winter daytime at SS contributes to a UTCI $9\text{--}10^\circ\text{C}$ higher on average during that same time frame. A weaker v and higher T also contribute to a WC 4 to 5°C warmer at SS (Fig. A2.5(c)), without much of a contrast between the daytime and nighttime (the ΔWC daytime average for October was obtained with a single observation). As stated previously, there is not much of an urban/rural contrast for the HX (Figs. A2.4(c) and A2.5(c)), explained by the lower e which offsets the higher T at SS. There appears to be a difference between the daytime and nighttime, however, the ΔHX nighttime curve in Fig. A2.5(c) should be interpreted with caution, since T at or above 21°C seldom occurs at night, resulting in very small sample

sizes available to calculate those averages. The daytime curve is indeed much closer to the “all day” curve.

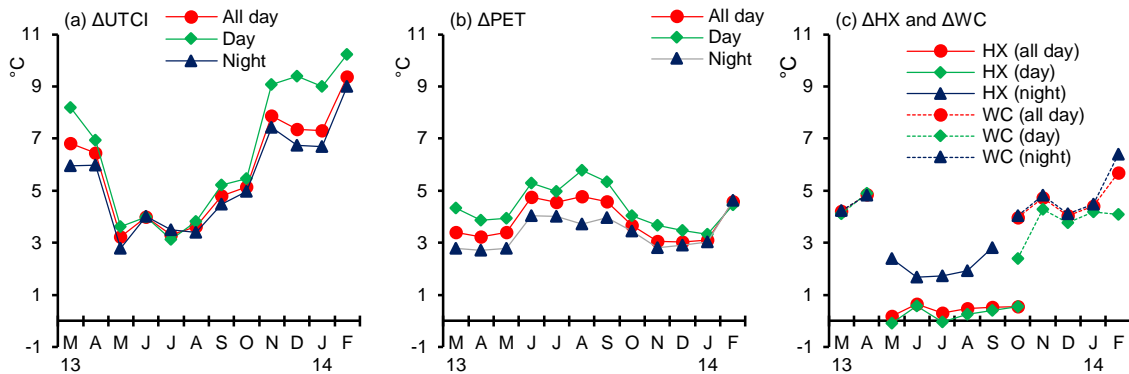


Fig. A2.5: Monthly average of the difference between SS and JL for (a) the UTCI, (b) the PET, (c) the HX and the WC from March 2013 to February 2014.

A2.3.2 Sensitivity analysis between the indices

The indices are all highly correlated with T . The UTCI and the PET also tend to be well correlated with T_{mrt} and e , largely due to the fact that T_{mrt} and e are also well correlated with T . This leaves ν weakly correlated with both indices, insinuating that ν plays a minimal role in the assessment of comfort. Given the close relationships between T , T_{mrt} , e and the indices, it is relevant to compare the offset of each index from T (e.g., $\text{UTCI}_{\text{off}} = \text{UTCI} - T$), rather than the index itself, to each one of the variables, including the offset of T_{mrt} from T (i.e., $T_{\text{mrt,off}} = T_{\text{mrt}} - T$) instead of T_{mrt} , to better assess how each of these impacts the indices.

We first perform such a comparison for the UTCI, graphed in Fig. A2.6(a–c) for SF. ν_{10} has a stronger correlation with UTCI_{off} , and therefore a stronger influence on the UTCI, followed closely by T_{mrt} and e . The influence of e seems to maximize around $\text{UTCI}_{\text{off}} = 10^\circ\text{C}$ while T_{mrt} and ν_{10} appear to have a somewhat more linear impact on the offset. The PET, on the other hand, is most strongly sensitive to T_{mrt} (Fig. A2.6(d)), followed by the much weaker correlations of e and ν_{10} (Fig. A2.6(e–f)). The impact of ν_{10} plateaus

around $PET_{\text{off}} = -11^{\circ}\text{C}$, suggesting that its influence on the PET fades off as it accelerates. The slopes of the trend lines shown in Fig. A2.6(a–f) are indications of how sensitive each index are relative to one another with respect to a given variable. The UTCI is indeed slightly more sensitive to T_{mrt} , moderately more sensitive to e and much more sensitive to ν_{10} than the PET. The slope and correlation statistics at JL and SS are tabulated in Tab. A2.3. The conclusions drawn on the data analysed at SF can be extended to JL as well; however, the generally different environmental conditions at SS create a different response between the indices and the variables. e and ν_{10} both lost influence on the UTCI to T_{mrt} 's benefit, and the PET is now slightly more sensitive to e and T_{mrt} than the UTCI. These differences appear to arise in part from the strikingly different ways that the UTCI and the PET assimilate ν to assess comfort. The slope at SS for the “ ν_{10} vs. PET_{off} ” comparison is steeper than at SF and JL, supporting the claim that the influence of ν_{10} on the PET diminishes as it grows stronger. The opposite is true for the UTCI, as interpreted from the “ ν_{10} vs. $UTCI_{\text{off}}$ ” column in Tab. A2.3. Following this logic, we could also state that the influence of e on the UTCI increases as it too increases, which would contradict the plateauing effect observed in Fig. A2.6(b). SS is indeed less humid than JL, however, the magnitude of Δe is quite low on average (below 1 hPa). The increase of the slope and correlation from SS to JL in the “ e vs. $UTCI_{\text{off}}$ ” column of Tab. A2.3 is the likely result of the interactions of other variables.

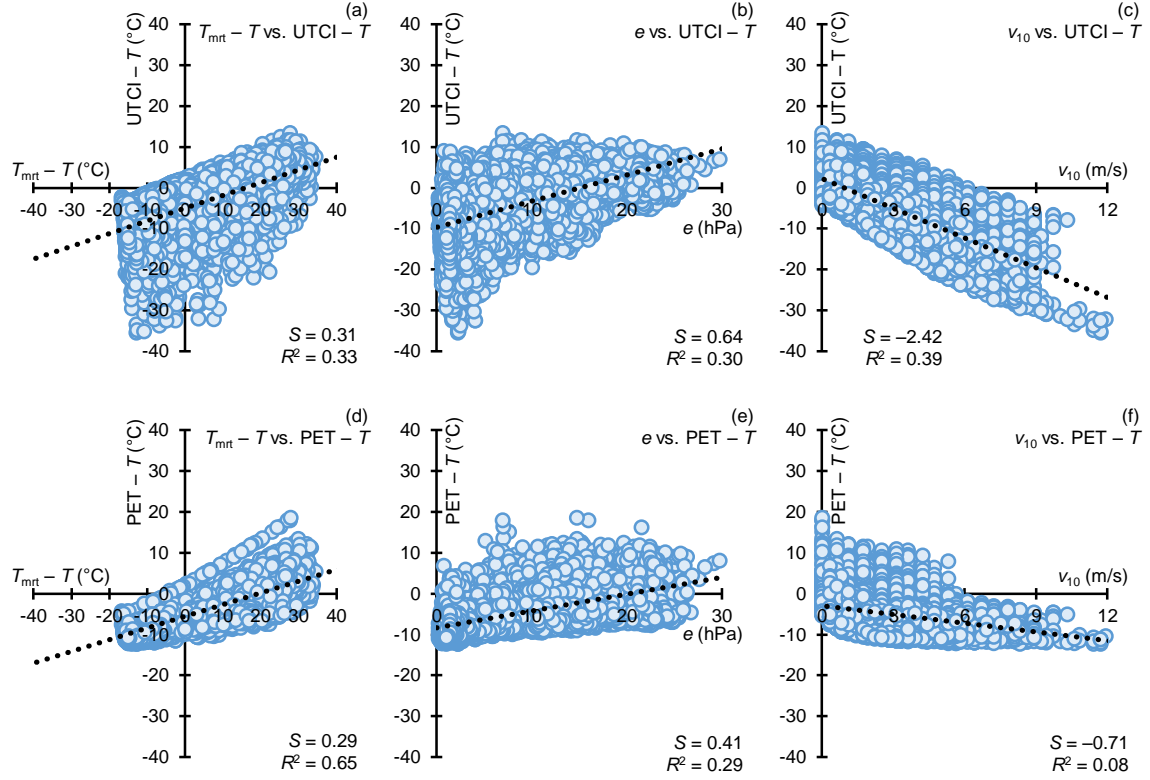


Fig. A2.6: Comparison between $UTCI_{off}$ and (a) $T_{mrt,off}$, (b) e and (c) v_{10} at SF, and (d-f) similarly for PET_{off} . The trend line is included, as well as its slope (S) and the coefficient of determination (R^2).

Tab. A2.3: Slope (S) and coefficient of determination (R^2) for comparison between the variables ($T_{mrt,off}$, e and v_{10}) and the offset of the indices ($UTCI_{off}$ and PET_{off}) at the three stations.

Station	$T_{mrt} - T$ vs.				e vs.				v_{10} vs.			
	$UTCI - T$		$PET - T$		$UTCI - T$		$PET - T$		$UTCI - T$		$PET - T$	
	S	R^2	S	R^2	S	R^2	S	R^2	S	R^2	S	R^2
JL	0.30	0.27	0.27	0.62	0.74	0.36	0.42	0.33	-2.50	0.41	-0.63	0.07
SF	0.31	0.33	0.29	0.65	0.64	0.30	0.41	0.29	-2.42	0.39	-0.71	0.08
SS	0.32	0.66	0.36	0.79	0.46	0.22	0.51	0.25	-2.18	0.15	-1.07	0.03

As stated previously, we only calculate the HX when $T \geq 21^\circ\text{C}$. In order to compare the influence of e between the UTCI, the PET and the HX, we restrict the calculation of the UTCI and the PET to this condition as well (Fig. A2.7(a-c) for SF). The HX is linearly proportional to e (Eq. A2.1), yielding a slope of $0.56^\circ\text{C}/\text{hPa}$ and a perfect correlation under all circumstances (Fig. A2.7(c)). For such high temperatures, however, e plays a small role on the UTCI and the PET (Fig. A2.7(a-b)). Our data suggest that, in hot weather, the UTCI and PET are indeed mostly driven by T_{mrt} , the PET being more sensitive to it than the UTCI (not shown). Similarly for the WC, we compare

the sensitivity of all indices to v_{10} by restricting the calculation of the UTCI and the PET to $T \leq 0^\circ\text{C}$ and $v_{10} > 0 \text{ m/s}$ (Fig. A2.8(a-c)). The UTCI is most strongly dependent on v_{10} during the winter when it is typically stronger, and T_{mrt} and e fluctuate much less. The UTCI is also much more sensitive to v_{10} compared to the PET and the WC. The slope in Fig. A2.8(a) is indeed stronger than in Fig. A2.6(c), supporting the assumption that the influence of v_{10} on the UTCI increases as it too increases, and vice versa for the PET. The PET remains most strongly sensitive to T_{mrt} , even in winter. The way the WC assimilates v_{10} is similar to the PET, in the sense that its influence fades off as it accelerates. The WC is nevertheless more sensitive to v_{10} than the PET.

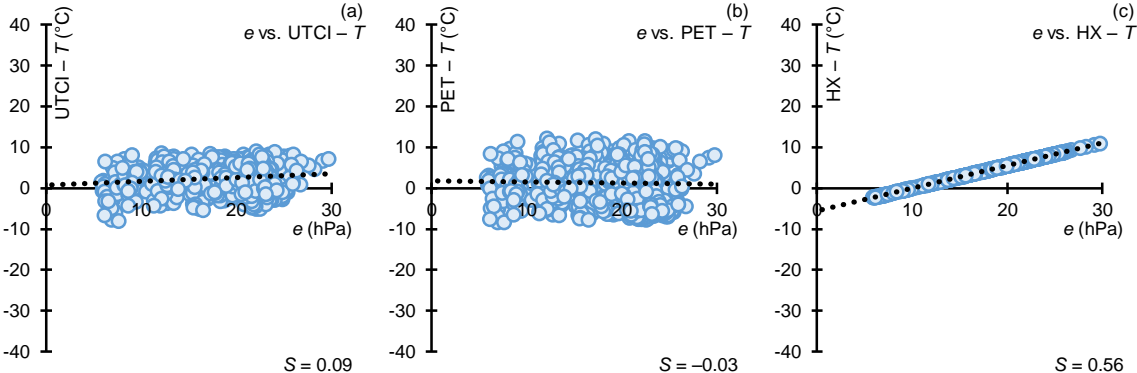


Fig. A2.7: Comparison between e and (a) UTCI_{off} , (b) PET_{off} and (c) HX_{off} at SF when $T \geq 21^\circ\text{C}$. The trend line and its slope (S) are included.

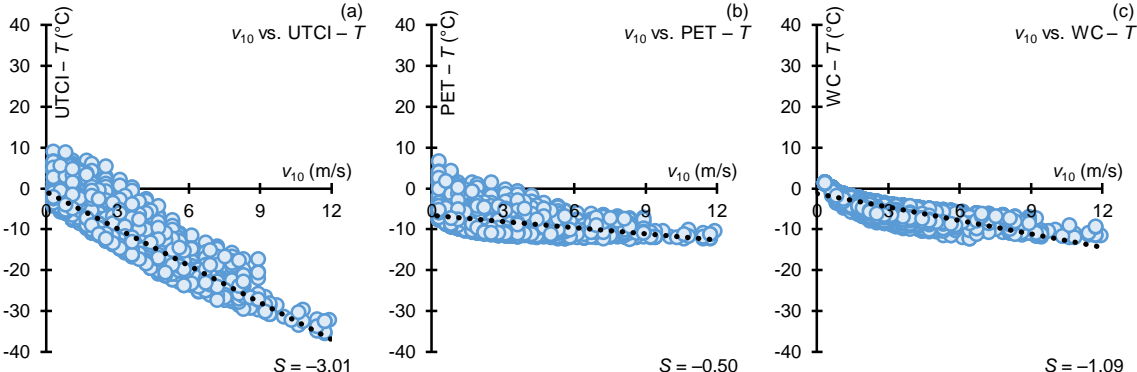


Fig. A2.8: Comparison between v_{10} and (a) UTCI_{off} , (b) PET_{off} and (c) WC_{off} at SF when $T \leq 0^\circ\text{C}$ and $v_{10} > 0 \text{ m/s}$. The trend line and its slope (S) are included.

A2.3.3 Identifying hazardous hot and cold weather events

In order to assess how the indices fare at identifying hazardous weather conditions, their hourly values at JL and SS are classified according to different levels of thermal comfort or stress as suggested by the literature. The frequency of occurrence of these levels is tabulated in Tab. A2.4. Over the course of the year, the UTCI identifies 9 h of very strong heat stress at SS but none at JL, which is not the highest level of stress but still potentially dangerous. The HX does identify 2 h at JL and 4 h at SS as being greatly uncomfortable, but still none at the dangerous level. The PET identifies 2 h of extreme heat stress at JL and 35 such hours at SS. At the other extreme, the UTCI identifies 90 h at JL and 2 h at SS of extreme cold stress, which is dangerous. The WC identifies 225 risky hours at JL and 98 such hours at SS, a level considered dangerous if outside for a long period of time without proper clothing. Interestingly, the PET calls for over half of the data to be “very cold” at both stations. The PET’s classification of a very cold sensation starts at 4°C, evidently too high to discretize a cold environment such as Quebec.

Tab. A2.4: Total number of hourly values for the UTCI, PET, HX and WC according to stress or comfort level at JL and SS. Stress levels for the UTCI are taken from Błażejczyk *et al.* (2013), comfort/stress levels for the PET are taken from Matzarakis *et al.* (1999), and HX and WC comfort levels are taken from Błażejczyk *et al.* (2012).

	Interval	Jean-Lesage		Saint-Sauveur	
		Hour(s)	%	Hour(s)	%
UTCI					
Extreme heat stress	[46°C, +∞[0	0.0	0	0.0
Very strong heat stress	[38°C, 46°C]	0	0.0	9	0.1
Strong heat stress	[32°C, 38°C]	42	0.5	175	2.2
Moderate heat stress	[26°C, 32°C]	390	4.5	555	6.9
No stress	[9°C, 26°C]	2,771	31.8	2,893	35.9
Slight cold stress	[0°C, 9°C]	1,545	17.7	1,440	17.9
Moderate cold stress	[-13°C, 0°C]	1,728	19.8	1,675	20.8
Strong cold stress	[-27°C, -13°C]	1,373	15.8	1,089	13.5
Very strong cold stress	[-40°C, -27°C]	770	8.8	216	2.7
Extreme cold stress]-∞, -40°C]	90	1.0	1	0.0
Total		8,709	100	8,053	100
PET					
Very hot / Extreme heat stress	[41°C, +∞[2	0.0	35	0.4
Hot / Strong heat stress	[35°C, 41°C]	37	0.4	150	1.9
Warm / Moderate heat stress	[29°C, 35°C]	139	1.6	326	4.0
Slightly warm / Slight heat stress	[23°C, 29°C]	383	4.4	435	5.4
ComforTab. / No stress	[18°C, 23°C]	485	5.6	581	7.2
Slightly cool / Slight cold stress	[13°C, 18°C]	780	9.0	774	9.6
Cool / Moderate cold stress	[8°C, 13°C]	993	11.4	880	10.9
Cold / Strong cold stress	[4°C, 8°C]	871	10.0	710	8.8
Very cold / Extreme cold stress]-∞, 4°C]	5,019	57.6	4,162	51.7
Total		8,709	100	8,053	100
HX					
Dangerous	[46°C, +∞[0	0.0	0	0.0
Great discomfort	[40°C, 46°C]	2	0.3	4	0.4
Some discomfort	[30°C, 40°C]	231	31.8	271	28.1
No discomfort]-∞, 30°C]	494	68.0	689	71.5
Total		727	100	964	100
WC					
No discomfort	[0°C, +∞[14	0.5	90	3.5
Slight discomfort	[-10°C, 0°C]	1,083	37.2	1,146	44.8
UncomforTab.	[-28°C, -10°C]	1,587	54.6	1,226	47.9
Risk	[-40°C, -28°C]	225	7.7	98	3.8
High risk	[-48°C, -40°C]	0	0.0	0	0.0
Very high risk	[-55°C, -48°C]	0	0.0	0	0.0
Dangerous]-∞, -55°C]	0	0.0	0	0.0
Total		2,909	100	2,560	100

July 15–17, 2013, were the three warmest days of the summer. During that 36-h period, T rarely ever dipped below 20 °C and was close to or above 30°C during the late morning and afternoon hours at SF (Fig. A2.9(a)). The indices are plotted in Fig. A2.9(b). The PET fluctuates the most, which reflects its stronger sensitivity to T_{mrt} in the summer. At the opposite, the HX, which does not consider T_{mrt} or v , fluctuates the least and stays consistently above T . A breeze can indeed attenuate the heat stress felt during a heatwave. This is reflected in the UTCI and PET during windy periods, such as July 15 at 1300 hours and occasionally throughout July 16 and 17, however, the relief appears to be minimal. Shade can also provide

stress relief during a heat wave. In order to evaluate how much so, the indices are recalculated for the hours when $T_{\text{mrt}} > T$ by setting T_{mrt} equal to T (Fig. A2.9(c)). The shade does indeed provide relief. In this particular context, the UTCI and PET reproduce a comfort value below the HX (which has not changed). The PET records the biggest difference between a sunny and shaded area, a difference of up to 14°C around noon, which reflects, once again, a higher sensitivity to T_{mrt} . The difference for the UTCI ranges between 6 and 8°C around noon.

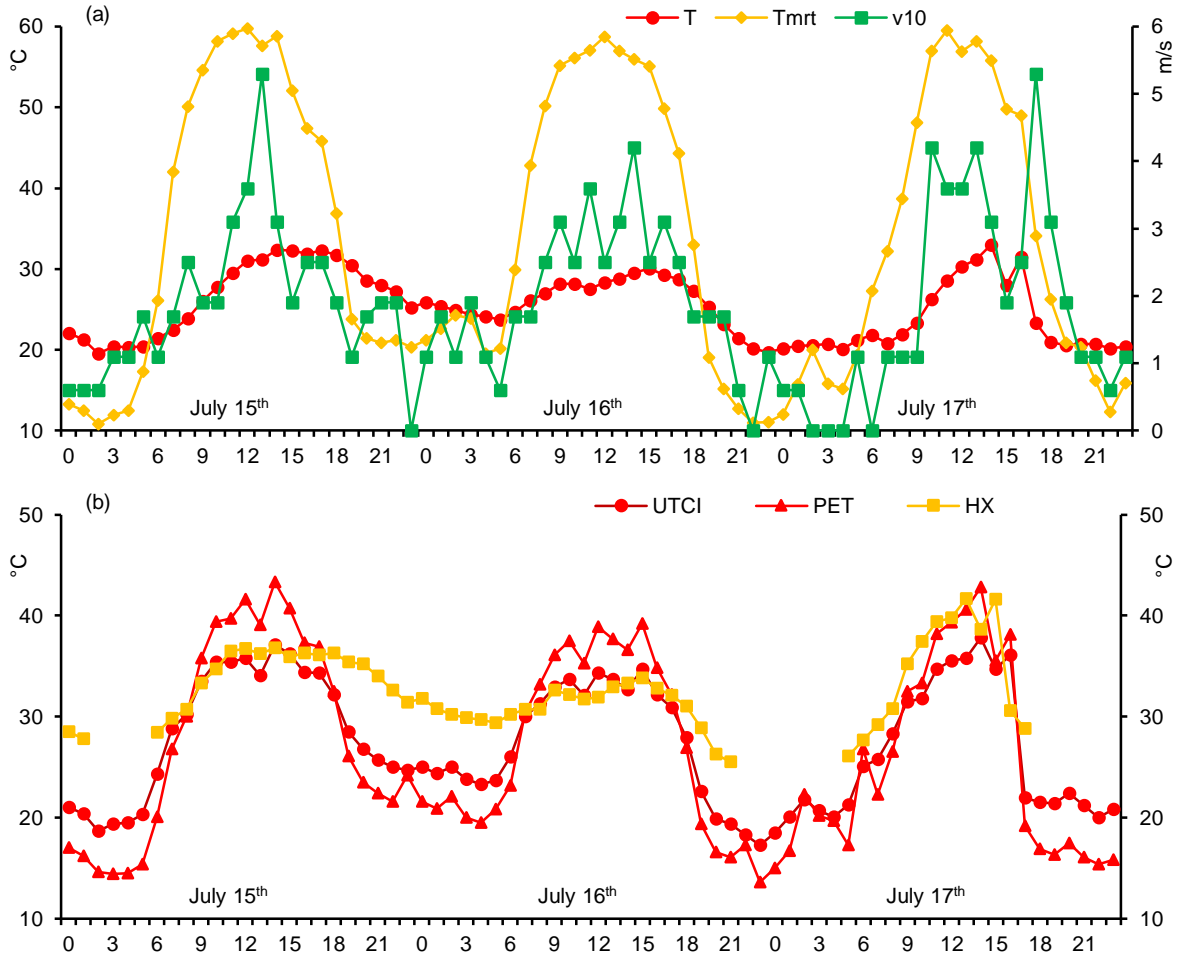


Fig. A2.9: Hourly (a) observations of T , T_{mrt} and v_{10} , (b) computations of the indices, and (c) computations of the indices in the shade for July 15–17, 2013, at SF.

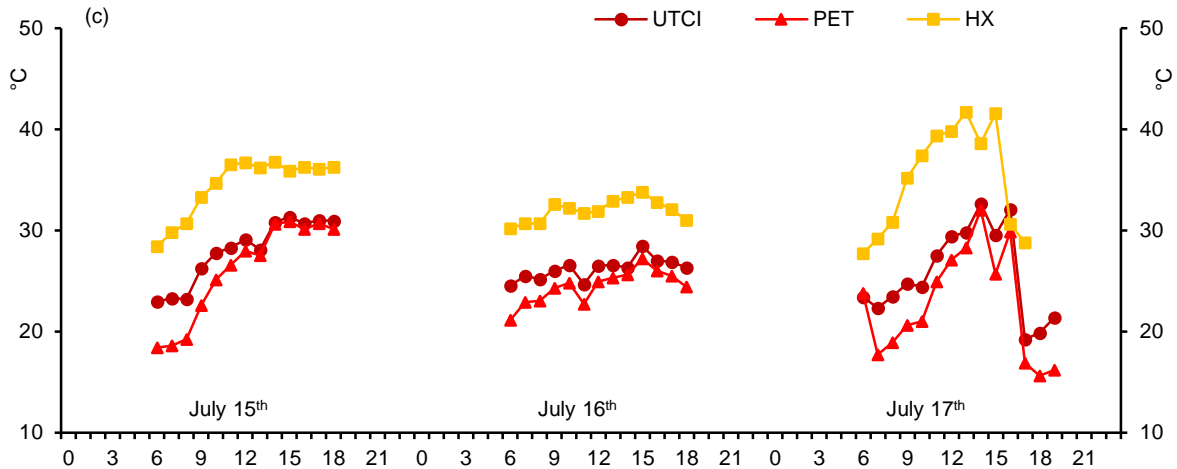


Fig. A2.9 (continued)

The three coldest days occurred from January 1–3, 2014. During that 36-h period, T rarely inched above -20°C (Fig. A2.10(a)). It was also very windy from sunset on January 2 to sunrise the following day. The most striking observation about Fig. A2.10(b) is how responsive the UTCI is during the windy period, dropping to dangerous levels, and throughout those 3 days, while the PET and WC are not nearly as affected. The UTCI and the PET tend to be colder than the WC, despite the PET's weaker sensitivity to v_{10} , except for the few hours of the day when $T_{\text{mrt}} > T$. The UTCI, however, might stay below the WC during those periods if the wind is strong enough.

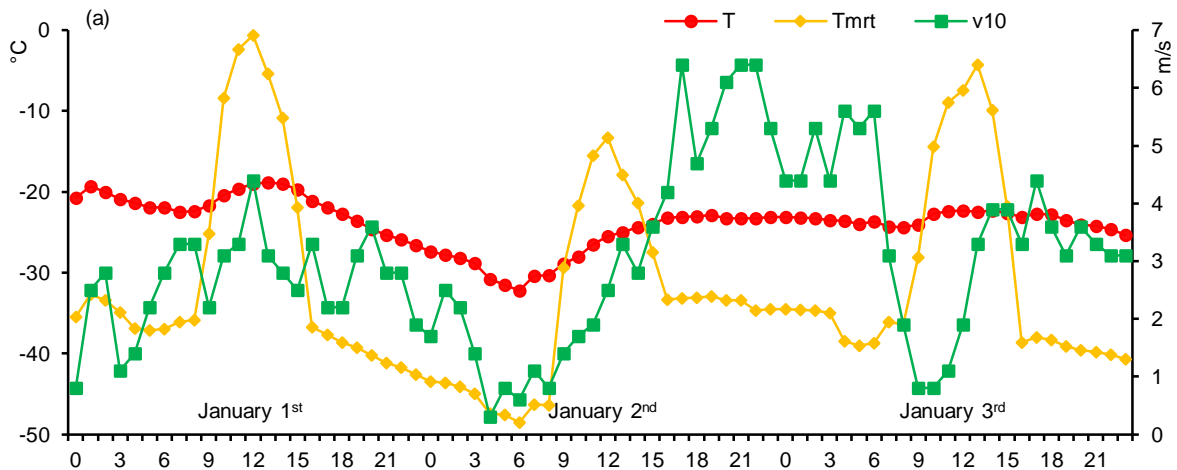


Fig. A2.10: Hourly (a) observations of T , T_{mrt} and v_{10} , and (b) computations of the indices for January 1–3, 2014, at SF.

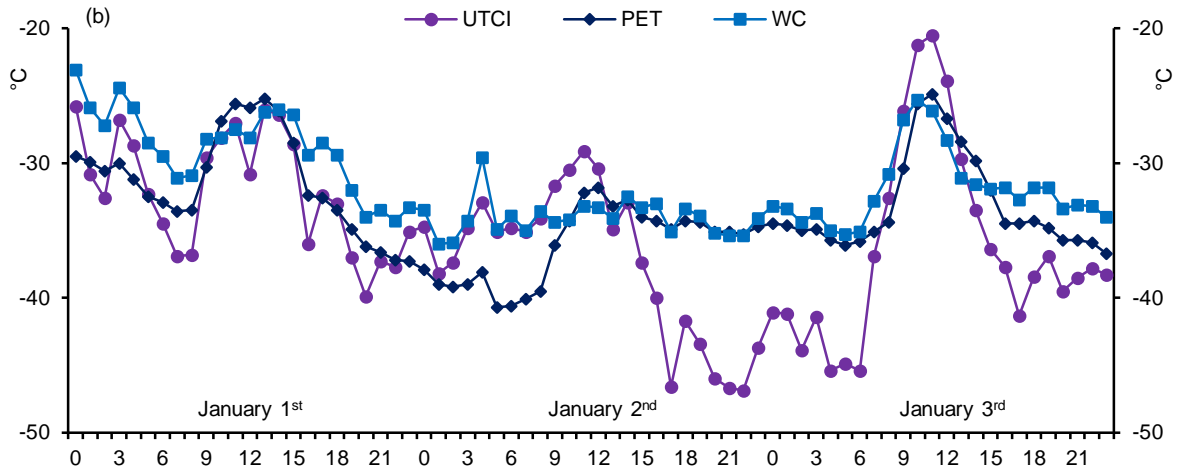


Fig. A2.10 (continued)

A2.4 Discussion

The UTCI is a more comprehensive and versatile index than the HX due to its consideration of T_{mrt} , which tends to warm the thermal sensation during the day and cool it at night. The UTCI does indeed fluctuate more than the HX on a daily cycle. Additionally, with some manipulation of T_{mrt} , it is possible to calculate the UTCI in shadowy areas, which is relevant information of public awareness during a heat wave. However, its strong sensitivity to v limits its capacity to reach high values, and it occasionally remains below the HX during the summer, since the HX does not consider v at all either. v does indeed supply some relief during a hot spell and should be taken into consideration when assessing the weather’s potential to be dangerous. The fact that e plays a lesser role in the calculation of UTCI in warm weather does not limit its capacity to identify hot thermal sensation, as was seen in Tab. A2.4.

The UTCI is also a more robust index than the WC due to its consideration of T_{mrt} and its higher sensitivity to v . The UTCI is a stress-based index, as opposed to the WC (and the HX) which is comfort based, making a comparison of different stress and comfort levels difficult (i.e., Tab. A2.4). However, if we consider the “extreme cold stress” expressed by the

UTCI to be comparable to the WC's "high risk" comfort level and other levels below, the UTCI does indeed capture dangerous cold weather more often.

Overall, the UTCI was found to be more sensitive to T_{mrt} , e and v_{10} in a suburban environment, and slightly less sensitive to T_{mrt} at the urban station, compared to the PET. During the summer, the PET was found to be more sensitive than the UTCI to T_{mrt} . In the summer daytime, the PET fluctuates more and reaches higher values (as seen in Fig. A2.9(b) and corroborated by a similar comparison by Błażejczyk *et al.* (2012) in Freiburg, Germany) and therefore identifies hazardous hot weather more often (Tab. A2.4). Błażejczyk *et al.* (2012) nevertheless concluded that the UTCI remains very sensitive to changes in all meteorological stimuli, including global radiation, on microclimatic time scales. The fact that the UTCI usually remains below the PET in the summer daytime is indeed explained in part by its stronger sensitivity to v . During the winter, hazardous weather is usually accompanied by strong winds. The UTCI, being much more sensitive to v than the PET, makes it a better index to identify such events. The UTCI's definition of the cold stress levels in Tab. A2.4 are also much more appropriate to interpret the impacts of dangerously cold weather as opposed to that of the PET.

With respect to the urban climatology analysis, SS is warmer and less windy than SF and JL, resulting in index values a few degrees higher there than elsewhere. Overall, the UTCI had the largest discrepancy between SS and JL, especially in the late fall, winter and early spring. In the daytime, when people are most likely to be outdoors, the UTCI and the PET were also warmer at SS, especially, once again, in winter for the UTCI. Downtown areas are therefore more comfortable environments in the winter season where people are less likely to suffer from the impacts of a cold wave. Indeed, JL (proportionally) records many more stressful cold hours than SS (Tab. A2.4). During the warm season, the UTCI is a few degrees warmer at SS on average. This difference creates potentially dangerous conditions that

remain unnoticed at JL (Tab. A2.4).

The implementation of the UTCI on a regular basis implies that real-time T_{mrt} estimates are readily available. There exists different methods to estimate T_{mrt} , such as measurements from a device measuring global radiation (a pyranometer or a globe thermometer), however, not all weather stations are equipped with such an instrument. The use of a software such as RayMan, like we used in this study, is always an option, but is not as accurate. Thorsson *et al.* (2007b) obtained consistent underestimations of T_{mrt} for low sun elevations by using the software as opposed to radiation measurements. Using constant values for the albedo, the Bowen ratio and the ratio of diffuse to global radiation is also a source of uncertainty, but we expect the errors that this might cause to be minimal, as Thorsson *et al.* (2007b) still obtained underestimations of T_{mrt} after manipulating the values of those variables.

A2.5 Conclusion

We calculated the newly developed UTCI and other popular thermal comfort indices such as the PET, the HX and the WC in Quebec City, a city with a wide climatic variability between the warm and cold seasons, in order to perform a sensitivity analysis of those indices with respect to meteorological variables within an urban climatology context.

The first objective of this study was to evaluate the added value of adopting the UTCI for the operational assessment of comfort on a daily basis and as a warning tool to forecast upcoming weather events that are potentially dangerous to human health, as oppose to relying on traditional and simpler comfort indices. The UTCI is indeed a more comprehensive index than the HX and the WC due to its consideration of T_{mrt} and high sensitivity to v . Overall, the UTCI is slightly more sensitive to T_{mrt} than the PET, although this varies in different conditions. When the weather was

prone to inflict hot stress, the PET was in fact more sensitive to T_{mrt} , making it more likely to reach dangerous levels. The UTCI is nevertheless capable of identifying conditions that are potentially hazardous, albeit not as often as the PET. The UTCI is in turn much more sensitive to v , which is a key feature when evaluating dangerous conditions in cold weather. Also, the PET's cold comfort levels as they are currently defined are inappropriate to assess comfort in cold environments. Taking this into consideration, the UTCI is therefore a better index to implement broadly.

The second objective was to evaluate the necessity to expand the network of urban weather monitoring for public awareness. This would be necessary given the different response of the UTCI between the urban and suburban stations. This argument is reinforced in the summer when many episodes of strong heat stress remain unnoticed by regionally representative observations made at airports.

References

Alduchov, O.A. and Eskridge, R.E. (1996). Improved Magnus form approximation of saturation vapor pressure. *J. Appl. Meteorol.* 35: 601–609.

Bergeron, O. (2014). *Caractérisation de la variabilité spatiale et temporelle de la température de l'air ambiant sur un territoire urbain : étude du cas de la ville de Québec*. Ministère du Développement durable, de l'Environnement et de la Lutte contre les changements climatiques, Quebec City.

Błażejczyk, K., Epstein, Y., Jendritzky, G., Staiger, H. and Tinz, B. (2012). Comparison of UTCI to selected thermal indices. *Int. J. Biometeorol.* 56: 515–535.

Błażejczyk, K., Jendritzky, G., Bröde, P., Fiala, D., Havenith, G., Epstein, Y., Psikuta, A. and Kampmann, B. (2013). An introduction to the Universal Thermal Climate Index (UTCI). *Geogr. Pol.* 86: 5–10.

Bleta, A., Nastos, P.T., and Matzarakis, A. (2014). Assessment of bioclimatic conditions on Crete Island, Greece. *Reg. Environ. Chang.* 14: 1967–1981

Bröde, P., Krüger, E.L., Rossi, F.A. and Fiala, D. (2012a). Predicting urban outdoor thermal comfort by the Universal Thermal Climate Index (UTCI)—a case study in southern Brazil. *Int. J. Biometeorol.* 56: 471–480.

Bröde, P., Fiala, D., Błażejczyk, K., Holmér, I., Jendritzky, G., Kampmann, B., Tinz, B. and Havenith, G. (2012b). Deriving the operational procedure for the Universal Thermal Climate Index (UTCI). *Int. J. Biometeorol.* 56: 481–494.

Budd, G.M. (2008). Wet-bulb globe temperature (WBGT)—its history and its limitations. *J. Sci. Med. Sport* 11: 20–32.

Burkard, K., Schneider, A., Breitner, S., Khan, M.H., Krämer, A. and Endlicher, W. (2011). The effect of atmospheric thermal conditions and urban thermal pollution on all-cause and cardiovascular mortality in Bangladesh. *Environ. Pollut.* 159: 2035–2043.

Cohen, P., Potchter, O. and Matzarakis, A. (2012). Daily and seasonal climatic conditions of green urban open spaces in the Mediterranean climate and their impact on human comfort. *Build. Environ.* 51: 285–295.

Environment Canada (2014). *Spring and summer weather hazards*. <https://www.ec.gc.ca/meteo-weather/default.asp?lang=En&n=6C5D4990-1>. Accessed 27 March 2015.

Environment Canada (2015). *Wind chill—the chilling facts*. <http://www.ec.gc.ca/meteo-weather/default.asp?lang=En&n=5FBF816A-1>. Accessed 27 March 2015.

Epstein, Y. and Moran, D.S. (2006). Thermal comfort and the heat stress indices. *Ind. Health* 44: 388–398.

Fanger, P.O. (1970). *Thermal comfort*. Danish Technical, Copenhagen.

Fiala, D., Lomas, K.J. and Stohrer, M. (1999). A computer model for human thermoregulation for a wide range of environmental conditions: the passive system. *J. Appl. Physiol.* 87: 1957–1972.

Fiala, D., Lomas, K.J. and Stohrer, M. (2001). Computer prediction of human thermoregulatory and temperature responses to a wide range of environmental conditions. *Int. J. Biometeorol.* 45: 143–159.

Fiala, D., Havenith, G., Bröde, P., Kampmann, B. and Jendritzky, G. (2012). UTCI-Fiala multi-node model of human heat transfer and temperature regulation. *Int. J. Biometeorol.* 56: 429–441.

Gagge, A.P., Stolwijk, J.A.J. and Nishi, Y. (1971). An effective temperature scale based on a simple model of human physiological regulatory response. *ASHRAE Trans.* 77: 247–260.

Gagge, A.P., Forbelets, A.P. and Berglund, L.G. (1986). A standard predictive index of human response to the thermal environment. *ASHRAE Trans.* 92: 709–729.

Havenith, G., Fiala, D., Błażejczyk, K., Richards, M., Bröde, P., Holmér, I., Rintamaki, H., Benshabat, Y. and Jendritzky, G. (2012). The UTCI-clothing model. *Int. J. Biometeorol.* 56: 461–470.

Höppe, P.R. (1993). Heat balance modelling. *Experientia* 49: 741–746.

Höppe, P. (1999). The physiological equivalent temperature—a universal index for the biometeorological assessment of the thermal environment. *Int. J. Biometeorol.* 43: 71–75.

Humphreys, M.A. (1994). *Field studies and climate chamber experiments in thermal comfort research*. In: Oseland, N.A. and Humphreys, M.A. *Thermal comfort: past, present and future*. Building Research Establishment, Watford, pp. 52–69.

Jendritzky, G., de Dear, R. and Havenith, G. (2012). UTCI—Why another thermal index? *Int. J. Biometeorol.* 56: 421–428.

Johansson, E. and Emmanuel, R. (2006). The influence of urban design on outdoor thermal comfort in the hot, humid city of Colombo, Sri Lanka. *Int. J. Biometeorol.* 51: 119–133.

Kántor, N. and Unger, J. (2011). The most problematic variable in the course of human-biometeorological comfort assessment—the mean radiant temperature. *Cent. Eur. J. Geosci.* 3: 90–100.

Kántor, N., Égerházi, L. and Unger, J. (2012). Subjective estimation of

thermal environment in recreational urban spaces—Part 1: investigations in Szeged, Hungary. *Int. J. Biometeorol.* 56: 1075–1088.

Krüger, E., Drach, P., Emmanuel, R. and Corbella, O. (2013). Assessment of daytime outdoor comfort levels in and outside the urban area of Glasgow, UK. *Int. J. Biometeorol.* 57: 521–533.

Landsberg, H.E. (1981). *The urban climate*. Academic Press, New York.

Leduc, R., Ferland, M., Gariépy, J., Jacques, G., Lelièvre, C. and Paulin, G. (1980). Îlot de chaleur à Québec : cas d'été. *Bound. Layer Meteorol.* 19: 471–480.

Leduc, R., Jacques, G., Ferland, M. and Lelièvre, C. (1981). Îlot de chaleur à Québec : cas d'hiver. *Bound. Layer Meteorol.* 21: 315–324.

Lin, T.P., de Dear, R. and Hwang, R.L. (2011). Effect of thermal adaptation on seasonal outdoor thermal comfort. *Int. J. Climatol.* 31: 302–312.

Makaremi, N., Salleh, E., Jaafar, M.Z. and Hoseini, A.G. (2012). Thermal comfort conditions of shaded outdoor spaces in hot and humid climate of Malaysia. *Build. Environ.* 48: 7–14.

Matzarakis, A., Mayer, H. and Iziomon, M.G. (1999). Applications of a universal thermal index: physiological equivalent temperature. *Int. J. Biometeorol.* 43: 76–84.

Matzarakis, A., Rutz, F. and Mayer, H. (2007). Modelling radiation fluxes in simple and complex environments—application of the RayMan model. *Int. J. Biometeorol.* 51: 323–334.

Matzarakis, A., Rutz, F. and Mayer, H. (2010). Modelling radiation fluxes in simple and complex environments: basics of the RayMan model. *Int. J. Biometeorol.* 54: 131–139.

Mayer, H., Holst, J., Dostal, P., Imbery, F. and Schindler, D. (2008). Human thermal comfort in summer within an urban street canyon in central Europe. *Meteorol. Z.* 17: 241–250.

MDDELCC (Ministère du Développement durable, de l'Environnement et de la Lutte contre les changements climatiques) (2015). *Normales climatiques 1981–2010*. <http://www.mddelcc.gouv.qc.ca/climat/normales/climat-qc.htm>. Accessed 27 March 2015.

Minard, D., Belding, H.S. and Kingston, J.R. (1957). Prevention of heat casualties. *J. Am. Med. Assoc.* 165: 1813–1818.

Oliveira, S. and Andrade, H. (2007). An initial assessment of the bioclimatic comfort in an outdoor public space in Lisbon. *Int. J. Biometeorol.* 52: 69–84.

Osczevski, R. and Bluestein, M. (2005). The new wind chill equivalent temperature chart. *Bull. Am. Meteorol. Soc.* 86: 1453–1548.

- Pearlmutter, D., Bitan, A. and Berliner, P. (1999). Microclimatic analysis of “compact” urban canyons in an arid zone. *Atmos. Environ.* 33: 4143–4150.
- Peel, M.C., Finlayson, B.L. and McMahon, T.A. (2007). Updated world map of the Köppen–Geiger climate classification. *Hydrol. Earth Syst. Sci.* 11: 1633–1644.
- Santee, W.R. and Wallace, R.F. (2005). Comparison of weather service heat indices using a thermal model. *J. Therm. Biol.* 30: 65–72.
- Spagnolo, J. and de Dear, R. (2003). A field study of thermal comfort in outdoor and semi-outdoor environments in subtropical Sydney Australia. *Build. Environ.* 38: 721–738.
- Steadman, R.G. (1984). A universal scale of apparent temperature. *J. Clim. Appl. Meteorol.* 23: 1674–1687.
- Steadman, R.G. (1994). Norms of apparent temperature in Australia. *Aust. Meteorol. Mag.* 43: 1–16.
- Taylor, N.A.S. (2006). Challenges to temperature regulation when working in hot environments. *Ind. Health* 44: 331–344.
- Thorsson, S., Honjo, T., Lindberg, F., Eliasson, I. and Lim, E. (2007a). Thermal comfort and outdoor activity in Japanese urban public places. *Environ. Behav.* 39: 660–684.
- Thorsson, S., Lindberg, F., Eliasson, I. and Holmer, B. (2007b). Different methods for estimating the mean radiant temperature in an outdoor urban setting. *Int. J. Climatol.* 27: 1983–1993.
- Toy, S. and Yilmaz, S. (2010). Thermal sensation of people performing recreational activities in shadowy environment: a case study from Turkey. *Theor. Appl. Climatol.* 101: 329–343.